Patterns of Crustal Deformation Resulting from the 2010 Earthquake Sequence in Christchurch, New Zealand

A thesis submitted in partial fulfilment of the requirements for the

Degree of Master of Science in Engineering Geology

in the University of Canterbury

by J.W.R. Claridge

University of Canterbury

2012

Abstract

The M_w 7.1 Darfield earthquake generated a ~30 km long surface rupture on the Greendale Fault and significant surface deformation related to related blind faults on a previously unrecognized fault system beneath the Canterbury Plains. This earthquake provided the opportunity for research into the patterns and mechanisms of co-seismic and post-seismic crustal deformation. In this thesis I use multiple across-fault EDM surveys, logic trees, surface investigations and deformation feature mapping, seismic reflection surveying, and survey mark (cadastral) re-occupation using GPS to quantify surface displacements at a variety of temporal and spatial scales. My field mapping investigations identified shaking and crustal displacement-induced surface deformation features south and southwest of Christchurch and in the vicinity of the projected surface traces of the Hororata Blind and Charing Cross Faults. The data are consistent with the high peak ground accelerations and broad surface warping due to underlying reverse faulting on the Hororata Blind Fault and Charing Cross Fault. I measured varying amounts of post-seismic displacement at four of five locations that crossed the Greendale Fault. None of the data showed evidence for localized dextral creep on the Greendale Fault surface trace, consistent with other studies showing only minimal regional post-seismic deformation. Instead, the post-seismic deformation field suggests an apparent westward translation of northern parts of the across-fault surveys relative to the southern parts of the surveys that I attribute to post-mainshock creep on blind thrusts and/or other unidentified structures. The seismic surveys identified a deformation zone in the gravels that we attribute to the Hororata Blind Fault but the Charing Cross fault was not able to be identified on the survey. Cadastral re-surveys indicate a deformation field consistent with previously published geodetic data. We use this deformation with regional strain rates to estimate earthquake recurrence intervals of ~7000 to > 14,000 yrs on the Hororata Blind and Charing Cross Faults.

Acknowledgements

I made it!

Many thanks must be first given to my Supervisors: Mark Quigley, Mike Finnemore, and David Barrell, this project would have been at a standstill and never made it anywhere without your input. Thanks to Mike for your commitment to helping me progress and grow the geophysical side of the project. U always managed to help me out when I needed it and it bit touch and go towards the end but we got there. I am forever grateful for everything you have done for me.

Mark a very special thanks must be dedicated to you. Your input and help through my project has been amazing, and you have always had faith in the project. or that I will be forever grateful for everything you did for me.

Brendan Duffy I have nothing but the utmost gratitude for everything you have done for me and this project. You were essentially an additional supervisor and it was greatly appreciated. I owe you a few beers for your commitment!!

To my fellow postgrads, Tim Stahl, Reuben Lo, Matt Banks, Blair Mason, Charlotte Stephen Brownie, Jelte Keeman, Sharon Hornblow; thanks for all your help in the seismic surveys it was not possible without your help.

To my family thanks for the support throughout the duration of this project. It was through your encouragement and guidance that. To my Dad, thanks for pushing me when I needed to be pushed and for countless hours editing my work. Kettie you are a champion, thanks so much for the countless hours editing it really meant a lot. I am very much looking forward to sharing a bottle of wine with you to say thanks.

TO my amazing girlfriend Sophie, I have appreciated your support throughout this project. You have always lent a hand when I've needed it and been there for support through the tough patches. I will never forget your help throughout this marathon of a project. You really help get me to the finish line. I will also miss the weekly batch of cookies to help me through.

Table of Contents

I. Scientific context

The tectonic setting of New Zealand and the Canterbury region, historical seismicity of Canterbury, and the geology and geomorphology of the Canterbury Plains are herein reviewed to provide background knowledge and a scientific context for the main body of research.

Tectonic Setting

The New Zealand micro-continent straddles the boundary between the Pacific and the Australian plates and its active tectonics are dominated by three main features that have evolved and shaped the New Zealand landmass visible today (see Figure 1) (Reyners and Cowan, 1993; Pettinga *et al.*, 2001). Firstly, beneath the North Island and the northern part of the South Island the Pacific plate is subducting obliquely beneath the Australian plate at Hikurangi trough (Reyners and Cowan, 1993). In contrast, the subduction is reversed in the Fiordland region in the southwest of the South Island, with the Australian plate subducting obliquely beneath the Pacific plate at the Puysegur trench (Reyners and Cowan, 1993). The final active feature along the plate boundary is positioned between these two areas of subduction within the central part of the South Island and is characterised by oblique continental-continental convergence (Sutherland, *et al.*, 2007; Stirling *et al.*, 2001). This occurs as the continental Chatham Rise section of the Pacific plate collides with the continental crust of the Australian Plate (Gledhill *et al.*, 2011; Allen *et al.*, 2010). Due to the both sections of the plates being comprised of the same density continental crust neither buoyant crust can subduct under the other as the plates converge. This leads to compressional movement forcing the Pacific Plate to be thrust over the Australian plate and subsequently results in crustal thickening and the uplift of the Southern Alps mountain range (see Figure 2). The Australia and Pacific plates converge obliquely at a rate of 39 - 48 mm/yr. The resultant collision zone is a distributed zone of large active faults that runs through Marlborough via the Marlborough Fault System and down the west coast of South Island (Allen *et al.*, 2010; Gledhill *et al.*, 2011; Pettinga *et al.*, 2001; Sutherland, *et al.*, 2007; Stirling *et al.*, 2001). It is marked by the Alpine Fault system connecting the northern and southern subduction zones.

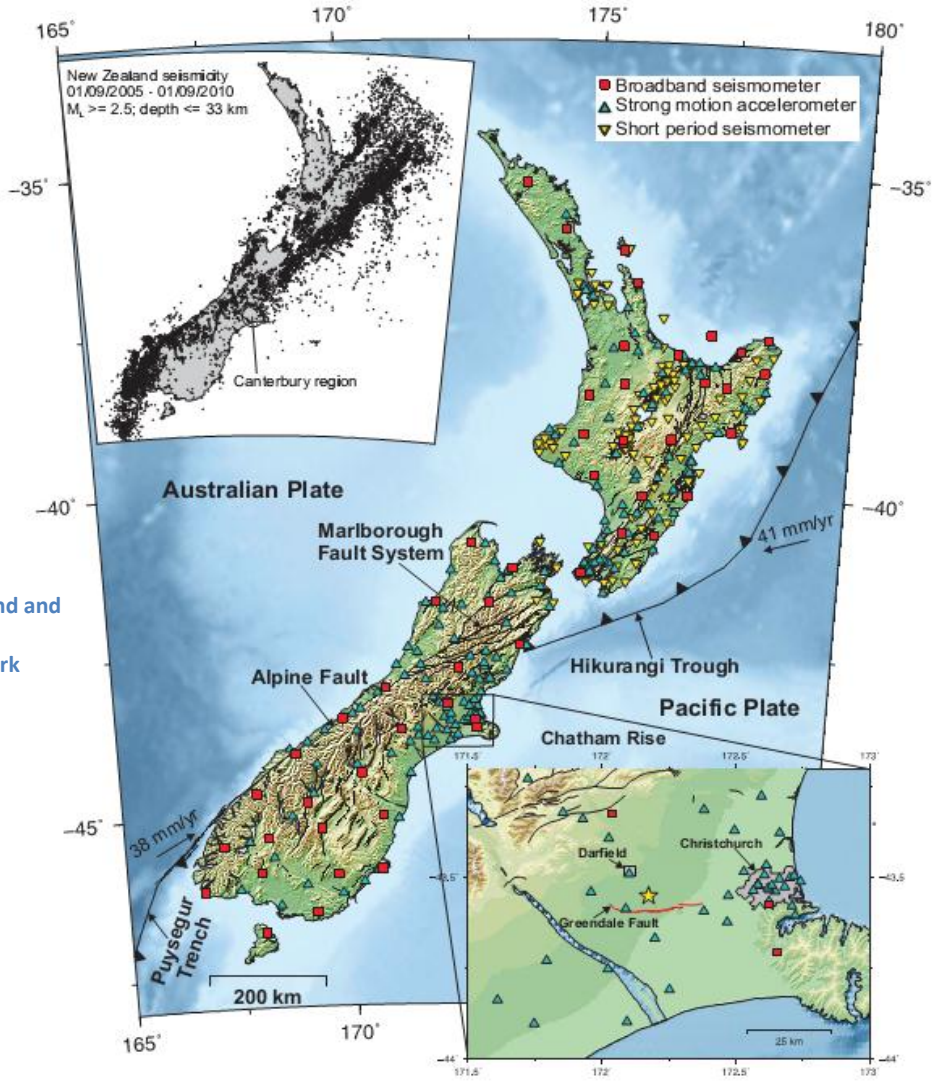

Figure 1: Tectonic setting of New Zealand and the Canterbury region, and the GeoNet seismometer and accelerometer network (Source: Gledhill *et al.*, 2011).

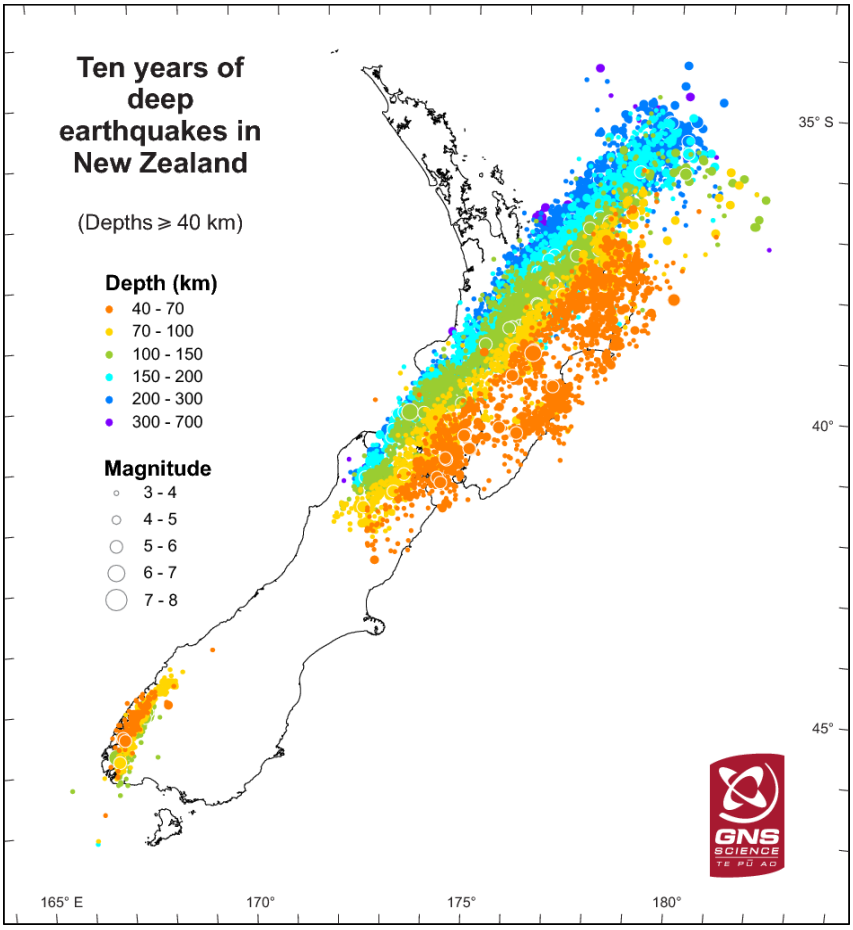

Figure 2: Signifies the oblique collision between the Australian and Pacific Plate in central Canterbury. As the image signifies there are no deep earthquakes in central Canterbury signifying that subduction is not occurring (Source: http://www.geonet.org.nz/var/storage/images/media/images/earthquake/deep_seismicity.png/36831-1-eng-GB/Deep_Seismicity.png.png).

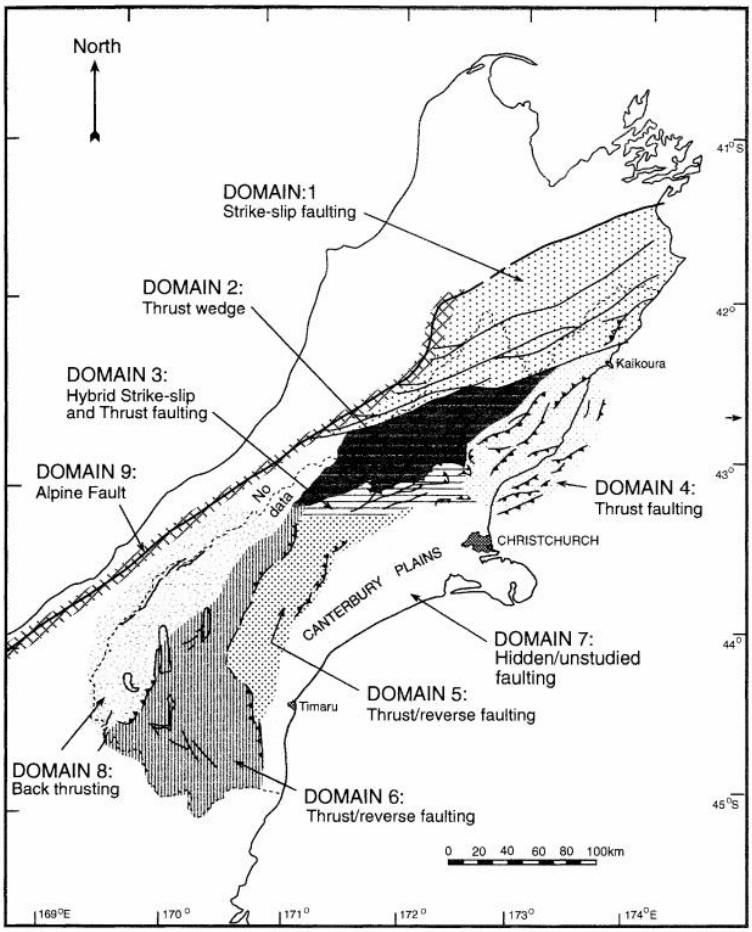

Figure 3: Structural domains of the Canterbury region: DOM 1 = Marlborough Fault Zone; DOM 2, 3 *and* 4 = West Culverden Fault Zone, Porters Pass-Amberley Fault Zone *and* North Canterbury Fold *and* Thrust Belt; DOM 5*and*6 = Mt Hutt-Mt Peel Fault Zone *and* South Canterbury Zone. Further explanation is in text. The towns and cities shown on the map are chosen by Environment Canterbury for site-specific hazard analysis in the original study (Stirling *et al.*, 1999). (Source: Pettinga *et al.*, 2001).

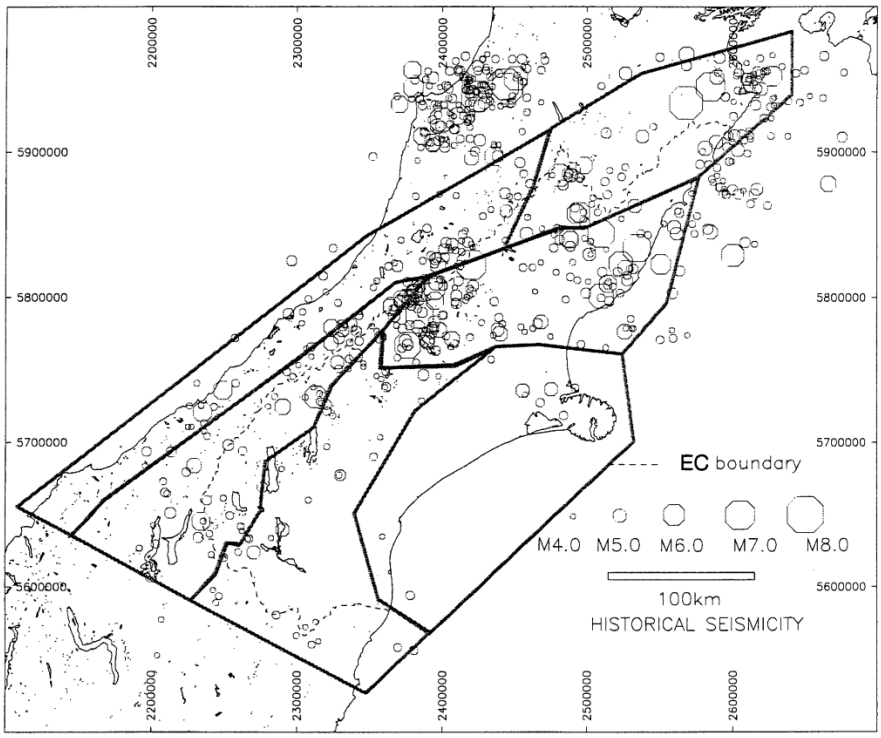

Figure 4: Historical seismicity of the Canterbury Region (Source: Stirling *et al.*, 2001)

Much of the Canterbury region is situated within the wide zone of active earth deformation where plate motion associated with the oblique collision between the Australian and Pacific Plates is approximately 40 mm/yr. (Pettinga *et al.*, 2001; Stirling *et al.*, 2001; De Mets *et al.*, 1990). The resultant motion is largely accommodated by the Alpine Fault, an approx. 650 km long right-lateral strike-slip (dextral-reverse) fault that runs along the western edge of the Canterbury region and the foothills of the Southern Alps mountain range (Allen *et al.*, 2010; Sutherland *et al.*, 2006; Norris and Cooper, 2001; Stirling *et al.*, 2001). It accommodates approx. 70 – 75 % of the total relative plate motion between the Australian and Pacific Plates (Allen *et al.*, 2010; Sutherland *et al.*, 2006; Norris and Cooper, 2001; Stirling *et al.*, 2001). The remaining approx. 30 % of the relative plate motion is accommodated by slip on a series of faults across the Southern Alps and Canterbury plains (Allen *et al.*, 2010). Comprehensive studies completed by Stirling *et al.* (2001) and Pettinga *et al.* (2001) have enabled the Canterbury and Southern Alps region to be divided into nine structural domains, each with distinctive neotectonic setting, style, geometry and rates of deformation. The domains are shown on Figure 3**,** and are outlined as follows:

Domain 1 - *Marlborough Fault Zone:* consists of a zone of strike-slip to oblique-slip faults, with the Wairau Fault marking the boundary of the northern domain (Stirling *et al.*, 2001; Pettinga *et al.*, 2001).

Domain 2 - *West Culverden Fault Zone:* is defined by a system of west-dipping thrust and reverse faults (Stirling *et al.*, 2001; Pettinga *et al.*, 2001).

Domain 3 - *Porters Pass - Amberley Fault Zone:* is at the south-eastern edge of the Southern Alps consisting of oblique strike-slip faults (Stirling *et al.*, 2001; Pettinga *et al.*, 2001).

Domain 4 - *North Canterbury Fold and Thrust Belt:* extends from the northwest Hope Fault to the southeast offshore Canterbury shelf. This zone is defined by thrust faults and folds (Stirling *et al.*, 2001; Pettinga *et al.*, 2001).

Domain 5 - *Mt Hutt - Mt Peel Fault Zone:* is comprised of thrust faults and folds forming the western margin of the central Canterbury Plains (Stirling *et al.*, 2001; Pettinga *et al.*, 2001).

Domain 6 - *South Canterbury Zone*: is the southernmost zone, which consists of thrust faults along the western edge of the southern Canterbury Plains (Stirling *et al.*, 2001; Pettinga *et al.*, 2001).

Domain 7 - *Canterbury Plains Zone*: is the furthest distance from the Australian and Pacific Plate boundary. Hence it is defined by a region with the lowest rates of deformation (Stirling *et al.*, 2001; Pettinga *et al.*, 2001).

Domain 8 - *Southern Alps Zone*: formed as result of back-thrusting from the Alpine Fault. It contains a number of oblique reverse/thrust faults (Stirling *et al.*, 2001; Pettinga *et al.*, 2001).

Domain 9 - *Alpine Fault Zone*: the furthest western domain, is defined by the oblique strike-slip Alpine Fault along the foothills of the Southern Alps. This zone accommodates the majority of plate motion over the region (Stirling *et al.*, 2001; Pettinga *et al.*, 2001).

Within these domains and the surrounding Canterbury region there are approximately 90 known major active earthquake source faults with recurrence intervals ranging from approx. 81 (– 200 years Hope Fault) to > 5,000 years (Stirling *et al.*, 2001; Pettinga *et al.*, 2001).

Historical Seismicity

Historical seismicity of the Canterbury region has largely occurred in the Southern Alps and its eastern foothills, within the northern and western domains (1, 2, 3, 6 and 8), where geological evidence for widespread active earth deformation is evident (Pettinga *et al.*, 2001; Stirling *et al.*, 2001).

Since 1840 a number of moderate to large (> Mw 6 – 7), shallow (≤ 15 km depth) earthquakes have occurred within the Canterbury region. The two largest historical earthquakes occurred within Domain 1 (Gledhill *et al.*, 2011; Stirling *et al.*, 2001; Pettinga *et al.*, 2001). The first was the M_w 7.5 Marlborough earthquake that occurred in 1848, rupturing the north-eastern section of the Awatere Fault (Stirling *et al.*, 2001; Grapes *et al.*, 1998). The second was the 1888 Mw approx. 7.2 Hope Fault earthquake, centred in Glen Wye, North Canterbury (Stirling *et al.*, 2001; Pettinga *et al.*, 1998; Cowan, 1991; Brown and Weeber, 1991). This earthquake ruptured the central section of the Hope Fault producing Modified Mercalli scale of intensity (MM) up to MMVIII in Christchurch. This is equivalent to significant occurrence of property damage and loss of life (Stirling *et al.*, 2001; Brown and Weeber, 1992). In fact, this earthquake resulted in damage to the Anglican Cathedral spire in Cathedral Square in central Christchurch (Brown and Weeber, 1992).

Other large earthquakes that have occurred within or near the region include the following (Stirling *et al.*, 2001; Pettinga *et al.*, 1998; Cowan, 1991; Brown and Weeber, 1991):

- 1929 M_w 7.8 Buller earthquake,
- 1929 M_w 7.0 Arthurs Pass earthquake,
- 1968 M_w 7.4 Murchison earthquake,

- 1969 M_w 4.7 – 4.9 Earthquake near Christchurch,
- 1970 M_w 5.6 – 5.8 Lake Ellesmere earthquake,
- 1994 M_w 6.7 Arthurs Pass earthquake, and the
- 1995 M_w 6.2 Cass earthquake.

Alpine Fault

Another fault of great significance that lies within the fringes of the Canterbury Region, within Domain 9 is the Alpine Fault. It accommodates the majority of strain along the plate boundary (Gledhill *et al.*, 2011; Stirling *et al.*, 2001). Paleoseismic investigations near the Alpine Fault have provided evidence demonstrating that earthquakes occurred in the years 1430, 1620 and 1717 with estimated moment magnitudes of 7.9 ± 0.4, 7.6 ± 0.3, and 7.9 ± 0.3 respectively (Gledhill *et al.*, 2011; Sutherland *et al.*, 2007; Rhoades and Van Dissen, 2003 Yetton *et al.*, 1998; Cooper and Norris, 1990). From this it has been suggested that the Alpine fault ruptures in major earthquakes, $M_w > 7.5$, and has a recurrence interval of approximately every 200–300 years (Gledhill *et al.*, 2011; Sutherland *et al.*, 2007; Rhoades and Van Dissen, 2003; Yetton *et al.*, 1998; Cooper and Norris, 1990).

As mentioned earlier the left over motion of the Australian and Pacific Plates, of approx. 40 mm/yr. is accommodated throughout the Southern Alps and Canterbury Plains by slip on a series of fault structures (Allen *et al.*, 2010; Stirling *et al.*, 2001; De Mets *et al.*, 1990). One of these structures, the Greendale Fault, was the source of the 2010 Darfield (Canterbury) earthquake. It was not a recognised fault prior to this earthquake (Quigley *et al.*, 2010). The fact that the Darfield earthquake was centred in the Canterbury Plains, where no active surface faults had been previously identified, confirms that the zone of active deformation extends well beyond the visible range front in the landscape on the eastern South Island (Pettinga *et al.*, 2001). Much of this motion is absorbed by other large faults in the eastern foothills of the Southern Alps, such as the Porter's Pass Fault, which has a slip rate of 3-7 mm/yr. (Howard *et al.* 2005; Cowan *et al.* 1996).

Darfield Region

Historical seismicity under the Canterbury Plains, in particular within the immediate region of the Greendale Fault and epicentre, was relatively low prior to the Darfield Earthquake (Gledhill *et al.*, 2011). Since written records began 170 years ago, no large earthquakes (> M_w 5) have occurred in the vicinity of the Greendale Fault. The strongest shaking of the area has been MMVII, which was experienced during local historical earthquakes. These include the 4th June 1969 Mw 4.7 – 4.9, which was a shallow earthquake near Christchurch and 31 August 1970 when a lower crustal rupture, M_w 5.6 – 5.8, occurred near Lake Ellesmere (Downes *et al.*, 2012; Gledhill *et al.*, 2011).

Geology of the Canterbury Plains

Beneath the Canterbury Region the basement rocks are Paleozoic to Mesozoic sedimentary and metamorphic rocks, termed Torlesse composite terrane, which originate as part of the Gondwanaland supercontinent (Forsyth *et al.*, 2008; Sutherland, 1999; Brown and Weeber, 1991). They are comprised of mainly thick deformed sections of indurated sandstone and mudstone, colloquially referred to as greywacke (Forsyth *et al.*, 2008). The Torlesse composite terrane is differentiated into two further terranes; the Rakaia and Pahau (see Figure 5) (Forsyth *et al.*, 2008; Sutherland, 1999; Brown and Weeber, 1991).

Within the foothills, beneath the Canterbury Plains, as well as on Banks Peninsula, Mid-Cretaceous volcanic, shallow intrusive and sedimentary rocks lie atop the Greywacke basement rock (Forsyth *et al.*, 2008). More extensive deposition of sedimentary rocks occurred during the Late Cretaceous period, continuing into the Pleistocene (Forsyth *et al.*, 2008; Brown and Weeber, 1991). These deposits generally formed a single large cycle of marine transgression and regression with sporadic intraplate volcanic events (Forsyth *et al.*, 2008). During the Miocene, basaltic volcanism formed Banks Peninsula which is the largest accumulation of Cenozoic volcanic rocks in the South Island (Forsyth *et al.*, 2008).

A shift in Australian-Pacific plate boundary dynamics during the Neogene lead to widespread faulting and folding that deformed the basement and overlying cover, resulting in uplift and the formation of ranges and basins (Forsyth *et al.*, 2008). As a result, the Late Cretaceous to Pliocene deposited sequence was eroded from uplifted areas but remained preserved in inland basins, such as in Northern Canterbury, offshore and beneath the Canterbury Plains (Forsyth *et al.*, 2008).

Above these deposits the Canterbury Plains in most part are comprised of coalescing fans and floodplains. They have been deposited by eastward flowing rivers emerging from the foothills of the Southern Alps during and following the end of the Last Glacial Maximum approx. 16,000 – 18,000 years ago (Forsyth *et al.*, 2008; Brown and Weeber, 1991). These deposits form a complex series of interbedded alluvial sand, silt, and gravel deposits up to and over 500 m in places (Forsyth *et al.*, 2008; Brown and Weeber, 1991).

It is therefore likely that erosion and/or deposition of gravels over the plains has obscured evidence of active faulting in this region. Seismic reflection surveys indicate that the Greendale Fault was pre-existing and was re-activated in the Darfield earthquake (Pettinga, J., pers. comm. 2011). Large up to

700 km long normal fault systems with the same east-west strike (direction) exist on the Chatham Rise, offshore east of Banks Peninsula (Field and Browne, 1989; Wood *et al.*, 1989).

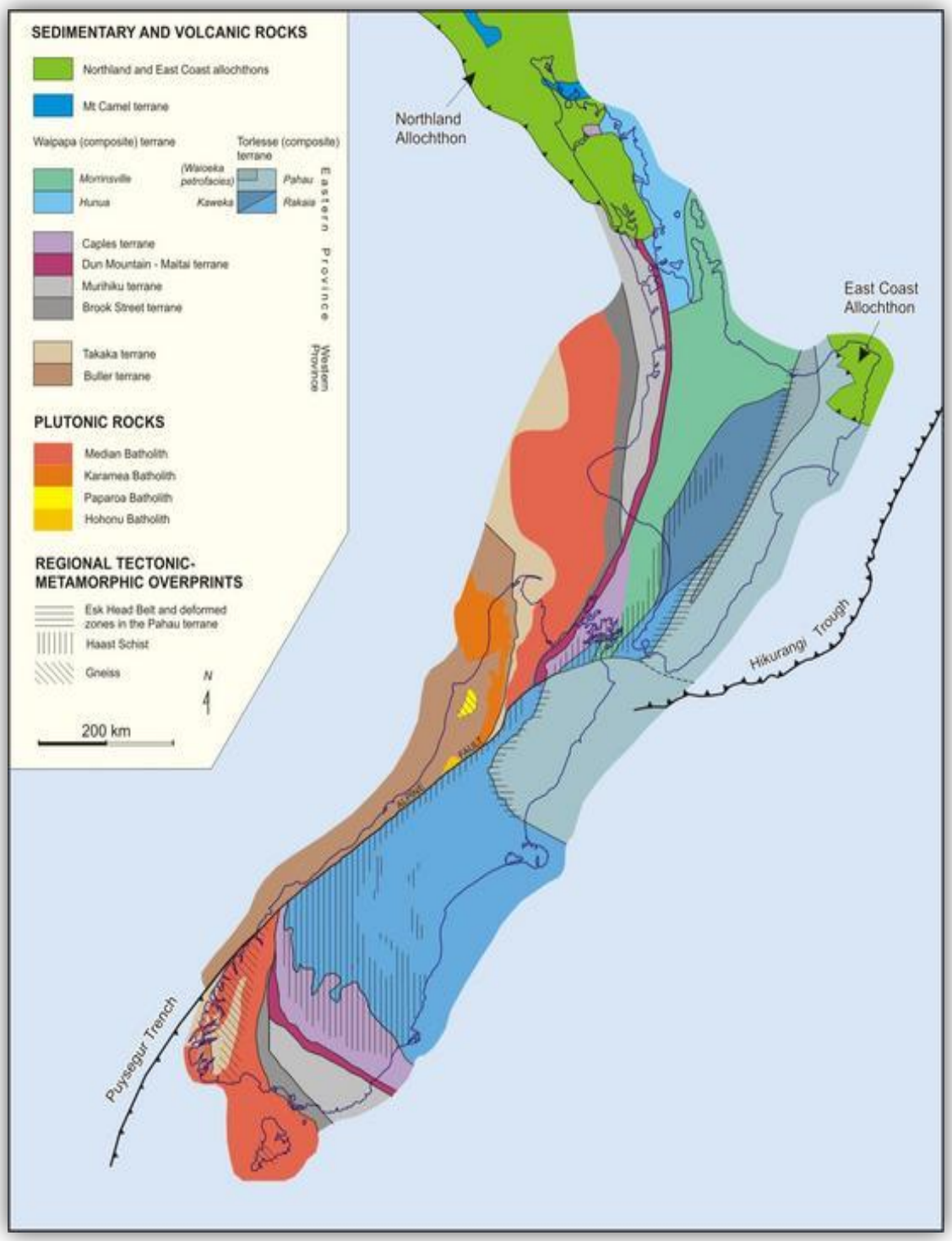

Figure 5: Basement rock and terranes of New Zealand (Source: http://www.gns.cri.nz/Home/Our-Science/Energy-Resources/Geological-Mapping/Geological-Origins-Research/Geological-Basement/Basement-terranes-of-New-Zealand

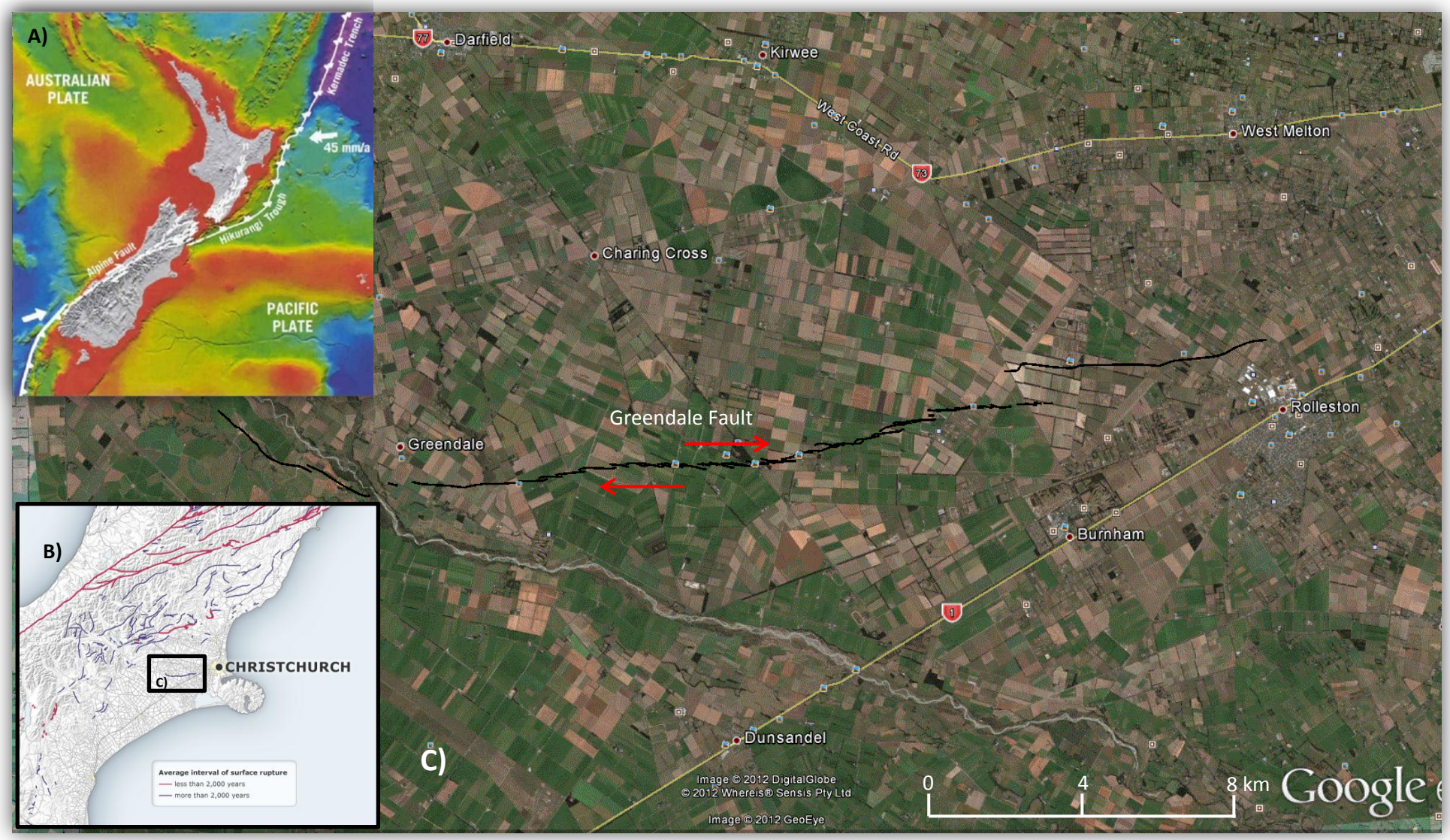

Figure 6: A)The tectonic setting in New Zealand (source: http://www.orc.govt.nz/Information-and-Services/Natural-Hazards/Great-Alpine-Fault-Earthquake/); B) The area and surface rupture length and extent with respect to the surrounding Canterbury landscape (http://www.teara.govt.nz/en/active-faults/1/1); C) Close up of the Greendale Fault (Source: Google earth, fault trace courtesy of N. Litchfield and D. Barrell).

II. Literature Review

To understand how the Greendale Fault behaved, this study and literature review focuses on:

1. Crustal Deformation
2. Elastic Rebound Theory
3. Earthquake Cycle
4. Surface Deformation
5. Relevant Historical Earthquakes
6. Recent Research into the Darfield Earthquake/Greendale Fault
7. A comparison of the Darfield Earthquake/Greendale Fault to relevant historical earthquakes
8. Research Ideas from the Literature
9. Summary

1. Crustal deformation

What is it and how does it occur?

Rock deformation is defined as a change in size, shape, orientation, or position of a rock mass in response to strain or a given stress, such as tectonic forces (MacDonald *et al.*, 2003). Crustal deformation occurs as a result of a number of different processes, including tectonic earthquakes, post-seismic slip events, mantle relaxation, fault morphology, tectonic tremors, volcanic earthquakes, low-frequency earthquakes, slow earthquakes, slow slip events, and induced earthquakes (McCaffrey & Gupta, 2011). Of particular note and relevance to this study are tectonic earthquakes, post-seismic slip events, and mantle relaxation.

Tectonic earthquakes

These occur in response to tectonic plate movement or other predominantly shearing sources, and they result primarily from the stick-slip behaviour of faults (McCaffrey & Gupta, 2011). As stress builds up across a fault surface frictional forces along the fault plane prevent the fault surface from slipping. However, once the stress surpasses the maximum shear strength of the fault, i.e. the point at which the frictional forces preventing slip or movement on the fault are exceeded, and then the two sides of the fault slip or rupture (see elastic rebound theory discussed below). This allows some or all of the elastic strain that has been built up over time to be released. The starting point of the (i.e. hypocentre) of the rupture propagates at 2-3 kilometres per second, (e.g. Holden at al., 2011)

and the rupture causes different types of seismic waves to be released. These earthquakes are by far the most common and the most destructive (McCaffrey & Gupta, 2011).

Post-seismic slip events

Post-seismic/post-mainshock slip or "afterslip" is another type of crustal motion that arises from continued slip along the fault at slow speeds following the mainshock during large tectonic earthquakes (McCaffrey & Gupta, 2011). During the mainshock, the stress along the slipping fault decreases and is shed to lower sections of the fault. If the fault responds to enforced stress by creeping in the lower crust, transient buried slip can occur (Segall, 2010). Aftershocks can account for a small part but the majority of slip occurs post-seismically and can last years, in some cases producing as much slip as the total slip produced during the main earthquake itself (McCaffrey & Gupta, 2011).

Mantle relaxation

Mantle relaxation occurs when the stress is redistributed in the crust and mantle following large earthquakes (McCaffrey & Gupta, 2011). This stress can cause the mantle to flow in a viscous manner, producing a long-period deformation of the crust above (McCaffrey & Gupta, 2011).

2. Elastic Rebound Theory

The elastic rebound theory is a simplified form of the earthquake cycle. Harry Reid (1910) was first to propose the theory of elastic rebound relating to the earthquake cycle following earthquake observations made in Sumatra and California. The theory postulates that the crustal blocks adjacent to a fault are locked or held together by frictional forces on the fault surface and their relative movement results in a build-up of strain in the blocks (see Figure 7a, b, and c) (McCaffrey & Gupta, 2011; Stein & Wysession, 2003; Reid, 1910).

The upper crust is thought to be comprised of linear elastic material, meaning the plastic strain increases over time as long as the blocks move at a constant speed (McCaffrey & Gupta, 2011). However, at some time (typically 10^2 to 10^3 years) when stress over the fault reaches a maximum limit, the fault responds suddenly by slipping/rupturing (see Figure 7c) resulting in an earthquake (McCaffrey & Gupta, 2011; Stein & Wysession, 2003). Subsequently, the fault rupture alleviates the accumulated strain in a matter of seconds. The term 'rebound' infers the notion that any feature on the surface (e.g. fence line, treeline, power poles or road) crossing the fault, will return to its original shape (i.e., free of strain) after the earthquake (McCaffrey & Gupta, 2011; Stein & Wysession, 2003). In reality this is not the case as the earthquake produces permanent strain on a regional scale by

displacing the crustal blocks along the fault (see the road and fence in Figure A) (McCaffrey & Gupta, 2011; Stein & Wysession, 2003).

The simplistic picture of the elastic rebound theory enables visualisation and insight into the rupture of earthquakes by reflecting the most dramatic part of a process that is the earthquake/seismic cycle. This takes place on segments of the plate boundary over hundreds to thousands of years (McCaffrey & Gupta, 2011; Stein & Wysession, 2003). But in reality it is a much more complex process that includes time-dependant deformation over many time-scales (McCaffrey & Gupta, 2011; Stein & Wysession, 2003).

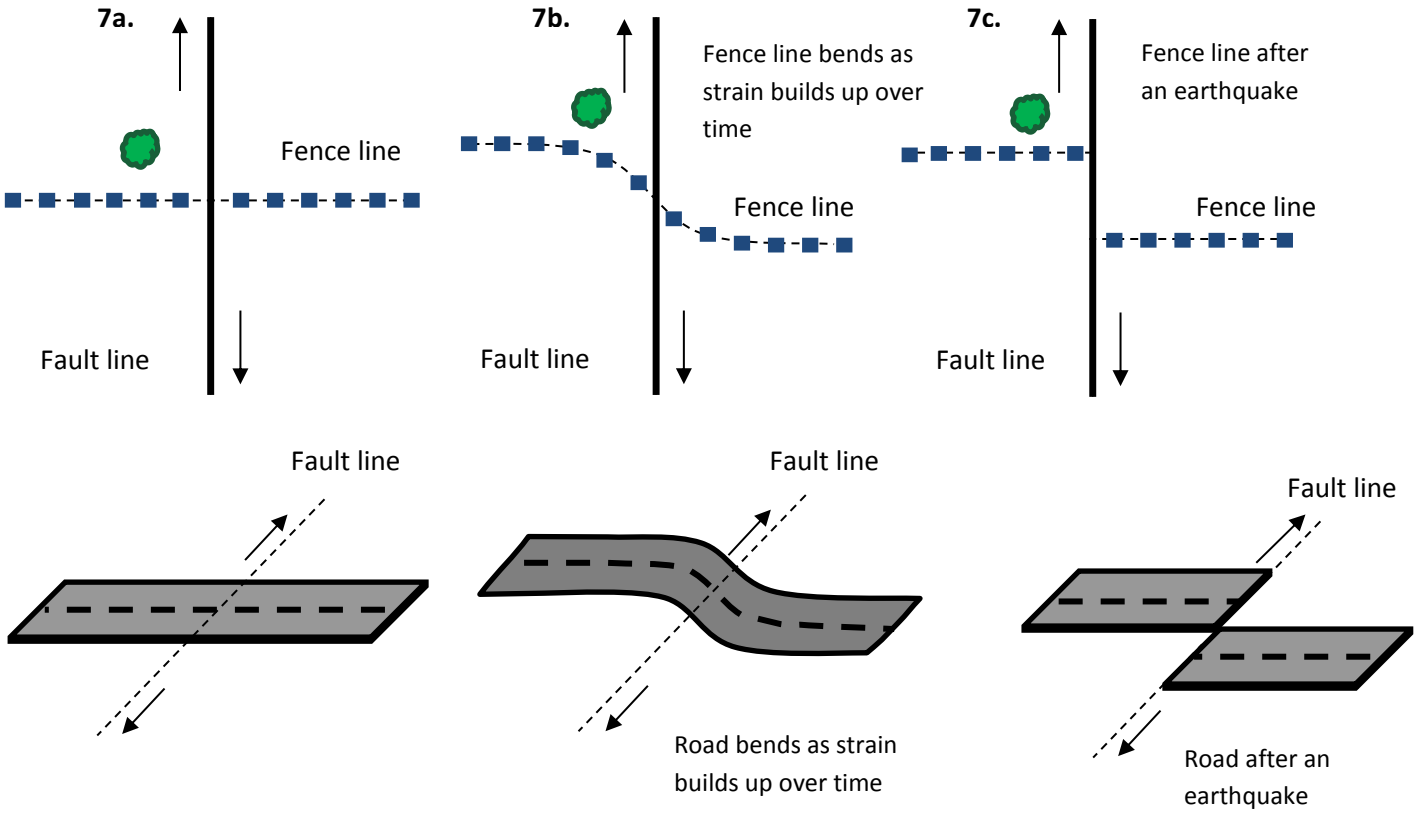

Figure 7: a, b, and c: The elastic rebound theory (Figure modified from models by Stein & Wysession, 2003; Burbank & Anderson, 2009; McCaffrey & Gupta, 2011).

3. Earthquake Cycle

For many years geologists have attempted to understand the deformation that precedes, accompanies, and follows earthquakes (Burbank & Anderson, 2009). The time and deformation that encompasses an earthquake and the entirety of the period between successive earthquakes is termed the earthquake cycle (Burbank & Anderson, 2009). The earthquake cycle consists of three stages:

- Inter-seismic stage,
- Co-seismic stage, and the
- Post-seismic stage.

Detail of each stage is as follows:

3.1 Inter-seismic stage

The stage between seismic events, termed inter-seismic, makes up most of the earthquake cycle. This stage reflects constant motion a long a fault that separates two nearby pieces of the earth's crust (Burbank *et al.*, 2009; Stein & Wysession, 2003). At some depth below the earth's surface, the fault is able to slip continuously and aseismically in a zone of ductile deformation, but in the brittle crust during the inter-seismic interval, the fault itself is locked such that no slip occurs along it, resulting in the building of elastic strain in the crustal mass surrounding the fault (although some faults such as San Andreas can release this strain through aseismic creep) (Burbank *et al.*, 2009; Stein & Wysession, 2003). Once the stress acting on a fault plane exceeds the frictional forces locking the fault together, rupture occurs.

3.2 Co-seismic Stage

Immediately prior to rupture, known as the pre-seismic stage, small earthquakes (foreshocks) or other precursory events may occur triggering the main rupture (Stein & Wysession, 2003). The co-seismic stage begins with the earthquake/fault rupture. This occurs as rapid slip along the fault generating seismic waves (Stein & Wysession, 2003). During these few seconds of rupture, the fault attempts to accommodate the elastic strain that had accumulated in the surrounding rockmass over hundreds or thousands of years (Stein & Wysession, 2003). Subsequently, this can generate many metres of slip at depth or along the surface, and can continue to slip following the main earthquake.

3.3 Post-seismic Stage

Following the main earthquake, aftershocks and transient post-seismic deformation can occur for a months to years before the fault system settles into its inter-seismic behaviour again (Stein & Wysession, 2003). For large shallow earthquakes, most aftershocks occur soon after the mainshock, and the remainder decay with time. The decay is inversely proportional to time, (1/t), described by a relationship known as Omori's Law (Omori, 1894; McCaffrey & Gupta 2011; Stein & Wysession, 2003). Post-seismic slip/deformation can also decay with time following Omori's Law. The temporal decay of aftershocks can be described using the modified Omori law (Omori, 1894; Utsu *et al.*, 1995; Wiemer, 2006), which can be expressed through the following equation: $R(t) = \frac{k}{(t+c)^p}$, where R (t)

is the rate of occurrence of aftershocks, and k, c, and p are constants (Kisslinger and Jones, 1991; Wiemer, 2006). Of these three parameters, p is the most important. Between different aftershock sequences, the value of p is in the range 0.8-1.2 in most cases (Utsu *et al.*, 1995). This decay represents the continued movement and adjustment of the surrounding region as the crust and mantle re-adjusts to the enormous stresses associated with the co-seismic stage of the earthquake ((McCaffrey & Gupta 2011; Pollitz *et al.*, 2006; Stein & Wysession, 2003).

Aftershocks and post-seismic deformation are the most common manifestations of stress relaxation following large earthquakes (Perfettini and Avouac, 2007). Since post-seismic deformation was first identified following the 1906 San Francisco earthquake (e.g. Thatcher, 1972 and 1983), research surrounding this stage of the earthquake cycle has revealed that this deformation occurs via multiple mechanisms (see Figure 8). These include:

- Creep or afterslip on or adjacent to the main fault rupture,
- Viscoelastic relaxation in the lower crust and upper mantle, and
- Poroelastic rebound through the flow of pore-fluids.

3.3.1 Afterslip

Afterslip can occur on or adjacent to the main fault rupture zone or below the rupture on the down-dip extension of the fault (McCaffrey and Gupta, 2011; Segall, 2010; Jonsson *et al.*, 2003). It reflects continued low magnitude slow slip or short term slip along the ruptured fault plane in response to the co-seismic earthquake stress (McCaffrey and Gupta, 2011; Segall, 2010; Ergintav *et al.*, 2009; Barbot *et al.*, 2009; Perfettini and Avouac, 2007; Freed *et al.*, 2006; Johnson *et al.*, 2006; Hsu *et al.*, 2006; Perfettini and Avouac, 2004; Ergintav *et al.*, 2002). The distribution of the afterslip characterises time-dependant stressing following earthquakes and directly reflects the material properties of the fault zone (Ergintav *et al.*, 2002).

The first documented event of post-seismic slip, or afterslip, was in California following the 1966 Parkfield earthquake (e.g. Smith and Wyss, 1968) (Marone *et al.*, 1991). Since then it has been measured following several large earthquakes worldwide, including the 1989 M_w 6.9 Loma Prieta earthquake (e.g. Burgmann *et al.*, 1997; Pollitz *et al.*, 1998), the 1999 M_w 7.3 Izmit earthquake, Turkey (e.g. Hearn *et al.*, 2002) and the 2004 M_w 6.0 Parkfield earthquake (Fialko and Barbot, 2010; Pertiffini and Avouac, 2004; Burgmann *et al.*, 2002; Marone *et al.*, 1991).

Recent research by Fialko and Barbot (2010), has shown that afterslip can be the dominant mechanism responsible for post-seismic deformation (e.g. Freed 2007; Barbot *et al.* 2009), or it may occur in combination with other mechanisms (e.g. Fialko 2004; Freed *et al.* 2006; Johnson *et al.*, 2009).

3.3.2 Viscoelastic relaxation

Viscoelastic relaxation is deep seated time dependant relaxation/adjustment of the lower crust or viscous upper mantle (lithosphere-asthenosphere boundary) in response to the stress induced by the mainshock (Grijalva *et al.*, 2007; Jonsson *et al.*, 2003; Pollitz *et al.*, 2006; Pollitz *et al.*, 2001; Pollitz *et al.*, 2000; Freed and Burgmann, 2004; Barbot *et al.*, 2008). Examples for this mechanism of post-seismic deformation include the 1992 M_w 7.3 Landers earthquake and 1999 M_w 7.1 Hector Mine earthquake (Freed and Burgmann, 2004).

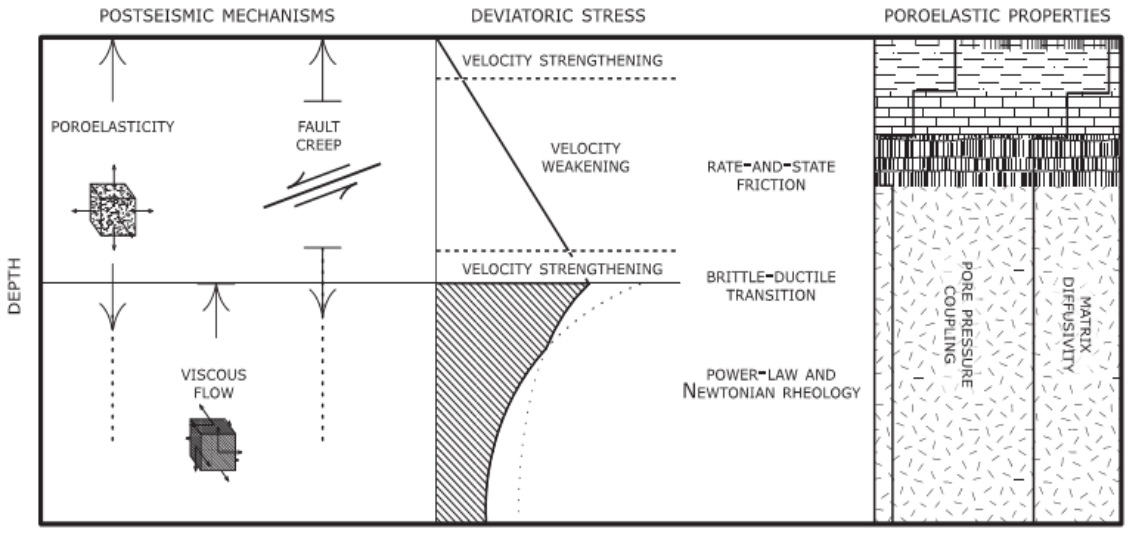

Figure 8: The mechanisms responsible for post-seismic deformation within the lithosphere and asthenosphere. Post-seismic deformation may be attributed to a combination of these transients. (Source: Fialko and Barbot, 2010).

3.3.3 Poroelastic Rebound

The Earth's crust is a heterogeneous material composed of solid and fluid phases, such as porous rocks and pore fluids (Fialko and Barbot, 2010). During a large earthquake or earthquakes the pore pressure is altered in the brittle upper crust by the imposed co-seismic stress, causing pore pressure to increase in areas of compression and decrease in areas of dilation (e.g. Bjornsson *et al.*, 2001; Nur & Booker, 1972) (Fialko and Barbot, 2010; Grijalva *et al.*, 2007; Jonsson *et al.*, 2003; Peltzer *et al.*, 1998). These pore-pressure gradients change groundwater flow and additional time-dependent strain (e.g. Roeloffs, 1996) (Jonsson *et al.*, 2003). This results in poroelastic rebound through

subsidence within (co-seismic) compressional quadrants and uplift in (co-seismic) extensional quadrants. The 1992 Landers earthquake in California (e.g. Peltzer *et al.*, 1998) is an example of post-seismic deformation as a result of poroelastic rebound.

4. Surface Deformation

Understanding the spatial and temporal distribution of slip accompanying and following large earthquakes will improve our understanding of the processes involved during the earthquake and the resulting ground shaking and surface deformation that pose a hazard to people and infrastructure. This section looks at what surface deformation is, how it occurs, what stops the continuation of surface ruptures, how it is measured, and reviews relevant historical studies.

What is surface deformation, how does it occur?

Beneath the surface, as the temperature increases with depth, rocks behave in a ductile manner. This means they will not break but instead undergo extensive plastic deformation (Segall, 2010; MacDonald *et al.*, 2003). Earthquakes, among other forces invoke stress changes within the subsurface. Ductile flow in response to these stress changes can lead to transient deformations at the Earth's surface (Segall, 2010). It is also recognised that rock is porous and liquid is saturated. Thus flow or pore fluids induced by co-seismic stress changes may also cause transient deformations that could be observed at the earth's surface (Segall, 2010). However, Reyners (2011) does not believe that there is a brittle-ductile transition zone beneath the Canterbury Region.

What causes a fault step over and how do faults stop from continuing rupture?

The question of what stops propagating fault rupture remains a problem, with researchers proposing a number of theories. Some investigations or researches have proposed that strong fault sections (barriers and asperities) stop propagation, (e.g. Aki, 1979), whilst others propose that it is weak sections of faults that stop earthquakes, (e.g. Husseini *et al.*, 1975; Harris *et al.*, 2002). Another group of researchers have proposed that it is the nucleation process itself that predetermines the eventual size of an earthquake, (e.g. Ellsworth and Beroza, 1995; Harris *et al.*, 2002). A third group have suggested that fault geometry helps to determine the overall rupture process (Wallace, 1970; Segall and Pollard, 1980; Sibson, 1985 and 1986; Harris *et al.*, 1991; Harris *et al.*, 2002).

The active fault traces on which earthquakes occur are generally not continuous (Wesnousky, 2006; Lettis *et al.*, 2002). Commonly, faults are composed of segments that are separated by discontinuities that appear as steps when mapped on the surface (Wesnousky, 2006). Stress concentrations resulting from slip at these discontinuities between segments may slow or terminate

rupture propagation and hence play an influential and somewhat controlling role in limiting the length of earthquake rupture (Wesnousky, 2006).

Following physical insight in to the dynamics of the earthquake rupture process through a study by Wesnousky (2006), it was observed that the limiting dimension of the step appears to be largely independent of the earthquake rupture length. It therefore follows that the magnitude of stress changes and the volume affected by the stress changes at the driving edge of laterally propagating ruptures are largely similar and invariable during the rupture process. This is regardless of the distance an event has propagated or will propagate (Wesnousky, 2006).

Wesnousky (2006) examined the mapped surface rupture traces of 22 historical strike-slip earthquakes with rupture lengths ranging from 10 to 120 km. The results from this study showed that approximately two thirds of the endpoints of strike slip earthquake ruptures are associated with fault steps or the termini of active fault traces (Wesnousky, 2006). It also showed that there exists a limiting dimension of fault step (3 – 4 km) exists above which earthquake ruptures do not propagate and below which rupture propagation ceases only about 40% of the time (see Figure 9) (Wesnousky, 2006). This is important finding for seismic hazard analysts and civil defence agencies as it places defining limits on the likely rupture length of future earthquakes on mapped active faults.

Other research has shown that historical strike-slip earthquakes with small to large displacements usually propagate through step-overs less than 1 – 2 km wide (e.g. Lettis *et al.*, 2002). However, with increasing displacement larger and larger step-overs can be ruptured through. Lettis *et al.* (2002) found that empirical data generally show a ratio ranging from 2:1 or 1:1 between step-over width (km) and strike-slip displacement (m) for a through-going rupture. However, from historical ruptures (see Appendix Table 1) step-overs as large as 4 – 5 km width arrest rupture propagation regardless of the amount of displacement. Thus, these results provide important constraints when evaluating the probability of multi-segmented ruptures on segmented strike-slip faults.

Measurement of the displacement of the Earth's surface during and after an earthquake (co-seismic and post-seismic respectively) either seismically or geodetically, enables an estimation of the distribution of fault slip along the rupture (Stein & Wysession, 2009; Reilinger *et al.*, 2000). Mapping the spatial distribution of this fault slip provides further insight into the mechanics of the earthquake process and the mechanical behaviour of the upper layers of Earth (Reilinger *et al.*, 2000). Understanding the distribution of co-seismic and post-seismic fault slip through displacement and strain diagrams also has implications for evaluating the potential for neighbouring faults to generate future earthquakes (Reilinger *et al.*, 2000).

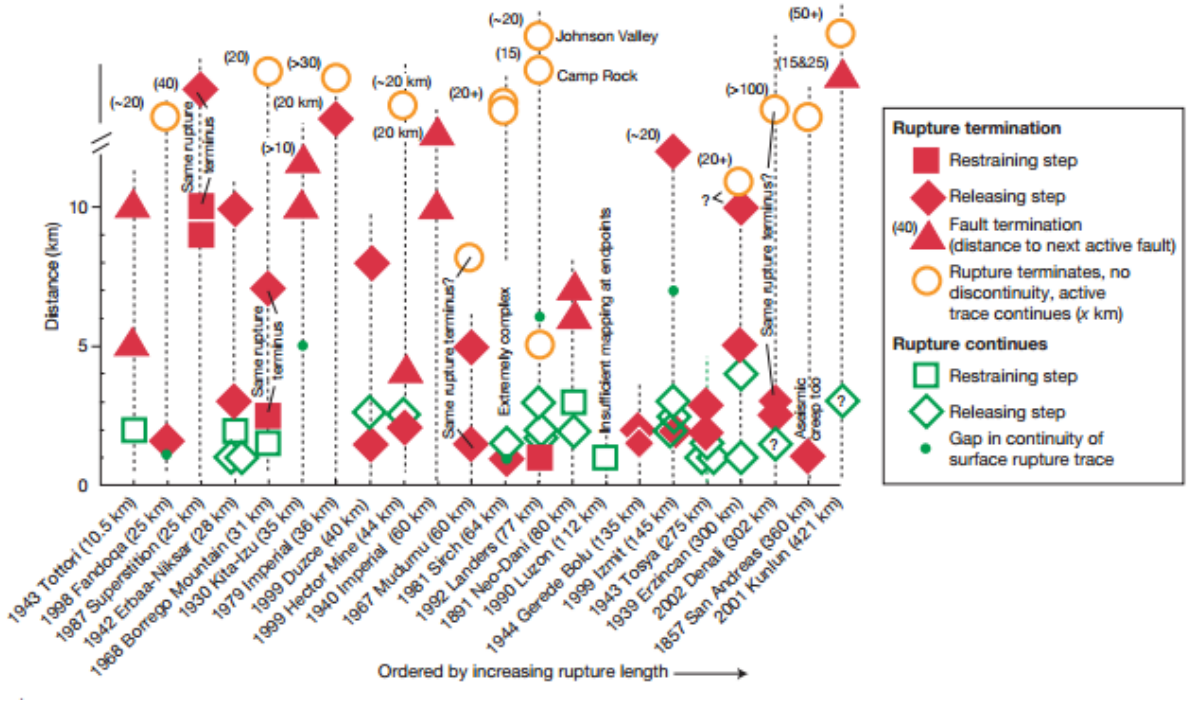

Figure 9: The relationship of geometrical discontinuities to strike slip endpoints from historical earthquakes (Source: Wesnousky, 2006).

Measuring surface deformation

Using techniques from geodesy - the science of the earth's shape, information about the processes before, during and after earthquakes, and consequently associated with fault locking and post-seismic slip can be obtained by measuring the slow ground deformation that occurs, (McCaffrey & Gupta, 2011; Stein & Wysession, 2009). Most of these techniques rely on detecting the motion of geodetic benchmarks or monuments, which are anthropogenic markers placed in the ground (Stein & Wysession, 2009).

Historically, measurements of the markers motion were made by triangulation or trilateration for horizontal motion. For vertical motion a precise level was used to sight on a distant measuring rod (Stein & Wysession, 2009). However, the advent of geodetic surveying from space enabled all three

components of position to be measured accurately (Stein & Wysession, 2009). Over the past decade further technological advancements in space borne surveying, in particular interferometric Synthetic Aperture Radar (InSAR) and construction of dense Global Positioning System (GPS) networks has enabled the production of high-resolution maps of earthquake induced surface deformation at centimetre-scale accuracy (Simons *et al.*, 2002; Fialko *et al.*, 2005).

Due to these technological advances in GPS and InSAR measurement accuracy and resolution, it is likely that new studies will rewrite what was previously understood about pre-seismic, co-seismic and post-seismic deformation (McCaffrey & Gupta, 2011; Segall, 2010; Reilinger *et al.*, 2000).

Historical geodetic surveys

The most iconic geodetic survey completed was by Lee *et al.* (2011) following the 1999 M_w 7.6 Chi-Chi earthquake in Taiwan. Lee *et al.* (2011) used the digital cadastral system, to calculate the co-seismic displacement around a pop-up structure in the Shihkang area of central Taiwan. This system was originally conceived to survey land and building boundaries.

This earthquake was the largest to strike Taiwan in the twentieth century, producing a surface rupture that extends more than 100 km in a north-south trend (Lee *et al.*, 2011). Interestingly, the northern end of this surface deformation terminates abruptly at a broad pop-up structure with east-to-northeast strike differing greatly from the main thrust feature striking north-south (Lee *et al.*, 2011). The pop-up structure consists of several regions of parallel thrusts and back thrusts resulting in a total shortening of about 9 m. To reveal the displacement field in the pop-up structure and slip vectors of branch faults, Lee *et al.* (2011) completed a cadastral survey using about 17,000 control points to calculate the co-seismic displacement around the Shihkang area. The digital cadastral system allows high density geodetic control points that reach about 2800 points per square kilometre with accuracy to within centimetres (Lee *et al.*, 2011). There have not been many surveys of this scale, which took approx. 8 – 10 years to complete.

In terms of space borne InSAR studies, the best documented historical earthquakes are the Landers, Izmit, Hector Mine earthquakes and the Darfield earthquake (e.g. Beavan et al., 2010 and 2012; Elliot et al., 2012).

5. Relevant Historical Earthquakes

A number of studies, such as Wesnousky (2008) and Lettis *et al.* (2002) have compared attributes such as, magnitude, surface displacement, rupture length, step-over sizes, depth, co-seismic slip and post-seismic slip rates from historical earthquakes. These studies were undertaken to examine questions surrounding these attributes. The most suitable earthquakes for comparison with the Darfield earthquake include Californian earthquakes M_w 7.3 Landers, M_w 7.1 Hector Mine, the M_w 7.6 Izmit earthquake in Turkey, M_w 7.9 Wenchuan in China, and the Bam earthquake in Iran. Details of each of the earthquakes and key findings are noted below.

M_w 7.3 Landers earthquake, California

The M_w 7.3 Landers earthquake occurred on the 28th June, 1992 in California. It ruptured five major faults, producing a total rupture length of approx. 80 ± 5 km (Peltzer *et al.*, 1998; Savage *et al.*, 1997; Freymueller *et al.*, 1994) with an average of approx. 3 m and a maximum of 6.2 m of right-lateral surface displacement (Freymueller *et al*, 1994; Peltzer *et al.*, 1998). The earthquake occurred in the southern part of the Eastern California Shear Zone (Freymueller *et al.*, 1994).

Key Findings

Slip models produced for the Landers rupture by Freymueller *et al.* (1994), Hudnut, *et al.* (1994), and Hudnut & Larson (1993), indicate there are two distinct zones of slip maxima. These occur where the surface fault traces step-over from the Johnson Valley to the Homestead Valley fault and from the Homestead Valley to the Emerson fault. Where the surface displacements are highest, the geodetic modelling indicates relatively low slip (averaged over 10 km in depth), which implies that locally the high surface slip overlies considerably lower slip at depth along that segment or strain localisation (See Figure 11) (Hudnut and Larson, 1993; Freymueller *et al.*, 1994).

The Freymueller *et al.* (1994) geodetic slip model identified two distinct patches of high slip, and correspondingly high moment release. The first patch, termed the southern zone, is located along the northern Johnson Valley fault. At this location, subsurface co-seismic slip of approx. 8 m occurred at a depth of 8 – 12 ± 2 km with 3 to 4 m of surface slip (Freymueller *et al.*, 1994). Further north, from the Johnson Valley Fault the slip decreases until the northern half of the Homestead Valley Fault. At this point, the second patch of slip starts on the Homestead, Emerson and Camp Rock faults. With overall maximum subsurface slip of 16 m occurring on the southern Emerson Fault at a depth of 2 to 6 km. Between these two zones of slip maxima a slip gap bounds them by a relative slip minima (Freymueller *et al.*, 1994; Hudnut *et al.*, 1994). Geological evidence identified the slip gap as a short, less than 3 km section of the Homestead Valley fault along which right-lateral

slip diminished to zero, but vertical displacement reached 1 m (with the west side up-thrown) (Freymueller *et al.*, 1994; Hudnut *et al.*, 1994; Sieh *et al.*, 1993).

In the months and years following the earthquake a number of studies (e.g. Peltzer *et al.,* 1998; Savage and Svarc, 1997) were completed monitoring the post-seismic surface displacement by repeated surveys. In particular, surveys of GPS networks, trilateration arrays, and creep meters. Fault slip models produced by Peltzer *et al.* (1998) using the GPS data from the first year indicate that post-seismic displacement of less than 0.10 m occurred along the northern and central sections of the fault and up to 0.18 m along the southern Johnson Valley and Eureka Peak Faults (Peltzer *et al.*, 1998). Furthermore, Savage & Svarc (1997) found over 3.4 years of surveying that the average post-seismic slip beneath the Landers rupture zone is approx. 0.6 m along the Emerson Fault at depth interval of 10 – 30 km. By comparison the average subsurface co-seismic slip was 4-4.7m at a depth of 0 – 10 km. This indicates that by 1995 the total amount of post-seismic slip was approx. 15% of the co-seismic displacement (Savage & Svarc 1997).

M_w 7.1 Hector Mine earthquake, California

The Mw 7.1 Hector Mine earthquake occurred on the 16th October 1999 in the Mojave Desert, California. It resulted in a 80 km wide zone of deformation with approx. 45 km of dextral surface rupture and a recorded peak ground acceleration (PGA) of 0.01 – 0.6 *g* (Treiman *et al.*, 2002). Like the Landers earthquake, the Hector Mine earthquake ruptured multiple faults – the northwest trending Bullion and Lavic Lake faults, which are part of the eastern Californian shear zone (Simons *et al.*, 2002). The overall rupture was complex comprising multiple strands; a northern, central and southern strand. The central segment is the simplest with a single segment crossing the Bullion Mountains (striking N10^{o}W), whereas the southern third of the rupture zone is made up of three sub-parallel segments extending about 20km in length in an N45^{o}W direction (Simons *et al.*, 2002). The northern third of the rupture zone is characterised by multiple slays, directions sub-parallel to strike in the southern and central strands.

Key Findings

Slip models produced for the rupture using geodetic InSAR and GPS data are consistent in suggesting that maximum subsurface co-seismic slip was greater than 5 m at a depth of 3 – 6 km, with the northern part of the fault accommodating the maximum slip (see Figure 12) (Simons *et al.*, 2002; Rymer *et al.*, 2002).

A study by Jacobs *et al.* (2002) using InSAR data from over the Hector Mine rupture area revealed a few centimetres of sub-surface post-seismic deformation along the uppermost several kilometres of the fault. This occurred especially on the north-northwest trending splay that did not rupture the surface during the earthquake. From an afterslip model they also suggest much of the afterslip occurs at depths of less than 3 to 4 km. The main deformation areas are a region of subsidence on the northern end of the rupture, an area of uplift located northeast of the primary fault bend, and a linear trough extending along the main rupture.

M_w 7.6 Izmit earthquake, Turkey

The Izmit earthquake approx. M_w 7.6 occurred on the 17 August 1999 in Turkey producing maximum PGA of approx. 0.4 *g* (Barka *et al.*, 2002; Langridge *et al.*, 2002; Lettis *et al.*, 2002; Erdik and Durukal, 2000). The earthquake caused extensive surface rupture, extending to a total distance of 126 km and involving four segments of the North Anatolian Fault (NAF). These are the Gölcük, Sapanca, Sakarya, and Karadere fault segments (Karakaisis, 2003; Barka, *et al.*, 2002; Lettis *et al.*, 2002). Each was separated by releasing step-overs of 1-4 km in width (Barka *et al.*, 2002). Surface rupture consisted primarily of right-lateral strike-slip surface displacement of up to 5.5 m, averaging 3 – 4 m (Barka *et al.*, 2002; Langridge *et al.*, 2002; Lettis *et al.*, 2002).

Key Findings

The Izmit rupture, which is almost purely right-lateral strike-slip faulting, is dominated by the bilateral breaking of a central asperity located about 10 km west of the city Gölcük, and eastern margin of Sapanka Lake, with subsurface slip reaching 6 - 8 m in the depth range of 6 to 12 km (see Figure 10a & b) (Barka *et al.*, 2002; Langridge *et al.*, 2002; Lettis *et al.*, 2002).

GPS data used to form the post-seismic deformation model for the Izmit earthquake, indicating rapid deformation occurring during the first two months following the mainshock, are not consistent with deformation rates expected from viscous relaxation of a broadly deforming lower crust (Reilinger *et al.*, 2000). Observed post-seismic displacements were modelled by transient strike-slip faulting after the Izmit earthquake using the same procedure used to model co-seismic displacements. The model fault geometry is identical to that for the co-seismic model, but it extends to a depth of 40 km. Also included was an additional segment along the trace of the 12 November 1999 Düzce rupture (Reilinger *et al.*, 2000). The Izmit rupture plane indicates maximum afterslip (post-seismic deformation) occurred below the co-seismic rupture reaching a total of 43 cm during the first 75 days after the main shock (see Figure 10b) (Reilinger *et al.*, 2000).

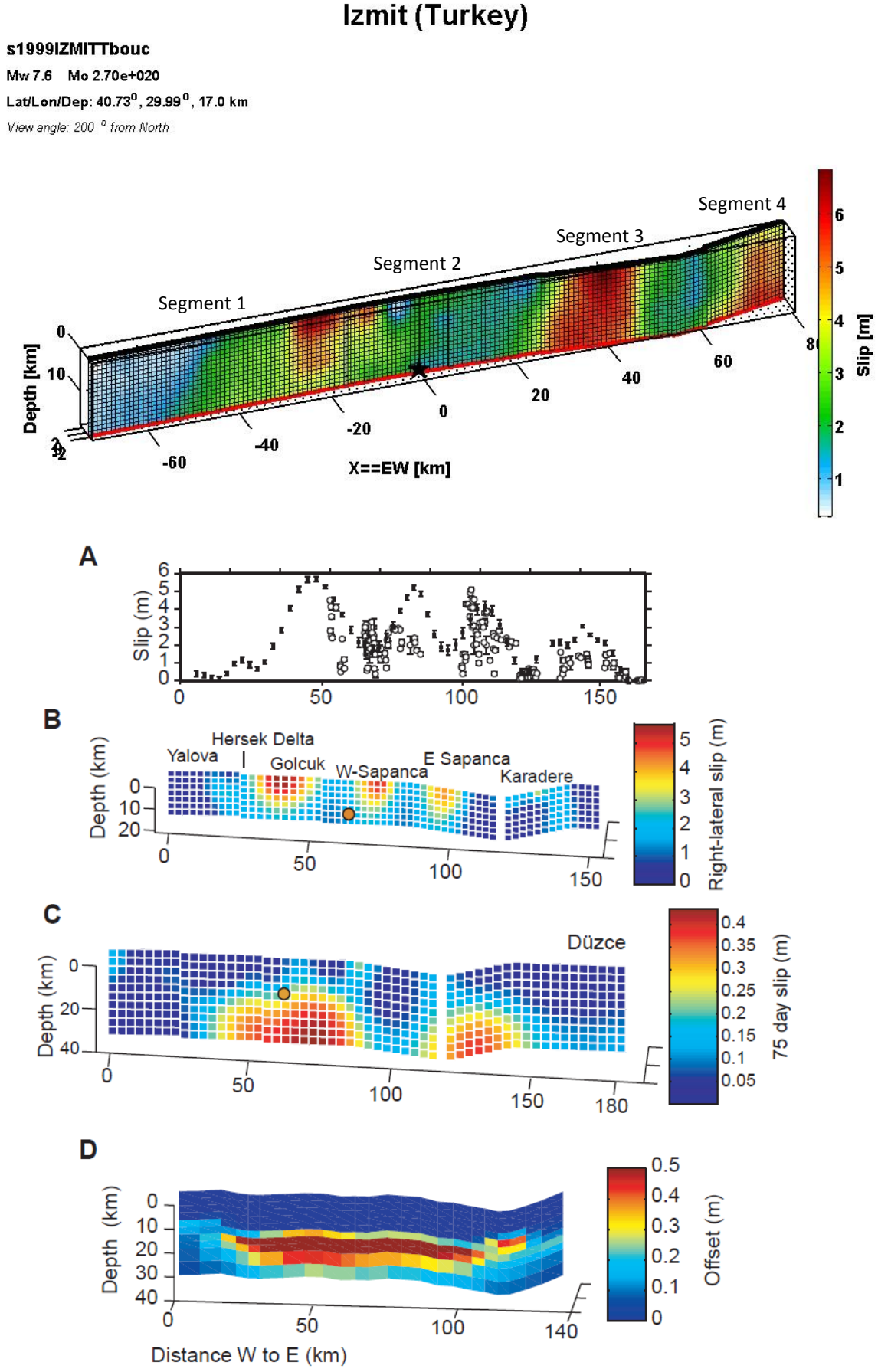

Figure 10 a &b: a) Co-seismic slip model for the Izmit Earthquake (Top) b) shows co-seismic and post-seismic slip models for the Izmit, Turkey earthquake (bottom) (Sources: Bouchon *et al.*, 2002; Reilinger *et al.*, 2000).

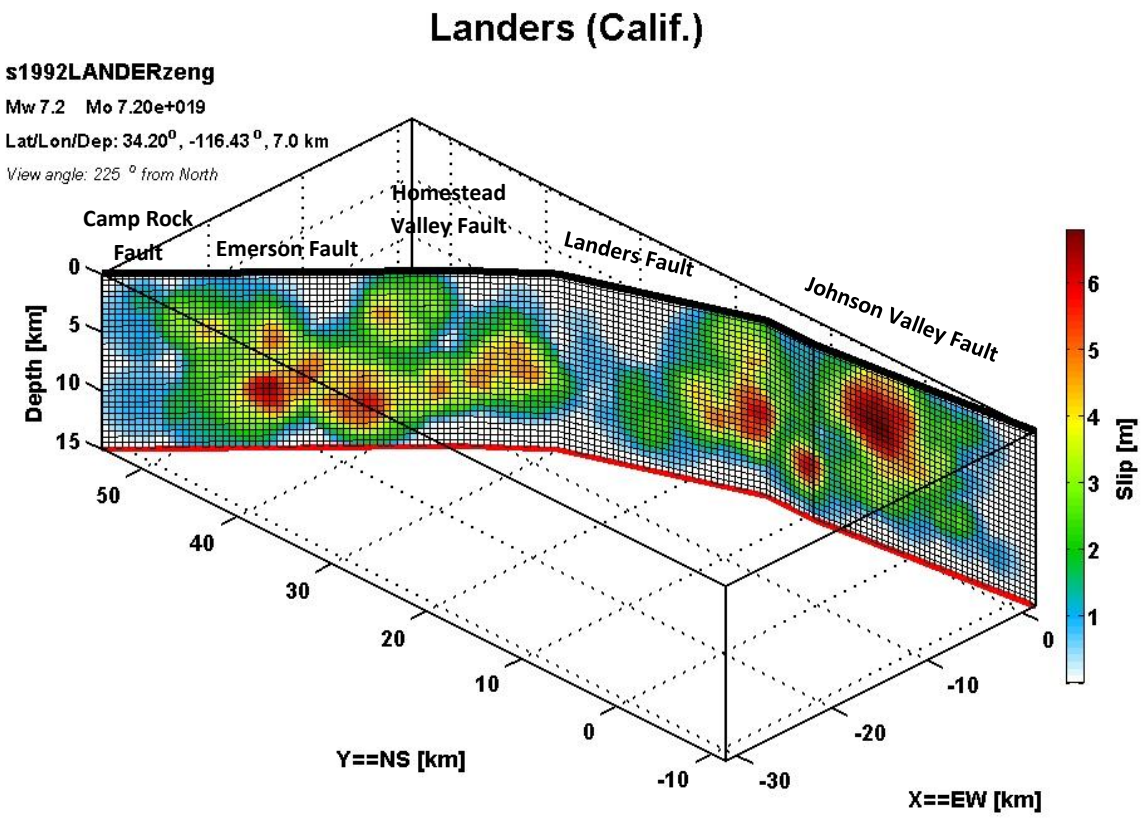

Figure 11: The co-seismic source model for the Landers 1992 earthquake, California (source: www.seismo.ethz.ch/static/srcmod/Eventpages/s1992LANDERzeng.html)

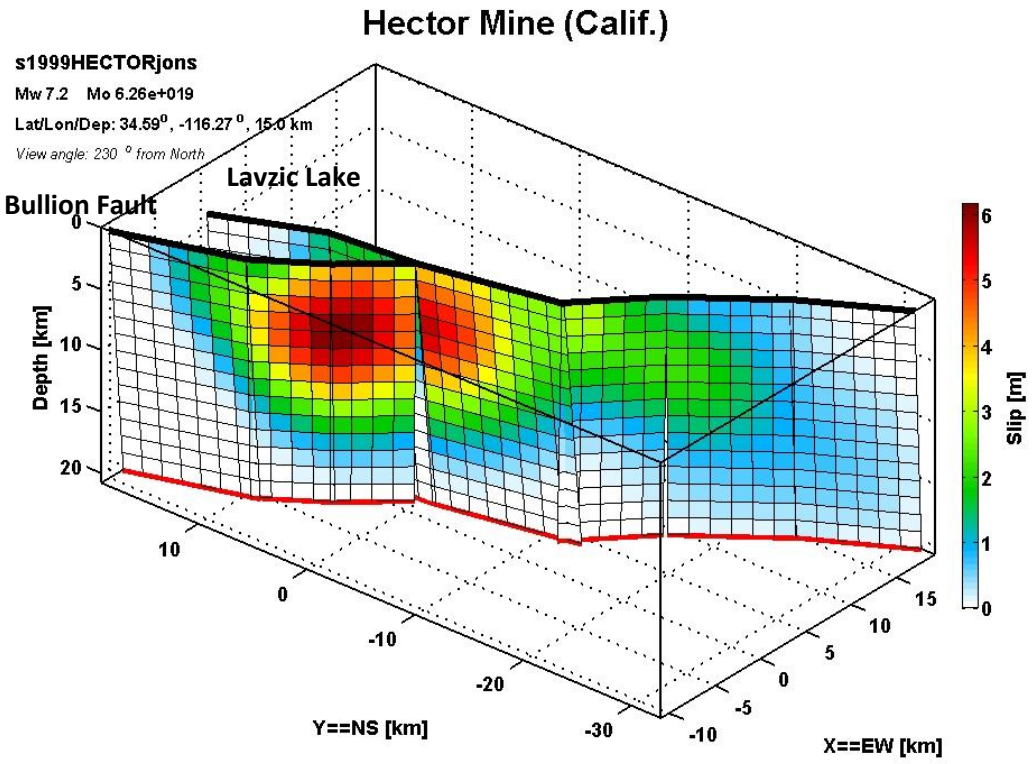

Figure 12: Source model for the Hector Mine earthquake (source: www.seismo.ethz.ch/static/srcmod/Eventpages/s1999HECTORjons.html)

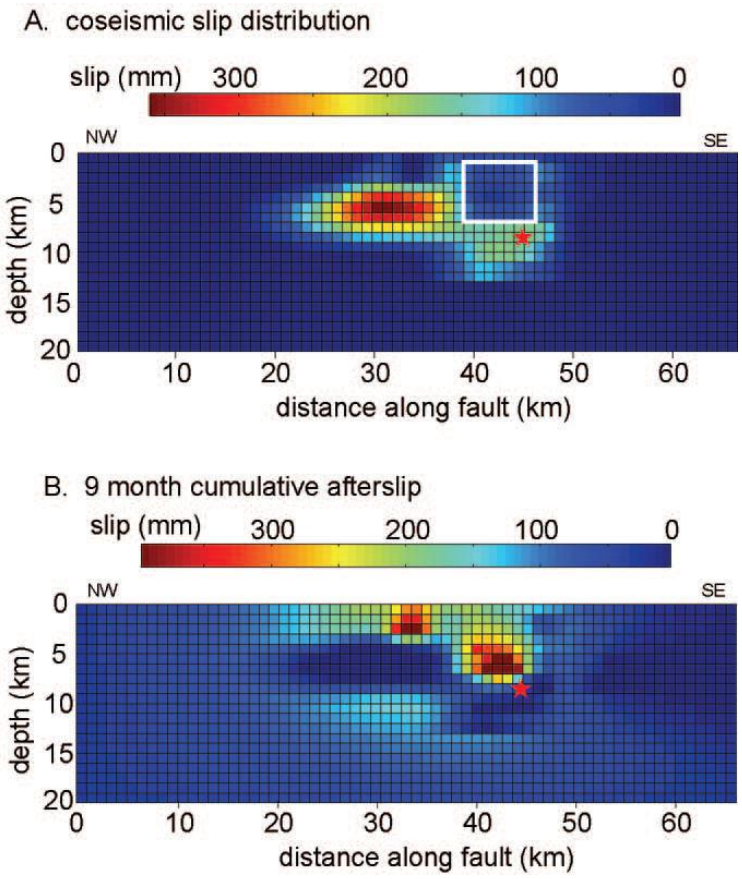

Figure 13: Parkfield earthquake slip model (Source: Johnson *et al.*, 2006)

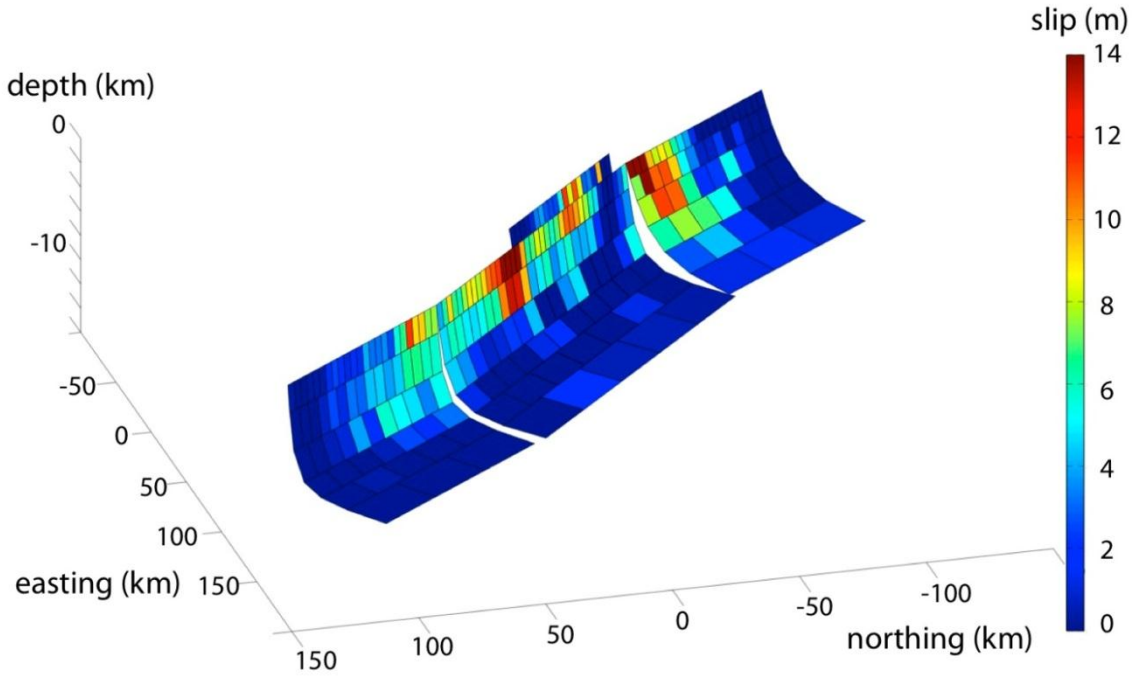

Figure 14: Wenchuan Earthquake slip model (Source: http://topex.ucsd.edu/wenchuan/listric_slip.jpg)

M_w 6.0 Parkfield earthquake, California

The Mw 6.0 Parkfield earthquake that occurred on 28th September 2004 was another of the many earthquakes (approx. 30 year recurrence interval) that have occurred along the Parkfield segment (south western fault zone) of the San Andreas Fault. The first occurred in 1966. This rupture produced approx. 32 km of surface fracturing dominantly northwest of the epicentre. It was most likely due to the Parkfield segment being situated between the aseismically creeping segment to the northwest and a locked Cholame segment to the southeast that last slipped in 1857 producing a M_w 7.9 earthquake in Tejon (Toke *et al.*, 2006). The Parkfield earthquake was only a moderately sized event compared to the others mentioned. However, it is one of the most observed and studied due to the abundance of geophysical instrumentation situated around Parkfield at the time of the rupture. These included such as arrays of continuous GPS receivers, creepmeters, strainmeters, borehole seismometers, and strong ground motion instruments all located near the fault (Langbein *et al.*, 2006; Johnson *et al.*, 2006). Therefore, it provided an unprecedented opportunity to study the physics governing slip on the fault and various other aspects of the co-seismic, post-seismic and, the inter-seismic periods of the earthquake cycle (Langbein *et al.*, 2006).

Key Findings

Due to the vast amount of instrumentation data available many studies were completed on this earthquake using the data available or combining it with space borne GPS and InSAR surveys. This produced a number of interesting findings as noted below.

Firstly the strong motion instruments showed these were highly varied peak accelerations over only a few kilometres, with the region near the fault ranging from 0.13 *g* to 1.2 *g* (Shakal *et al.*, 2006). The largest accelerations occurred near the northwest end of the rupture zone because the southern end was locked (Shakal *et al.*, 2006). Furthermore, co-seismic slip models produced by Johnson *et al. (*2006), and Langbein *et al. (*2006) for the earthquake identified two main areas of subsurface slip extending 25 km north of the hypocentre. The maximum subsurface co-seismic slip of approx. 0.5 m occurred approx. 10 km northwest of the hypocentre. This was at approx. 5km depth below Middle Mountain, whilst the other area of significant subsurface slip occurred slightly northwest of the hypocenter approx. 7-8 km deep (see Figure 13). Whereas, the majority of the accumulative post-seismic slip was located in similar subsurface locations but at a shallower depth, with a range of slip of 0.1 to 0.5 m or more occurring at a depth of approx. 5 km just above the hypocentre and 2-3 km beneath Middle Mountain (see Figure 13).

Johanson *et al.* (2006) also found that main earthquake rupture was followed by aseismic afterslip that was about three times the co-seismic slip (see Figure 13).

Mapped locations of fault step-overs and jogs or bends were compared to mapped locations of features following the 1966 rupture (Rymer *et al.*, 2006). Interestingly, both mapped locations of surface fractures on the south western fault zone were comparable over the two events.

M_w 7.9 Wenchuan earthquake, China

The M_w 7.9 Wenchuan, China earthquake of 12 May 2008 produced a 285 km long surface rupture zone and PGA of approx. 0.65 *g* (Shao *et al.*, 2011). The type of motion was a predominantly thrusting slip accompanied by a right-lateral component along the central-northern segments of the zone, and left-lateral component along the southern segment, along the Longmenshan Thrust Belt, eastern margin of the Tibetan Plateau (Shao *et al.*, 2011; Ran *et al.*, 2010; Lin *et al.*, 2009).

The amount of co-seismic deformation and its distribution provide important scientific information for revealing the mechanisms of earthquake propagation. Thus, the large surface rupture length provided a number of locations at which ground surface investigations took place to measure the amount of surface co-seismic slip. In particular Lin *et al.* (2009) and Ran *et al.* (2010) completed surveys that involved measuring displacements of major terrain features such as roads, stream channels, and terrace risers that were cut perpendicular by the surface rupture zone, as well as dislocated building displacements. All measurements were completed using total station instruments and differential GPS.

Key Findings

The key findings from these studies for Wenchaun earthquake were as follows:

- The co-seismic ruptures mainly occurred along the pre-existing Yingxiu–Beichuan, Guanxian–Anxian, and Qingchuan faults, which are the main faults of the Longmenshan Thrust Belt (Lin *et al.*, 2009).
- The co-seismic surface displacements measured from field investigations and surveys, are approximately 0.5 – 10 m of vertical displacement, accompanied by an average left-lateral component of less than 2 m along the 50 km long southernmost segment of the rupture zone and an average right-lateral component of approx. 1 – 2 m along the 150 km long central-northern segments, particularly in Shaba Village (see Figure 14) (Ran *et al.*, 2010; Lin *et al.*, 2009).

- The overall rupture length (approx. 285 km) and maximum vertical displacement (thrust slip) approx. 10 m, accompanied by 9 m of shortening across the rupture zone are the largest among all intra-continental thrust-type earthquakes reported to date (Ran *et al.*, 2010; Lin *et al.*, 2009).
- GPS observations of the fault following the first 14 days after the main rupture, initially identified what was perceived by Shao *et al.* (2011), as significant post-seismic deformation. The mechanisms were assumed to be afterslip on the earthquake rupture plane and viscoelastic relaxation of co-seismically stress change in the lower crust or upper mantle (Shao *et al.*, 2011).
- It was, however, later confirmed that aseismic fault slip was responsible for the near-fault post-seismic deformation, whereas the viscoelastic stress relaxation was seen to be the major mechanism behind the far-field post-seismic deformation (Shao *et al.*, 2011).

Mw 6.5 Bam earthquake, Iran

The M_w 6.5 earthquake, which occurred in south-eastern Iran on the 26th December 2003, was one of the deadliest in the region's history, devastating the town of Bam and causing casualties estimated to be in the order of tens of thousands (Fialko *et al.*, 2005; Talebian *et al.*, 2004). Bam lies within the western zone of two north-south trending strike-slip fault systems located either side of the Lut desert, which together accommodate the motion between central Iran and Afghanistan. It is part of the Eurasian plate, which is a diffuse boundary between the Arabian and Eurasian plates.

It is common for blind earthquakes to occur and produce long term surface deformation and morphological effects by which their existence may be recognised (Talebian *et al.*, 2004). A study by Talebian *et al.* (2004) concluded from an earthquake that destroyed the city of Bam that there was a complete absence of morphological features. The study discovered that the majority of the co-seismic slip (approx. 2 m) occurred subsurface at a depth of 2 – 6 km, with maximum surface displacements of approx. 0.2 m recorded and an average of less than 10 cm sporadically over a distance less than 12 km (see Figure 15) (Tablian *et al.*, 2004). This discovery was made through geological mapping of the surface displacement features and Envisat (European Space Agency) mapped decorrelation effects.

A study by Fialko *et al.* (2005), however, dismissed these surface displacements after Envisat satellite analysis (ASAR) of surface deformation indicated that most of the seismic moment release occurred at a shallow depth of 4 – 5 km. Yet it did not break the surface. However the ASAR data within the central part of the Bam rupture later showed surface displacements that did not exceed a few

centimetres (Fialko *et al.*, 2005). Furthermore, that these displacements are much smaller than the maximum horizontal displacements of 0.5 – 0.6 m at a distance of 1.5 km away from the rupture trace.

Key Findings

Findings from the Bam studies include:

- Both studies agreed that the majority of co-seismic slip, approx. 2 m, occurred in the subsurface at a depth of 2-6 km (see Figure 15).
- Surface rupture measurements indicated right lateral movement of up to 0.2 m with an average surface displacement of less than 0.1 m (over distance less than 12 km). Displacements were recorded at 0.5 – 0.6 m 1.5 km away from the rupture trace.
- Peak ground accelerations (PGA) recorded for the earthquake was 0.7 – 0.8 *g* for the horizontal component and 1.01 *g* for vertical component (Hosseini *et al.*, 2004).

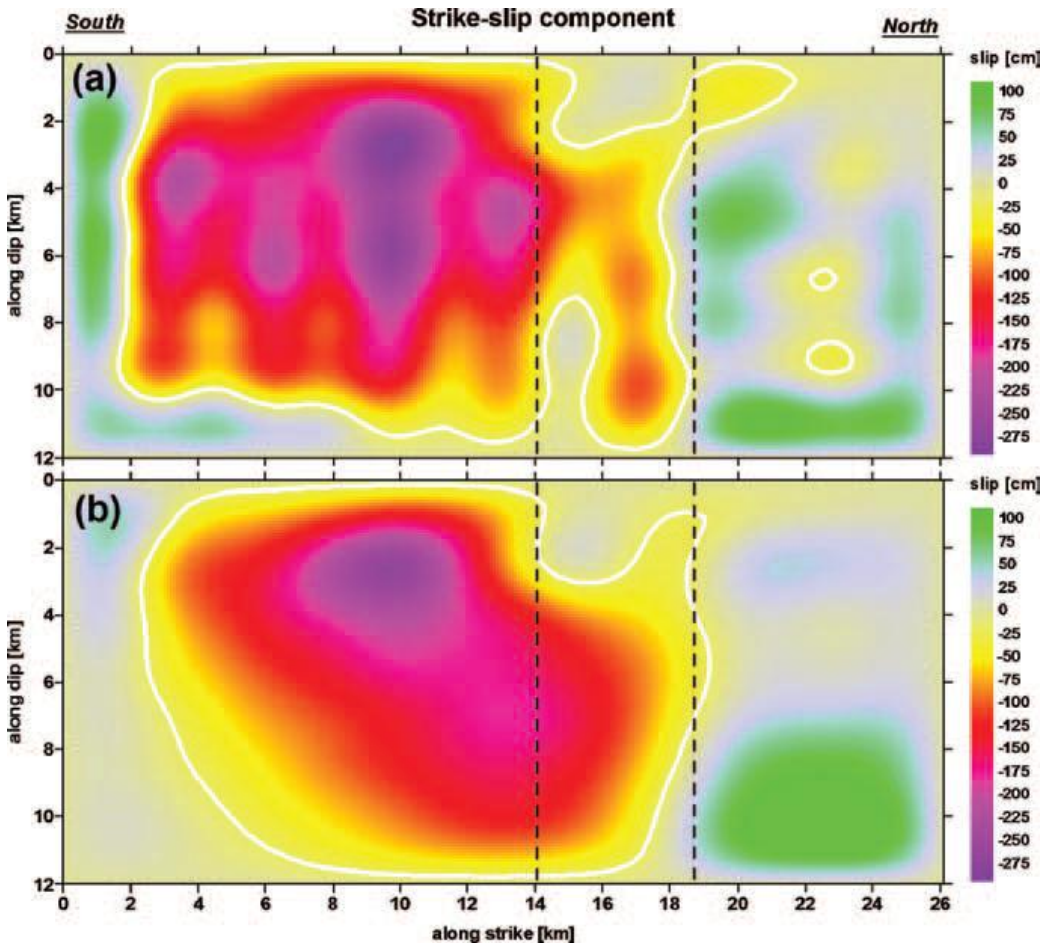

Figure 15: Bam earthquake slip model. (a) Represents the use of the successive approximation method and (b) the least-squares fitting method with the smoothing condition. (Source: Wang *et al.*, 2004)

Summary of Historical Earthquakes

From the studies reviewed, regarding the historical earthquakes outlined above, a number of key components have been identified:

- All the earthquakes summarised show maximum subsurface seismic moment release in the middle of the seismogenic layer, at average depths of 4-6 km (Fialko *et al.*, 2005).
- There is a wide range in surface rupture lengths for each of the earthquakes with the smallest being the Bam earthquake at approx. < 12 km and the largest being the Wenchuan earthquake with up to a trace 285 km along the surface.
- Maximum surface slip varies from 0.1m in M_w 6.0 Parkfield earthquake to approx. 9 m vertical with approx. 2 m horizontal for M_w 7.9 Wenchuan earthquake.
- Average surface displacements for the earthquakes range from 0 (Bam) to 4 - 5 m (Izmit and Wenchuan).
- Relative co-seismic to post-seismic slip at depth of 2- 10 km ranged from 0.5 to > 10 m with less than 0.5 m of post-seismic slip for all of the earthquakes.
- PGA values for each of the earthquakes reviewed ranges from 0.01 *g* – approx. 1.2 *g*. However, due to some older earthquakes the data presented for the PGA may not be as reliable as the newer projected values.
- The Landers earthquake had a small step over or jog associated with the fault rupture. In contrast, the Izmit earthquake had releasing step-overs of 1-4 km in width separating the four segments.

6. Darfield Earthquake literature

The M_w 7.1 Darfield earthquake was a complex event involving rupture of multiple fault planes (Beavan *et al.*, 2010), propagating to the surface and extending east-west for 29.5 ± 0.5 km (Quigley *et al.*, 2012).The majority of the earthquakes moment release resulted from slip on the previously unmapped Greendale Fault (Holden *et al.*, 2011; Van Dissen *et al.*, 2011; Quigley *et al.*, 2010). Quigley *et al.* (2012) identified the gross rupture morphology as that of two definable east - west striking segments (an eastern and a central segment), as well as a third NW-striking western segment. Collectively these segments are referred to as the Greendale Fault.

The Darfield earthquake has become one of New Zealand's best-recorded of this magnitude. This is because equipment was readily available, as New Zealand has evolved to include a relatively intricate research capability into earthquakes and associated phenomenon. Seismic data from the rupture was recorded by accelerometers, a dense network of broadband and strong motion

seismometers. The geological data was recorded by ground surveys and mapping surface displacements, using GPS techniques and geodetic data by GPS and InSAR (Bevan *et al.*, 2010; Quigley *et al.*, 2012; Holden *et al.*, 2011; Van Dissen *et al.*, 2011; Gledhill *et al.*, 2011; Quigley *et al.*, 2010; Cousins & McVerry, 2010).

Seismic instruments, in particular accelerometers, recorded PGA generated during the mainshock. The PGA's were recorded by 130 GeoNet accelerometers. They ranged from 0.3 - 0.8g with the maximum recorded value occurring near Greendale with 1.25*g* (Cousins & McVerry, 2010). From the geological surveys co-seismic slip was a maximum of 5.3 ± 0.5 m with an average of 2.5 m over the approx. 29 km fault trace (Holden *et al.*, 2011; Van Dissen *et al.*, 2011; Gledhill *et al.*, 2011; Quigley *et al.*, 2010). Surveys also found that the eastern and central fault segments are defined by a series of left-stepping '*en echelon'* east-west striking surface traces (Quigley *et al.*, 2012; Van Dissen *et al.*, 2011). The width of the largest step-over was measured as approx. 1 km (950 ± 500 m) perpendicular to the average strike of adjacent rupture trace and occurred between the eastern and central segments (Quigley *et al.*, 2012; Van Dissen *et al.*, 2011). A multitude of smaller steps, ranging in size from less than 75 m to approx. 500 m, separated the western and central segments (Quigley *et al.*, 2012; Van Dissen *et al.*, 2011). Also co-seismic deformation patterns were identified on the step-over to the east-west striking segment (near Rolleston) that differed to those on the main central segment.

The geodetic InSAR images from 1 - 8 weeks following rupture of the fault indicate a slight amount of post-seismic slip less than 0.01 m corresponding to approximately 1% of the co-seismic slip (Beavan *et al.*, 2010).

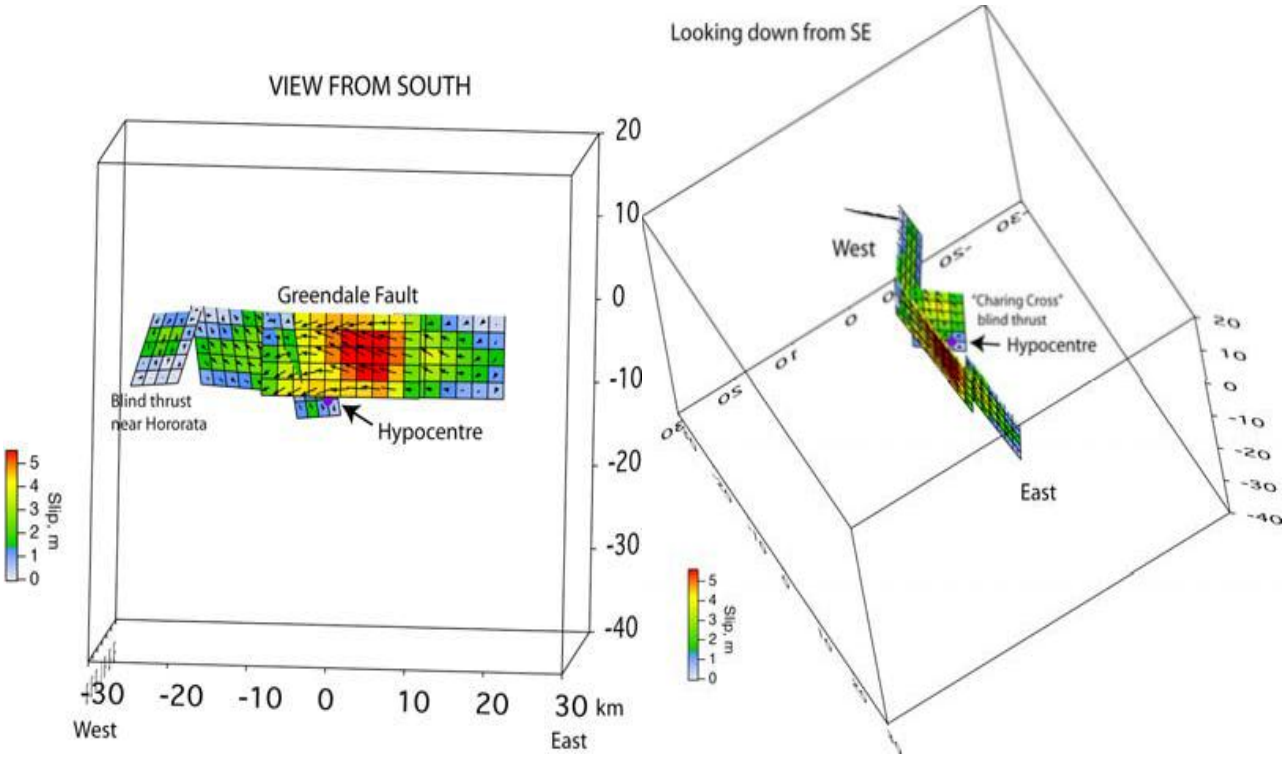

Figure 16: Fault slip model for the Greendale Fault produced by the geodetic and GPS data (Source: Holden *et al.*, 2011).

The complexity of this rupture was also reflected in the models produced from the extensive high-quality geological, geodetic and seismic/strong motion data sets (Holden *et al.*, 2011; Gledhill *et al.*, 2011; Quigley *et al.*, 2012). The models produced some interestings findings, as noted below.

- Combing the geodetic and strong motion data (see Figure 16 above) aided clarity into the rupture pattern by highlighting the presence of blind faults as well as defining them (Holden *et al.*, 2011; Gledhill *et al.*, 2011; Quigley *et al.*, 2012). In addition, it showed the likely rupture sequence with initiation of the rupture occurring on a steeply dipping blind reverse fault 4 km north of Greendale (Charing Cross). This was followed by a major rupture of the Greendale Fault, resulting in a further rupture on a blind reverse fault near the western tip of the Greendale Fault south of Hororata (Holden *et al.*, 2011).
- All of the models produced underestimated the overall magnitude of the earthquake, which strongly suggests that more blind sources were involved in the rupture process (Beavan *et al.*, 2010).

- Dissipation of seismic energy in the gravels may account for the absence of clearly defined fault scarps despite the modelled predictions of near-surface fault slip for the Hororata and Charing Cross ruptures (Holden *et al.*, 2011).

Geodetic Surveys on the Greendale Fault

There have been two geodetic surveys completed in Christchurch and Canterbury area following the September 4th earthquake (e.g. Beavan *et al.*, 2010; Holden *et al.*, 2011). Beavan *et al.* (2010) completed the data acquisition in 3 stages. Firstly from September 7th-13th a survey of 80 geodetic sites was completed within 80 km of the earthquake to determine the co-seismic (a few days of post-seismic) ground surface displacement field. The second stage from September 27th-30th involved reoccupying 45 sites closer to the earthquake and measuring two additional sites, with at least 2 hour sessions in the lower quality sites and at least one session of 24 hours at five of the high quality locations. This was completed to see if a significant amount of post-seismic displacement (afterslip or poroelastic effects) had taken place in the period between the first survey and the second survey 3 weeks after the earthquake (Beavan *et al.*, 2010). The third and final stage occurred from 26th-29th October which involved an additional 12 lower quality sites with a 24 hour session, again to provide data for future post-seismic studies. Holden *et al.* (2011) completed a geodetic study of 8 sites within 80 km of the epicentre in the week following the earthquake to include as little post-mainshock slip as possible.

Summary of Key Findings

A summary of the key findings on the research on the Darfield Earthquake shows:

- The Greendale Fault has the highest ratio of surface slip to surface rupture length for any fault rupture compared with the data from the studies on historical earthquakes (Quigley *et al.,* 2012).
- The PGA recorded for the earthquake ranged from 0.3 - 0.8 g with the maximum recorded value of 1.25 *g* occurring near Greendale.
- Geological surveys found that the eastern and central fault segments are defined by a series of left-stepping '*en echelon'* east-west striking surface traces. The largest step-over width was measured as approx. 1 km (approx. 950 ± 500 m) between the eastern and central segments. In addition, there were a multitude of smaller steps, ranging in size from less than 75 m - approx. 500 m separating the western and central segments
- Co-seismic slip was a maximum of 5.3 ± 0.5 m with an average of 2.5 m over the approx. 30 km fault trace. Whereas post-seismic deformation is small ≤ 0.01 m, determined from GPS

displacements during the first 8 weeks after the earthquake (Beavan *et al.*, 2010; Reyners, 2011).

7. Darfield Compared to Relevant Historical Earthquakes

Details of the relevant earthquakes have been tabulated for direct comparison with the Darfield earthquake in Table 1 and Table 2. Comparisons focus on surface attributes, co-seismic activity, post-seismic activity, and maximum recorded PGA.

Surface Attributes

Some interesting findings occur when comparisons are made between the Darfield and historic earthquakes. In particular, comparisons included surface attributes such as maximum displacement, average displacement over the surface rupture length, maximum displacement and average displacement for the geological moment magnitude generated during the reviewed earthquakes.

Following on from the Quigley *et al.* (2012), by comparing the ratio between the maximum displacement and surface rupture length, average displacement and surface rupture length, maximum displacement and geological moment magnitude, average displacement and the geological moment magnitude from the Darfield earthquake with additional earthquakes; Izmit, Bam, Wenchuan, and Parkfield (see Table 1). Once again, the Greendale Fault has the highest surface displacement, maximum (SD_{max} 5.3 m) and average (SD_{avg} approx. 2.5 m) with respect to surface rupture length. Furthermore, comparing the Greendale Fault to tabulated earthquakes used in studies by Wesnousky (2008) and Lettis *et al.* (2002) (shown by Appendix Tables 1 – 2) the maximum and average surface displacement values relative to the surface rupture length for the Greendale Fault are still among the highest ever recorded.

The maximum surface displacement for the Greendale Fault (SD_{max} 5-6 m) is larger than the 1943 M_w 7.6 Toysa earthquake, Turkey (SD_{max} 4.4 m) and 1968 M_w 7.2 Dasht-e-Bayaz earthquake, Iran (SD_{max} 5.2 m) with rupture lengths > 80 km. The average surface displacement for the Greendale Fault (SD_{avg} approx. 2.5 m) is the same or greater than the following earthquakes:

- 1939 M_w 7.9 North Anatolian Fault, Erzincan earthquake, Turkey; SD_{max} 6-8 m, SD_{avg} 2.5 m with a approx. 360 km long rupture length.
- 1943 M_w 7.3 North Anatolian Fault, Kargil earthquake, Turkey; SD_{max} 6 m, SD_{avg} 2.5 m with a approx. 360 km long rupture length.

- 1943 M_w 7.6 Toysa earthquake, Turkey; SD_{max} 4.4 m, SD_{avg} 2.5 m with a approx. 275 km long rupture length.
- 1968 M_w 7.2 Dasht-e-Bayaz earthquake, Iran; SD_{max} 5.2 m, SD_{avg} 2.3 m with a approx. 80 km long rupture length.
- 2001 M_w 7.8 Kunlin earthquake, China; SD_{max} 8.3 - 8.75 m, SD_{avg} 2.4 – 3.3 m with a approx. 438 km long rupture length.

The majority of earthquakes that do have higher surface displacement values (SD_{max} and SD_{avg}) than the Greendale Fault are equal to moment magnitude, M_w 7.9 or greater.

Surface rupture lengths are another interesting comparison between surface attributes. The Greendale Fault has a surface rupture length similar to Mw 6.0 Parkfield earthquake which had an approx. 32 km surface rupture, yet the Bam earthquake (M_w 6.5) resulted in a surface rupture of less than 10 km, with the majority of moment release occurring at 4-5 km depth. Whereas, similar moment magnitude earthquakes Hector Mine (M_w 7.1) and Landers earthquakes (M_w 7.3) have a large jump in rupture length from approx. 10 to 45 km further than the Greendale Fault.

The variety in rupture lengths for each of the earthquakes outlined indicates the rupture length is dependent on the fault setting, as well as properties of the subsurface crustal material. The upper few kilometres of brittle crust are known to have mechanical properties that differ from those of the rest of the upper crust (Fialko *et al.*, 2005). In particular, the shallow layer has a higher density of cracks, pores and voids, a higher co-efficient of friction and may exhibit velocity straining behaviour (Fialko *et al.*, 2005). The latter may explain why co-seismic slip is impeded in the upper crust, but it does not make clear how the resulting deficit of shallow slip is accommodated throughout the earthquake cycle (Fialko *et al.*, 2005). Suggestions include steady state shallow creep, shallow post-seismic afterslip, or distributed inelastic failure of the shallow crust either during earthquakes or in the inter-seismic period (Fialko *et al.*, 2005). However, this does point out the ability of near surface material to dissipate slip/rupture energy and in the case of Greendale Fault it asks the question what role the gravels played in dissipating slip.

Table 1: Comparisons of the magnitude, type of faulting, depth, surface rupture length and maximum surface offsets of historical earthquakes with the Darfield Earthquake (Sources: Quigley *et al.*, 2010 and 2010; Van Dissen *et al.*, 2011; Beavan *et al.*, 2010 and 2012; Wesnousky, 2008; Peltzer *et al.*, 1998; Fialko *et al.*, 2005; Harris *et al.*, 2002; Ergintav *et al.*, 2002; Treiman *et al.*, 2002; Barka *et al.*, 2002; Langridge *et al.*, 2002; Lettis *et al.*, 2002).

Event/ Location	Date	Magnitude (M_w)	Type of Faulting	Depth (km)	Length (km)	Surface Rupture Length (km)	Max. Surface Offset (m)
Izmit, Turkey	17th August 1999	7.6	Right-lateral strike-slip	13	107	~60	5.5 avg. 1.1
Hector Mine, California	6th October 1999	7.1	Right-lateral strike-slip	12	44	~ 41	4.5 - 5.2 avg. 1.56
Landers, California	28th June 1992	7.3	Right-lateral strike-slip	15	~ 80	~ 75	6.2 avg. 2.3
Bam, Iran	26th December 2003	6.5	Right-lateral strike-slip	~5	20	< 10	0.2 avg. < 0.1
Parkfield, California	September 2004	6.0	Right-lateral strike-slip	7.9	~ 36	32	0.1
Wenchuan, China	12 May 2008	7.9	Thrust with right lateral component	19	~ 290	285	0.5 - 9 V. and <1 - 2 H.
Greendale Fault, New Zealand	4th September 2010	7.1	Right-lateral strike-slip	~10	~40	~ 29	~ 5.3 avg. 2.5

Table 2: Comparisons of historical earthquake to Darfield earthquake, this time looking at average and maximum co-seismic slip at depth and post-seismic slip (Sources: Beavan *et al.*, 2012; Elliot *et al.*, 2011; Geonet, 2012; USGS, 2012; Treiman *et al.*, 2002; Barka *et al.*, 2002; Langridge *et al.*, 2002; Lettis *et al.*, 2002; Erdik and Durukal, 2000; Wang *et al.*, 2004; Johanson *et al.*, 2006; http://peer.berkeley.edu/smcat/index.html).

Event/ Location	Magnitude (M_w)	Avg. co-seismic slip (m)	Max. co-seismic slip (m)	Depth (km)	Post-seismic slip (m)	Peak Ground Acceleration (*g*)
Izmit, Turkey	7.6	2.3	3	≤ 4	0.4	0.4
Hector Mine, California	7.1	1.56	5.2	3- 6	0	0.6 max < 0.3 avg.
Landers, California	7.3	2.3	6.2	< 5	≤ 0.04	0.818 max < 0.2 avg.
Bam, Iran	6.5	1.5	2.5	4-5	≤ 0.19	0.7 - 0.8
Parkfield, California	6.0	< 0.4	0.4	5 – 10	0.1 - 0.3	<1.2 max (1.1 km) 0.2 – 0.6 avg.
Wenchuan, China	7.9	1	9 V. and 2 H.		N/A	0.65
Greendale Fault, Darfield New Zealand	7.1	2.5	8 - 9	4 - 6	?	1.25 max (1.3 km) 0.66 (27 km) 0.6 – 0.8 avg.

Co-seismic and Post-seismic Slip

Looking at the co-seismic slip at depth in Table 2, the Greendale Fault rupture once again has one of the highest max slip (8 - 9 m) and average slip values (approx. 2.5 m) when considered relative to the moment magnitudes and rupture lengths. This indicates that the overall co-seismic subsurface displacement that occurred during the rupture of the Greendale Fault was remarkably high in comparison to other historical earthquakes of similar magnitude and rupture length (this could also have something to do with the way this earthquake was measured). From the literature and slip models (see Appendix A Figures A1 - A6), it was also found that the earthquakes all show a maximum co-seismic slip in the middle to the top of the seismogenic layer, at average depths of 4-6 km or less.

By comparing these values for post-seismic slip, it was found that all of the earthquakes have less than 0.5 m of slip. GPS displacements from initial surveys by Beavan *et al.* (2010) have indicated that there is slight post-seismic deformation/slip, ≤ 0.01 m, along the Greendale Fault. Currently published research into the post-seismic deformation along the Greendale Fault is limited to a few months following the rupture (e.g. Beavan *et al.*, 2010).

Peak Ground Acceleration

Also worth mentioing is the maximum and average PGA values measured during each of the earthquakes. The M_w 7.1 Darfield has a maximum and average values of PGA at 1.25 *g* and 0.6 - 0.8 *g,* resptively. The M_w 6.0 Parkfield rupture has a maximum reocrding of < 1.2 *g* and an on average 0.2 – 0.6 *g*, respectively, compared to the other earthquakes. However, both of these earthquakes reflect much large PGA values than any of the other earthquakes.These high values have been recorded by instrumentation close to the epicentre, hence why a similarity in result does seem unusual as the Darfield earthquake had much larger values for maximum and averagere surface slip and slip at depth as previously discussed.

This is confirmed as the Greendale Fault the maximum value was recorded approx. 1.3 km from the epicentre, whilst a value for 0.66 *g* was recorded 27 km from the epicentre in Ferrymead/ Heathcote area of Christchurch and a value of 0.91 g was recorded near Lincoln (see Figure 17) . With the Parkfield earthquake the maximum recording of approx. 1.15 *g* was made 1.1 km from the epicentre. The Parkfield had a maximum surface displacement of 0.1 m and co-seismic slip 0.4 m, with an average of less than 0.3 m subsurface slip at approx. 5 – 10 km depth along the 32 km fault plane. Reasons for this include the following possibilities; firstly it may be due to the fault settings as the Parkfield was situated between the aseismically creeping segment to the northwest and a locked segment to the southeast since the 1857 Fort Tejon rupture. Secondly, the fact that Parkfield also

showed a high PGA value indicates that data presented for the older earthquakes may not be as reliable as the newer projected values. This is likely due to advances in technology and the wide range of instrumentation used to record the Parkfield and Darfield earthquakes.

Comparing surface attributes, co-seismic activity, post-seismic activity, and PGA for the Greendale Fault rupture and historical earthquakes, the salient points to emerge are:

- The Greendale Fault has surface attributes, in particular maximum and average surface slip displacements, which are among the highest recorded for an earthquake of that magnitude and rupture length.
- The Greendale Fault and the relevant historical earthquakes reviewed for this study show maximum seismic moment release in the middle to the top of the seismogenic layer, at average depths of 4 – 6 km or less (see Appendix Figures A1-6). Indicating maximum slip distribution was concentrated at shallow depths.
- The Greendale Fault has a surface rupture length similar to 2006 M_w 6.0 Parkfield earthquake which had a approx. 32 km surface rupture. Whereas, similar moment magnitude earthquakes M_w 7.1 Hector Mine and M_w 7.3 Landers earthquakes have a large jump in rupture length from approx. 10 to 45 km further than the Greendale Fault.
- Post-seismic slip is less than 0.5 m for all of the earthquakes. GPS displacements have indicated post-seismic deformation along the Greendale Fault, though it is slight due to measurements only covering the first eight weeks after the earthquake.
- The rupture of the Greendale Fault produced relatively high PGA values over the Canterbury Region (average of 0.6 – 0.8 *g*) for the reviewed earthquakes.

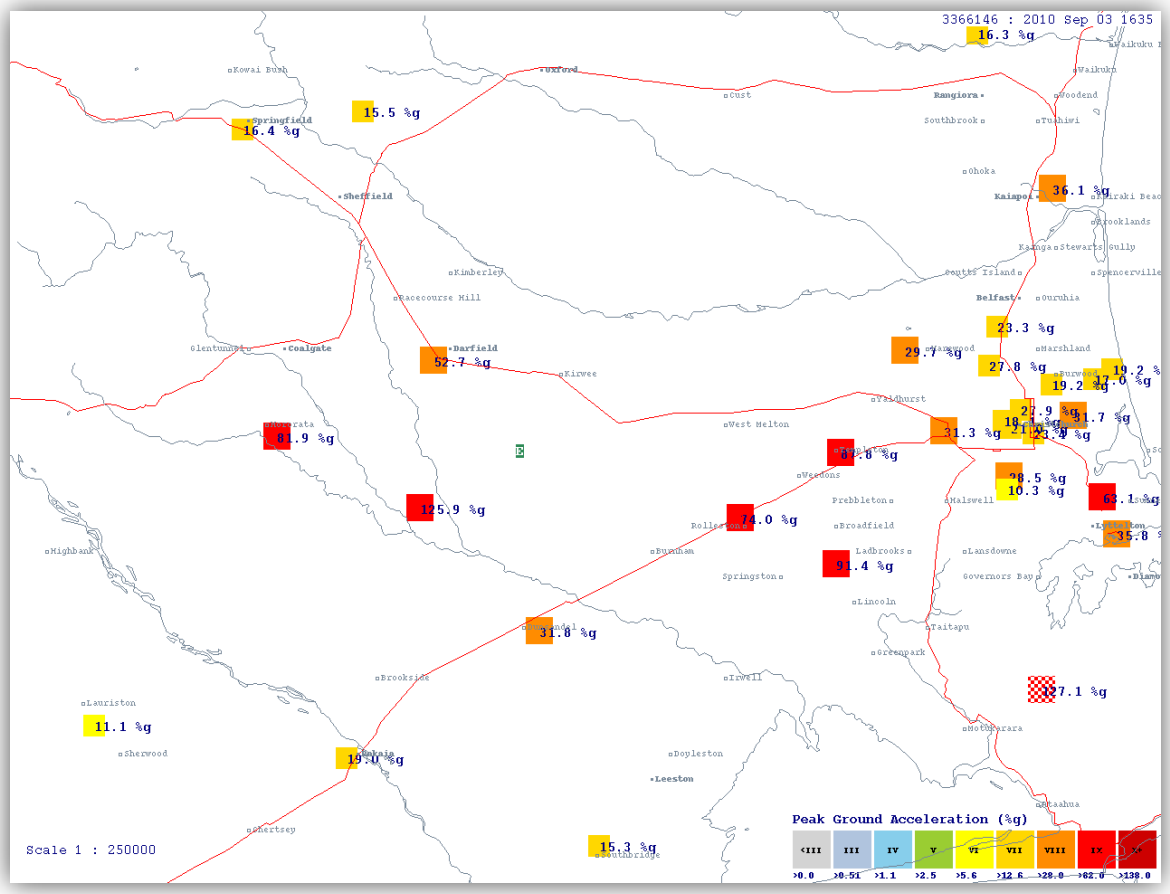

Figure 17: Peak ground acceleration values for the Darfield earthquake (Source: http://www.geonet.org.nz/var/storage/images/media/images/news/2010/darfield_pga/44949-1-eng-GB/darfield_pga.png)

8. Research Ideas from the Literature

A lot of questions need to be addresses surrounding earthquake fault zones and particularly deformation in fault zones. These include:

- How faithfully does post-mainshock surface displacements record displacement at depth?
- What is the role of gravels in dissipating slip?
- How do faults behave after earthquakes?
- How long should we wait to repair fault zones?

The litereature review also found reasearch surrounding the following areas of the Darfield Earthquke and Greendale Fault was limited and/or inconclusive to date:

1. Postseismic creep on the Greendale Fault.

2. How much surface deformation occurred on the Hororata and Charing Cross areas southwest of Christchurch rupture during the Darfield earthquake sequence?
3. Can the New Zealand geodetic network be used for repeat cadastral surveys in determining surface deformation? What do they reveal about the patterns of surface deformation in the Canterbury earthquake sequence?

8.1 Post-seismic Creep

Currently no study has been completed looking into post-seismic creep on the Greendale Fault using near source or near fault high resolution markers of post-seismic deformation. Beavan *et al.* (2010) completed a study collecting data for the post-seismic slip on the Greendale Fault over 8 weeks, which was limited in time and space on a region scale.

Using a smaller scale survey, this study aims to be the first to provide conclusive evidence as to whether the Greendale Fault exhibits post-mainshock creep over a period of 18 months through across fault post-seismic analysis on the Greendale Fault.

8.2 How much surface deformation occurred on the Hororata and Charing Cross areas southwest of Christchurch rupture during the Darfield earthquake sequence?

For the areas southwest of Christchurch, within the literature completed to date, only seismic and geodetic models of the Hororata and Charing Cross faults have been produced. InSAR images have revealed that there was deformation in the vicinity of the Hororata and Charing structures. However, these techniques are limited in their ability to resolve finite geometries. Therefore, a study can be undertaken to resolve these geometries by completing a near surface seismic reflection survey.

8.3 Can the New Zealand geodetic network be used for repeat cadastral surveys in determining surface deformation? What do they reveal about the patterns of surface deformation in the Canterbury earthquake sequence?

The previous cadastral studies completed on the Darfield earthquake (e.g. Beavan *et al.*, 2010) are widespread, looking at the movement in the Canterbury Region using 1^{st}-3^{rd} order geodetic survey marks. They do not focus on the areas surrounding the Charing Cross and Hororata thrust features. This study aims to test the credibility of the cadastral surveying network by surveying localised to these blind features (less than 50 km from the fault) using 3^{rd} to 12^{th} order geodetic survey marks to reveal information about the pattern of surface deformation within close proximity of the fault trace resulting from the Canterbury earthquake sequence. In addition, it will complement the studies already completed for widespread motion maps.

By completing research into these aspects, this study will not only answer these questions but also shed some light on some of the grey areas when it comes to patterns of crustal deformation resulting from earthquakes.

9. Summary

The literature reviewed made it clear that there are a number of unanswered questions when it comes to deformation at fault zones. In particular the review found reasearch surrounding the following areas was missing, limited and/or inconclusive to date:

- Postseismic creep on the Greendale Fault,
- The Hororata and Charing Cross blind structures rupture and,
- Cadastral network research and surveys localised to the fault vacinity.

Events like the Darfield earthquake are pivotal in helping to bridge the knowledge gap around earthquakes, as it is one of the best recorded earthquakes in the world. Therefore it provides a unique opportunity to answer unknown questions, like those aforementioned, through research into the behaviour of earthquakes and key aspects surrounding earthquakes.

III. Scientific contributions arising from the thesis

Completion of research into the patterns of crustal deformation resulting from the 2010 Earthquake Sequence in Christchurch, Canterbury, New Zealand will provide:

- A better understanding of post-seismic deformation within the near surface following large (> Mw 6.5) shallow strike-slip earthquakes.
- Additional knowledge of surface deformation associated with the Hororata and Charing Cross Blind Faults.
- Co-seismic surface deformation patterns associated with the Darfield earthquake sequence. Furthermore, the knowledge of whether the New Zealand cadastral network is viable for use as deformation monitoring of active faults within the landscape.

Publications:

Van Dissen, R; Barrell, David; Litchfield, Nicola; Villamor, P; Quiley, M; King, A; Furlong, K; Begg, J; Townsend, D; Mackenzie, H; Stahl, T; Noble, D; Duffy, B; Bilderback, E; Claridge, J; Klahn, A; Jogens, R; Cox, S; Langridge, R; Ries, W; Dhakal, R. 2011. Surface rupture displacement on the Greendale Fault during the Mw 7.1 Darfield (Canterbury) earthquake, New Zealand, and its impact on man-made structures. *Proceedings of the Ninth Pacific Conference on Earthquake Engineering Building an Earthquake Resilient Society* (pp. 1-8). Auckland, New Zealand: NZSEE

IV. Thesis structure

This thesis is devoted to understanding the patterns of crustal deformation through three key topics surrounding the Greendale Fault/Darfield Earthquake. To structure the research around these topic, the thesis has been separated into 3 parts. The structure within each of these parts begins by introducing the question it intends to answer; identifies the selected work area; outlines the methodology behind the research; presents the results and discusses them with relation to the question; concluding with a summary of the overall findings from that part.

At the end of Part III, there is an overall conclusion which entails a summary of the findings from the entire thesis.

Part I: Post mainshock creep on the Greendale Fault, detected in repeat surveys.

Outline:

1.1 Introduction

The M_w 7.1 Darfield earthquake on the 4th September 2010 at approximately 4:35 am caused widespread damage, significant ground rupturing and surface deformation throughout the Canterbury Region. It was a complex event involving rupture of multiple fault planes (Beavan *et al.*, 2010); including a surface rupture that extended east-west for 29.5 ± 0.5 km (Quigley *et al.*, 2012). The previously unidentified Greendale Fault was responsible for the majority of earthquake moment release (Beavan *et al.*, 2010; Holden *et al.*, 2011; Van Dissen *et al.*, 2011; Quigley *et al.*, 2010).

Major earthquakes provide opportunities to study lithospheric deformation phenomena (Pollitz *et al.*, 1998; Ergintav *et al.*, 2002). This includes co-seismic and post-seismic effects, such as short-term afterslip (scale of years) and long-term viscoelastic relaxation (scale of 10^3 years). By measuring the displacement of the Earth's surface during and after an earthquake valuable evidence about the mechanics of the earthquake process on the main fault zone can be obtained. Furthermore, measuring the Earth's surface during and following an earthquake provides insight into the mechanical behaviour of the region surrounding the fault and in deeper parts of the earthquake generation zone, including the crust and upper asthenosphere (Ergintav *et al.*, 2002; Scholz, 1988; Tse and Rice, 1986; Thatcher, 1983; Savage, 1980). Numerous studies of co-seismic and post-seismic fault motion/deformation have been conducted after M_w 6.9 -7.2 earthquakes, including events in Turkey, California, and Iran (e.g. Peltzer *et al.*, 1998; Savage *et al.*, 1997; Freymueller *et al.*, 1994; Treiman *et al.*, 2002; Simons *et al.*, 2002; Barka *et al.*, 2002; Langridge *et al.*, 2002; Lettis *et al.*, 2002; Shakal *et al.*, 2006; Langbein *et al.*, 2006; Johnson *et al.*, 2006; Shao *et al.*, 2011; Ran *et al.*, 2010; Lin *et al.*, 2009; Fialko *et al.*, 2005; Talebian *et al.*, 2004).

Understanding this distribution of co-seismic and post-seismic deformation and associated stress changes in the surrounding region enables estimates of seismic loading to be calculated and an evaluation to be made of the potential for neighbouring faults to generate future events (Ergintav *et al.*, 2002). In addition to the spatial pattern of surface displacements, the temporal development of post-seismic deformation helps to define the rheology of the fault zone and the surrounding crust (Ergintav *et al.*, 2002). These studies show that it is very important to investigate the mechanisms for pre-seismic, co-seismic and post-seismic crustal deformations to understand the complete processes of the major earthquakes (Miyashita *et al.*, 2001). These mechanisms include; poroelastic effects; viscoelastic relaxation; fault creep, and seismically or aseismically triggered subsidence.

The Darfield earthquake provides a great opportunity to advance knowledge of post-seismic effects in fault zones. In particular, it should provide useful information on near surface deformation

mechanisms such as fault creep, and seismically or aseismically triggered subsidence, surrounding the near surface rupture and deformation zone.

Before conducting data collection for this thesis, my hypothesis is that post-seismic deformation on the Greendale Fault following the Darfield earthquake will be detectable by near field surveying techniques. Furthermore, it will be concentrated at shallow levels due to a surface slip deficit relative to the co-seismic slip at 4 to 6 km depth. This is worth investigating as the Greendale Fault had one of the highest co-seismic displacements with respect to the surface rupture length ever recorded. It was found that 5.3 ± 0.5 m with an average of 2.5 m displacement occurred over the approx. 29 km fault trace (Quigley *et al.*, 2012). This large amount of co-seismic surface slip corresponds to a significant static stress drop of 13.9 ± 3.7 MPa (Quigley *et al.,* 2012), typical of an intraplate earthquake. Therefore, this drop in stress could result in either more or less production of post-seismic deformation. An earthquake of this size and magnitude has the potential to provide answers to the following questions;

- Did the high levels of co-seismic deformation minimise the amount of measurable post-seismic displacement?
- Did this co-seismic slip also minimise any residual slip gradients in the near surface?
- Will post-seismic slip be more likely to occur, as the near surface attempts to recover, settle, or overcompensate for the large co-seismic displacement?
- Or in a broader sense, what happens to the near surface of fault zones following major earthquakes.

To test this hypothesis and answer the outlined questions, repeat surveys were conducted at several locations, where marker pins had been inserted either side of the Greendale Fault trace. Surveying these pins at different intervals over a period of approx. 1.5 years enables measurement of across fault displacements to be calculated along the Greendale Fault and related segments.

1.2 Study Area

Selecting the study sites was an important initial stage in this project. A desirable site needed to be intersected by the fault trace, as well as having a line of sight from one side of the fault to the other. Therefore, roads were decided to be the best sites. To get robust results, the survey also required sites that provided a good representation of the different levels of displacement occurring along the length of the Greendale Fault. The selected sites are highlight by the blue, red and green areas in Figure 18.

- Telegraph and Highfield Roads, the green area, represent sites where high co-seismic slip was recorded - approx. 5 m horizontal and < 1 m vertical.
- Kivers Road, intersected by the fault within the blue area, reflects a site where moderate displacement occurred - approx. 3 m horizontal and 0.2 m vertical.
- Kerrs and Railway Roads highlighted by the red area along the eastern tip of the Greendale Fault recorded small amounts of co-seismic displacement – approx. 1.6 m horizontal and 0.2 m vertical.

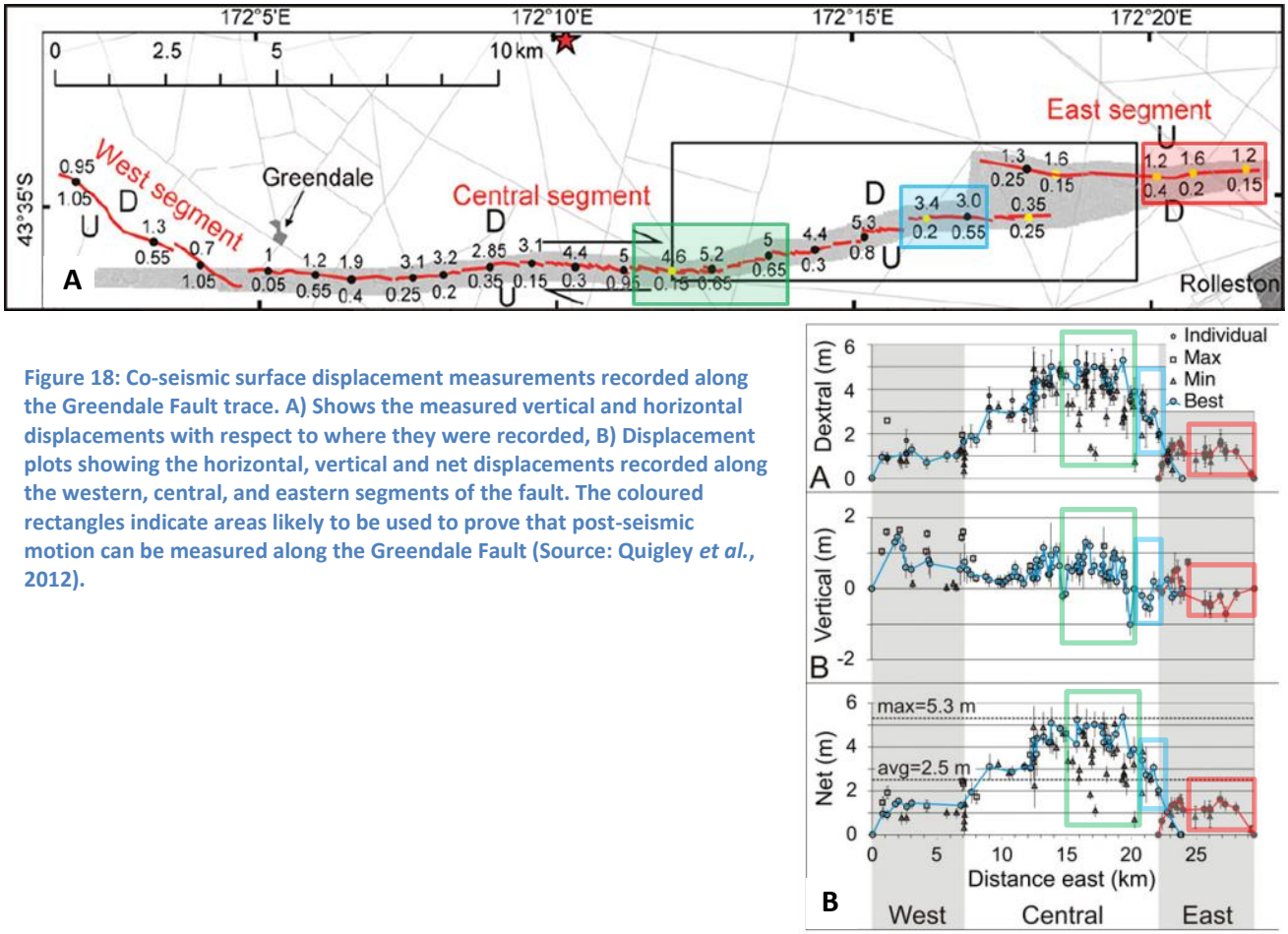

Figure 18: Co-seismic surface displacement measurements recorded along the Greendale Fault trace. A) Shows the measured vertical and horizontal displacements with respect to where they were recorded, B) Displacement plots showing the horizontal, vertical and net displacements recorded along the western, central, and eastern segments of the fault. The coloured rectangles indicate areas likely to be used to prove that post-seismic motion can be measured along the Greendale Fault (Source: Quigley *et al.*, 2012).

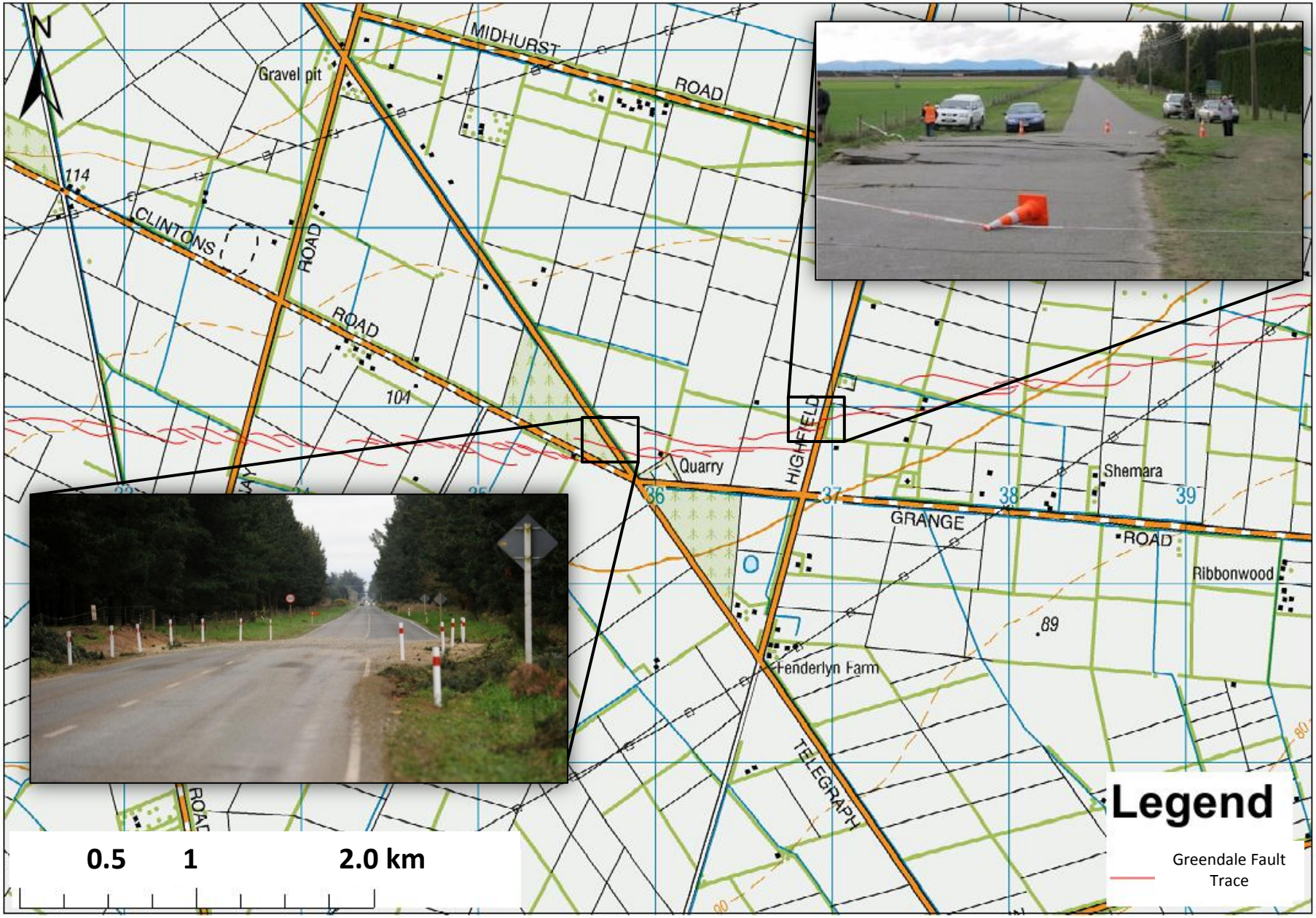

Figure 19: Illustrates where the Greendale Fault passes through Telegraph Road and Highfield Road (Sources: left image http://4.bp.blogspot.com/_kybPIQ2Rhjk/TI1SitAetzI/AAAAAAAAAAc/YeoAGhJ_UME/s1600/Telegraph+Rd+sm.jpg; right image Barrell, 2011; Fault trace courtesy of N.Litchfield and D. Barrell).

Figure 20: The Greendale Fault trace passing through the Kivers Road and Kerrs/ Railway Road in Mid Canterbury (Sources: Fault trace courtesy of N.Litchfield and D. Barrell).

1.3 Methodology

The Greendale Fault displaces a number of visible landmarks along the approx. 29 km trace (Quigley *et al.*, 2012). Immediately following the Greendale Fault rupture, a group from the Engineering department at the University of Canterbury led by Dr Kevin Furlong, inserted marker pins (100 mm x 4 mm galvanised nails) into the ground at five different locations where the fault trace intersected the road. The marker pins were installed to record or identify the presence of near surface post-seismic deformation or movement occurring along the Greendale Fault at the following locations (see Figures 19 - 21):

- Telegraph Road (T),
- Highfield Road (H),
- Kivers Road (K), and
- Kerrs Road/ Railway Road (KR).

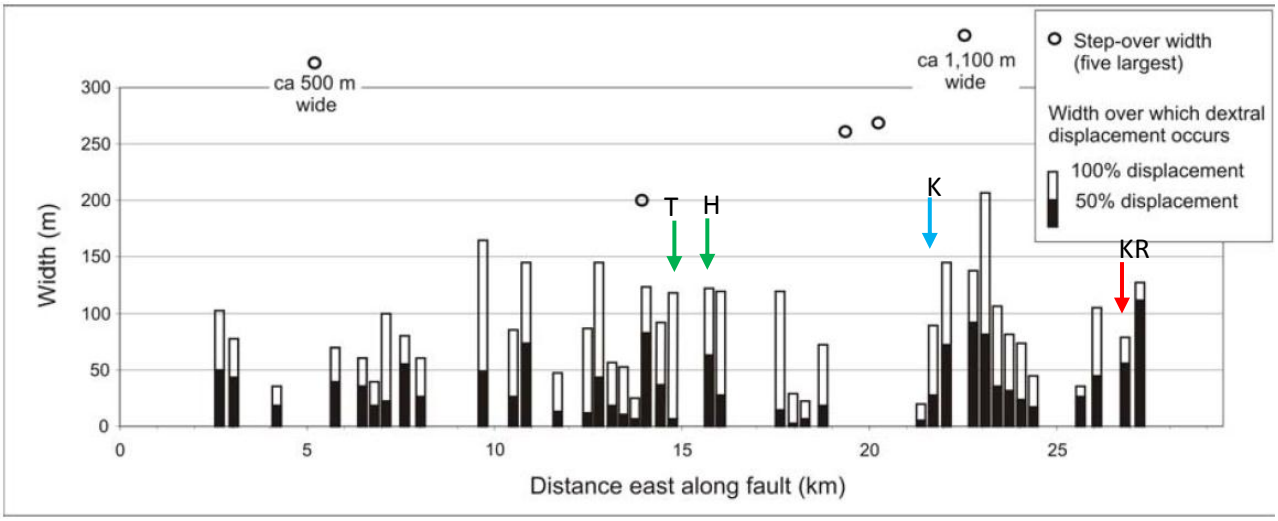

Figure 21: Fault zone widths (horizontal distance) from 40 sites along the Greendale Fault. T corresponds to Telegraph Road; H, for Highfield Road; K for Kivers Road and KR for Kerrs and Railway Roads. These were measured perpendicular to fault strike over the distance is takes to accumulate 50% and 100% of the total co-seismic dextral surface rupture displacement (Source: Van Dissen *et al.*, 2011).

1.3.1 Telegraph Road

The Telegraph Road study site is located mid-way along the central segment of the Greendale Fault. It was set up approx. 7 km south of Charing Cross. Close to the intersection of Telegraph, Clintons and Grange Roads, where approx. 4.6-5.2 m of horizontal and 0.6 m of vertical surface displacement occurred. This displacement is depicted in Figure 19, which shows the road edge lining up with the centreline of Telegraph Road across the fault. At this location a total of 15 marker pins (road nails, RN) were inserted into the ground with pins 1 - 8 on the northern side of the fault and 9 - 15

covering the southern side of the fault (see Figure 23). A base marker was inserted on a post, up the road to reference the equipment from RN 1 before surveying at the location. This was completed so that the azimuths measured in the surveys were reference angles from the back sight or reference frame or marker point (see Figure 23). It is important to note that all coordinates and elevations are measured relative to the initial benchmark and backsight.

1.3.2 Highfield Road

Highfield Road is interesting amongst the selected locations, as the fault crosses the road at a high angle within the highly displaced central section of the Greendale Fault. A spectacular array of shears and cracks were formed in the tarseal road (see Figure 19) (Barrell *et al.*, 2011). Also the surface rupture displaced the roadside fences, hedges and power-poles, as the landscape responded to approx. 4.5 m right lateral horizontal movement as well as an upthrow or vertical displacement of approx. 1 – 2 m of vertical displacement (Barrell *et al.*, 2011). Highfield Road was an ideal location to provide evidence as to whether there was any on-going surface deformation because of these patterns of deformation.

A total of 13 marker pins were inserted in Highfield Road, with pins 1 – 5 on the northern side of the fault and 6 - 13 covering the southern side of the fault. A reference marker pin was inserted in the top of a wooden fence post approx. 250 m up the road of pin 1.

1.3.3 Kivers Road

Heading east along the Greendale Fault trace just after two small steps the trace passes through Kivers Road, a secluded single lane tarsealed road (see Figure 20). This is the last road intersected by the fault trace before the largest en-echelon step approx. 1 km wide (Quigley *et al.*, 2012).

At this site a total of 11 marker pins were installed with 1-5 on the northern section of the fault and pins 6-11 on the southern section of the fault. Along the western fenceline north of pin 1 a reference marker pin was also inserted in for surveying (see Figure 25).

1.3.4 Kerrs Road and Railway Road

The last two sites were positioned along the eastern tip of the Greendale Fault trace at Kerrs and Railway Roads near Rolleston (see Figure 20). Kerrs Road was set up with 8 marker pins installed, with 5 on the northern section for the fault and 3 on the southern section. Railway Road, however, is slightly different to the other sites as the point at which the fault passes through the road is not a

sealed section of road making it difficult to position the pins across a clearly defined fault. Fortunately, Railway Road intersects Kerrs Road perpendicularly along a sealed section of the road. Six marker pins were installed (see Figure 26). Further west along Railway Road (approx. 300 m), an iron waratah was selected as ideal position for the reference marker.

Following the insertion of the pins at each of the above locations, they were then resurveyed over the period of 2010-2012 to monitor for displacement relative to the reference marker or frame. This was completed using; a surveyor's total station, tripod, reflector staff and reflector prism (see Figure 22). The surveying process involved the following steps:

- Step 1: Set the total station and tripod over marker pin 1, or A in the case of Railway Road making sure it is positioned level and in the centre of the marker pin.
- Step 2: Reference nail (RN) 1 at the location with the reference point or marker (see Figures 24-26). To do this the reflector was placed on the reference marker pin and by observing the reflector through the total station site gauge, a reading was taken. In doing this the azimuths measured in the survey were reference angles from the back sight or reference point. It is important to note that all coordinates and elevations taken were therefore relative to this backsight or reference frame or marker. Once referenced the survey could begin as the azimuth would now be consistent through each of the surveys assuming the reference point remained in the same position.
- Step 3: move the reflector to the second marker pin. Once the reflector had been sited through the total station, a reading can be taken. This will measure the distance and angle with respect to the total stations location. Make sure this measurement has been recorded.
- Step 4: repeat step 3 for the remaining marker pins. Taking note of the of the distances and azimuths measure for each point.

Figure 22: The equipment required to complete the outlined survey; 1) tripod, 2) reflector staff, 3) protection case for the theodolite/total station, 4) data card for the total station, 5) total station, and 6) reflector prism (Source: activetectonics.asu.edu/Total station/checklist.html

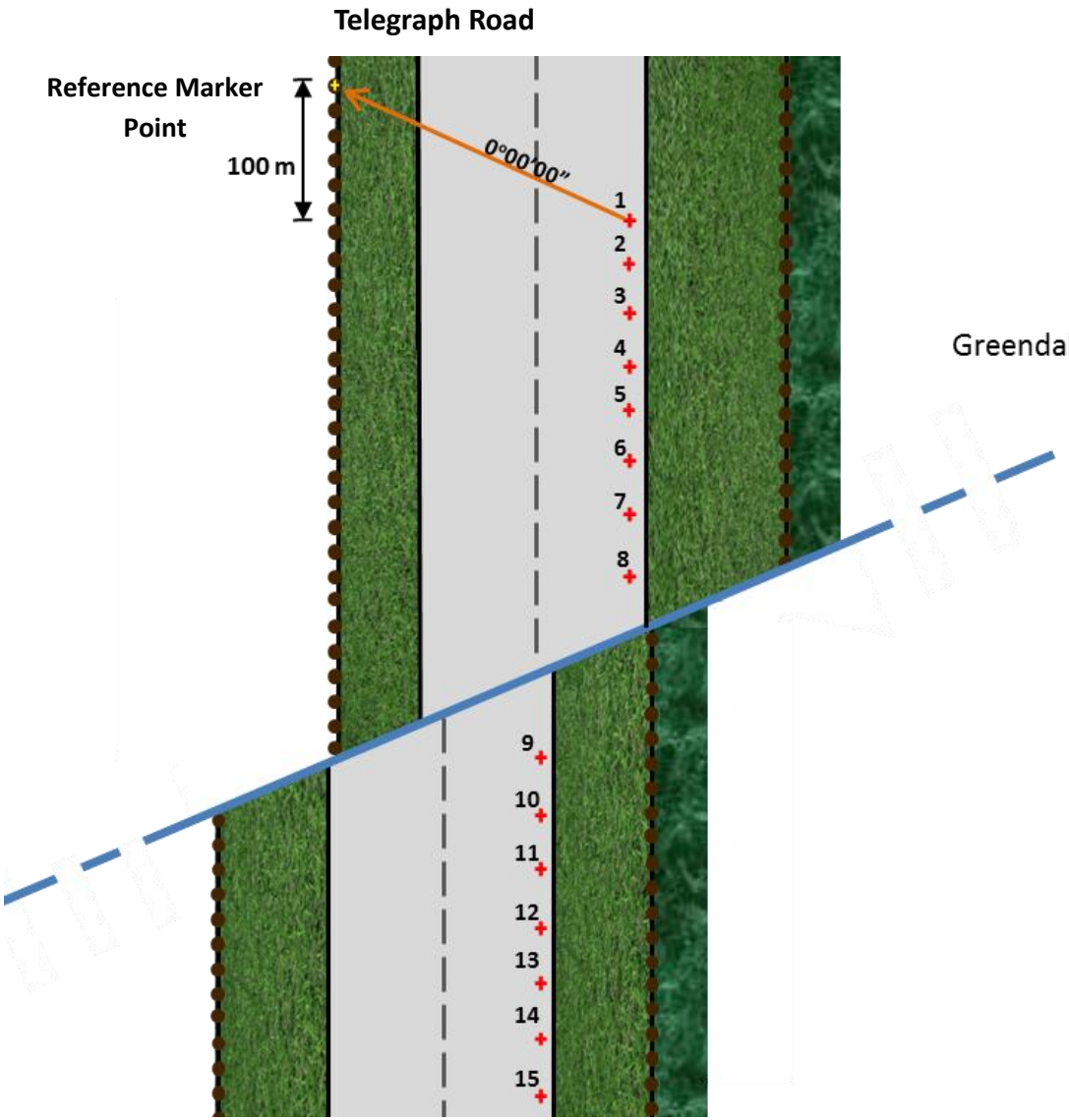

Figure 23: Schematic representing the fault creep survey setup along Telegraph Road, and identifies the locations of marker pins RN 1-15 with respect to the intersecting fault trace

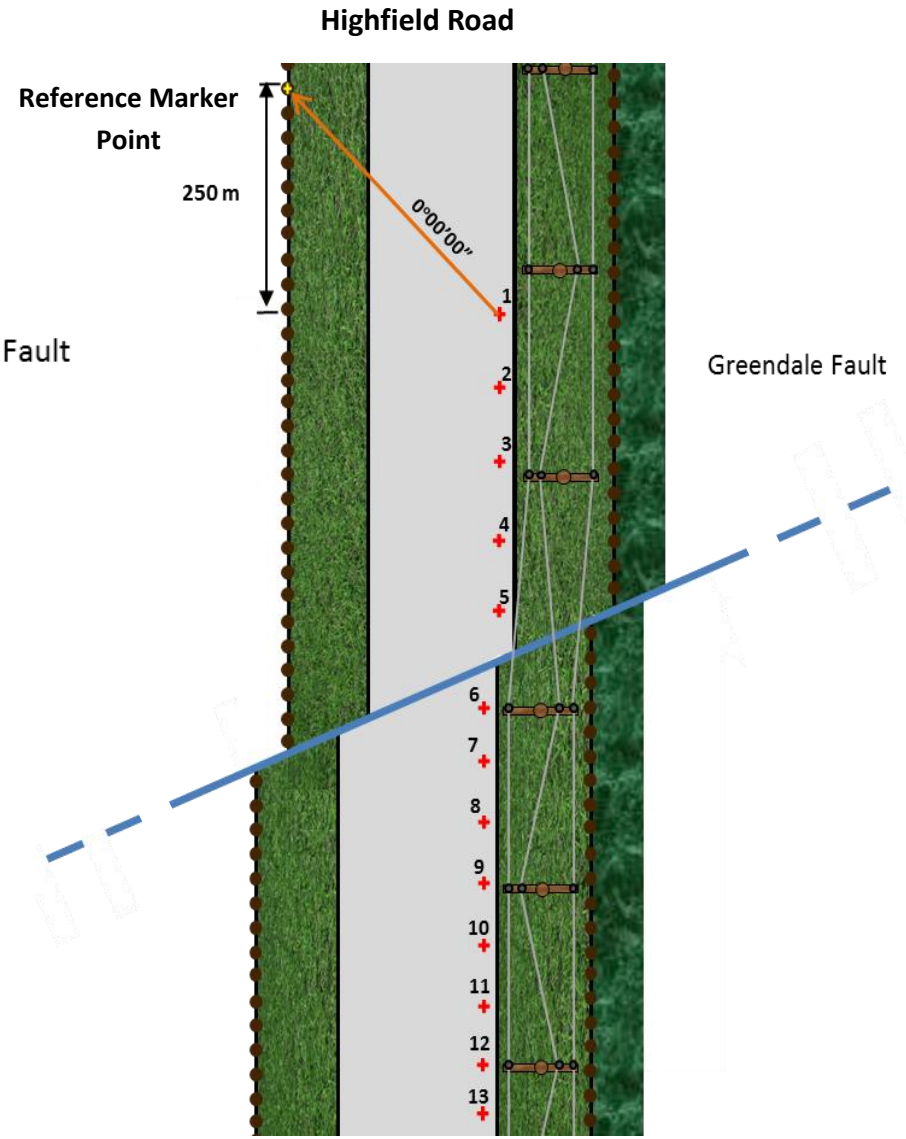

Figure 24: Schemtaic setup for the fault creep survey along Highfield Road whilst also identifying each of the marker pins RN 1-13 positions with respect to the intersecting fault trace.

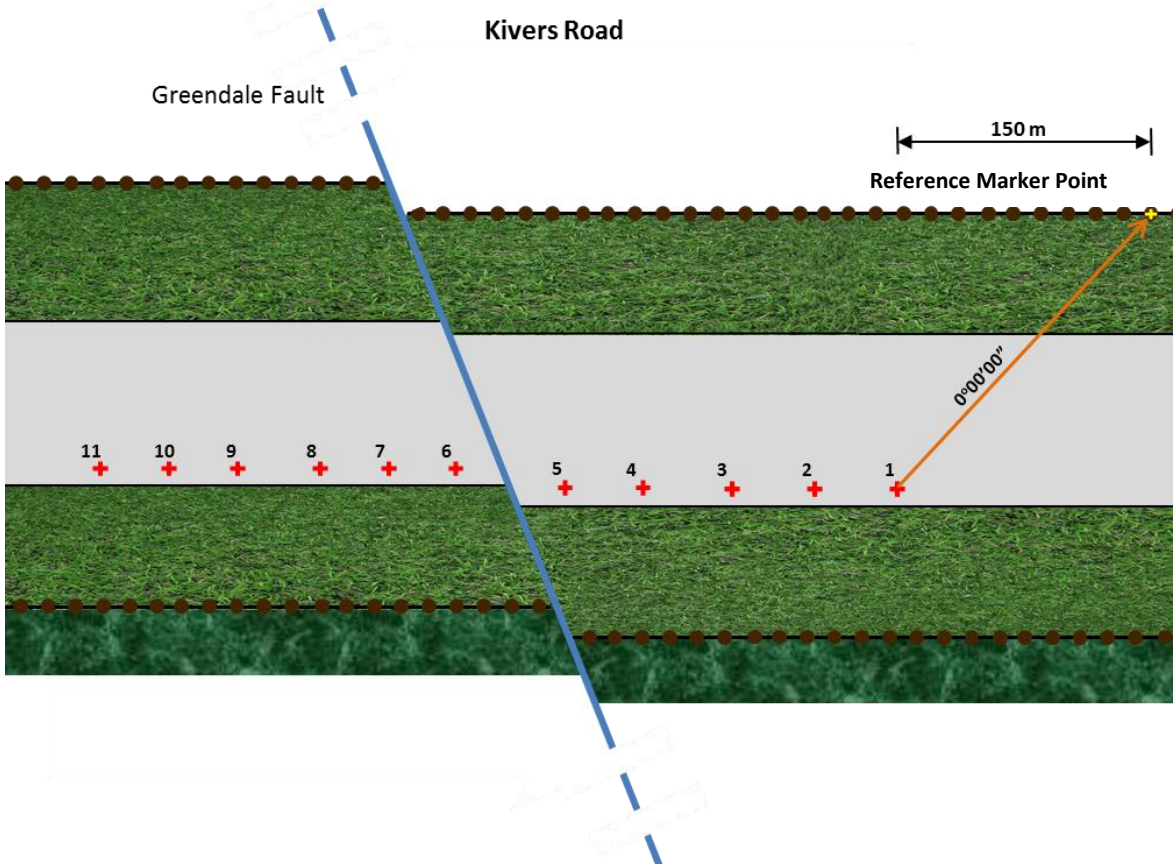

Figure 25: represents a schematic of the Kivers Road survey setup identifying the marker pin locations of RN 1 – 11.

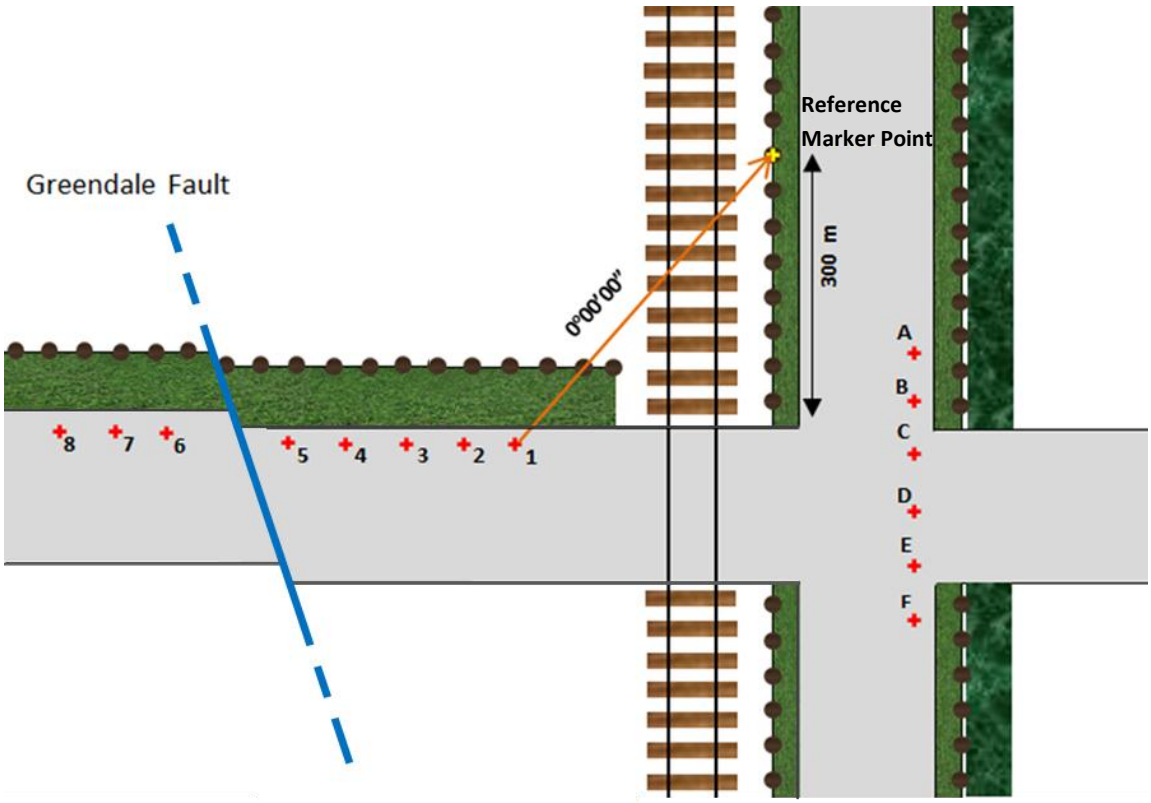

Figure 26: is a schematic of the layout for the Kerrs Road and Railway Road show marker pins RN 1-8 and RN A-F. Note that position of the Railway survey markers running almost parallel to the fault.

1.4 Results

This section outlines the quality of the data presented and the results found from surveying the marker pins at the each of the five locations. The raw data can be found under the heading fault displacement data in Appendix B.

1.4.1 Data Quality

To create robust quality data, instrumental and surveying induced error was calculated and a number of assumptions were also made. The details for the each are as follows.

Total stations are equipped with distance-measuring electronic theodolites capable of detailed mapping and position-measuring tasks. Top of the line models have a wide range of accuracy capable of reaching 0.5 angular seconds and 2 mm + 2 mm/km, with a range of action up to 5 kilometres (see Table 3) (Rick, 1996; Totalstation, 2012). The type of instrument used in this survey was between a low and middle range. This was established after calculating the error in the dataset.

Table 3: Standard error with total station instruments (source: Rick, 1996). The total station used for the surveys was believed to be in between a low-end and a middle range instrument.

Specification	Low-end Instruments	Middle-range Instrument	High-end Instrument
Angular Accuracy	10'-20'	5' (sometimes 3')	1-3'
Distance accuracy	5 mm + 5mm per km	2-3 mm + 2-3 mm per km	2mm + 2mm per km
Maximum Distance with 1 reflector	300 – 1.0 km	1.0 – 1.5 km	2.0 – 3.0 km
Maximum error at 100m	Angle: 5-10 mm Distance: 5.5 mm	Angle: 2.5 mm Distance: 2.2-3.3 mm	Angle: 0.5-1.5 mm Distance: 2.2 mm

Derivation of measurement error

Error calculated for the surveys, is shown as error bars in the results below (Figures 25-30). The error was calculated for each of the marker pins/points at each location. For example see the derivation of error for RN 2 in Table 4. Using the regression function under data analysis in Microsoft Excel, the range of numbers collected for RN 2 at Telegraph labelled x and y were input. The X column corresponds to a difference in the horizontal position or azimuth of the marker pin with respect to the data from the prior survey (see Table 4). The Y column corresponds to the distance of the pin

from the previous recorded location (see Table 4). Calculating the standard error for each of the survey marker pins provided propagating error along the survey line, which is believed to best indicate whether the displacements are true or fit within the limits of error.

Table 4: a) Results from fault displacement surveys for RN 2. The x and y values were calculated using the following formulas. X=03*SIN(RADIANS(degrees+minutes/60+seconds/3600-(AngleCorectionRN2)) Y=03*COS(RADIANS(degrees+minutes/60+seconds/3600-(AngleCorectionRN2)) with the formula for correcting the angle being (Degrees-180+minutes/60+seconds/3600). B) Output from excel showing the calculated standard error for RN2 at Telegraph Road.

Point	Date	Bearing (D,M,S)			Distance (m)	X	Y	Angle Correction
RN 2	9 Sep 10	186	03	50	20.879	0.000	-20.879	6.0639
RN 2	13 Sep 10	186	03	25	20.882	0.003	-20.882	
RN 2	18 Sep 10	186	01	50	20.880	0.012	-20.880	
RN 2	13 Oct 10	186	03	00	20.875	0.005	-20.875	
RN 2	1 Jul 11	186	01	06	20.860	0.017	-20.860	
						Standard Error	0.007059	

B) SUMMARY OUTPUT

Regression Statistics	
Multiple R	0.724834
R Square	0.525384
Adjusted R Square	0.367179
Standard Error	0.007059
Observations	5

Assumptions

The data and results produced from the fault monitoring surveys rely on a number of assumptions to establish the quality of the data:

1. The installation of each marker pin and reference point at the selected locations were completed and the azimuthal distance recorded accurately on the 9th September 2010.
2. The marker pins were not disturbed throughout the duration of the survey by anthropogenic processes, which was checked and verified throughout the survey. Therefore, the measured displacements reflect natural geological processes.
3. The reference phase or marker provides a quasi-stable orientation marker for the survey line, in which the near field displacements reflect movement of the other pins relative to the location.
4. To produce across fault displacement plots showing the relevant positions of the marker pins with respect to the Greendale Fault trace assumptions were also required. With the

exception of Railway Road which is not intersected by the fault at the survey site, these assumptions include the following:

- At Telegraph Road it was assumed that the principle slip surface of the Greendale Fault trace passed evenly between points RN 8 and 9 (see Figure 21) , whereas,
- For Highfield, Kivers and Kerrs Roads it was assumed that the Greendale Fault trace passed evenly between points RN 5 and 6 (see Figures 22-24).

Overall it is believed the data collected in the surveys and presented in the results to determine whether there is evidence to suggest that there is post-seismic creep on the Greendale Fault are honest and accurate.

1.4.2 Overview of Results

The results for each site are described and presented below. These were calculated from data collected during the surveys completed on the 9th, 13th, and 18th of September 2010; 13th October 2010; and 1st July 2011. These data have been presented graphically showing the displacement along the survey line with respect to the base position, RN 1, as well as the across fault displacements for each location. The raw data and calculation are shown under the heading fault displacement surveys in Appendix B. Note all displacements and direction of motion discussed will be relative to the reference marker at each location. Furthermore, the displacements are internally relative and should not be interpreted as absolute displacements for the Greendale Fault.

1.4.2.1 Telegraph Road

Displacement from RN 2-15with respect to RN 1 for Telegraph Road

Figure 27a Telegraph Road RN 2 to 15 displacements with respect to RN 1, shows the results for displacements occurring along the length of the survey line. Following installation of the marker pins and survey set up on 9th September 2010 the pins were resurveyed on the 13th September. This survey revealed that an initial movement had occurred of approx. 1 cm eastwards. The eastward motion relative to the reference marker continued through until a survey on the 18th September 2010. This indicated that a combined eastward shift of 2 - 4 ± 1 cm had occurred along the survey line. Following this survey, a reoccupation of the points on the 13th October revealed a change in the direction of movement occurred. With 2 - 4 ± 1 cm of westward motion occurring. After an approx. 9 month period the line was resurveyed on the 1st July 2011, revealing that there had been another shift in motion back east. This time approx. 2 – 8 ± 1 cm of eastward motion relative to the reference marker had occurred exceeding the initial movement recorded during the first few weeks (13th and 18th September surveys) following the Darfield earthquake. Overall the northern side of the fault in

Figure 27a illustrates a trend in the shift of motion by 1 - 2 ± 1 cm to towards the east. The southern side of the fault also reflects this eastwards trend in motion though the pins moved 2 ± 1 cm.

Across Fault Displacement for Telegraph Road

Looking at the results for the surveys in a different manner by viewing the marker pins position with respect to the central position of the fault trace (see Figure 27b) the following result were observed.

Following the start of the survey on the 9th September 2010, an inspection of the marker pins on the 13th of September illustrated ≤ 2 ± 1 cm of westward propagation along the northern side of the fault. This motion continued in the period from the 13-18th of September with an additional 5 - 1 ± 1 cm and a maximum of 6 cm by RN 2 occurring. This resulted in a combined average motion of 3 - 4 ± 1 cm westward for the period from 9th-18th September. Smaller westward movement continued until the next survey was completed on the 13th of October 2010. This trend of westward propagating continued to the final survey on the 1st July 2011. The southern side of the fault, however, reflected a general trend of 1 ± 1 cm eastwards throughout the 9th September 2010 to 1st July 2011 surveys. The only exception was the 13th October 2010 survey which showed small westward motion of less than 2 ± 1 cm. Interestingly, Figure 27b indicates that the majority of movement is occurring furthest from the fault trace, marker pins RN 2-5 on the northern side and RN 11-15 on the southern side.

Overall, Figures 27a and b indicate that near surface post-seismic or aseismic movement is occurring outside the bounds or limits of error at Telegraph Road. This movement looks sporadic and does not appear to reflect a trend with time. The majority of movement associated with Telegraph Road appears to be on the southern section/block of the fault with respect to the Greendale Fault trace.

1.4.2.2 Highfield Road

Displacement from RN 2-13 with respect to RN 1 for Highfield Road

The survey results for along the line displacements from RN 2 – 15 with respect to RN 1 for Highfield road are shown in Figure 28a. In the week following installation of the pins and resurveying on the 13th September, the survey line revealed initial eastward movement less than 2 ± 0.7 cm on the northern side and up to 5 cm on the southern side of the fault. This was followed by approx. 1 - 3 ± 0.7 cm of western motion, through to the 18th September 2010. A resurvey of the marker pins on the 13th October 2010 revealed a change in the direction of movement had occurred. The pins now indicated movement of 2 ± 0.7 cm eastwards. By looking at the separate sides of the fault, overall the northern side of the fault illustrates a trend in the shift of motion by 1 ± 0.7 cm to towards the

east with respect to the position of the original survey (9th Sept). The southern side of the fault also reflects this eastwards trend in motion though the pins moved approx. 0.02 - 0.04 ± 0.007m.

Across Fault Displacement for Highfield Road

The results for the markers pins positions with respect to the fault trace can be seen in Figure 28b. From 9th to 13th September an initial westward trend in motion occurred for the northern side of the fault. RN 2 was an exception to this as the point illustrates significantly larger movement in the order of approx. 0.07 ± 0.007 m. The 18th September 2010 survey showed a directional change with the marker pins shifting 0.005 m eastwards. Once again the motion from RN 2 was significantly larger (0.06 m). This movement did not exceed the original position of the marker pins on the 9th September. The next survey on the 13th October showed that this movement had been recovered and was again heading westwards. The movement of the pins during this period tracked close enough to be in the same positions as when the marker pins were measured in a month earlier, on the 13th September. On the southern side of the fault, Figure 28b illustrates an initial movement of 0.01 – 0.04 ± 0.007 m to the west with RN 11-13 reflecting the larger range of movement. Resurveying the points on the 18th September 2010 revealed that 0.005 - 0.02 ± 0.007 m of westward movement had occurred in the interval between surveys. Eastward motion continued once again during the period following, with 0.01 - 0.02 ± 0.007 m of movement being recorded by the 13th October 2010 survey.

The results in Figures 28a and 28b also identify one erroneous point; RN 10 that was consistently dissimilar to the motion detected in the other survey pins. The irregularity in this point is most likely due to an incorrect setup position. Though less likely, it could also reflect different motion e.g. subsidence, within its setting than other areas of the survey line. Also worth mentioning, is that there was no data available for the 1st July 2011 survey along Highfield Road. This is because the road around the trace of the Greendale Fault was repaired in this interval covering over the marker pins and thus they were not able to be located. Overall, Figures 28a and b also provide evidence to suggest that post-seismic movement occurred along the fault trace at Highfield Road.

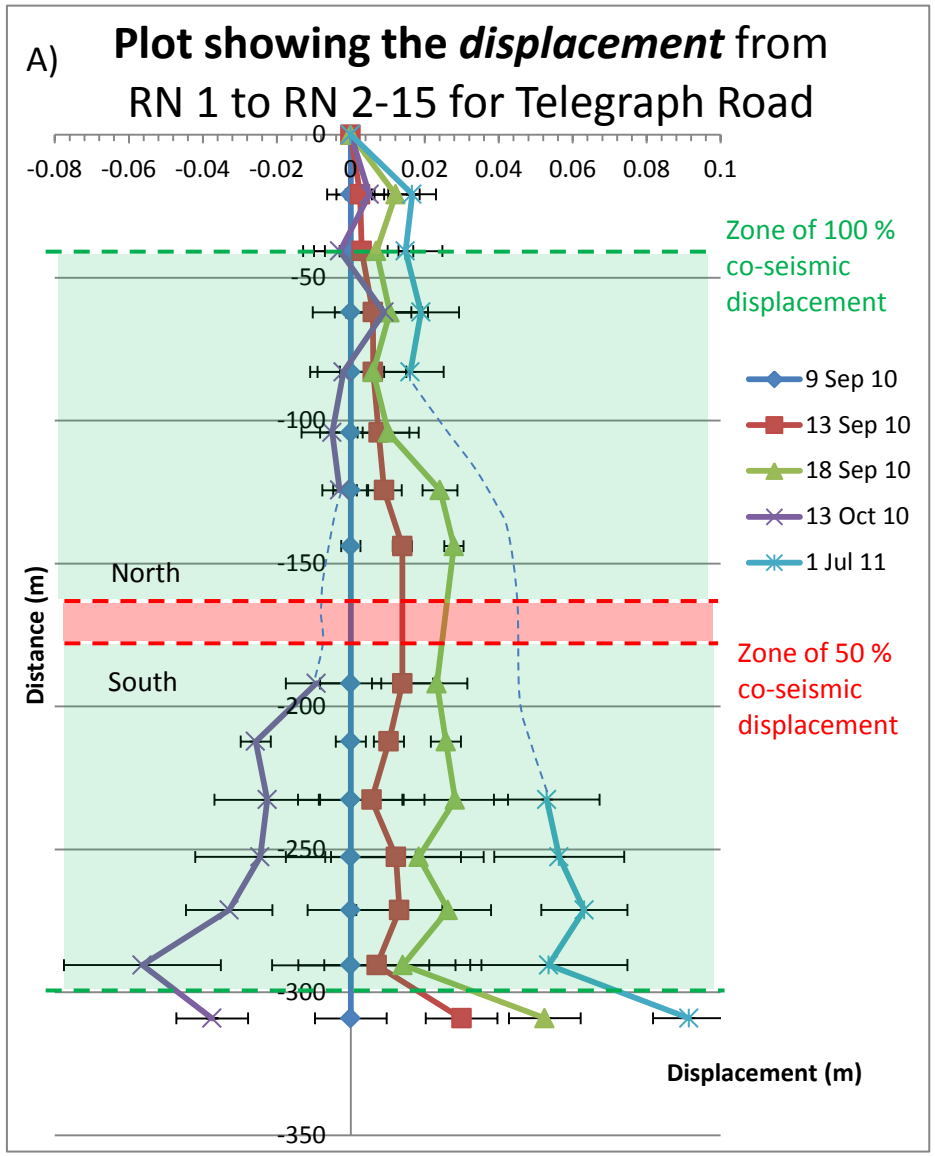

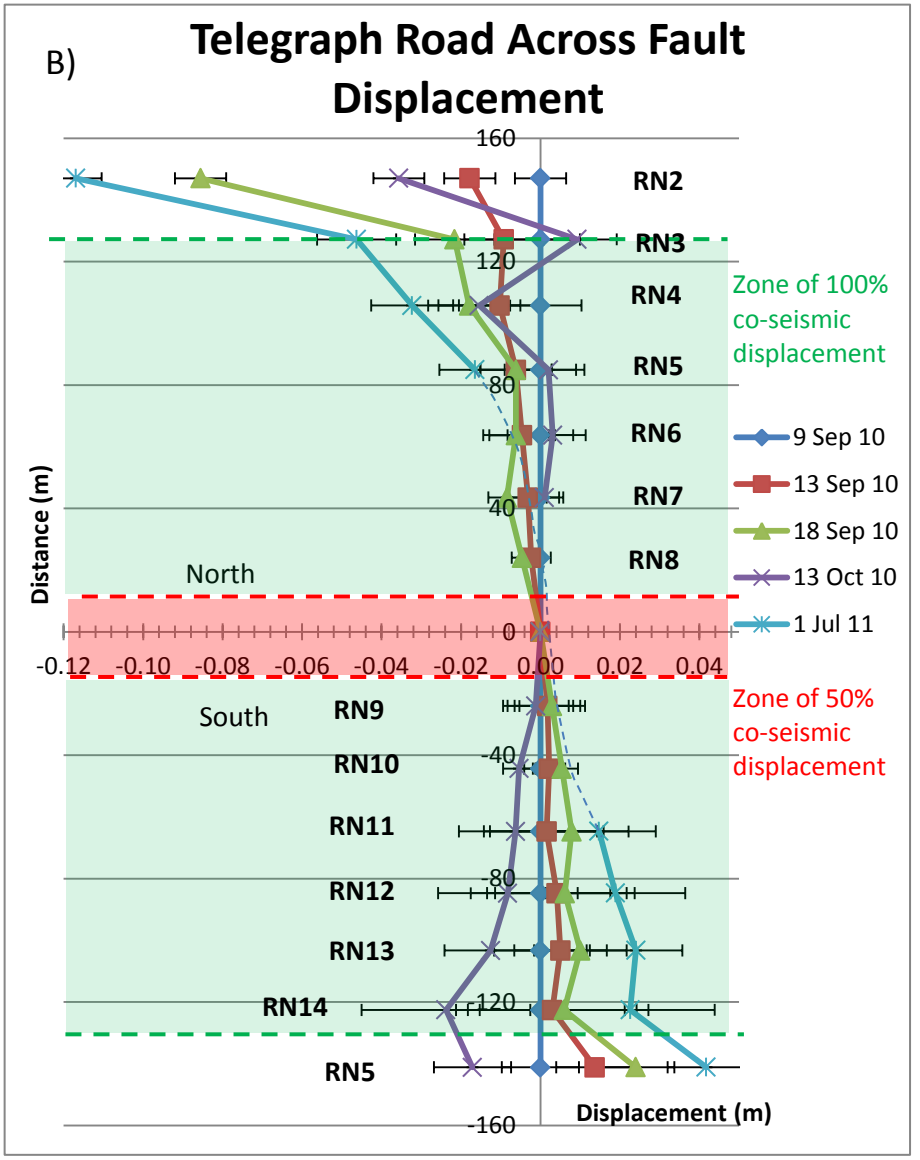

Figure 27a & b: Results from the fault creep surveys along Telegraph Road. The the dashed red line represents the Greendale Fault Trace and the red and green zones reflect zones of strike over which it takes to accumulate 50% and 100% of the total dextral surface rupture displacment at this site along the Greendale Fault. These distances were sourced from Figure 3 in Van Dissen *et al.*, 2011.

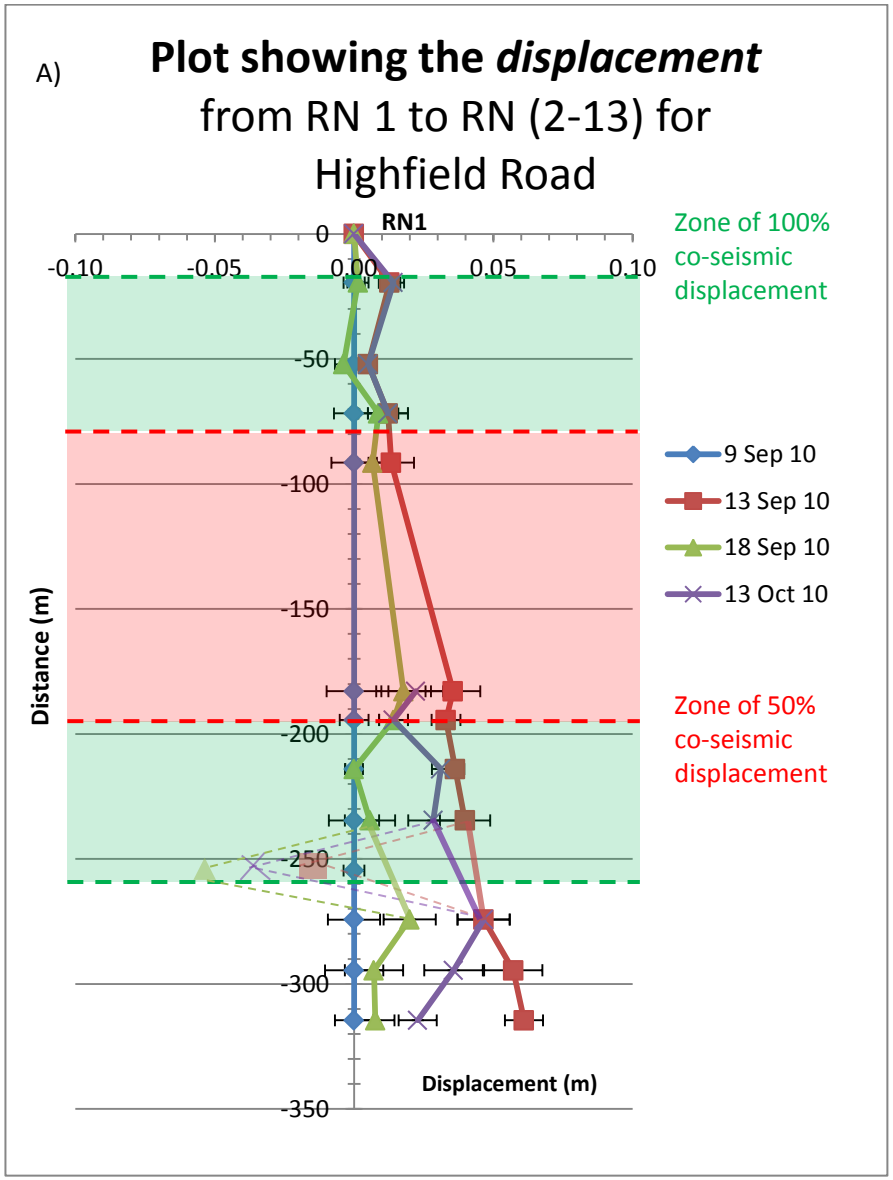

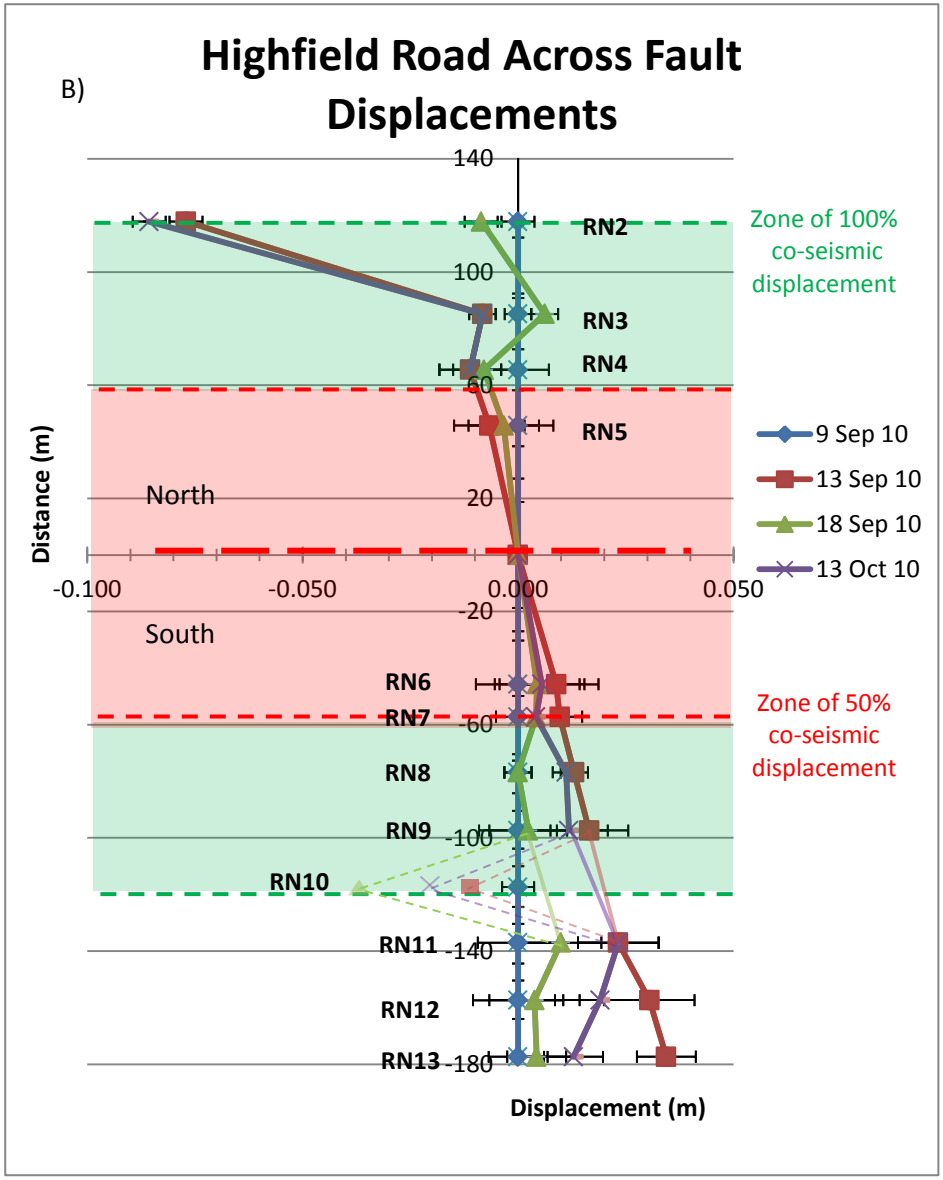

Figure 28a & b: Results form the fault creep surveys along Highfield Road. The the dashed red line represents the Greendale Fault Trace and the red and green zones reflect zones of strike over which it takes to accumulate 50% and 100% of the total dextral surface rupture displacment at this site along the Greendale Fault. These distances were sourced from Figure 3 in Van Dissen *et al.*, 2011.

1.4.2.3 Kivers Road

Displacement from RN 2-11 with respect to RN 1 for Kivers Road

Figure 29a shows the displacements for marker pins RN 2-11 with respect to RN1 for Kivers Road. The northern side of the fault in Figure 29a shows movement patterns of the marker pins that correspond to both eastward and westward movement. Marker pins RN 2, 4 and 5 reflect a shift of ≤ 2 ± 1 cm eastwards, whereas RN 3 indicates approx. 1 ± 1 cm of westward motion. This back and forth motion is only reflected in the 13th October survey for the southern side of the fault in Figure 29a. The rest of the surveys; 13th and 18th September 2010, and 1st July 2011 indicate a general eastern trend in motion with respect to the original positions of the survey line on 9th September.

The southern section/side of the fault, on the other hand illustrates patterns of post-seismic motion taking place with initial eastward movement of less than 4 ± 1 cm between installing the pins on 9th September and resurveying on the 13th September 2010. This initial motion is compensated by a change in direction, with westward motion of less than 1 ± 1 cm occurring in the intervals between surveys on the 18th September and 13th October 2010. After the survey of the 13th of October the movement shifts back eastward with less than 1 ± 1 cm of motion occurring up until the 1st July 2011.

Across Fault Displacement for Kivers Road

Looking at Figure 29b a similar trend to 29a is apparent, with alternating eastern and western motion for the northern section of the fault. However, by labelling the motions displayed by RN 3 as erroneous and therefore disregarding them the northern side of the fault starts to reflect some more obvious trends. Following the 13th September 2010 survey RN 2, 4 and 5 illustrate initial westward motion of approx. 1, 0.1 and 0.1 ± 1 cm, respectively. This westward trend in motion continued slightly following the next survey on the 18th September 2010 for RN 4 and 5. These points both show small indications of movement < 0.1 ± 1 cm. RN 2, however, reflects a shift to the east in its position, with 0.6 ± 1 cm motion. After a three week period the 13th of October survey reflects a pronounced westward shift in motion along the northern side of the fault. RN 2 and 5 shifted west by approx. 1 ± 1 cm, whilst RN 4 illustrates close to 2 ± 1 cm of motion. After this period of movement a change in direction occurs for RN 4 shifting eastward slightly by 1 ± 1 cm from 13th October to 1st July 2011. RN 2 on the other hand continued moving west by 1 ± 1 cm. The marker pin, RN 5 could not be located during the 1st July survey, thus no data was collected for its position.

In contrast, the southern side of the fault illustrates a trend in relative eastward motion with RN 9, 10 and 11 producing the majority of motion. The 13th September 2010 survey illustrated a starting shift in motion eastwards of 2 ± 1 cm tapering off to < 1 ± 1 cm the closer it got to the fault. This initial motion was followed by a westward shift of approx. 0.1 (RN 6 and 7) - 1 (RN 9, 10 and 11) ± 1 cm, following the 18th September survey. Surprisingly, survey markers RN 10 and 11 did not move following the next survey on the 13th of October 2010. The other sites, however, reflected a small transposition, up to 0.4 ± 1 cm, west with the exception of RN 8. This point showed a shift east by 0.2 ± 1 cm. The final survey on the 1st July 2011 shows the majority of the marker pins moving east again by less than 1 ± 1 cm. RN 8 is again an exception shifting west by 4 ± 1 cm.

From Figure 29b the northern side of the fault reflects a general western shift in motion with respect to the position of the marker pins at the beginning of the surveying, on the 9th September 2010. Whereas, the southern side of the fault indicates an overall trend in the shift of points RN 6-11 relatively eastward for the period of monitoring.

The overall results for Kivers Road, outlined above, fit within the limitations of error reflected by the error bars in Figures 29a and 29b. This makes it difficult to confirm if post-seismic motion actually occurred or whether apparent displacements are a result of measurement error or limitations of the equipment used. This could also be used to explain why these results reflect complicated trends of motion.

1.4.2.4 Kerrs Road

Displacement from RN 2-8 with respect to RN 1 for Kerrs Road

Looking at the results for Kerrs Road displacements in Figure 30a the northern side of the fault indicates both relative eastwards and westward motion following the September 13 2010 survey. RN 2 and 3 indicate 0.1 ± 0.5 cm motion east, whereas RN 4 and 5 shift west by 0.6 ± 0.5 cm. In contrast, the marker pins on the southern side of the fault (RN 6-8) illustrate a clear indication of westward motion ≤ 1.8 ± 0.5 cm. The next survey on the 18th September 2010 reveals a period of eastward movement along the whole survey line. This movement corresponds to approx. ≤ 2 ± 0.5 cm. Following a three week interval in surveys, a trend in eastern motion continued. The northern side of the fault with the exception of RN 4 had very little or no eastern movement of < 0.1 cm. The southern side of the fault however, reflected approx. 0.2 ± 0.5 cm eastwards motion. The last period of motion from 13th October 2010 until 1st July 2011 portrays an apparent westward motion of less than 0.5 ± 0.5 cm.

Across Fault Displacement for Kerrs Road

Following the installation of the marker pins on 9th September 2010 and a resurvey of RN 2-8 on the 13th September 2010, a combination of western and eastern motion can be seen in Figure 30b for the northern side of the fault. RN 2 and 3 shifted west by 1 and 0.5 ± 0.5 cm, respectively. RN 4 and 5, however, can be seen to shift east by 0.5 ± 0.5 cm. On the southern side of the fault the initial motion was solely illustrated as a westward shift up to 0.8 ± 0.5 cm, relative to the original position of the marker pins.

The next survey on the 18th September 2010 illustrates a trend in a westward shift along the northern side of the fault, with RN 2 and 3 shifting 2 and 1.2 ± 0.5 cm respectively. RN 4 and 5 reflected smaller motion west of less than 0.5 ± 0.5 cm. This motion changed to the east, crossing over the fault and heading onto the southern side of the fault. It was, however, only small offsets occurring. RN 6 moved 0.1 ± 0.5 cm, RN 7 moved 0.2 ± 0.5 cm, whilst RN 8 shifting by approx. 0.6 ± 0.5 cm.

The 13th October 2010 survey continued this trend of different movement patterns on either side of the fault, with the northern side of the reflecting less than 1 ± 0.5 cm of western movement. The southern side of the fault illustrates an eastern shift of up to 1 ± 0.5 cm in the location of the marker pins. Even with this eastern movement, the marker pins on the southern side of the fault after the 13th October 2010 survey are still located to the west of the original position from the 9th September 2010 survey.

The final survey, approx. 10 months later on the 1st July 2011, indicates an eastern shift in the direction of the marker pins along the northern section of the fault, less than 0.5 ± 0.5 cm. Unfortunately only one marker pin was able to be located on the southern side of the fault, RN 8. This indicates small, less than 0.2 ± 0.5 cm of western change in the position of the marker pin.

Overall Figure 30a shows a general trend in the northern side of the fault moving eastwards, from their original position on the 9th of September 2010, with respect to the southern side. Whereas, the southern side of the fault shows a trend in motion westwards, from their original position on the 9th of September 2010, with respect to the northern side. The across fault displacements in Figure 30b show the northern side reflecting an overall trend to the west of the original position of the pins from the 9th September 2010 survey. In contrast, the southern side shows a tightly grouped trend in motion to the west of the original position of the marker pins. The results for Kerrs Road, summarised above, reflect obvious trends that are believed to reflect post-seismic motion. However,

in a lot of cases this movement is within the limitations of error, making it difficult to confidently validate this as movement.

1.4.2.5 Railway Road

Displacement from RN A-F with respect to RN 1(on Kerrs Road) for Railway Road

Due to its location and orientation to the fault Railway Road provides a unique look at post-seismic motion along the Greendale Fault (referred to above but see Figure 26). Figure 31 shows the displacement plot of the results for the surveys at Railway Road. It shows a clear trend of movement south towards the fault trace. This is reflected in the period of motion between the 9th and 13th of September surveys, with points RN A-F reflecting a minimum movement of 3 ± 1 cm up to a maximum of 6 ± 1 cm. Surveys on 13th October 2010 and 1st July 2011 also reflect the position of the pins around the same location as the 13th survey. The only survey showing significant movement back toward the original position of the marker pins is the 18th September survey. This reflects approx. 2 ± 1 cm of northern motion. However, at this point in time the pins were still reflecting at least 2 up to 4 ± 1 cm of motion towards fault or the south.

These results for Railway Road indicate there is at least 2 – 4 ± 1 cm of motion towards the fault or south of the original position of the marker pins on 9th September 2010. Some of the movement reflected in the figure fits within the limitations of error, but at this site it is believed this does not affect the overall confirmation of post-seismic displacement present.

Overall, the results outlined for each of the surveys locations provides evidence to confirm that the post-seismic deformation or displacement is occurring along the Greendale Fault trace. However, discussion is required to determine the mechanisms behind this movement.

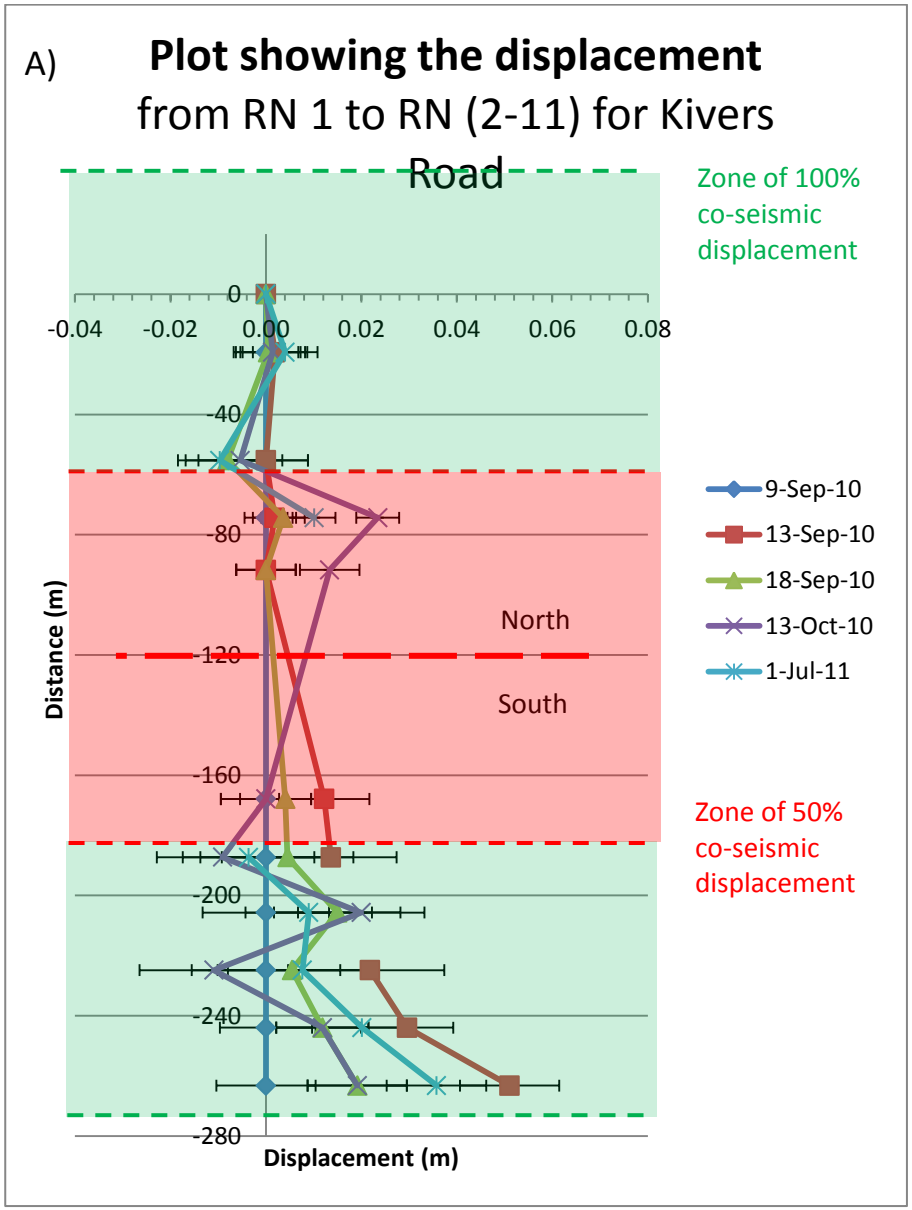

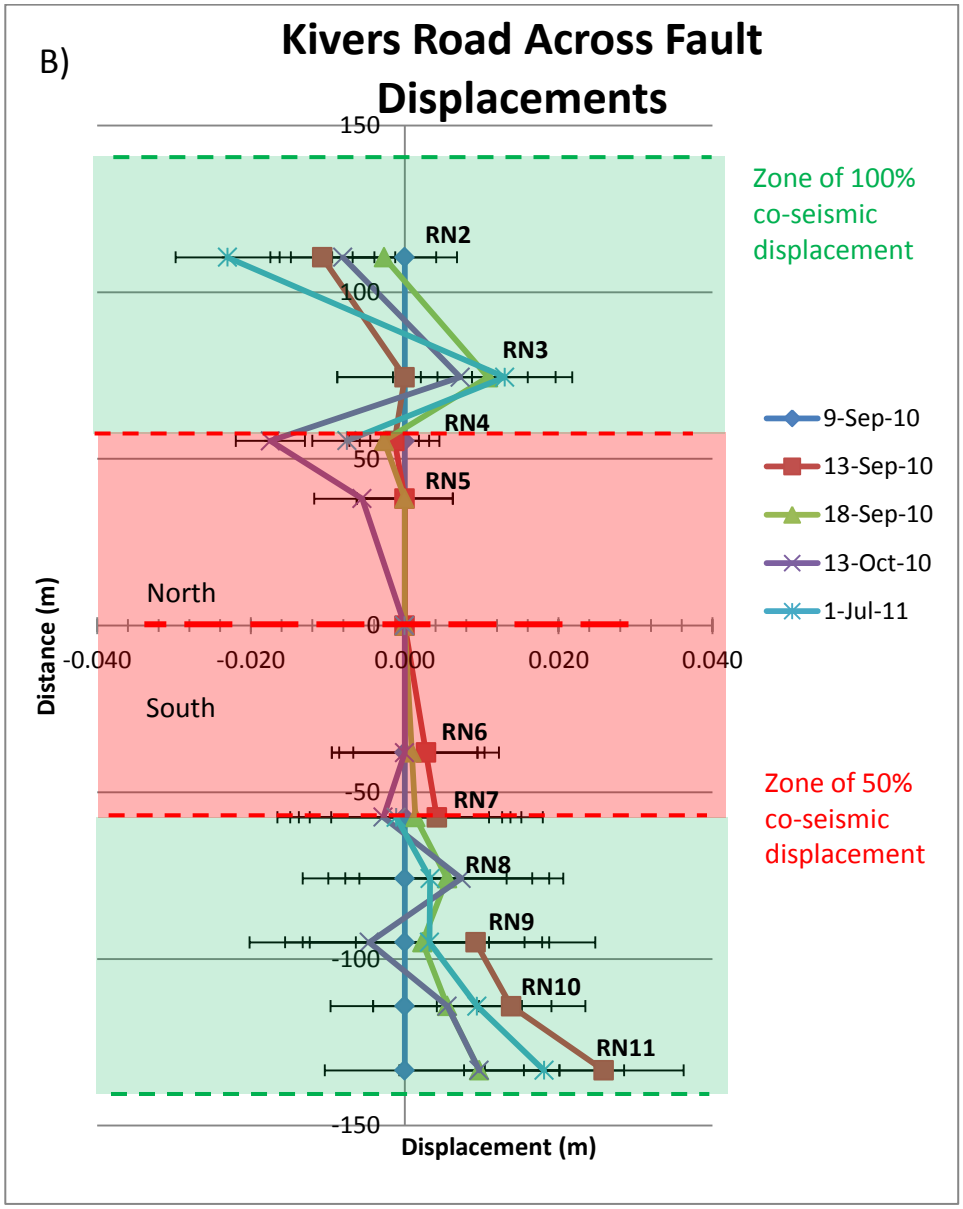

Figure 29a & b: Results from the fault creep surveys along Kivers Road. The the dashed red line represents the Greendale Fault Trace and the red and green zones reflect zones of strike over which it takes to accumulate 50% and 100% of the total dextral surface rupture displacment at this site along the Greendale Fault. These distances were sourced from Figure 3 in Van Dissen *et al.*, 2011.

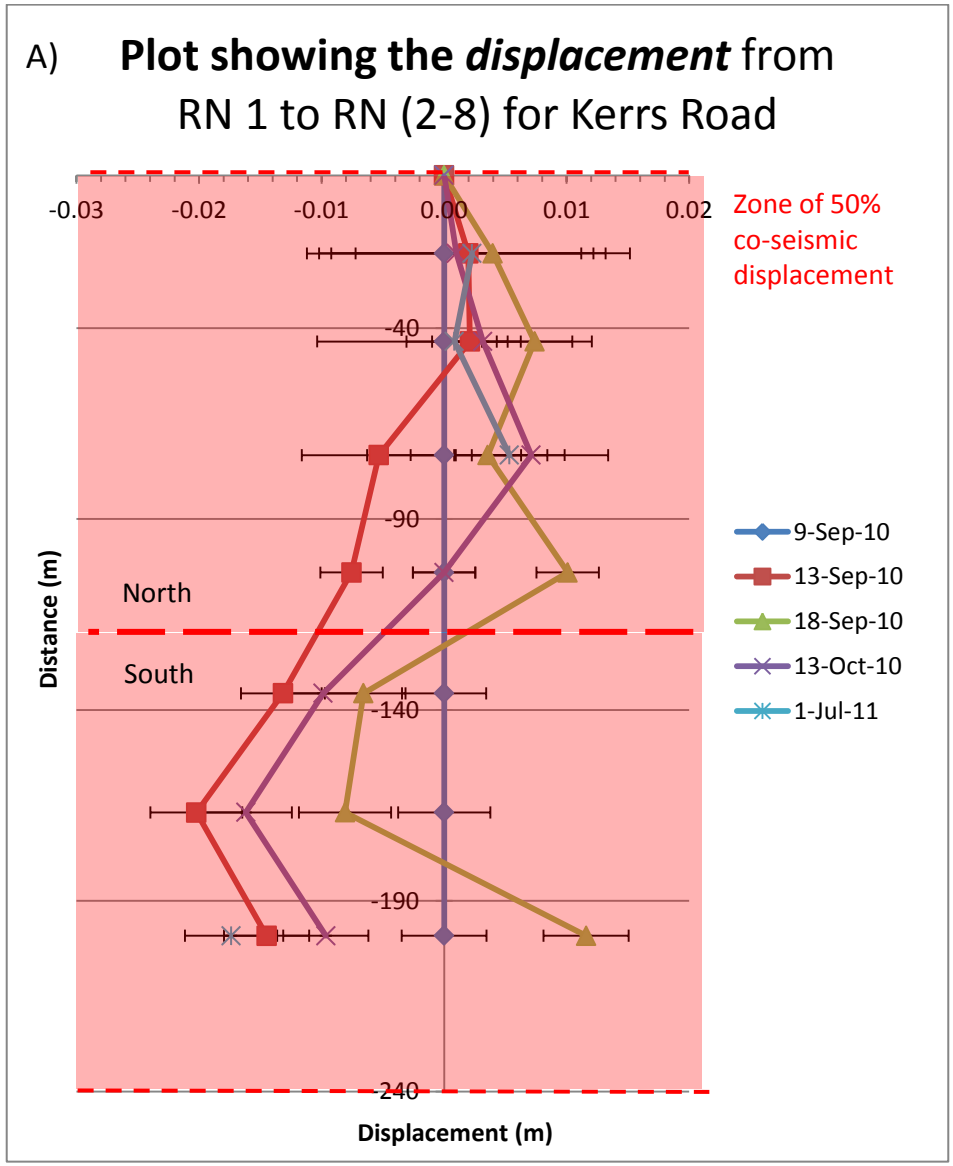

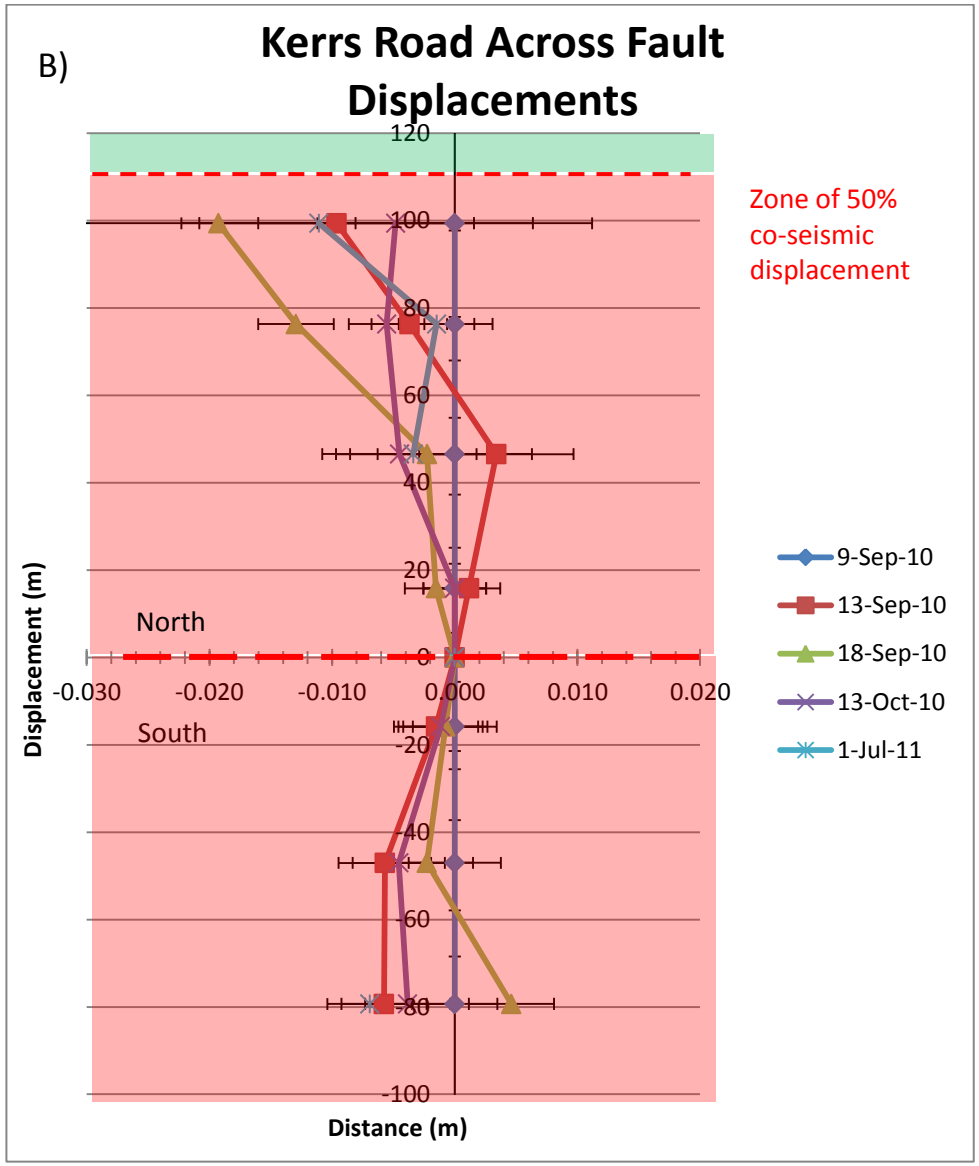

Figure 30 a & b: Results from the fault creep surveys along Kerrs Road. The the dashed red line represents the Greendale Fault Trace and the red and green zones reflect zones of strike over which it takes to accumulate 50% and 100% of the total dextral surface rupture displacment at this site along the Greendale Fault. These distances were sourced from Figure 3 in Van Dissen *et al.*, 2011 note: the dashed red line represents the Greendale Fault Trace.

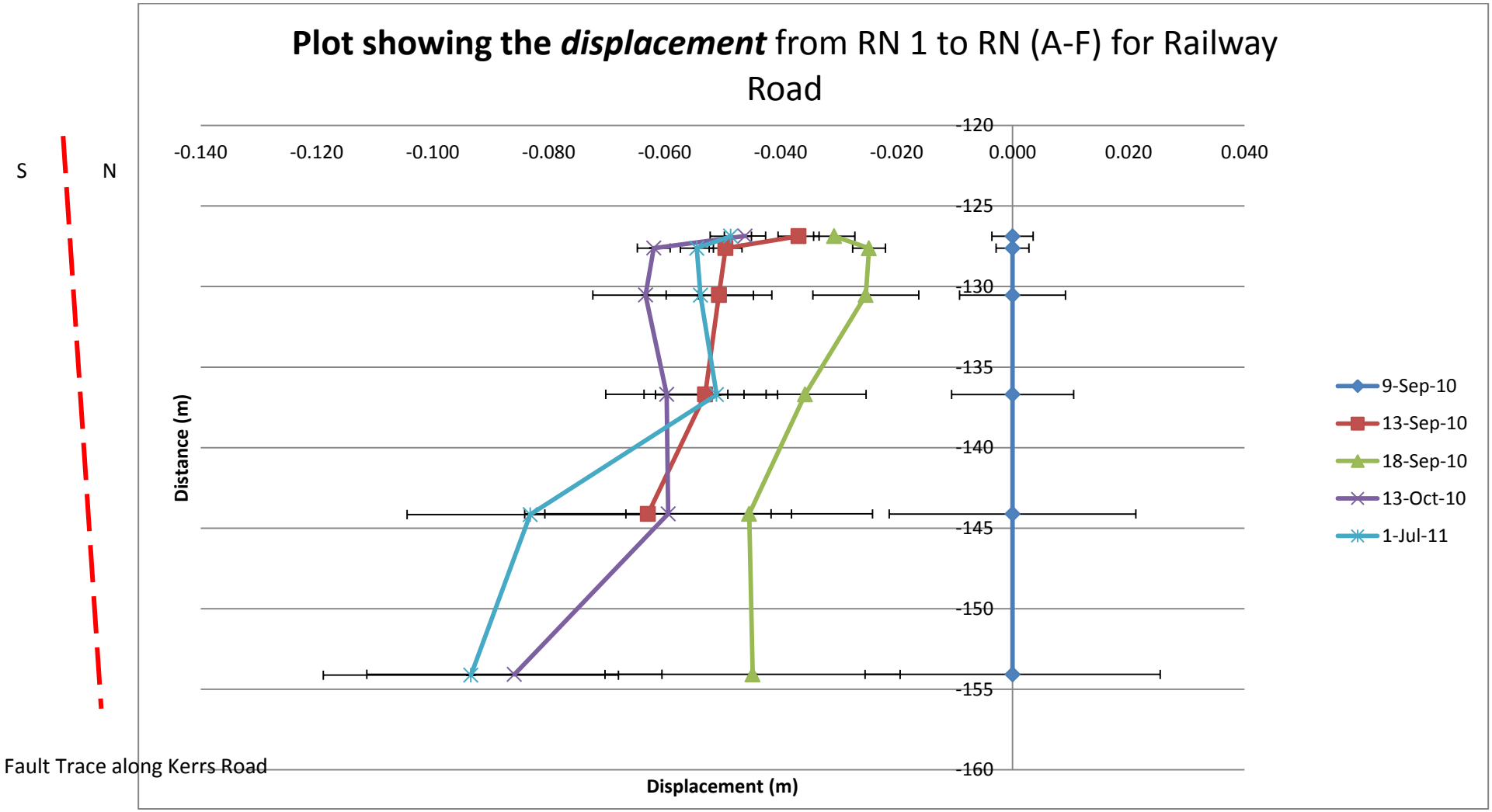

Figure 31: Results from the fault creep surveys along Railway Road. Due to its setting identified in the methodology section it does not cross the fault but reflects the same northern side of the Greendale Fault with Kerrs Road (points RN 2-5). It is also to far from the fault zone to have any zone of co-seismic displcament.

1.5 Discussion

This section discusses the results outlined in the previous section, as well as suggesting possible mechanism(s) behind the recorded post-seismic motion. It also looks at evaluating whether these mechanisms are robust and if so, what the most suitable mechanism responsible for the observed movement could be. Theories are explored to explain how these mechanisms resulted and their implication on societal issues such as rebuilding on or near fault zones.

1.5.1 Discussion of the Results

Overall, the results for this section provide confirmation that post-seismic movement is occurred along the Greendale Fault. This is reflected by the results outlined at four of the five surveying locations; Kerrs Road and Railway Road at the eastern tip of the Greendale Fault and Highfield Road and Telegraph Road within the central segment of the fault trace. Telegraph Road and in particular Highfield Road depict the best indications of post-seismic movement or displacement. Kerrs and Railway Road provide an indication of post-seismic motion but the results seem more complicated than the other two sites. Kivers Road, which sits between the other areas, exhibits no direct trend in post-seismic motion because all measured displacements fit comfortably within the limitations of error.

The confirmation of post-seismic motion by this study is in agreement with a GPS displacement survey by Beavan *et al.* (2010), although dextral displacements were recorded in this study. Beavan *et al.* (2010) revealed that post-seismic deformation was taking place during the first 8 weeks following the main fault rupture, although only a small amount, ≤ 1 cm, had been detected (less than 2% of the co-seismic motion). However, it is believed the 8 weeks of surveying underestimated the amount of post-seismic motion occurring along or within the deformation zones of 100% co-seismic displacements. Furthermore, the direction of motion changed after an initial recovery period of weeks to a month.

1.5.2 Logic Trees

Production of the logic trees was useful in highlighting the thought processes behind trying to understand the datasets and results. In particular it enables a robust dataset by showing the processes used to determine the likely mechanism(s) behind the post-seismic movement. At the same time it provides explanations as to how these mechanism(s) may have resulted. The logic trees are as follows:

Figure 32: Telegraph Road logic tree

Telegraph Road Logic Tree

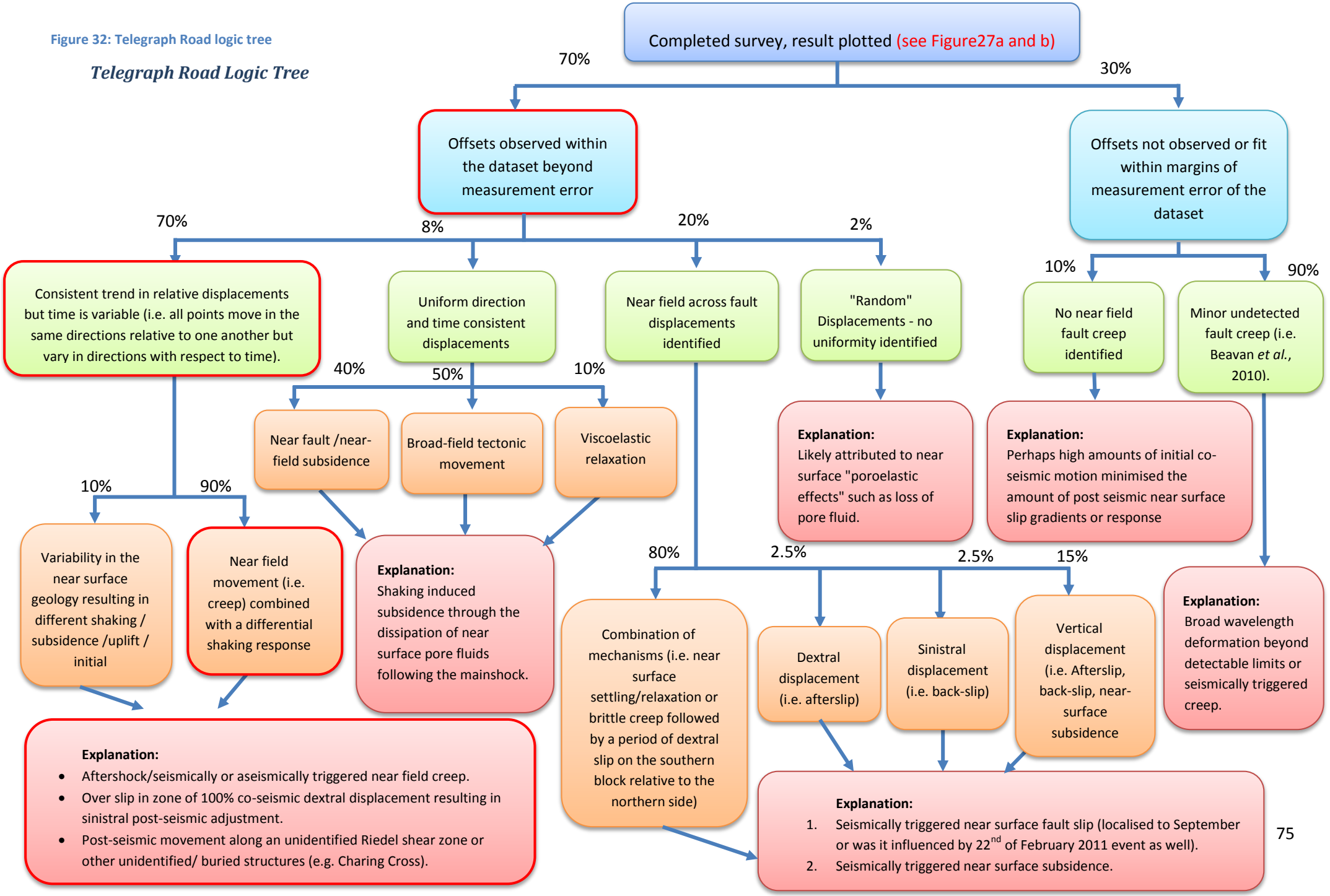

Figure 33: Highfield Road Logic Tree

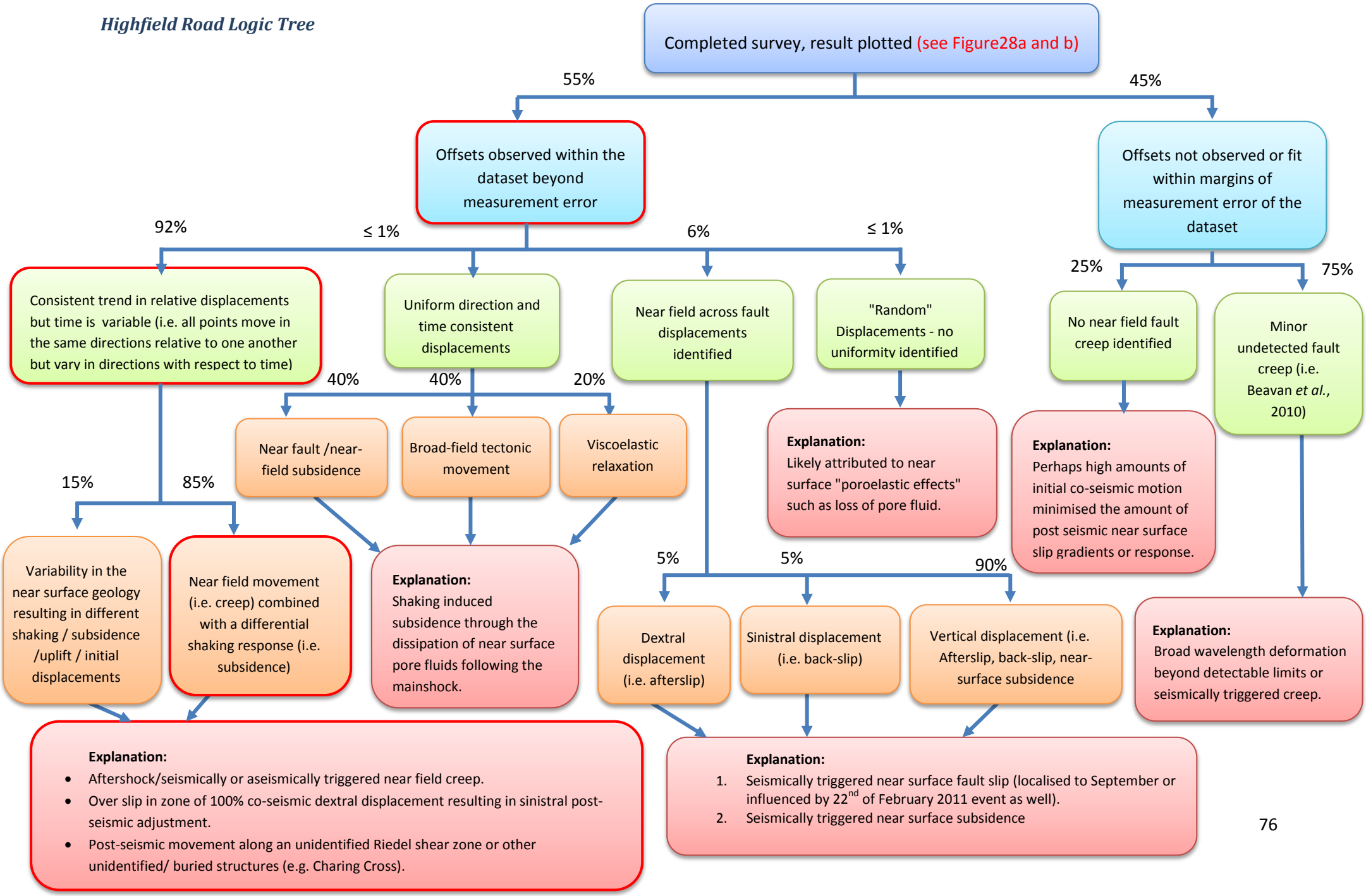

Figure 34: Kivers Road Logic Tree

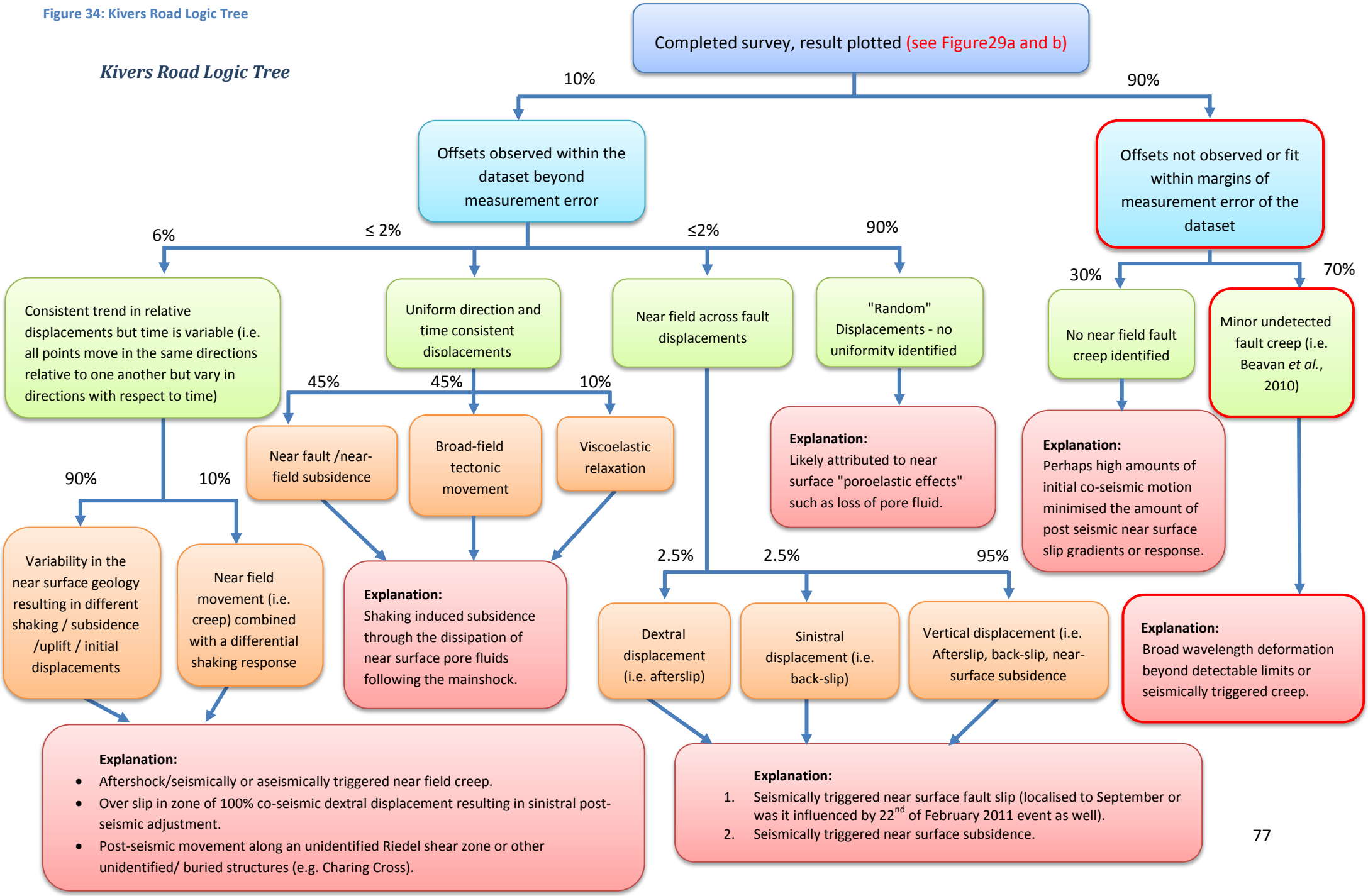

Figure 35: Kerrs Road Logic Tree

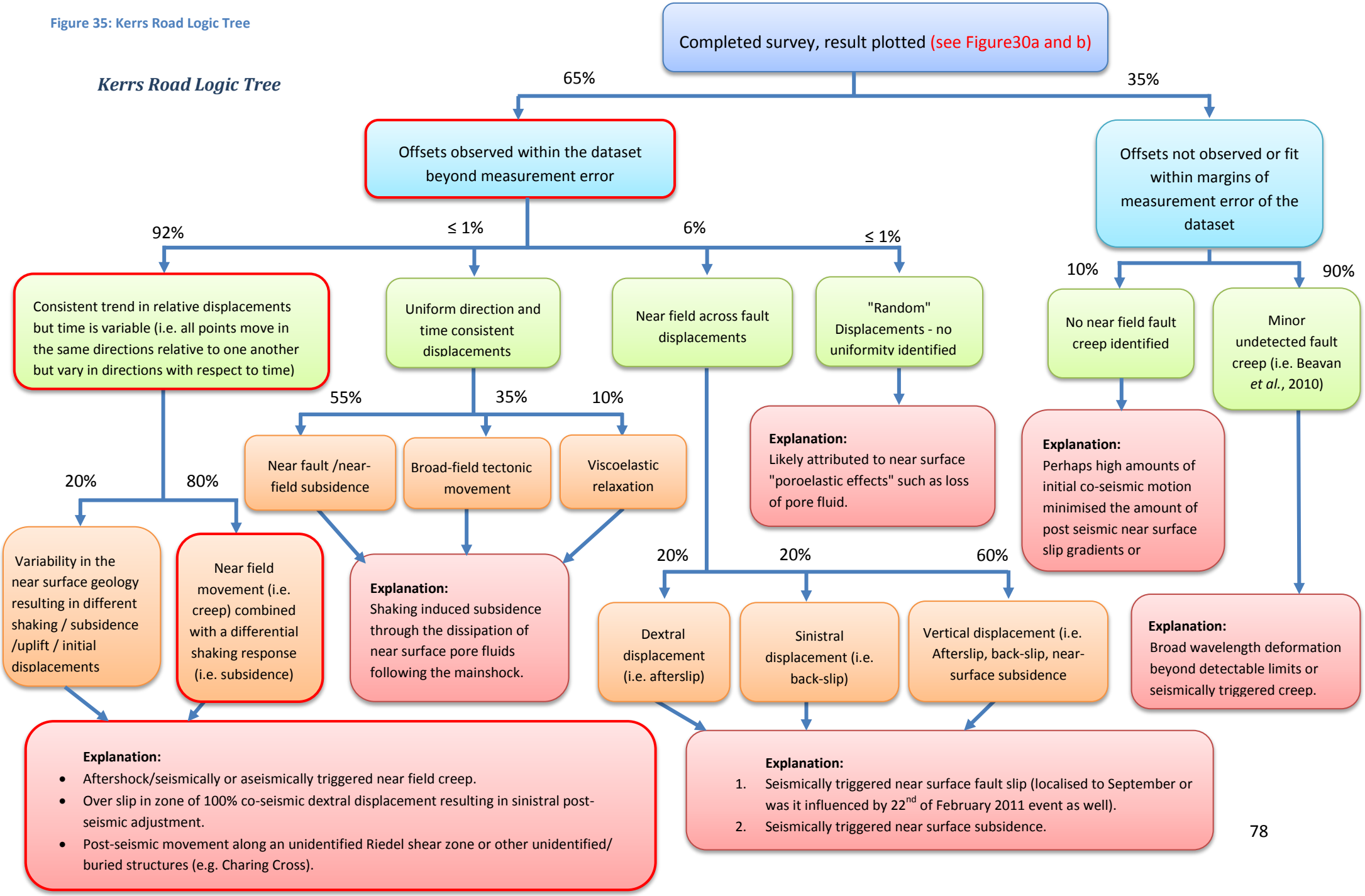

Figure 36: Railway Road Logic Tree

Railway Road Logic Tree

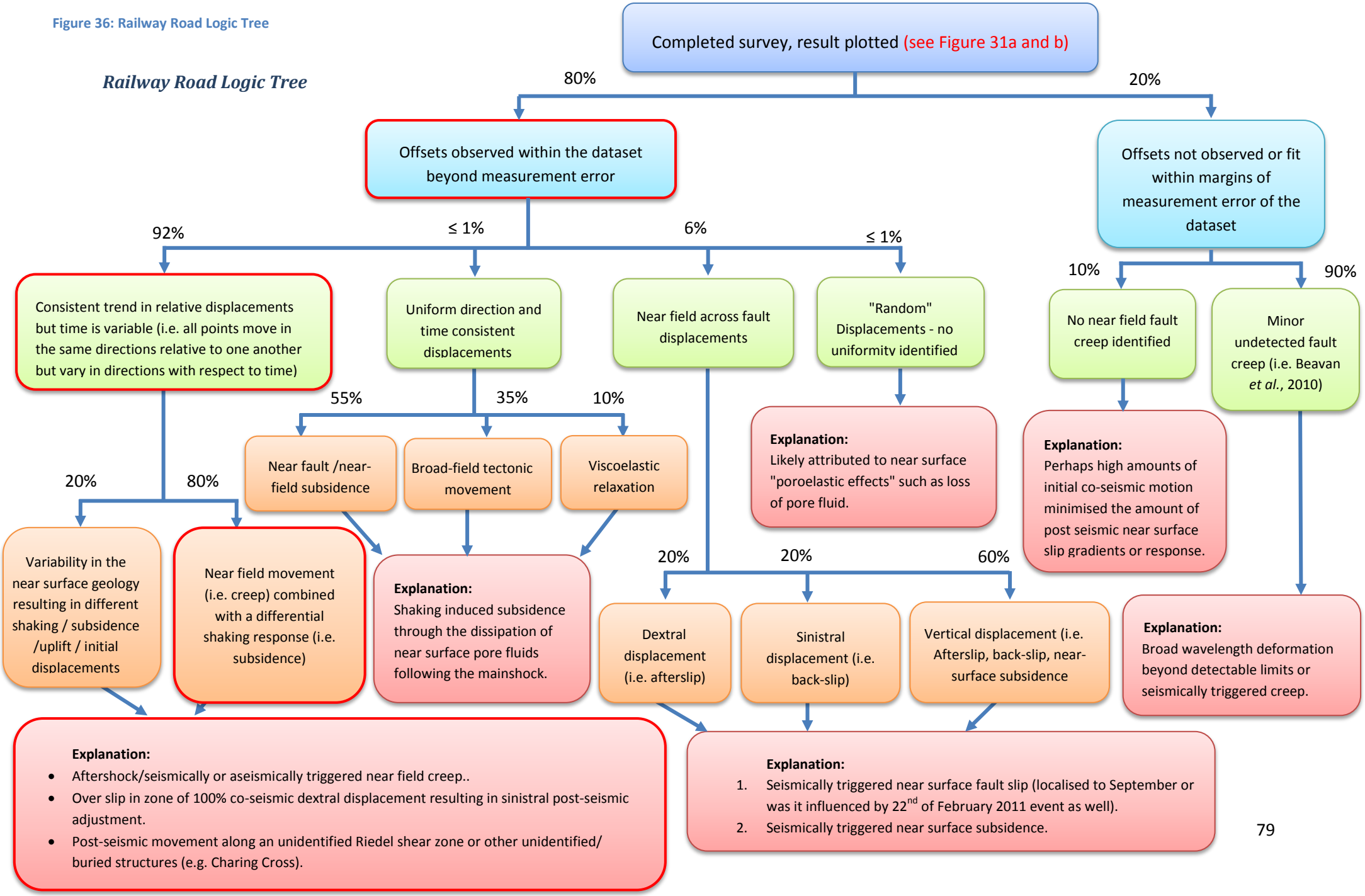

Figure 37: Combined Logic Tree

Combined Logic Tree

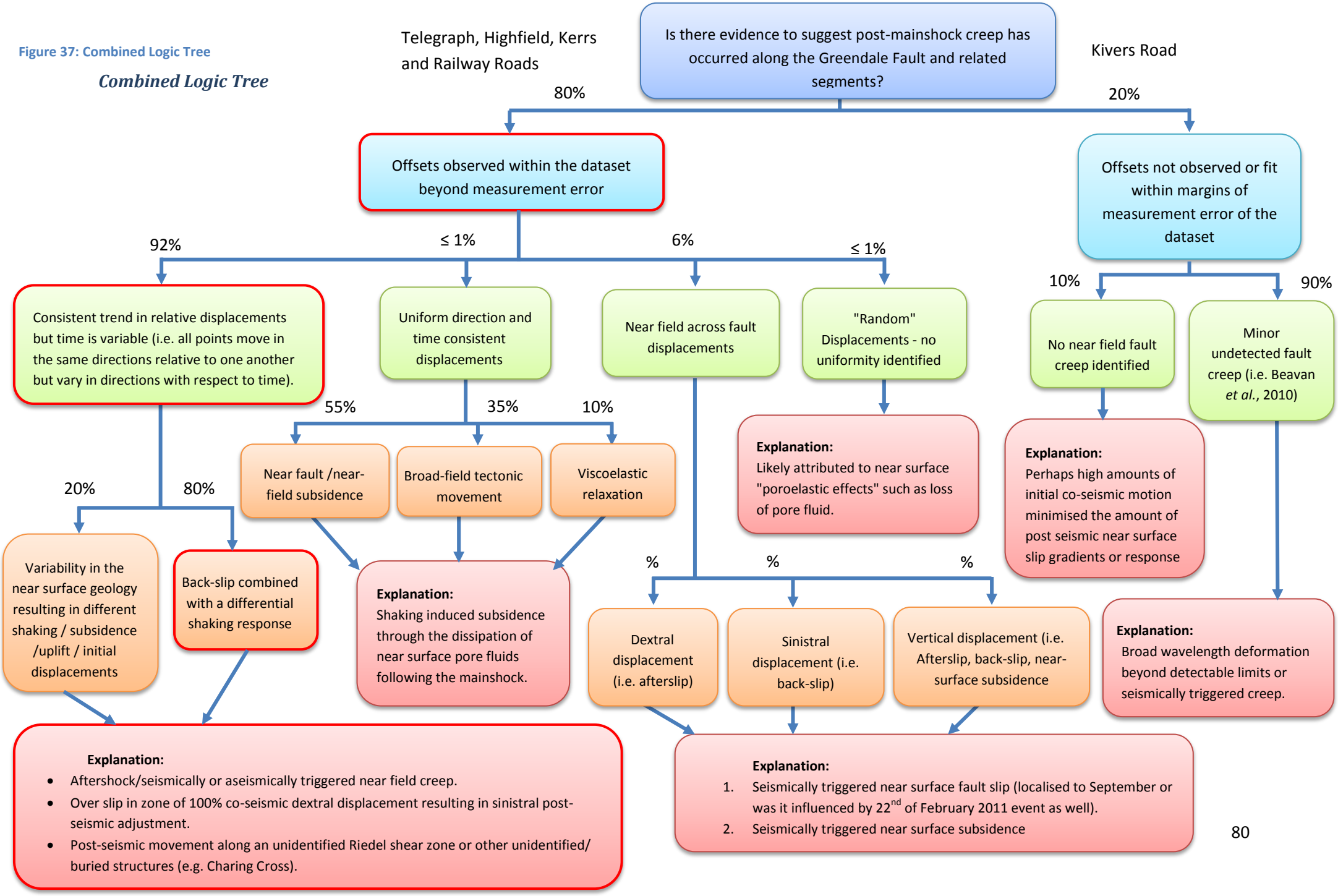

1.5.3 Suggested mechanisms for post-seismic motion

To discuss the recorded displacements it was important to first check and see whether there was any seismically induced movement from large aftershocks in the periods between surveying. Using the online historical earthquake database at Geonet.org.nz it was discovered the following earthquakes ≥ M_w 4 (see Table A1-3 in Appendix B):

- 9th and 13th of September 2010 – x13 M_w 4 aftershocks occurred,
- 13th to 18th September 2010 - x14 M_w 4 aftershocks occurred,
- 18th September to 13th October 2010 – x16 M_w 4 and x2 M_w 5 aftershocks occurred.

Of these aftershocks outlined, the two significant ones M_w 5, occurred approx. 4 km northeast of Kerrs and Railway Roads. However, referring to the displacement plot for this period these earthquakes did not seem to have any influence on resultant displacement plots for these areas.

Looking back at the results for across fault displacements for each location, a clear pattern emerges within each of the figures (see Figures 27b – 30b). This trend was that the northern side of the fault moved dominantly westwards relative to the southern side of the fault, and/or the southern side moved eastwards relative to the northern side. In other words, the southern side of the fault was moving left laterally with respect to the northern side of the fault and vice versa. Telegraph Road and in particular Highfield Road depict the best indications of this post-seismic creep (see Figures 27b and 28b). This is believed to be post-seismic creep as the same offsets visible at these sites would not result with just subsidence as the mechanism. This mechanism would show all the points moving in the same direction, which is not the case on the northern and southern side of the fault. Normally backslip localised to the fault trace would cause the marker pins closest to the fault to move the most. However, the recorded displacements from each of the survey sites in this study indicate the marker pin furthest from the fault reflecting the most movement. Thus, it was described as post-seismic creep.

Kerrs Road also provides evidence to support the presence of post-seismic creep as the main mechanism behind the post-seismic motion. However, Figure 30b, looks different to the across fault plot for Highfield Road which was deemed to reflect the best example of post-seismic creep occurring along the fault (see Figure 28 b). ON the northern side of the fault, however, the displacement looks to be moving in a more complex pattern. This resulted in movement patterns that cannot be completely explained by post-seismic creep. For example following the installation of the marker pins on 9th September 2010 and a resurvey of RN 2-8 on the 13th September 2010 along

Kerrs Road, a combination of western and eastern motion was reflected for the northern side of the fault (see Figure 30b). RN 2 and 3 shifted west by 1 cm and 0.5 ± 0.5 cm, respectively, whereas, RN 4 and 5 can be seen to shift east by 0.5 ± 0.5 cm. The southern side of the fault the initial motion was solely illustrated as a westward shift up to 0.8 ± 0.5 cm, relative to the original position of the marker pins.

Furthermore, the next survey on the 18th September 2010 illustrates a trend in a westward shift along the northern side of the fault, with RN 2 and 3 shifting 2 cm and 1.2 ± 0.5 cm respectively. RN 4 and 5 reflected smaller motion west of less than 0.5 ± 0.5 cm. This motion changed to the east, crossing over the fault and heading onto the southern side of the fault. However, only small offsets occurred. RN 6 moved approx. 0.1 ± 0.5 cm, RN 7 moved 0.2 ± 0.5 cm, whilst RN 8 shifting by approx. 0.6 ± 0.5 cm. Though this motion is only small and within the limits of error it does reflect the same trend in motion as Highfield Road, which shows the best example of relative post-seismic creep motion. Overall the northern side of the fault does still reflect an overall trend in motion to the west, indicating relative post-seismic creep. But the southern side of the fault reflects a general trend in relative motion to the west. This is not the case in any of the other plots, including Kivers Road. Kerrs Road looks to be reflecting a different trend in motion as well. This could be linked to another near surface mechanism controlling part of the post-seismic deformation.

By comparing the Kerrs Road and Railway Road displacement plots with respect to RN 1 on Kerrs Road, it was found that the movement of the marker pins towards the fault trace in the Railway road was likely the result of subsidence or vertical motion. This is because limitations with the equipment used throughout the surveys, meant only the horizontal displacements of the pins were able to be recorded. Therefore vertical motion could be misinterpreted as horizontal displacement. This could be one of the possibilities for explaining why the pins shifted at least 2 - 4 ± 1 cm south. The second possibility is that there could be contraction occurring within this location along the fault trace. Therefore, because Railway Road intersects Kerrs Road and the motion recorded at this site is with respect to the total station position at RN 1 on Kerrs Road it is likely the same motion is also incorporated within this data. Thus, a component of either vertical motion through subsidence/settling of the near surface or contraction of the near surface as horizontal displacement could explain the relative motion reflected in Figures 30a and b for Kerrs Road. Furthermore, these additional mechanisms may also explain why these sties reflected different motion patterns to Highfield Road in Figure 28b, where the relative motion was believed to reflect post-seismic creep. Telegraph Road to a degree may also reflect some vertical motion or contraction within the data set. This is because Figures 27a and b for Telegraph Road highlight similarities to Kerrs Road patterns of

displacement motion. This provides further support that there is evidence to suggest an additional mechanism(s) are influencing motion at some of the survey sites.

The results also indicate difficulties and complexity of understanding or trying to understand the processes in fault zones. In particular post-seismic deformation around fault zones following large scale near surface and surface ruptures. Therefore, to establish a robust data set supporting these mechanisms as the source for the observed post-seismic motion at Telegraph Road, Highfield Road, Kerrs Road and Railway Road; logic trees were created for each location, including Kivers Road (see Figures 32 - 37). This was suggested as it allows all possible near surface mechanisms to be evaluated from within the datasets or results for each location.

Summary of Logic Trees

From the production of the logic trees for each of the locations and a combined tree we argue that there is a differential near-field post-mainshock response of the Greendale Fault Zone. The results and logic trees highlight the likelihood that multiple mechanisms contribute towards the overall post-seismic movement along the Greendale Fault. A summary of the each of the logic trees follows:

Telegraph Road

For Telegraph Road the logic tree (see Figures 32) suggests the mechanism(s) most responsible for the observed post-seismic deformation is near-field creep combined with a differential shaking response (e.g. near-field settling/deflation or contraction). The evidence to support the mechanism behind the majority of the movement is near-field OFBS combined with a differential shaking response and is shown in Figure 27b. The marker pins closest to the fault trace on either side seemingly show little or no displacement. Surface settling/relaxation or contraction was believed to play a part initially (9-18th September) in causing the lack of consistency in direction of motion with time. Some settling or relaxation of the near surface could be identified as a component of horizontal displacements during the early surveys, because only the horizontal displacements of the pins were able to be recorded.

Highfield Road

From the results, Highfield Road was identified to have only one main mechanism behind the observed post-seismic displacements/offsets. Figures 26a and 26b indicated this as near-field creep, which was due to the northern side of the fault moving left laterally relative to the southern side and vice versa. The logic tree for Highfield Road also confirmed this interpretation (see Figure 33). Possible explanations for this mechanism are:

- Aftershock/seismic or aseismically induced, or
- Over slip in zone of 100% co-seismic dextral displacement resulting in sinistral post-seismic recovery, or
- Post-seismic movement along an unidentified riedel shear zone.

Kivers Road

Kivers Road was the only location to have displacements/offsets encompassed within the limitations of error. Therefore it was grouped into the appropriate right hand side of the logic tree (see Figure 34). The next step of the logic tree was to determine whether any near field creep was identified or whether it was just minor undetected creep. If no slip was identified, then it was likely that the large co-seismic slip along the Greendale Fault minimised any post-seismic slip gradients in the near surface along Kivers Road. However, an InSAR and GPS study by Beavan *et al.* (2011) identified less than 1 cm of post-seismic motion occurring along the Greendale Fault. This verifies that Kivers Road is likely to be reflecting post-seismic motion, but the offsets are just small and within the limitations of error.

Kerrs and Railway Roads

The logic trees for Kerrs and Railway Roads (see Figure 35 and 36) provide evidence to suggest that the mechanism behind their movement is near-field creep. This is combined with a significant component of differential shaking response likely to be subsidence.

Only being able to measure horizontal displacements meant that it is likely part of the horizontal motion reflected in the Kerrs and Railway Road results (see Figures 28 and 29) is attributed to incorporating components of vertical motion through subsidence of the near surface. A good example of this is displayed Figure 29, as it identifies the displacements on Railway Road where marker pins show motion that may reflect the pins being pulled towards the fault trace along Kerrs Road.

Combined Logic Tree

Overall the most consistent post-seismic motion at each of the sites, Telegraph Road, Highfield Road and Kerrs Road is near field creep triggered displacement combined with a component of differential shaking. This is indicated by a combined logic tree for all of the sites (see Figure 37).

This is reflected along the majority of sites with the north side of the fault moving left laterally with respect to the southern side and vice versa. Furthermore, Railway Road, Kerrs Road, and to a smaller

extent Telegraph Road provide evidence (see Figures 33 and 34) that suggests subsidence is occurring as a secondary mechanism controlling post-seismic motion along the eastern end of the fault.

1.5.4 Explanations for Mechanisms

The results and logic trees highlight near-field creep combined with varying amounts of a differential shaking response as the main mechanism controlling post-seismic slip along the Greendale Fault. Looking for evidence to support this claim, I searched within the literature, to locate studies where post-seismic creep was recorded away from the fault trace. Unfortunately, I could find no studies showing strike slip creep.

The lack of information in the literature is because the majority of studies are more focused on the deeper mechanisms controlling post-seismic slip or displacement. Examples include; viscoelastic relaxation (Grijalva *et al.*, 2007; Jonsson *et al.*, 2003; Pollitz *et al.*, 2006; Pollitz *et al.*, 2001; Pollitz *et al.*, 2000; Freed and Burgmann, 2004; Barbot *et al.*, 2008) or afterslip along the downdip extents of the fault plane (McCaffrey and Gupta, 2011; Segall, 2010; Ergintav *et al.*, 2009; Barbot *et al.*, 2009; Perfettini and Avouac, 2007; Freed *et al.*, 2006; Johnson *et al.*, 2006; Hsu *et al.*, 2006; Perfettini and Avouac, 2004; Ergintav *et al.*, 2002). These mechanisms induce deeper processes, like the adjustment of the upper mantle or lithosphere, to explain the post-seismic deformation, whereas, the near surface deformation monitored in this study is not influenced by these processes. These studies measure this deeper deformation using InSAR and GPS instruments to observe displacements over known landmarks or survey marks/reference points with established accuracy over a defined period (weeks to years) following a large earthquake.

Therefore, to provide support for the findings in this study it is only possible to discuss what is controlling or producing this observed near-field creep along the Greendale Fault. The logic trees (see Figure 32-37 above) highlighted the following theories to explain the occurrence of post-seismic creep and an explanation for the associated differential shaking induce subsidence:

1. Over slip in the zone of 100% co-seismic dextral displacement,
2. Post-seismic movement along an unidentified Riedel shear zone or other unidentified/ buried structures (e.g. Charing Cross),
3. Differential displacement of far field 'base station', and
4. Aftershock/seismically or aseismically triggered differential shaking.

Over slip in zone of 100% co-seismic dextral displacement resulting in sinistral post-seismic adjustment.

Highfield Road reflects the best example of post-seismic creep occurring along the Greendale Fault (see Figures 28a and b). Co-seismic surface deformation recorded at this site was larger than the other sites, with a maximum of 5.00 to 5.20 m of right lateral (dextral) horizontal displacement and up to approx. 0.7 m of vertical displacement (Van Dissen *et al.*, 2011; Quigley *et al.*, 2010). As a result the 50% and 100% co-seismic deformation zones for this location extend approx. 60 m and 120 m, respectively (see Figure 28 a and b). This indicates that a distance of 60 m perpendicular from either side of the fault trace at Highfield Road was required to accumulate and distribute 50 % of the total dextral surface rupture displacement or deformation of 5.0 - 5.2 m. At 100 % of the total dextral surface rupture displacement or deformation, the distance required to accumulate and distribute this deformation stretches out to 120 m from the fault trace.

Subsequent to these large co-seismic displacements, a broad area is clearly highlighted where the near surface was impacted along the fault and within the 50 % and 100 % zones of deformation. The near surface in the Canterbury Region and at each of the selected sites is comprised of weak materials, such as gravels silts and sands. These materials accommodated both brittle failure and inelastic strain during the Darfield Earthquake. To relieve the strain close to the fault and to generate the displacement observed at Telegraph Road or Highfield Road (approx. 5 m), the areas furthest from the fault trace within the 100% co-seismic displacement zone over-slipped as they were dragged or pulled by the surface materials closer to the fault trace. This overcompensated slip therefore required adjustment or settlement post-seismically. Thus, OFBS (also termed 'sinistral') displacement is generated. The ideas behind this theory are depicted in Figure 38.

This theory also explains why the marker pin results for Telegraph Road, Highfield Road, and Kerrs Road across fault displacements (referring to Figures 27b, 28b and 30b) indicated the near surface furthest from the fault produced the most post-seismic. These areas required more displacement to recover from large co-seismic enforced strain. On the other hand, the amount of displacement tapered off towards the fault trace where the co-seismic slip was sufficient in releasing strain and did not generate overslip. Hence, minimal post-seismic movement was required. This was observed to be occurring until 1st July 2011 when surveying ceased.

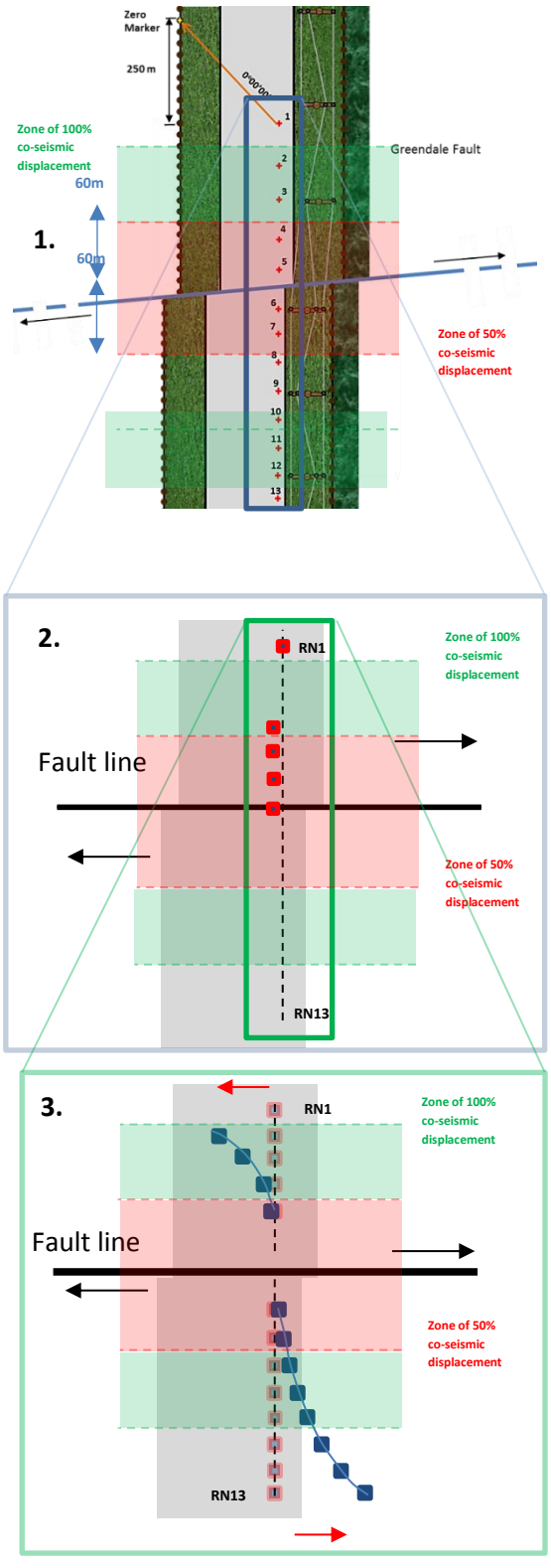

1. Indicates the position of the maker pins along Highfield Road.

2. The marker pins were inserted after the mainshock and co-seismic slip had occurred along Highfield Road. The schematic represents a close up of the marker pins location with respect to the fault trace and displacement zones. This was completed so the pins would record only post-seismic movement.

3. This indicates the post-seismic response to the large mainshock displacement. Note how the direction of motion opposes the co-seismic slip direction. This “post-seismic creep” acts to re-equalise areas where the co-seismic displacement was overcompensated. This is likely to be further away from the fault trace as the fault dragged or over stretched these areas during the mainshock.

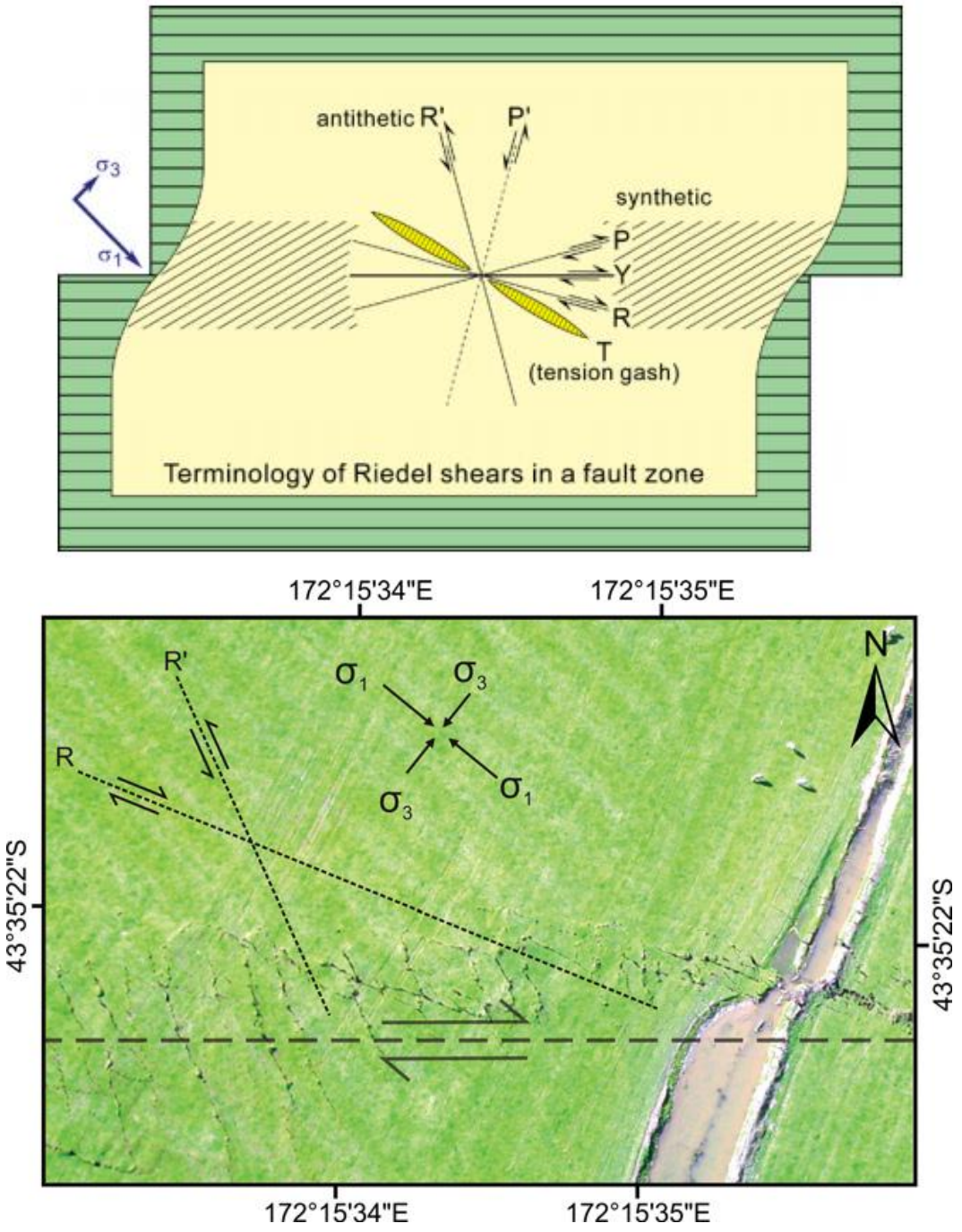

Figure 39: Top) Riedel shears in a dextral fault zone (Source: Burg, 2011). Where P is the p-shear and P' is the antithetic conjugate shear, whilst T is the tension fracture or gash. Bottom) Dextral Riedel shears and sinistral conjugate Riedel shears identified along the Greendale surface rupture trace between Highfield and Kivers Roads (Source: Quigley *et al.*, 2012).

Post-seismic movement along an unidentified Riedel shear zone or other unidentified/buried structures.

Following the Darfield earthquake, studies by Quigley *et al.*, (2010:2012) and Van Dissen *et al.*, (2011) located a multitude of features over the reach of the fault. These were commonly observed features found within earthquake ruptures dominated by simple shear (e.g., Terres and Sylvester, 1981) and contained within 50 % and 100% co-seismic surface rupture zones where the average surface co-seismic displacement exceeded the average of 2.5 ± 0.5 m (Quigley *et al.*, 2010 and 2012; Van Dissen *et al.*, 2011). They include;

- East-west striking dextral faults,
- West-northwest oriented and east-southeast synthetic Riedel (R) dextral shear fractures,
- North-northwest and south-southeast oriented antithetic (R') sinistral shear fractures,
- Northwest to southeast oriented tension or extensional fractures,
- Northeast to southwest oriented folds and thrust/reverse faults,
- Horizontal flexure, and
- 0.1 m-amplitude vertical flexure and bulging (Quigley *et al.*, 2012; Van Dissen *et al.*, 2011).

Of particular interest, a number of Riedel shear structures were identified. Riedel shears (R-shears) are synthetic strike slip faults that propagate a short distance out of the main fault but are coeval with it (Burg, 2011 Davis and Reynolds, 1996; Terres and Sylvester, 1981). They form at an acute angle, of about 10-20^{o} clockwise to the main line of dextral faulting or anticlockwise for sinistral faulting and are generally the first subsidiary fractures to occur and build the most prominent form (see Figure 39) (Burg, 2011; Davis and Reynolds, 1996). Their arrangement often forms a spectacular en échelon and overstepping array synthetic to the main fault. Meaning they evolve as a sequence of linked displacement surfaces parallel to one another and arranged along a common line of bearing (Burg, 2011; Davis and Reynolds, 1996).

The term, Riedel shears, may also refer to as many as five directional groups of associated fractures or antithetic fractures when looking at a large scale fault pattern (Burg, 2011), all of which are depicted and explained in Figure 39. Interestingly, it is possible individual fractures may remain active even after the other types have developed (Burg, 2011). This is so synchronous movement on all fractures can accommodate strain within the fault zone (Burg, 2011; Davis and Reynolds, 1996).

The antithetic strike-slip faults are conjugate Riedel shears (R'-shears), which means they move with a sense of direction that opposes the bulk movement along the fault (Burg, 2011; Davis and

Reynolds, 1996). For example the Greendale Fault is a dextral (right lateral) strike slip fault and thus the R'-shears movement will be sinistral (left lateral) (see Figure 39). R'-shears form at a high angle of about 75^{o} to the main line of faulting, i.e. clockwise for a dextral fault plain and anticlockwise for a sinistral fault plane, with the direction of greatest principle stress (σ_1) bisecting the angle between R and R' (see Figure 39) (Burg, 2011; Davis and Reynolds, 1996). These shears preferentially occur in the overlap zone between two parallel R shears, where they often connect these two R shears. Also important is that they may develop with or after R shears (Burg, 2011). Therefore, the second theory to explain near-field back slip occurring along the Greendale Fault is from subsidiary shear fractures, known as Riedel shears.

Neither of these studies pinpointed R'-shears at the locations selected for surveys. Although a number of R-shear fractures were identified close to and between Telegraph and Highfield Roads, and Highfield and Kivers Roads. Several R' shear fractures were identified between Highfield and Kivers Roads (Van DIssen *et al.*, 2010; Quigley el al., 2012). These can be seen in Figure 39. Burg, (2011) stated that R'-shear fractures can develop in conjunction with R shears but they may also develop after. This means it is possible that R'-shears were not identified in or near to the selected surveying sites because they could have formed in the days or weeks following the mainshock and formation of the R shears. It could also mean that discrete R' structures were not generated at the surface.

Therefore, in support of this theory, if an R' shear fracture did occur at or close to the survey locations it would have reflected sinistral motion approx. 75^{o} to the fault trace in the results from across fault displacement surveys. This sinistral motion would be detected on both sides of the fault trace as the R' shear crossed thorough the fault zone. The results for each of the Telegraph Road, Highfield Road, and Kerrs Road sites highlighted post-seismic creep as the mechanism behind motion. Furthermore, to be used for surveying these sites were required to have an across fault line of sight, i.e. perpendicular or 90^{o} to the fault. Therefore the results observed could have occurred through adjustment along R' fractures.

In contrast these R' shear structures, shears fail to address or explain why the marker pins furthest from the fault trace reflect the most amount of motion tapering off closer to the fault trace. In addition, it seems unlikely that all of these sites, Telegraph, Highfield and Kerrs Roads, are reflecting post-seismic creep motion along a R' shear fractures. It could then be proposed that the explanation for the results could be a combination of readjustment from co-seismic overslip (theory one) and R' shear fractures.

Also worth consideration is the possibility that other unidentified structures are present within the near surface, and could generate the displacements recorded at each of the survey sites. A good example of these unidentified structures is post-mainshock folding within the fault interaction zones (see Figure 40). Folding or small localised areas of thrusting occurring analogous to Charing Cross fault structure and close to Telegraph and Highfield Roads could explain the relative post-seismic creep observed through surveying at these sites (see Figure 40). If the reference marker was placed within or near one of these structures, like illustrated, it is possible that observed movement would appear as sinistral. This occurs as the marker pins appear to be moving left laterally closer to the reference marker. When in reality if the marker pins reference station moves then all of the survey marks would reflect this movement. In this case they would appear to be moving closer to these zones.

Another likely option is that the Charing Cross is continuing to move or adjust post-seismically. Recent cadastral studies indicated that a survey mark along telegraph road shifted northwest relative to its original location. This fits with the observed patterns “apparent” left lateral post-seismic creep.

Differential displacement of far field reference station

It is possible that all of this movement has arisen from the development of differential displacement of far field 'reference station or marker', used to reference the total station and measure the azimuths for each of the survey marker pins. If this reference station moved at all during the period of surveying it would be reflected in the results as movement completed by the survey pins. However, this movement would then be the same down the full length of the fault, which is not the case. This theory does not address or explain why there a visible across fault displacements. The northern side and southern side of the fault clearly reflect different directions of motion with respect to one another. Thus, because this theory fails to address this motion it is believed this is not the appropriate explanation for the post-seismic creep occurring at selected locations along the Greendale Fault.

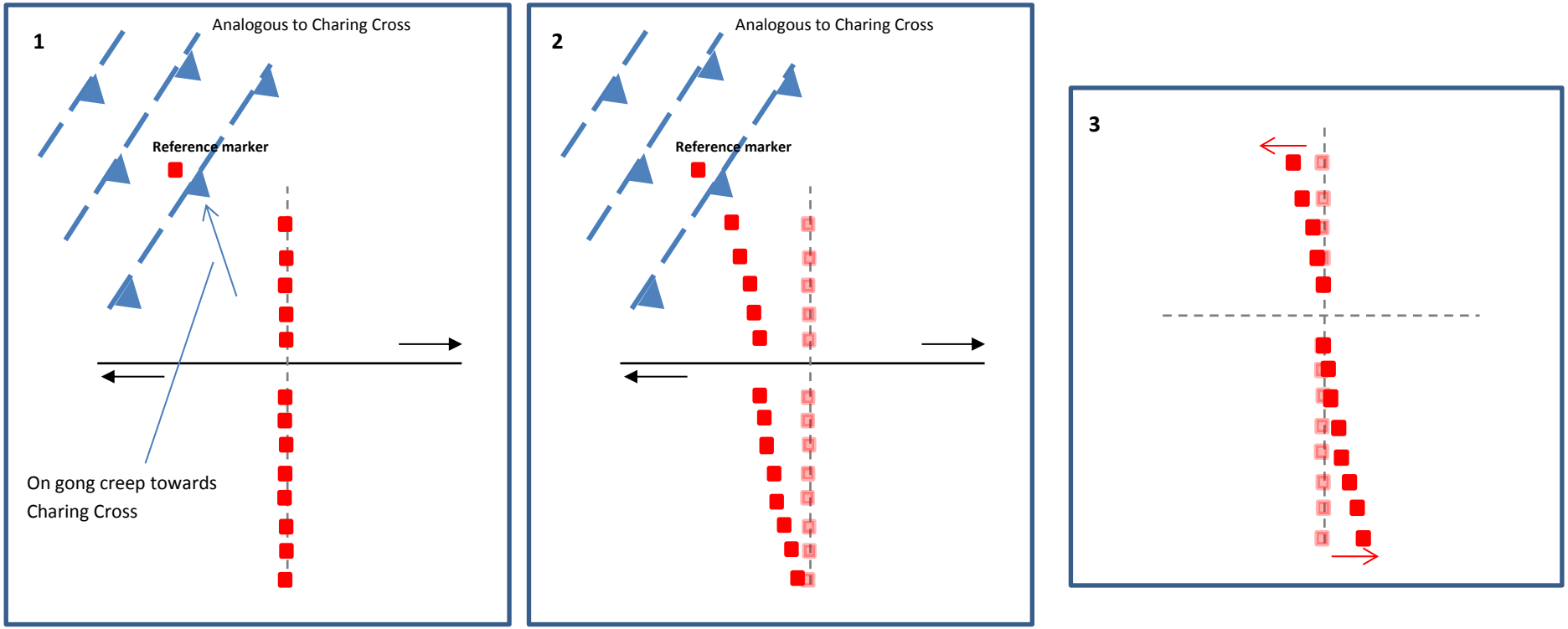

Figure 40: Likely source mechanism for the post-seismic creep.

Aftershock/seismically or aseismically triggered differential shaking

An explanation for some of the associated secondary motion is seismically or aseismically triggered differential shaking, i.e. subsidence, which added to motion detected in the surveying of the selected locations.

Firstly it is possible that aftershocks seismically induced subsidence along the Greendale Fault.

- Local high magnitude aftershocks resulting in resettling of the near surface,
- Large regional earthquakes i.e. 26 December 2010, February 22nd 2011 and 13th June 2011.

Aseismic movement, without seismic waves, could explain subsidence occurring as a secondary mechanism as the ground tries to resettle following the large co-seismic deformation. For example large amounts of water was brought to the surface as a result of ground motions experienced during the mainshock therefore the subsurface materials need to recover, thus poroelastic recovery may have occurred.

In particular Railway Road showed the most obvious amount of differential shaking, i.e. subsidence, with a minimum of 0.02 – 0.04 ± 0.005 m occurring over the approx. 10 month period following the installation of the marker pins on the 9th September 2010. It is believed this is because the orientation of the marker pins is different to the other sites. At Railway Road the pins are in a northwest to southeast array rather than approx. north to south orientation at the other survey site.

Kerrs Road and Telegraph Road also indicated a secondary mechanism was affecting the results, although, on a much smaller scale than Railway Road.

Each of these possibilities discussed has merit as the likely explanation for the production of post-seismic creep displacements along the Greendale Fault. Hovever, it is believed that the motion obsereved is reflected by Near filed post-mainshock deformation across the Greendale Fault appears to be driven by on-going creep on adjacent thrust faults (e.g. Charing Cross) which results in the “apparent” sinistral displacement.

From a societal point of view these findings are important for understanding how faults behave in the nearfield following large earthquakes. This is particularly relevant for rebuilding damaged or demolished homes close to fault zones and to be applied to other large faults across New Zealand.

1.5.5 Societal Issues

Earthquakes are devastating and largely unpredictable events with a low probability of occurrence but high impact (Kerr *et al.*, 2003; PCE, 2001). However, it is possible to mitigate some of the most damaging effects of earthquakes by the correct seismic building design standards and avoiding obviously hazardous areas, such as known active faults (PCE, 2001). This section aims to discuss the results from this thesis with respect to:

- The current standards for building on or next to fault lines, and
- The timeframe for rebuilding or building at sites on or close to a ruptured fault.

Throughout historical ruptures it has been shown that buildings positioned across fault lines that ruptured during an earthquake will be, in general, more badly impacted than building built adjacent to a fault line (Kerr *et al.*, 2003; PCE, 2001). For this reason councils and the government have established and implemented "fault avoidance zones" (FAZ). These guidelines are quantified using the likely fault rupture zone or 'fault location' and the interval between events, "recurrence interval". The current guidelines were established under the auspices of the Ministry for the Environment (MfE) by Kerr *et al.* (2003) state the following:

> "A fault avoidance zone is an area created by establishing a buffer zone either side of the known fault trace (or the identified likely fault rupture zone). These Guidelines recommend a minimum buffer zone of 20 metres either side of the known fault trace or likely fault rupture zone. Twenty metres has been chosen because intense deformation and secondary ruptures are commonly experiences as a result of fault movement within this distance from the primary plane of the fault rupture. These effects can occur because near-surface weak materials deform instead of breaking cleanly, and structures built near an area of fault rupture can cause surface rupture to divert around them unpredictably. Twenty metres also represents a precautionary approach to ensure a level of life safety in regard to the protection of life.
>
> Defining a fault avoidance zone on district planning maps, which is supported by policies and methods (including rules) will allow a council to:
>
> - Restrict development within the fault avoidance zone, and
> - Take a risk-based approach to development in built-up areas.
>
> The determination of the extent of a fault avoidance zone is closely related to *fault complexity* (refer section 8). A wide and complex likely fault rupture zone is likely to have a significant fault avoidance zone. Displacement across a fault usually decreases with its distance from the fault trace. The fault avoidance zone

can be reduced if a detailed fault study shows that the zone of intense deformation and secondary rupture is less than 20 metres from the likely fault rupture zone." [1]

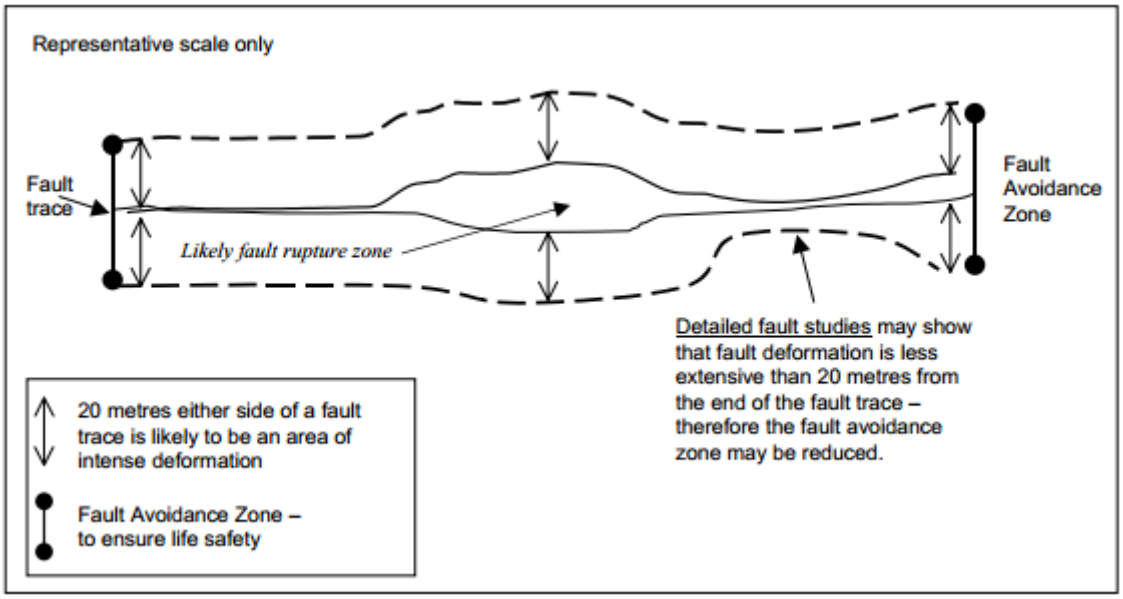

Figure 41: A fault avoidance zone on a district planning map (Kerrs *et al.*, 2003).

Fault complexity refers to a classification of the surface rupture. This is because surface ruptures are complex and can vary considerably along the length of the fault rupture. The MfE guidelines recommend different limitations depending upon the type of fault complexity. They are divided into three classifications shown in Table 5. The final fault avoidance zone is determined through combining the fault complexity area and the 20 m set back distance.

Table 5: MfE Fault Complexity Classifications (Source: Kerr *et al.*, 2003)

A) Well Defined	A fault trace of limited geographic width, typically a few metres to a few tens of metres wide.	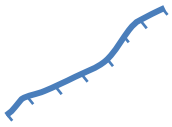
B) Distributed	Deformation is distributed over a broad geographic width up to hundreds of metres in width, sometimes with multiple fault traces, folds, or both.	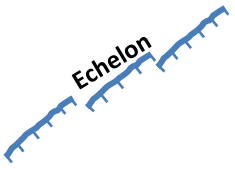
C) Uncertain	Location of fault trace(s) us uncertain as it either has not been mapped in detail or it cannot be identified, typically as a result of	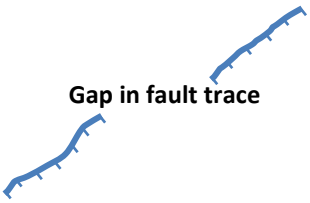

[1] Kerr, J., Nathan, S., Van Dissen, R., Webb, P., Brunsdon, D., King, A. 2003. **Planning for Development of Land on or Close to Active Faults - A guideline to assist resource management planners in New Zealand.** Ministry for the Environment Report produced in conjunction with Geological & Nuclear Sciences. Section 6.1, pp.12.

gaps in the trace(s) or erosion or coverage of the trace(s).

Looking at the sites where surveying took place, the surface trace within these areas can be categorised as complex classification B or distributed. Therefore using the MfE current guidelines the final FAZ can be determined by combining the distributed complex zone with a 20 m set back distance. In contrast, the results from the near surface fault surveys combined with the 50 % and 100 % co-seismic displacement zones from Van Dissen *et al.* (2011) (Figures 27-30) indicate a broad zone further beyond the MfE FAZ. Furthermore, the standard does not mention or take consideration of post-seismic motion along the fault. This motion as previously mention can last for weeks, months or even years in some cases. For example, 7 years of post-seismic deformation followed the Zemmouri earthquake in Algeria in 2003 (Cetin *et al.*, 2012).

Along the Greendale Fault at Telegraph Road and Highfield Road survey sites, motion of approx. 5 – 12 cm was recorded up to approx. 140 m (Telegraph Road) from the fault trace. This motion had not stopped following the completion of this surveying. Although movement of less than 15 cm seems small, it could have a massive impact on existing structures, especially residential, within these deformation zones. Buildings on piles within these areas are the most vulnerable and likely to be affected as the piles will move with the ground. This will result in buckling or warping of the piles and home producing serious structural damage to the building. Thus, these results indicate that the current guidelines of 20 m for building on or next to fault lines could be understated.

Figure 42: Home located northeast of Telegraph Road badly damaged by distributed surface deformation by the Darfield earthquake. It is a timber-framed brick clad house with a concrete slab foundation (at most lightly reinforced) and a light-weight roof. The home is located within a ~150 m wide deformation zone accommodating 4 – 5 m of dextral displacement. (Source: Van Dissen *et al.*, 2011; photo A (looking south) by Richard Cosgrove; B (looking WNW) and C (looking SSW) by Hayden Mackenzie; D (looking ESE) by Dougal Townsend).

Secondly, in terms of rebuilding or building on or next to a ruptured fault, these results were monitored over a period of approx. 10 months, with motion continuing following the final survey on the 1st July 2011.

Over the surveying period, it was noticed that several damaged homes on or near to the fault trace were being demolished. A few examples include one home near Telegraph Road (see Figure 41) and on Kerrs Road near the railway line where a home was built over the hidden fault. This sparked the questions:

- Would they rebuild?
- How long they would wait to rebuild?
- Would they wait or commence rebuilding as soon as possible?
- Is there a standard in place to determine the required length of time before rebuilding or building could occur?

Unfortunately, no standard was applied. However, it is still worth pointing out that with motion continuing at the end of the final survey it is likely any building that went up within the timeframe could have been impacted by the observed post-seismic creep.

It is believed the current guidelines for fault avoidance zones need to be readdressed or revised to include a clause for post-seismic deformation. Furthermore, these guidelines may need to be readdressed following major earthquakes worldwide as more information becomes available surrounding the unknown aspects of fault zones.

1.7 Conclusions

1. No discrete displacements across the Greendale Fault indicates no resolvable Greendale Fault Creep.
2. Near filed post-mainshock deformation across the Greendale Fault appears to be driven by on-going creep on adjacent thrust faults (e.g. Charing Cross) which results in “apparent” sinistral displacement.
3. Cannot preclude that creep on other unrecognised strikes like incipient R’ shears that don’t rupture the surface could create this pattern of motion we observe.
4. In absence of vertical displacements, differential subsidence may also explain some of our data.

Part II: Characterisation of the Hororata and Charing Cross faults using site investigations, RTK and seismic reflection surveys.

Outline:

2.1 Introduction

The Darfield earthquake produced very strong ground motion with violent shaking following rupture on the 4th September 2010. This resulted in widespread damaged and earthquake associated features throughout the Canterbury region because the earthquake caused ground rupturing, shaking damage and surface deformation (Quigley *et al.*, 2010; Van Dissen *et al.*, 2011).

Approximately 10 to 20 earthquakes, greater than $M_w \geq 7.0$, occur worldwide each year (USGS, 2012). Few provide such an opportunity for detailed research as the Darfield Earthquake because this caused a surface rupture in an agricultural landscape, containing an abundance of anthropogenic, linear fault displacement markers including roads, tree lines, fence lines, shelterbelts, powerpoles and hedges (Quigley *et al.*, 2010).

In addition to the obvious offset features that define mapped fault trace, there are other subtle features that also relate to fault rupture, and can allow the mapped length to be extended. Documentation of these earthquake induced surface features provided a new and unique opportunity for research to be undertaken into addressing the questions:

- What is the subsurface geometry of these structures?
- Would the slip on this structure be recognized geologically? Is it possible to characterise these structures through near surface investigations?
- What role do the subsurface alluvial gravels play in dissipating fault slip?

The hypothesis for this section is to better characterise the Hororata and Charing Cross faults, southwest of Christchurch, which ruptured during the Darfield Earthquake. This hypothesis will be tested through site investigations and real-time kinematic (RTK) surveys to identifying earthquake associated geological manifestations and attributing factors to shaking and rupture deformation. These features will provide a location were seismic reflection surveys can be used to characterise or image these features.

2.2 Study Area

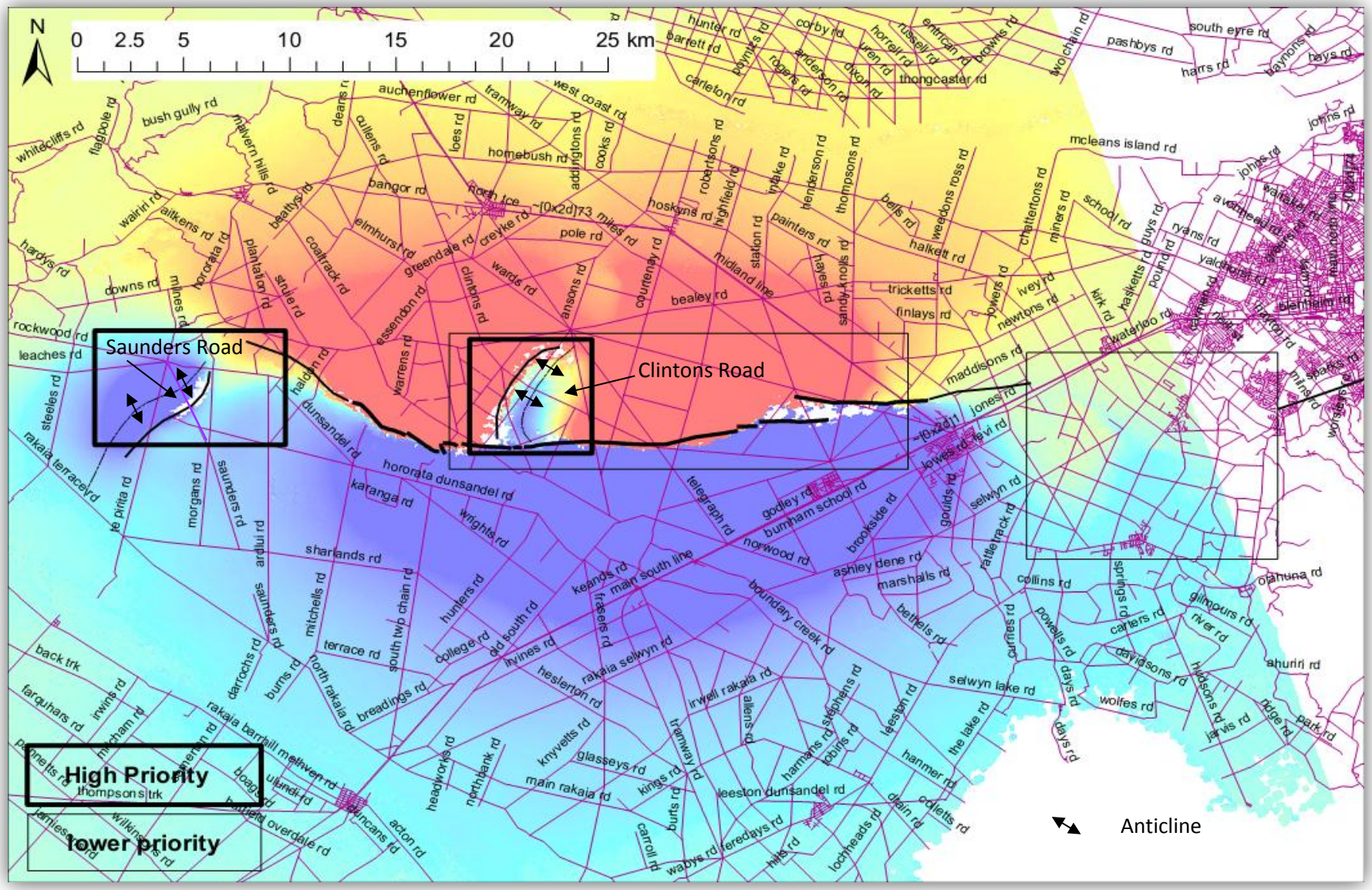

Figure 43: The study areas for the site investigations for this section. Hororata and Charing Cross areas are highlighted as high priority areas for undertaking investigations working towards testing the hypothesis for this section. This is because the background InSAR image highlights two distinctive patches of deformation anomalies within them. Whereas the area south of Christchurch is regarded as a lower priority in order to balance the work load in the respective sites.

2.3 Methodology

To achieve the hypothesis and answer questions relating to the Greendale Fault zone, an in depth study was undertaken involving multiple site investigations, RTK GPS measurements, and geophysical surveys. The methodology involved in each of these investigations is outlined below.

2.3.1 Site Investigations

An initial site investigation took place following earlier observations by those first on hand and resident information. This entailed investigating areas within close proximity of the Greendale Fault and related segments, then moving to south of Christchurch and the wider Canterbury region (see Figure 43). Each location had to be scrutinized by car and on foot, recording information on features that had deformed or showed deformation post-earthquake rupture. The sites of particular interest and focus were Hororata and Greendale/Charing Cross areas but Lincoln to Ladbrooks, and Tai Tapu to Halswell areas were also investigated (see Appendix C for the results from these).

At each of the above locations, features of interest varied in scale from the large obvious land movement to subtle offsets visible to those only interested in looking for it. They included:

- Tensioned fence lines,
- Cracks in roads whether offset or not,
- Offset fence posts and powerpoles, and
- Offset treelines.

Once identified, a location was taken on a hand held GPS, as well as written notes about the feature so that it could be found when the real time kinematic surveying began.

2.3.2 RTK Surveying

Using the information collected during the site investigations, the next step was to document the observed deformation patterns and offsets to produce a map of the wider Greendale Fault area. This involved taking accurate GPS locations of these features using a Real-time kinematic (RTK) GPS. This was a Leica system 500 provided courtesy of Geological and Nuclear Science (GNS) (see Figure 44).

The RTK mode of the instrument involves having the base station, a GPS receiver station, set on an established point and the rover, also a GPS receiver, connected to the base station via radio contact. The base and rover communicate to each other the details of their locations by satellite signals. This

means that much greater precision of position is achieved than a hand held receiver making it well suited for measuring subtle offset features.

Figure 44: Equipment required for the RTK survey (Source: http://ww.ebay.com/itm/Leica-SR530-GPS-L1-L2-RTK-Base-Rover-Survey-SET-/190552613517#ht_3661wt_1396).

2.3.3 Seismic Surveying

The technique of seismic surveying was originally developed in the early 1930s as a means for the oil exploration industry to delineate subsurface structure (Keuken and Groenewoud, 1992). As the use of seismic surveys became more accepted during the 1960s through to 1980s, and as funds were available for research, the technique evolved. It became an effective way to view and interpret large-scale subsurface geologic structural features through different types of surveys, such as seismic reflection, refraction and multichannel analysis of surface waves (MASW) (Keuken and Groenewoud, 1992). Nowadays the seismic survey technique is widely accepted and used by Environmental, Geological and Engineering Industries. It is this ability to image subsurface structural features that provides a suitable tool when trying to determine features beneath the Canterbury Plains. A study by Dorn *et al.* (2010) seismic reflection surveys in an attempt to characterise some of the vast seismogenic structures beneath the Canterbury Plains. In particular, the studies focus was to provide a greater understanding of the potentially active structures northwest of Christchurch (Dorn *et al.,* 2010).

This study aimed to emulate Dorn *et al.* 2010, using seismic reflection surveys to better characterise the Hororata and Charing Cross Faults. From reviewing the RTK data, and overlaying it on to an InSAR image taken of the area after the September rupture a number of sites were identified where further investigations were required, in particular, Clintons Road (Charing Cross) and Saunders Road (Hororata). Therefore, seismic surveys were undertaken along Clintons Road and Saunders Road (see Figure 43).

Currently only seismic and geodetic models of the Hororata and Charing Cross faults structures exist (Beavan *et al.*, 2010), but these techniques are limited in resolving finite geometries, such as the angle of the fault. Thus, through near surface seismic reflection survey this study proposes to better characterise the shallow structure and extent of the Hororata and Charing Cross blind fault structures. The following outlines the survey designs, setup equipment, testing and procedure required for the Clintons Road and Saunders Road seismic reflection surveys.

2.3.3.1 Survey Design

Clintons Road, Charing Cross

Using information from the site investigations, RTK surveys and the InSAR image, it was decided the optimal way to cover the area was to run a line approximately 4.5 kilometres long from the corner of Clintons Road/ Milton Road – running through until approximately Adams Road. This meant the line would cut perpendicular to the deformation structure and provide the best opportunity of imaging the fault.

Using four cables each with 24 geophones spaced approx. 6.5m apart (i.e. a total of 96 geophones), the survey was run along the margin of Clintons Road (see Figure 45). The “dog box” was positioned between in the central point of the cables. The first shot, using an accelerated weight drop (see Figure 48), was positioned approx. 13m behind the start of the line, shotpoint 100 (i.e. geophone 1)(see Figure 45). The next shot was then taken at shotpoint 100, then shotpoint 103, so as to shoot on every third geophone (shown in Figure 45). The locations of the geophones were also mapped using a GPS to provide the location and geometry of the seismic line during processing.

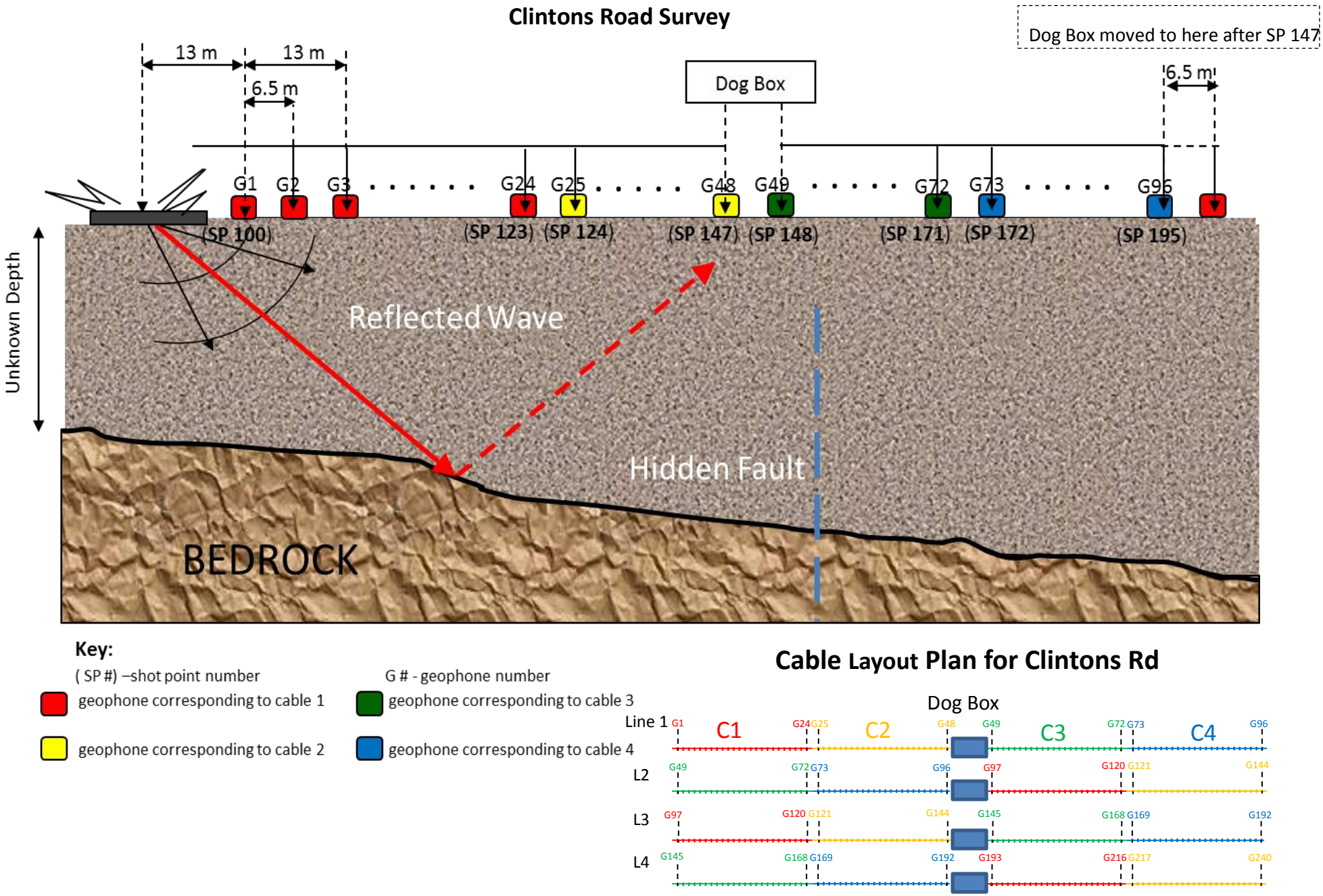

Figure 45: Design and cable layout plan for the Clintons Road seismic reflection survey. The layout plan shows the movement of the dog box and cable for running an end over end seismic reflection survey along the verge of Clintons Road.

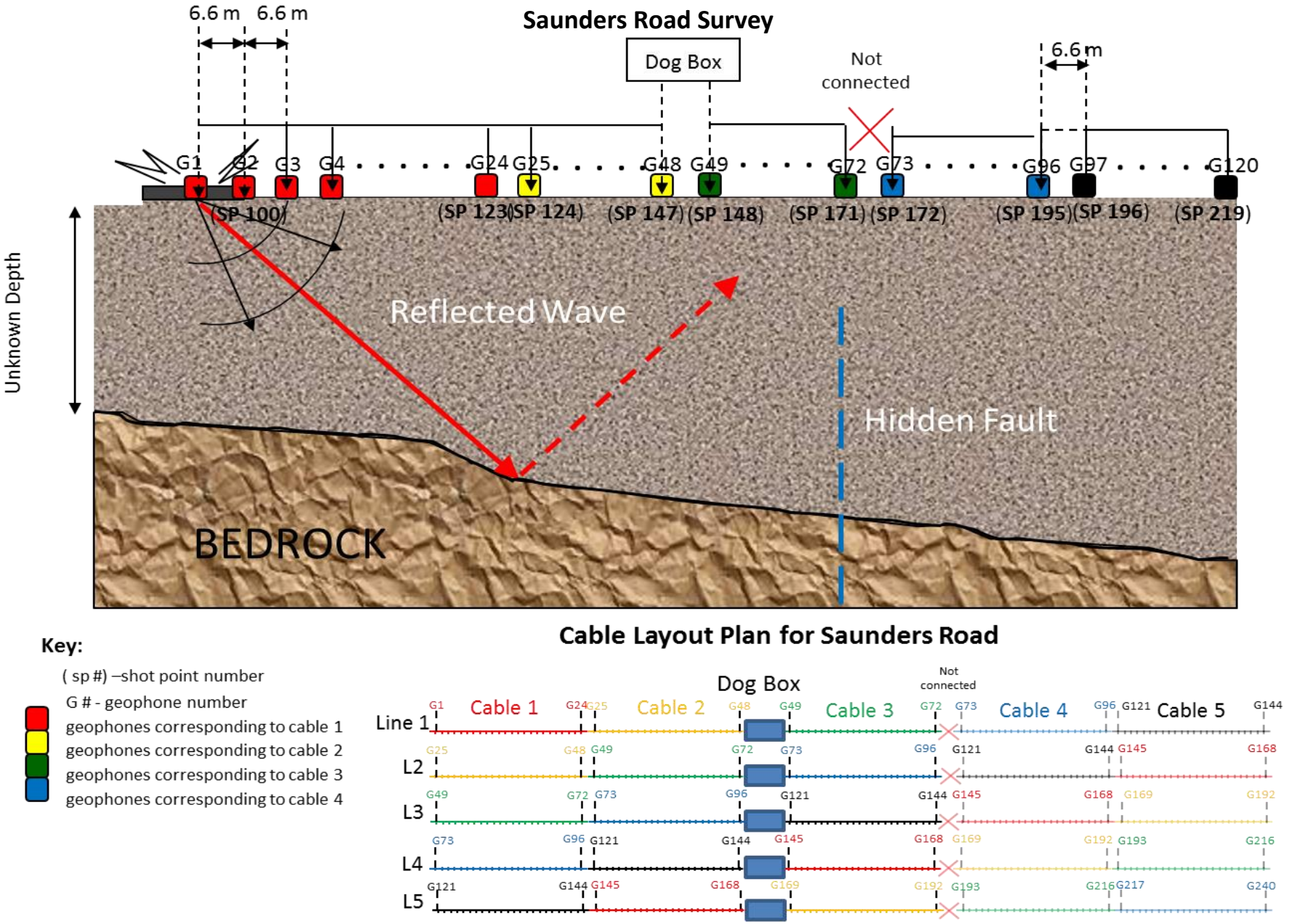

Figure 46: Design and cable layout plan for the Saunders Road seismic reflection survey

Saunders Road, Hororata

Fortuitously, the position of the Hororata Blind Fault was perfect for a survey to be run approx. 2.8 km along Saunders Road, cutting perpendicular to this feature. Saunders Road is a farm track therefore no traffic volume meant a different survey technique to what was used along the verge of Clintons Road. This time five cables were used each with 24 geophones spaced approx. 6.6m apart (i.e. a total of 120 geophones), with only three lines active at one time. The dog box was positioned so that there would be two lines behind it and one in front, with the accelerometer shooting on the lines behind the dogbox (see Figure 46). The first shot was positioned on the starting cable at shotpoint 100 (i.e. geophone 1). The next shot was then taken on shotpoint 100, then shotpoint 103, so to shoot on every third geophone (shown in Figure 46). Following this the locations of the geophones were mapped using a GPS in order to provide the location and geometry of the seismic line for the processing phase.

2.3.3.2 Equipment

The following equipment was required for both seismic reflection surveys:

- 2x vehicles (one for the dog box the other for the accelerated weight drop),
- 'Dog Box', i.e. Seismograph and roll-a-long switch, (see Figure 47)
- Accelerated weight drop + spare rubber bands (see Figure 48)
- Quad bike,
- 2x Steel plates
- 2x 50 m Tape measures,
- Geophones x 96, + 24 spare
- 5x CDP cables (4 for the survey + 1 spare) – including connectors
- 6x 'Two-way line-of-sight radios', i.e. two way radio transceivers,
- 6x cans spray paint
- Portable computer and battery,
- Field notepad for observers' report,
- Camera,
- High visibility vests, and
- GPS unit.

Using the labelled cable layout plans (see Figures 45 and 46) and a quad bike; each cable was laid down and positioned using a tape measure so the cables were taunt and the last and first geophone were 6.5 m apart for Clintons Road and 6.6 m for Saunders Road.

2.3.3.3 Device Setup

Using the quad bike the survey was setup with four CDP cables laid out at the desired 6.5 m intervals using tape measures. Once this was completed the geophones were connected along the cables and placed into the ground, whilst the cables were attached to the seismograph and roll-a-long switch in the 'Dog Box'. The next step was to ensure the seismograph was set at:

- Frequency of 30 Hz,
- O m offset,
- Station interval approx. 6.5 m,
- Spread type is set as single geophone.

Setup for the Saunders Road survey was slightly different; it involved attaching the geophones to the CDP cable at approx. 6.6 m intervals, then attaching the cables to the 'Dog Box'. This time the seismograph was set at:

- Frequency of 30 Hz,
- O m offset,
- Station interval approx. 6.6 m,
- Spread type is set as off-end centre.

It was also necessary to check that the seismograph had been connected to the trigger at the base of the shot source (accelerated weight drop). This switch instantaneously starts the seismograph recording the inputs from the geophones, when connection with the plate occurs.

2.3.3.4 Testing

Once the devices were set up, the next step was to testing to make sure the geophones, seismograph and accelerated weight drop were working effectively. This step was fundamental as the geophones, in particular, need to be checked to ensure that they were all working and connected in the right orientation (i.e. not reversed). This was completed by a couple of trial shots, using the accelerated weight drop. A signal test was also required, which was sent out by the seismograph.

Note: It is common for sand, grass, water and dirt to get stuck in the connection between the geophone and cable which obstructs the signal. Therefore be sure to complete frequent checks throughout the length of the survey.

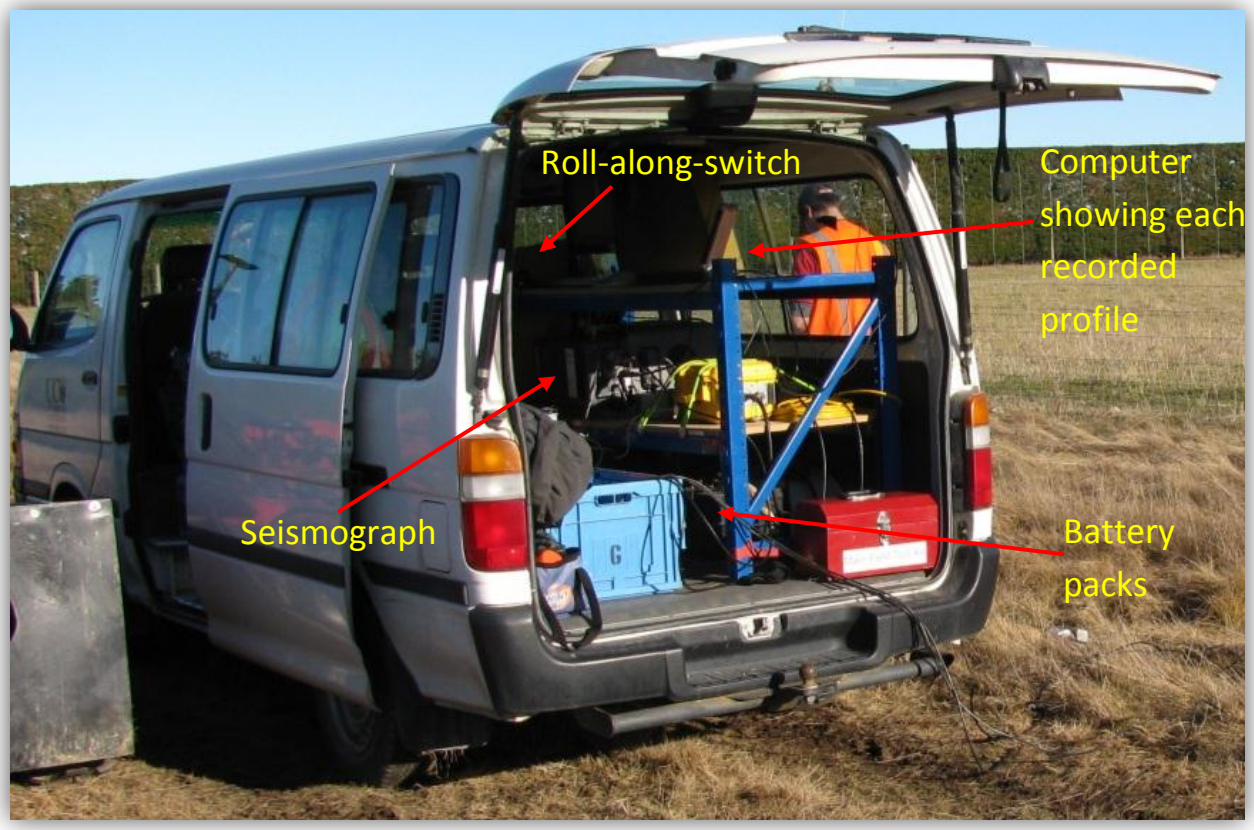

Figure 47: The dogbox used in the seismic surveys. It is where all the controlling and recording instrumentation is kept. This includes a seismograph, a roll-a-long switch which tells the seismograph the location of the shotpoint, i.e. roll it along each time you shoot at a new location, as well as batteries to power the seismograph, and the survey lines. Having the equipment positioned inside a vehicle enables the dogbox to be repositioned throughout the survey.

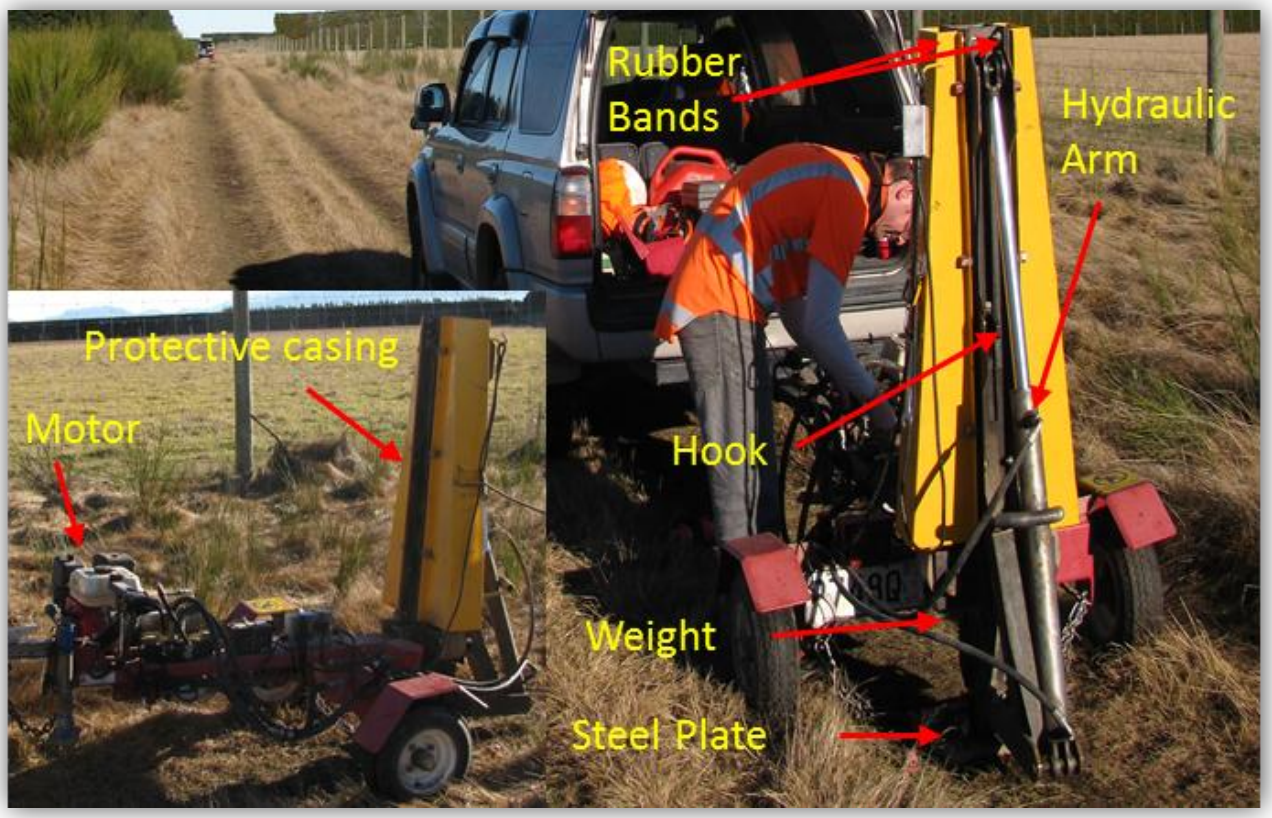

Figure 48: Accelerated weight drop generates the seismic wave in the seismic surveys. It works like a slingshot. A 25 kg steel weight, behind the yellow cover is attached to two large rubber bands. At the push of a button the hydraulic arm locks on the weight lift it up and stretching the rubber bands. Just before the top the hydraulic arm drops the weight. This allows the tensioned rubber bands to slingshot the weight at the ground hitting a steel plate placed underneath generate a seismic wave. Accelerated weight drop was courtesy of Southern Geophysical Ltd.

2.3.3.5 Survey procedure

The steps undertaken for the survey procedure for both surveys were completed as follows:

Step 1: 'Shot crew' (wave generators) position themselves approx. 13m from the first geophone (Shot point 100) for Clintons Road or on the first geophone for Saunders Road and signal to the seismograph team that they are ready. Seismograph team in the Dog Box position roll switch at number 1 and signal over the radio the survey can begin.

Step 2: The shot person, operating the accelerated weight drop, hits the steel plate 'x' number of times (for both surveys an average of 6-8 shots were used), ensuring to allow for an approx. 2 second interval between shots. This pause provides enough time for the geophones to pick up the p and s waves via reflection, refraction or ground roll without the waves from the next shot interfering.

Step 3: the shot crew then move again, another 3 m to the next shot point 101, the first official geophone. The seismograph team roll the switch to change number, and signal they are ready to proceed.

Step 4: Repeat step 2, by hitting the steel plate, and then proceed to the next shot point, 102. Wait for confirmation from the seismograph team continue, if given repeat step 2 again.

Step 5: Once shot point 124 has been completed, i.e. SP 100, 101, 102, 103... 123 and 124 have all been completed then the first cable can be disconnected and reconnected at the end of the last cable CDP cable 4 (refer to cable layout plans in Figures 45 and 46).

Step 6: Continue on new cable at Shot point 125 and repeat steps 2-5 for the new cable.

2.4 Results

The results entailed in this section are from initial investigations, RTK surveying and seismic surveys within the western and eastern study areas around the Greendale Fault trace.

2.4.1 Initial Investigation

Following the review of satellite interferometry (InSAR) images, for the period between 13 August 2010 (pre-quake) and 28 September 2010 (post-quake), movement anomalies were identified to have occurred in Charing Cross/Greendale and south of Hororata following the rupture of the Greendale Fault (Barrell, 2010). Through collaboration with David Barrell of GNS Science an introductory site investigation took place into identifying surface deformation features in the Hororata and Greendale and Charing Cross areas. Below are the results from these investigations, results made through discussion and collaboration with D. Barrell have been identified, but the majority are individual findings on what was observed.

2.4.1.1 Hororata Area

Following contact with residents and through site investigations a number of deformation features were identified within the Hororata area. The following section summarises key locations the in which surface deformation features were identified and outlines what was seen.

- *Rockwood Road,*
    - Severe fence damage was found along Rockwood Road in the large deer fences. Damage involved deformation of wire, buckling of posts, possible offset fence lines and broken posts with freshly exposed wood (see Figure 50a and d).
    - A number of hairline cracks were also found running through the tarseal on Rockwood road, within the same vicinity as the deformed fences.
- *Saunders Road,*
    - Similar deformation of fence lines (tensioned and warped wire and buckling of posts) to those seen along Rockwood Road. Unfortunately, the road is a farm track not tarseal so if cracking existed, it was not visible.

Tracking this deformation in a line Southwest, Te Pirita Road was the next road inspected. No obvious damage to the fences or road was visible along this road, indicating that the deformation petered out further southwest. Heading back towards Rockwood and Hororata to recapture the deformation pattern, a review along Leaches Road (west of Rockwood/Te Pirita intersection) identified taunt fence lines on either side of the road for approximately one kilometre (D. Barrell pers. com. 24 October, 2010). This marked the furthest westward deformation point.

Heading back towards Hororata and northwest towards Derretts road, a number of other deformation features were identified, including:

- *Cotons Road*,
    - Located directly behind the main street of Hororata, the fence lines along Cotons had very strained and deformed fence lines shown in Figures 53 and 54.
- *Hartnells Road*,
    - North of the Horarata River, a visual inspection of the fence line and powerpoles running the length of Hartnells road towards Substation Road suggested the possibility of a slight bend (D. Barrell., pers. coms. 24 October, 2010).
    - South of Hororata River, from Board Road to Rockwood Road, Hartnells Road turns from a gravel road into a grassed over farm track. This unfortunately concealed any evidence of surface cracking near the intersection with Rockwood Road. But, the fence lines reflected strain on the area. As the wire was stretched and taunt in places heading north towards Morgans Road. Crossing the intersection with Morgans road the tension in the fences dissipates.
- *Morgans Road*,
    - At first sight Morgan Road further reflected the taunt fence lines inspected along Derretts Road. However, through discussion it was later deemed that this was just as a result of overtightened wire by the farmer (D. Barrell., pers.com. 24 October, 2010).
- *Derretts Road,*
    - A series of cracks were seen to cut through the road tarseal in an east-west orientation, between the two bridges along Derretts Road.
    - Liquefaction in the form of sand volcanoes sprung from these cracks, following the September earthquake, as documented by Simon Cox on 5 September (D. Barrell., pers coms. 24th October, 2010).
    - Standing at the northern or southern end of Derretts road looking toward the middle section, where the cracks are visible. This reflects what is believed to be small subtle dextral bend (D. Barrell., pers. coms. 24 October, 2010).

The last part of the search for this area involved scouring roads north of Hororata for signs of rupture features. The only thing located were several small cracks visible in the tarseal along Duncans Road, which were deemed the result of road embankment failure (D. Barrell., pers.coms. 24 October 2010).

2.4.1.2 Greendale / Charing Cross Area

Following the review of InSAR images, for the period between 13 August 2010 (pre-quake) and 28 September 2010 (post-quake), a displacement anomaly was identified in the vicinity of Clintons, Ridgens and Adams Roads following the rupture of the Greendale Fault (Barrell, 2010). The images also identified the best place to begin was Adams Road, as it was aligned along a strong fringe (D. Barrell., pers.coms. 24 October 2010).

After reaching the location it was immediately evident that discovering surface deformation features was going to be more challenging than initially perceived. This was due to the fact that the majority of the roads around Charing Cross and Greendale area are gravel not tarseal. So they are less suited to expressing features such as subtle cracks (D. Barrell., pers.coms. 24 October 2010).

Of the roads that were sealed the results are as follows:

- *Greendale Road*,
    - At the south-western (SW) tip of Adams Road, Greendale Road did not show any visible signs of deformation. No cracks could be found in the tarseal, and the fence lines were not offset or over tensioned.
    - Through correspondence with landowners at this point, it was discovered that the only surface deformation in Greendale was near the substation at the corner of Coaltrack and Ridgens Roads (the SW end of the Greendale fault).

Following discussions with landowners, surface deformation likely to be attributed to the extension of the Greendale fault trace was tracked to Gallenders Road. Here, a number of features were present and documented, including an offset fence lines and power-poles as well as deformation of fence posts (see Figures 52c and d).

Surveying within close proximity of the Charing Cross displacement anomaly, shingle roads: Dip, Hawthorne, Storeys and part of Clintons Road (between Ridgens and Bealey Roads) were inspected. Unfortunately, any features present along these roads were masked by the shingle. However, the sealed section of Clintons Road (southeast of Ridgens Road) as well as the sealed Ridgens Road (oriented NE-SW) provided some interesting observations attributed to the displacement anomaly. They included:

- *Clintons Road,*

- From approx. 300 m to 640 m southeast of Ridgens Rd, a set of prominent cracks existed in the tarseal within a topographic low previously located D. Barrell (pers.com. 24 October, 2010). The furthest crack at approx. 640 m from Ridgens coincided with the crest of a topographic rise, leaving the low lying section.
- The cracks ranged in size from hairline (< 5mm) nearer to Ridgens Road becoming more prominent (approx. ≤ 10 mm) further southeast. Due to no centreline along Clintons Road it was not possible to determine if there was any laterally movement associated with these features.
- Through collaboration with D. Barrell these cracks were identified to have a typical trend of 010°/190° to 020°/200° (pers. coms. 24 October, 2010).

- *Ridgens Road,*
  - Next inspected was Ridgens Road northeast of Clintons Road. Heading northeast along the road, sparse hairline cracks were evident for approximately before becoming more prominent from 250 m from the intersection of the roads.
  - The most prominent cracks were observed at approx. 700 m from the intersection with Clintons Road. Beyond this point the cracks continued for nearly a kilometre before becoming progressively less frequent and wide (D. Barrell., pers.com. 24 October 2010).
  - No cracks were found beyond approx. 1.5 km from the intersection of Clintons and Ridgens Roads.
  - Another interesting surface feature identified was the change in the gradient plain heading northeast along Ridgens road such that the road bends out of line of sight (D. Barrell., pers.com. 24 October 2010).

Having identified these cracks, it was decided a wider investigation should be undertaken. This involved examining the adjacent sealed roads, which included Ridgens Rd (southwest of Clintons Road), Hollands Rd, Clintons Road (further southeast) and Bealey Road (between Adams and Ridgens Roads). Unfortunately, there were no obvious signs of cracking found in any of these roads, nor was there any sign of deformed or taunt fence lines with the exception of Hollands Road whether the Greendale Fault trace was visible through the offset fence line (see Figure 58).

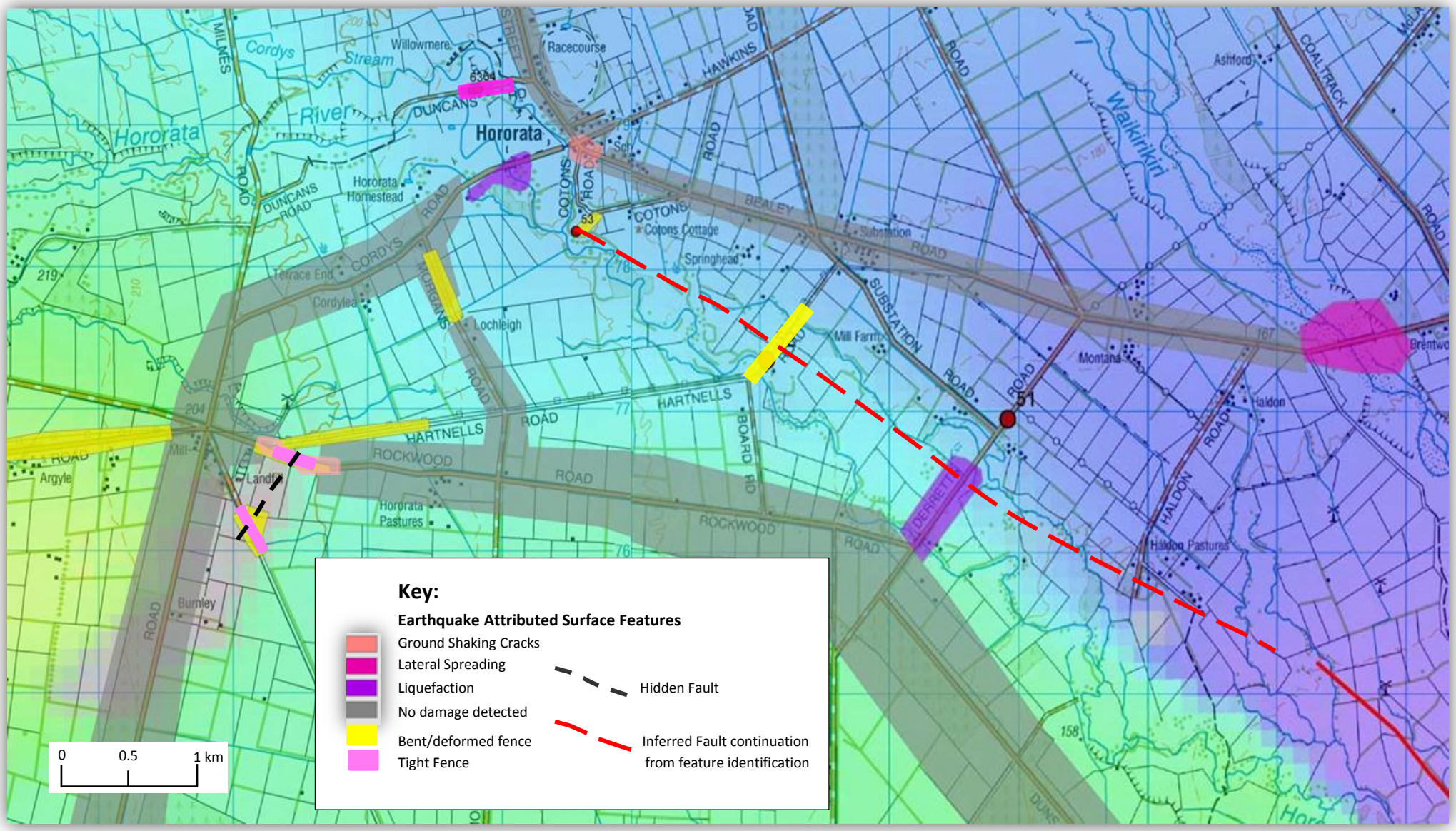

Figure 49: Features identified in site investigations of the Hororata area. The map identifies a number of damage features particularly to the Southwest of Hororata (Sourced and modified from Barrell, 2010).

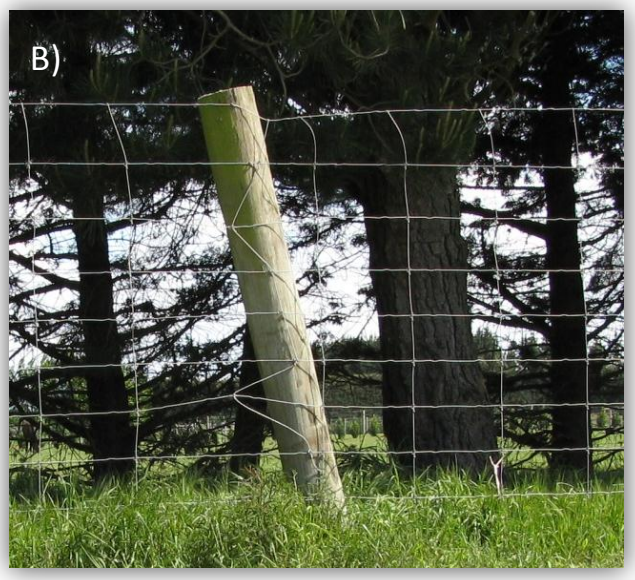

Figure 50: Deformation caused to fencelines as a reuslt of the earthquake. Starting at the top, A) shows the deformed fenceline along Rockwood Road in Hororata, B) shows how the wire is streched as the fenceline is offset by the fault trace near Highfield Road, C) Shows a deformed fenceline along Old TaiTapu Road south of Halswell, D) shows the strain on the wire as a result of the Darfield earthquake along Rockwood Road.

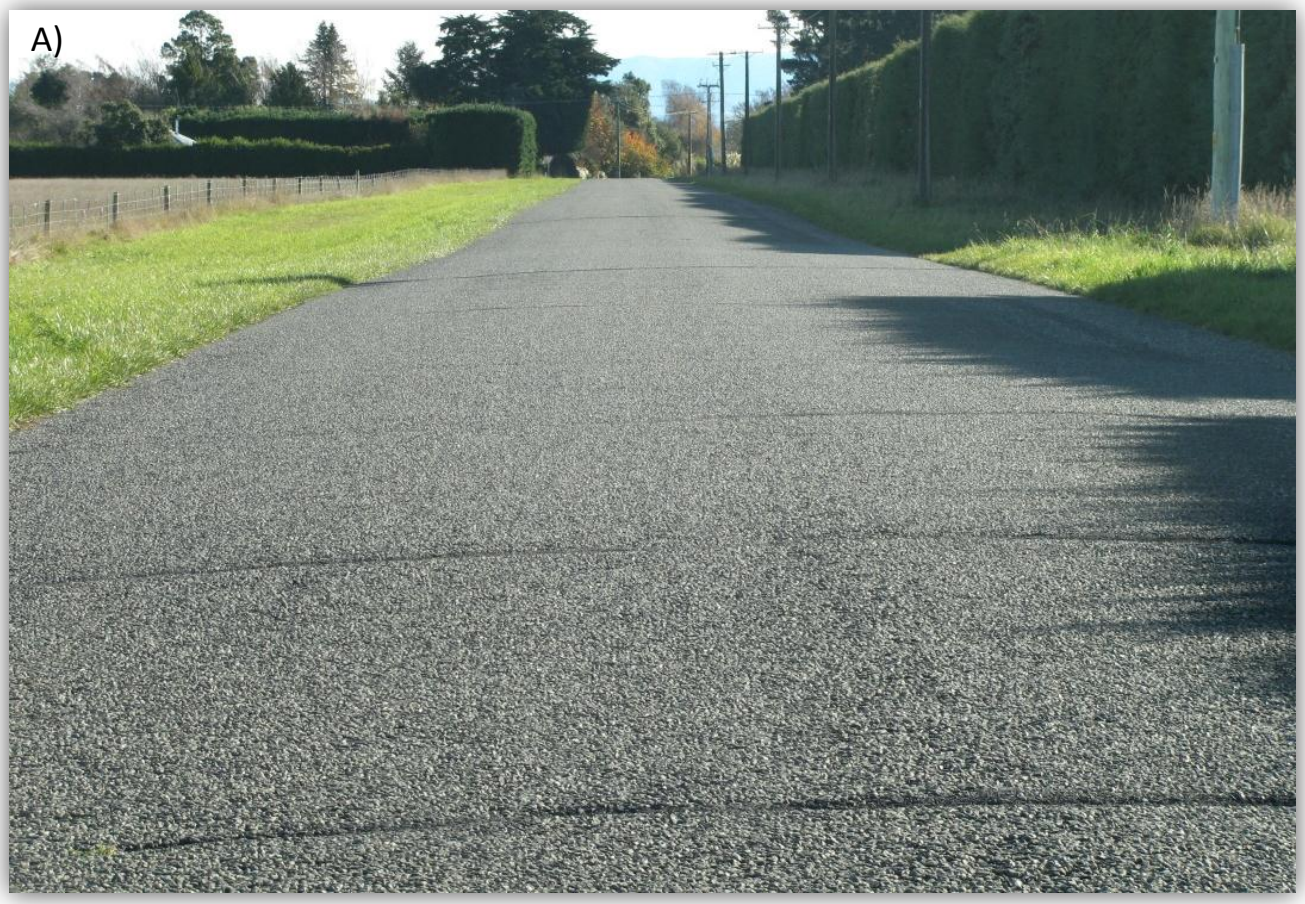

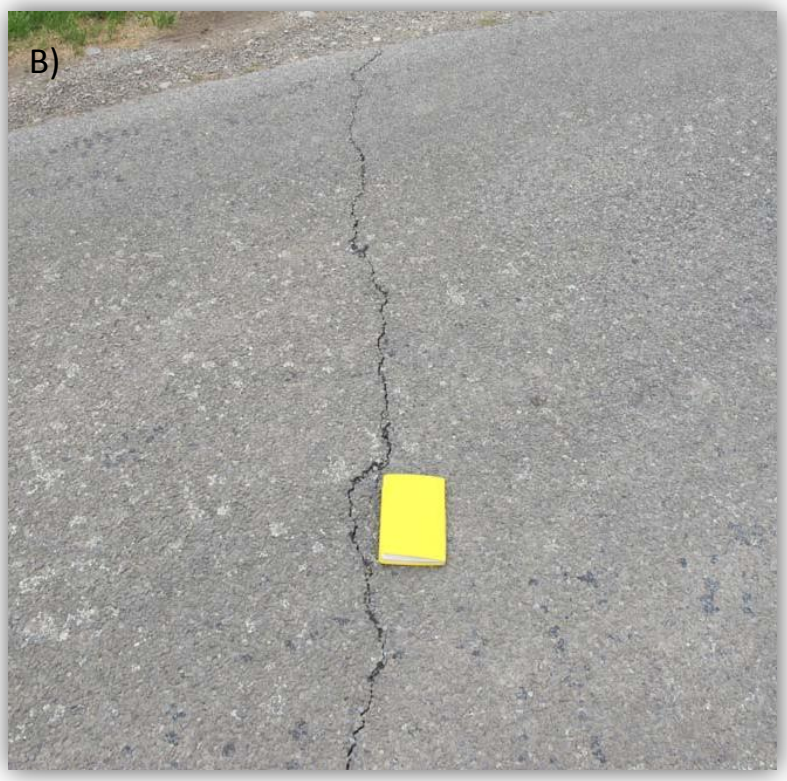

Figure 51: Cracks observed in the road around the Canterbury region attributed to the earthquake. A) shows Clintons Road cracks possibly due to the rupture of a blind fault at the same time as the Darfield earthquake, B) crack along Old Tai Tapu road, south of Christchurch, C) Crack running through Coaltrack Road south of Bealey Road.

Figure 52: Offsets in the hedges, power-poles and fence lines in the landscape around Canterbury.

Figure 53: Taunt and deformed fence line on Cotons Rd, looking towards the NE (Hororata less than 200m north), and detail of the fence can be seen in the lower photo (Image courtesy of D. Barrell).

Figure 54: Close up of the strained and deformed fence on Cotons Rd (Image courtesy of D. Barrell).

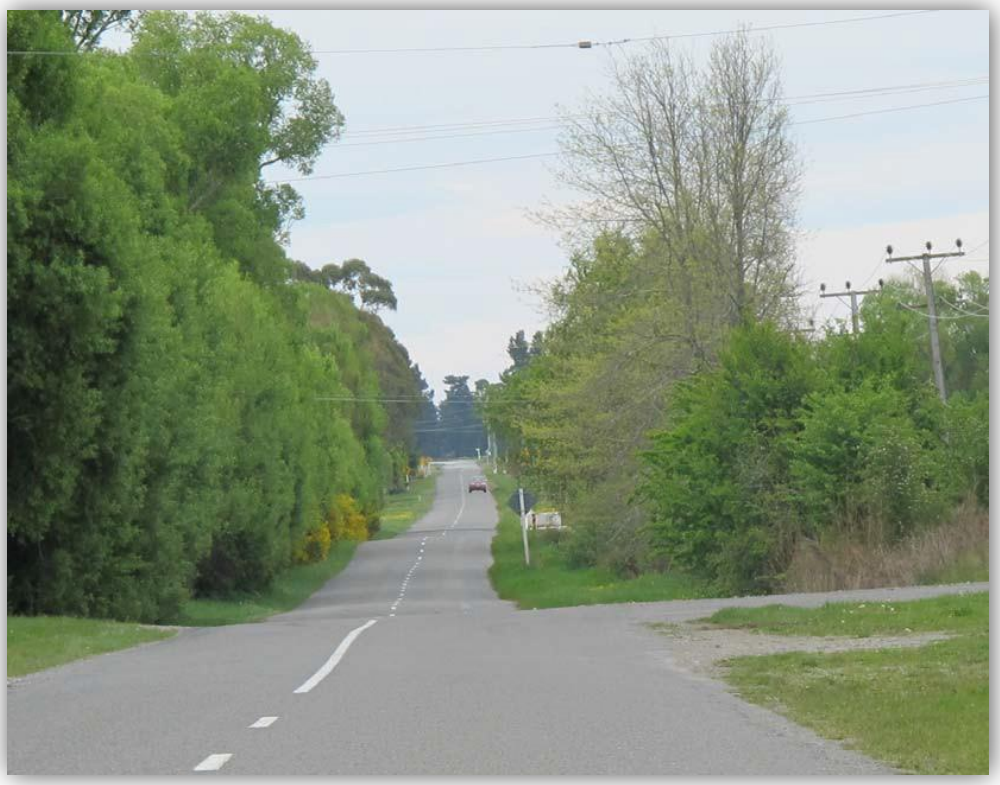

Figure 55: Possible dextral bend in the centreline of Derretts Rd, looking southwest form Substation Rd location 51 in Figure 3 (Image courtesy of D. Barrell).

Figure 56: Possible subtle dextral bend in the fence on Hartnells Rd, looking NE towards Hororata Substation, and Location 52 in Figure 3 (Image courtesy of D. Barrell).

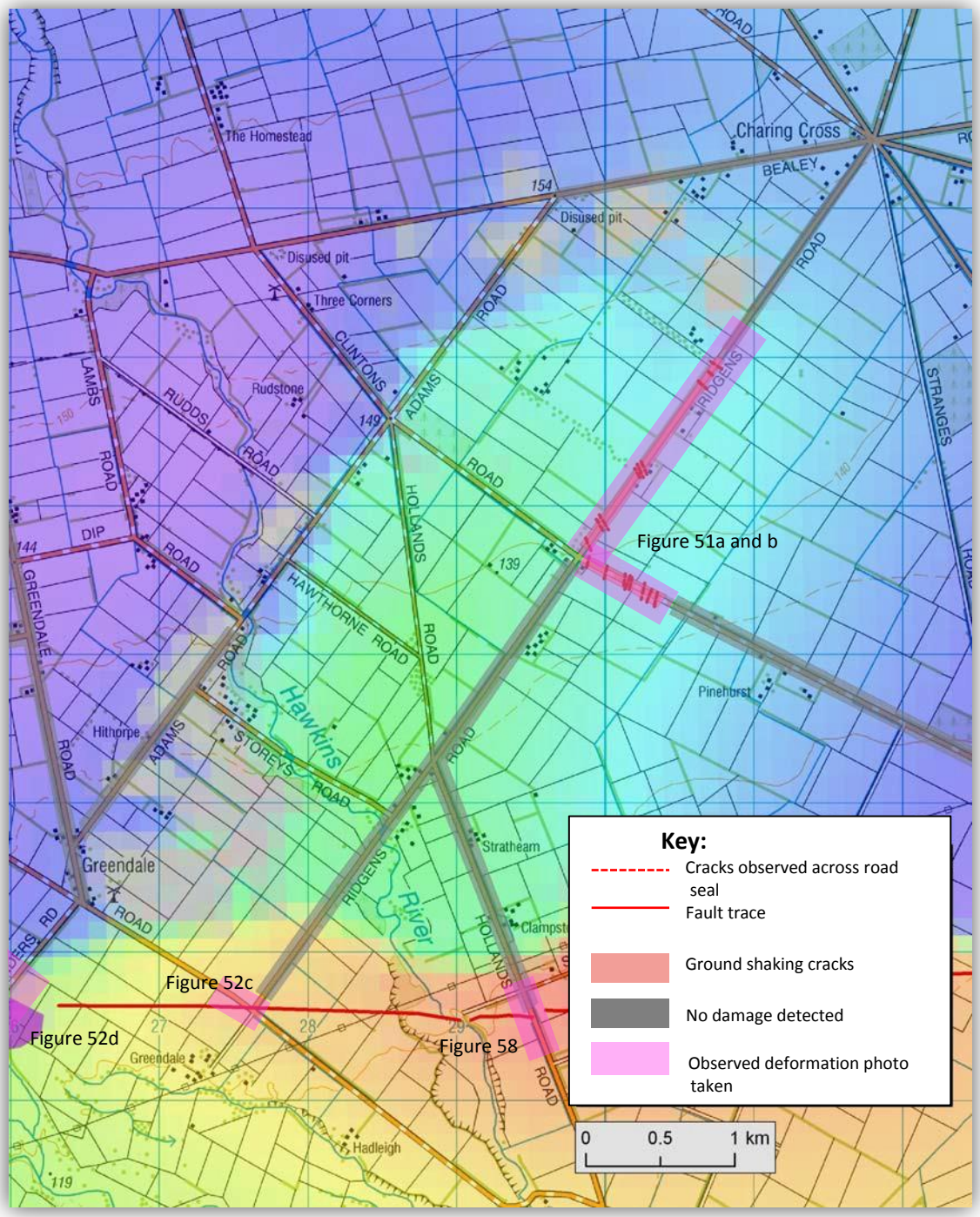

Figure 57: Map of damage features in the Charing Cross area. Red lines along Clintons and Ridgens Road are a schematic depiction of the cracks found in an investigation to the region with D. Barrell. Features are overlayed on the InSAR image used in the investigation of the area (Sourced and modified from Barrell, 2010).

Figure 58: Greendale Fault Trace observed in the offset fence line and power poles along Hollands Road (Image courtesy of S. Orsbourn)

2.4.2 RTK Surveying

Following the completion of the site investigations, a detailed record of all the identified features was compiled using a RTK GPS. The raw data was then corrected following post-processing by Nicola Litchfield at GNS in Wellington. The results from these surveys are represented by western and eastern sections as well as a map showing everything. Individual site map were also produced these can be found under the heading RTK in Appendix C.

Western Section

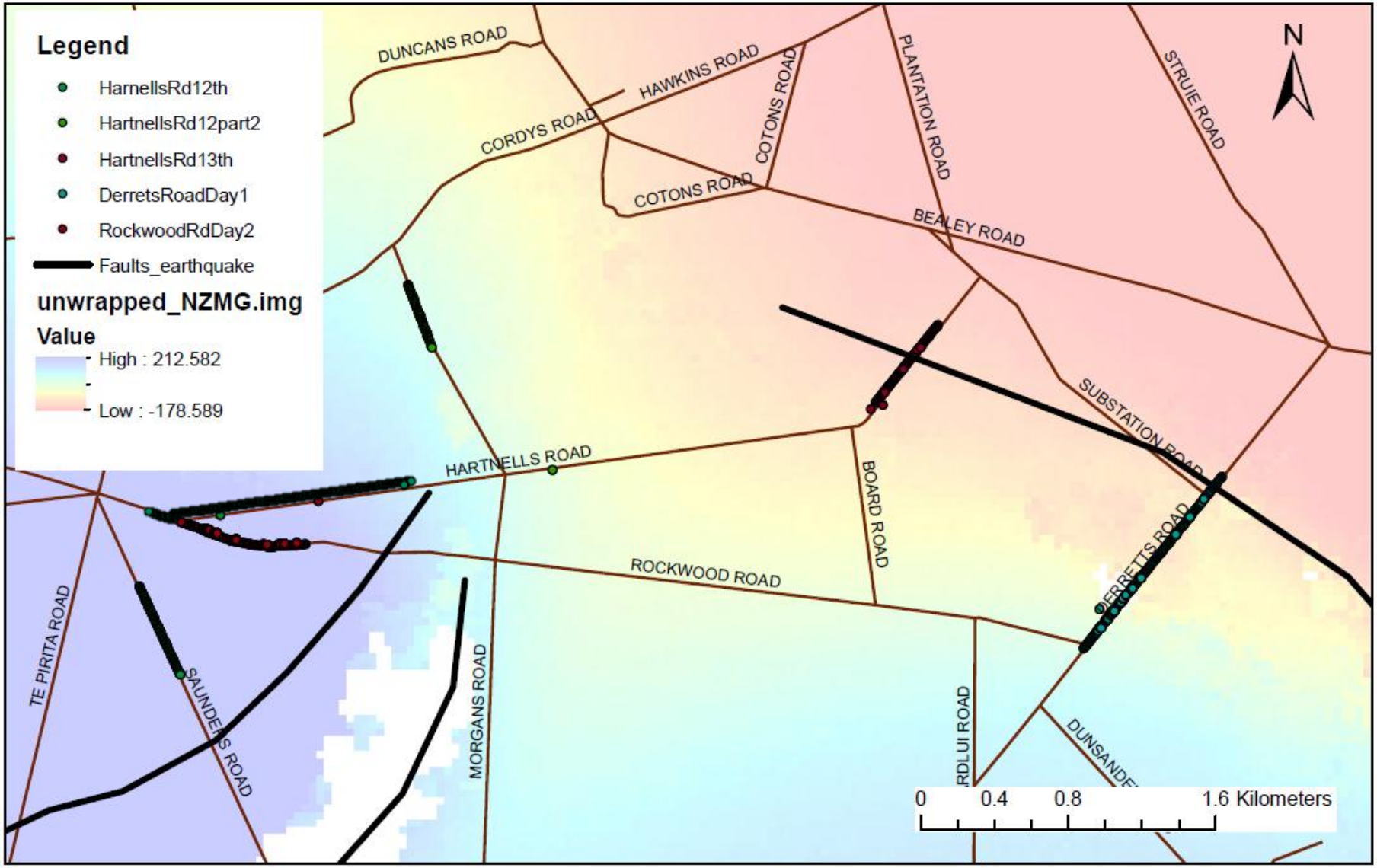

Figure 59: RTK sites along the western end of the Greendale Fault Trace.

Map of Everything

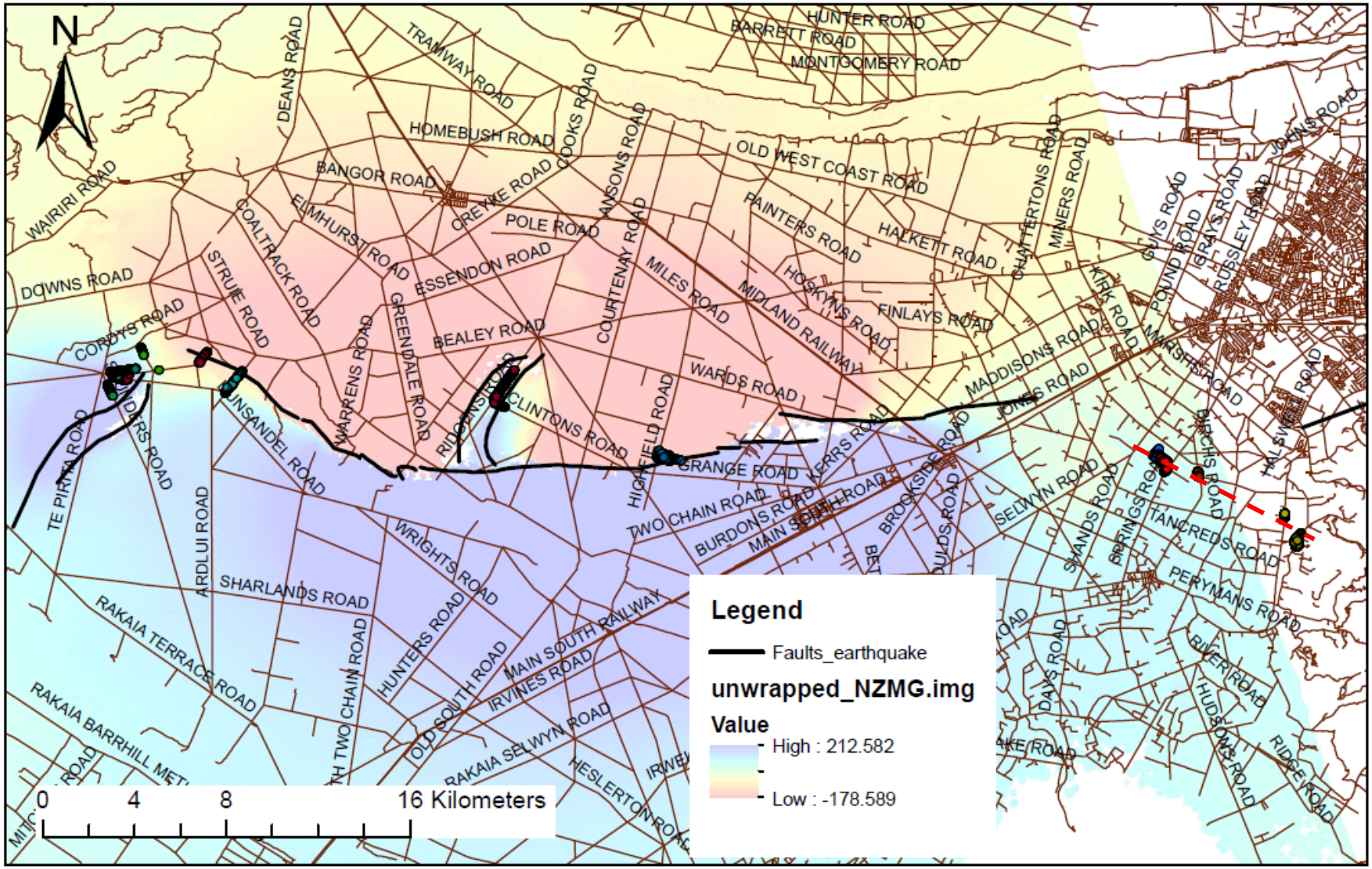

Figure 60: RTK sites with respect to the Greendale Fault Trace. The red line represents possible continuation of the fault trace east.

2.4.3 Seismic Surveying

This section outlines the steps required to process the data and formulate the results. It also depicts the survey profiles and outlines the interpretation of the results from the Clintons Road and Saunders Roads survey profiles.

2.4.3.1 Processing

Following the collection of the survey data, processing was required to produce the wave profiles for the sites; this step was completed by Mike Finnemore at Southern Geophysical Ltd. The first step of processing, involved converting raw seismograph generated data (SEG-2) into a recognised format such as Seismic UNIX (SU). This was followed by inputting the geometry, which aligns the location and position of the geophones and shotpoints to match the dataset.

After this was completed the next step was to apply a filter to screen the unwanted noise, such as airwaves from wind, and seismic refractions. However, the data recorded was particularly low frequency, therefore this step required a particular software package. The low frequency data meant it was difficult to distinguish between the low frequency reflections and ground-roll. The low frequency data occurred as a result of the low water table at the sites, making it harder for the induced wave to propagate deep into the subsurface.

Southern Geophysical did not have the required software to perform FK filtering which extracts the low frequency reflections from the strong ground roll. Therefore the data was sent to Excel Geophysical Ltd where the processing and filtering occurred courtesy of Anne Melhuish. Following a quick review of the data by Anne it was discovered that it was not worth processing Clintons Road as this would not alter the image. The data itself was chaotic. Therefore the following processing steps were completed to produce Figure 66 for the Saunders Survey:

- Elevation statics,
- Bad trace edit – removal of bad traces,
- Amplitude recovery and surface consistent deconvolution,
- Spectral whitening,
- Bandpass filter – applies a frequency filter(s) to each input trace using an algorithm,
- Velocites/residuals - two passes of each,
- Normal moveout correction (NMO correction) applied to enable stacking,
- Interactive top mute,
- Automatic gain control (AGC),

- Stacking and additional spectral whitening,
- FX Deconvolution, and AGC again to finish.

An F-K filter was also considered, however upon trial, the frequency filter removed most of the ground-roll energy and some of the wave. Thus, it was not used in the end. This signified the completion of processing Saunders Road data. It then enabled the production of a stacked and migrated survey profile shown in Figure 66.

After the production of the stacked profile the final stage involved converting the depth profile from the measured units of time (milliseconds, ms) into a more commonly recognised metres scale. This involved using the simple velocity equation $V = d/t$ or rearranged to $d = V\,x\,t$, where d is the distance in metres (m), V is the selected profile p-wave velocity in metres per second (m/s), and t is the time in seconds (s). This was applied to all the time values shown on the y axis of the seismic profile figures. For example, through processing the stacked and migrated image selected for the Saunders Road profile in Figure 66, has a p-wave velocity of 2000 m/s. Thus, to obtain the depth in metres for time = 800 milliseconds (ms) or 0.8 s on the profile, the process is as follows:

$$d = V\,x\,t = 2000\,m/s\;x\;(0.8/2) = 800\ \text{m}$$

This indicates that time (ms) is directly proportional to the depth in the Saunders profile. It is worth noting that t/2 or 0.8/2 in this case is because the time reflected is a two way time. I.e. the travel time for the wave to propagate down in the subsurface and then reflected back to the surface where it is measured by the seismograph.

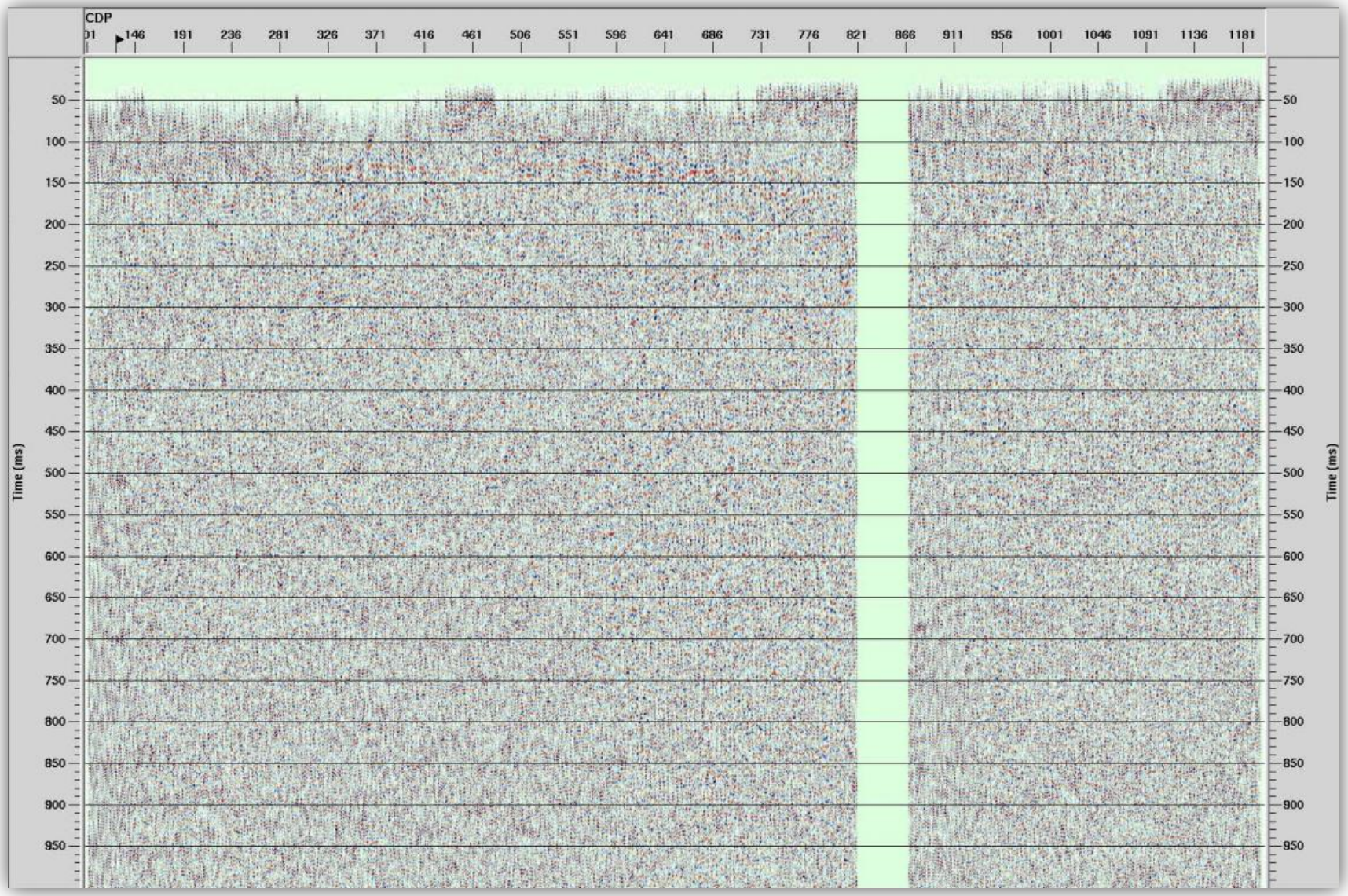

Figure 61: Raw stacked results from the seismic reflection survey along Clintons Road (Image courtesy of Mike Finnemore from Southern Geophysical Ltd).

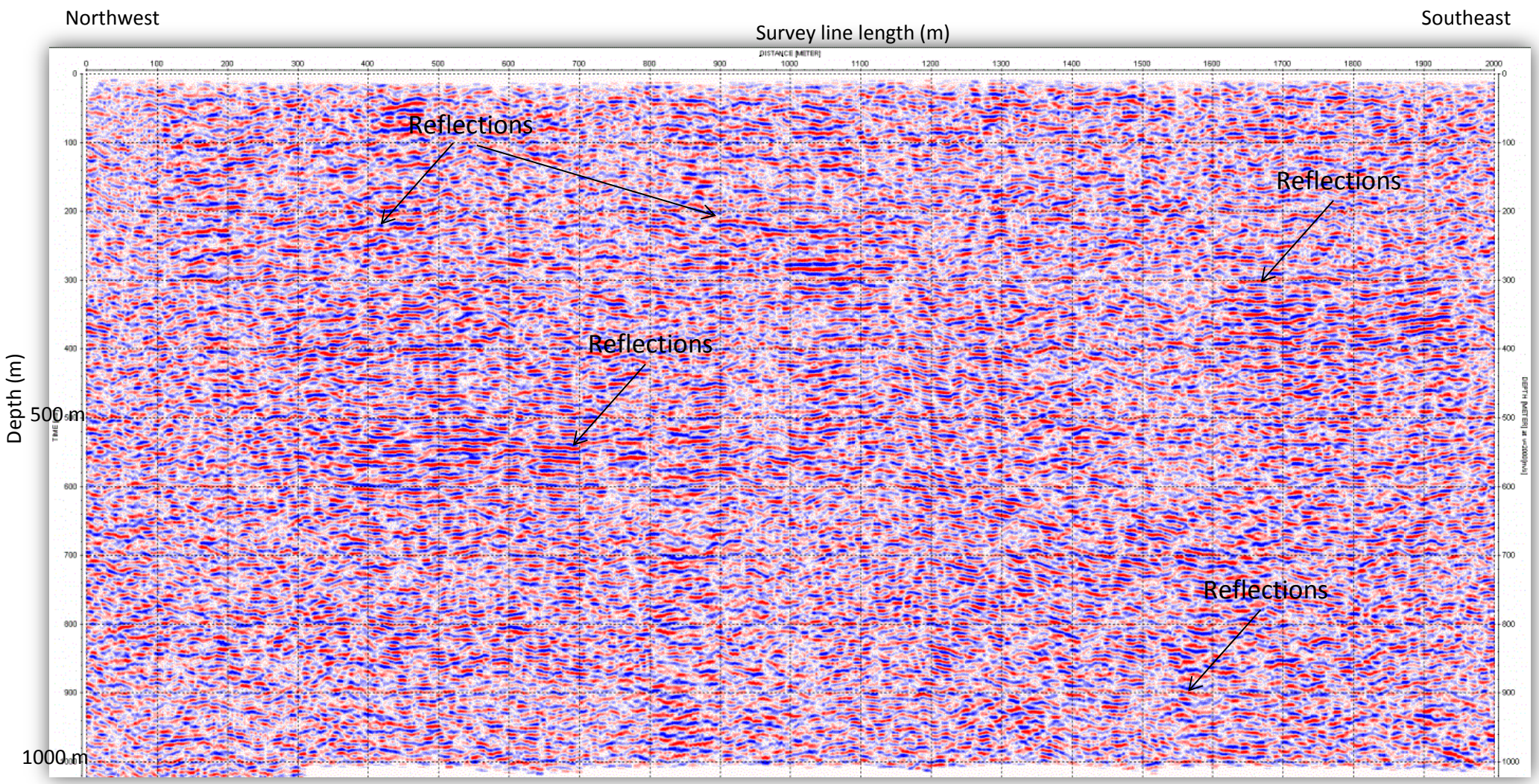

Figure 62: Stacked and migrated seismic reflection profile for Saunders Road. Note the horizontal reflection packages present (Image courtesy of Mike Finnemore from Southern Geophysical Ltd).

2.4.3.2 Profiles

Figures 61 and 62 show the results for Clintons Road and Saunders Survey, respectively. Overviews of each profile are described below.

The results from the Clintons Road survey are represented by the raw stacked image in Figure 61. The image reflects a survey under 1.181 km in length running from the south to north. Not being able to full process this survey meant identifying anything within the raw data was difficult. However, within this profile several small non continuous reflectors are visible in the near surface. Unfortunately with depth these reflectors become less prominent and blend in with the low frequency background noise making it nigh on impossible to differentiate between the two. The distinctive gap in the profile corresponds to Ridgens Road. This section of the survey line was leapfrogged for safety reasons and to avoid damage to surveying equipment. Overall the Clintons Road profile reflects a very disrupted and chaotic sequence.

In contrast, Figure 62 reflects a fully processed stacked and migrated profile for Saunders Road survey. It is represented as a depth and chainage cross-section running from the northwest corner to the southeast corner along a 2 km stretch of Saunders Road. To provide an indication of what the processing achieve the raw stacked pre-processing Saunders Road image can be found in Appendix B along with survey field notes. On first glance it is immediately obvious that a number of reflectors are visible throughout this profile. In particular, Figure 61 reveals multiple variously thick horizontal reflection packages northwest to southeast in orientation. These can be seen to be more continuous than in the Clintons survey, with reflectors able to be traced along the survey line. Interpretation of this line will help to provide a greater understanding of these reflections.

2.4.3.3 Interpretation

Saunders Road

Through interpretation of previous seismic reflection studies around the Canterbury Plains (e.g. Dorn *et al.*, 2010 and Jongens *et al.*, 2012) it was determined that the following sub-surface layers expected in Hororata were Quaternary gravels, Pliocene Kowai Formation, Paleogene layer, and depending on the depth of the profile a Late Cretaceous layer (Jongens *et al.*, 2012). A consistent reflector at approx. 200 ± 50 m near the northwest end of the survey profile becoming 100 ± 50 m towards the southeast was interpreted as the boundary between the Quaternary gravel layer and Pliocene Kowai Formation. This was approximately consistent with Jongens *et al.* (2012) study, which located the layer at just over 250 m (Figure 64).

The next obvious reflector identified was 550 ± 50 m at the northwest end of the profile. Tracing this reflector along the survey line towards the southeast it disappears at approx. 1250 m. A similar strong reflector can be seen to appear approx. 1600 m along the line, although it is at a significantly shallower depth (350 ± 50 m) (Figure 63). This appears to be the same boundary, correlating to the start of the Paleogene deposits, whilst reflectors at the bottom of the survey profile represent the boundary between the bottom of the Paleogene and start of the Late Cretaceous deposits (see Figure 69). A variation in the change in the depth of 200 m was also identified noticed along this boundary. Starting at approx. 1000 m deep at the northwest end of the line by 1500 m, it reaches 800 m at 1500 m along the line before dropping back down to 900 m at 2000 m the southeast end of the survey (see Figure 63). This significant change in the depth along the Pliocene/Paleogene and Paleogene/Late Cretaceous boundaries is interpreted as offsets from the northwest dipping Hororata blind fault and anticline. After identifying this fault a number of possible splays can be seen to the northwest between 900 -1200 m along the survey line corresponding with changes in the lithology boundaries (see Figure 63).

Comparing these identified faults to the Jongens *et al.* (2012) study it was found a similar set of splayed faults were identified, although at a significantly deeper depth between 1 and 1.25 km (approx. 300 – 400 m deeper). This discrepancy in depth could be explained by slip on these faults during the Darfield sequence displacing shallower layers and enabling identification closer to the surface. This is supported by Beavan *et al.*, (2012), which revealed the top of the Hororata Blind Fault is at a depth of approx. 500 m beneath the surface using InSAR data.

Clintons Road

It was not possible to interpret the Charing Cross raw profile from Clintons Road as the low frequency data and background data could not be differentiated with any degree of accuracy. However, through discussion with M. Finnemore it is possible that the profile is in fact reflecting what is beneath the area (pers.com. September 2012).

A study by Beavan *et al.*, 2012 using InSAR interpretations of the Charing Cross Fault found the top of the fault is 500 m beneath the surface. This ruled out the possibility that top of the Charing Cross Fault is located deeper than penetration depth of the survey.

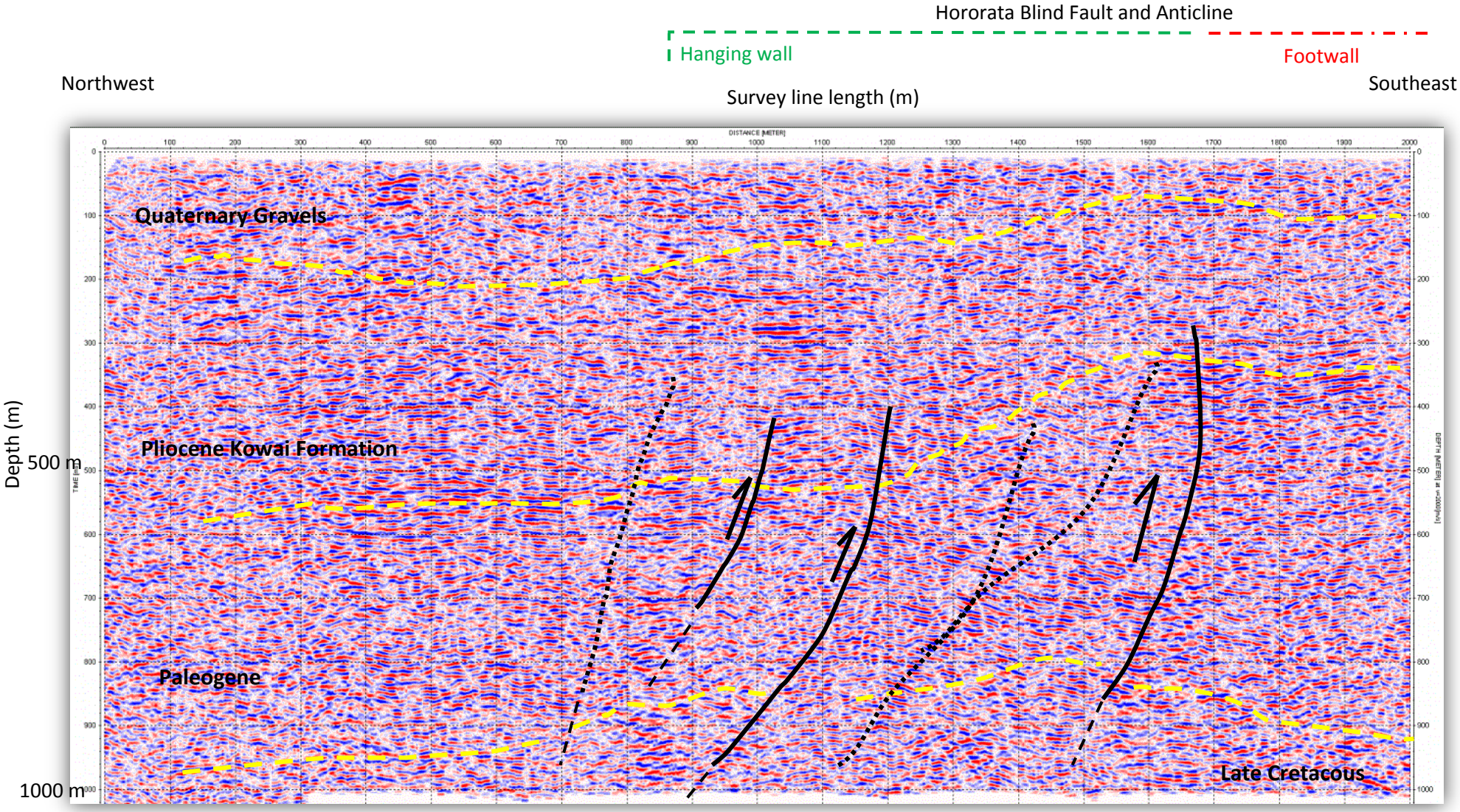

Figure 63: Saunders Road interpreted seismic profile. Yellow dotted lines represent lithology boundaries; black bold lines represent likely fault splays with black dotted lines alternative positioning of the faults.

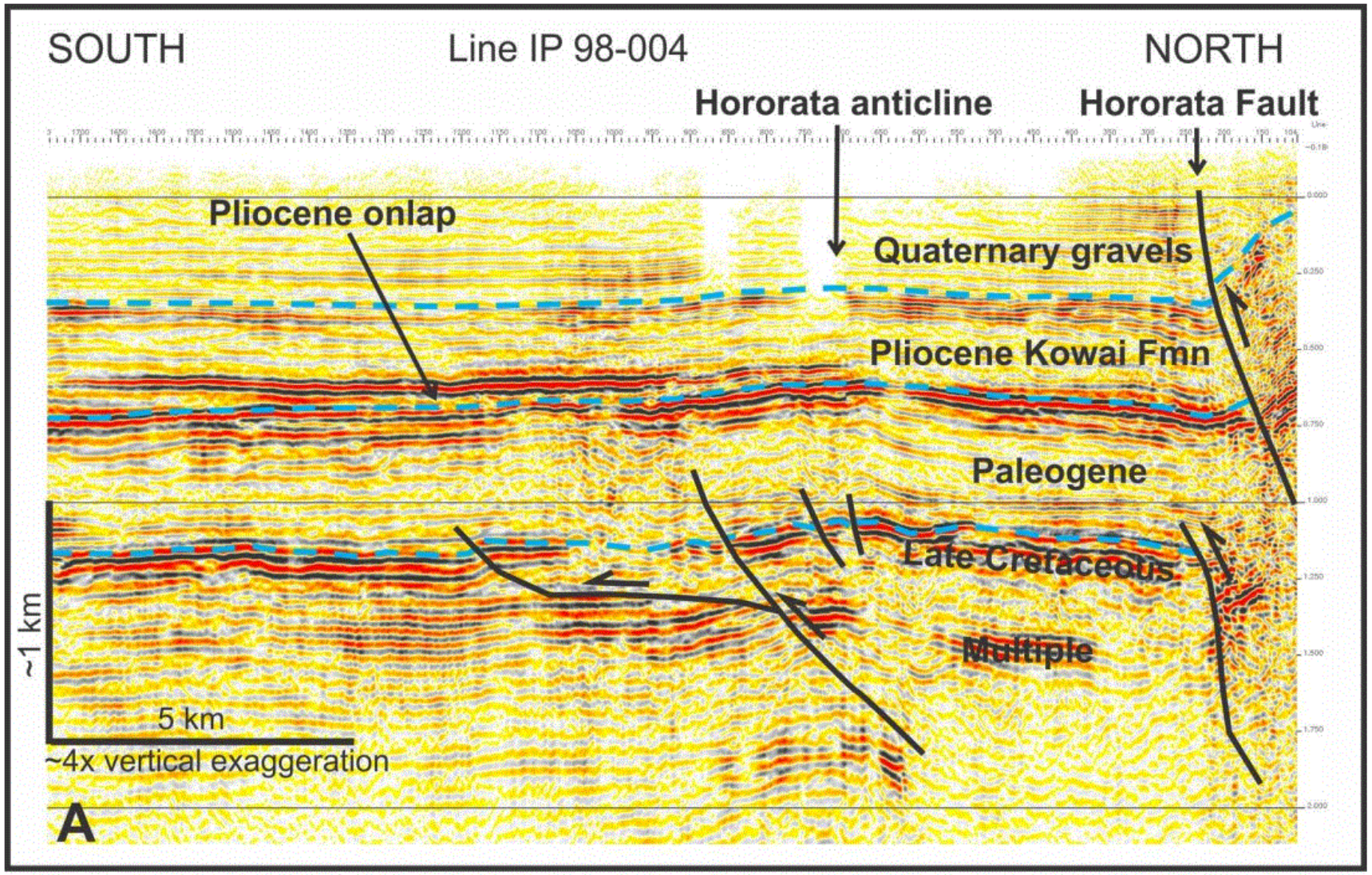

Figure 64: Survey profile produce and adapted by Jongens *et al.*, (2012) from an oil exploration investigation of the Canterbury Plains by Indo-Pacific Energy 1998 (Source: Jongens *et al.*, 2012; 1999).

2.5 Discussion

From the site investigations and RTK surveying results multiple earthquake attributed features were located within the landscape southwest of Christchurch. This section discusses the results from the combined site investigations, RTK surveys and seismic reflection surveys relative to the hypothesis and related questions for this chapter.

My interpretations of the seismic profile for Saunders Road in Figure 63 shows the Hororata Blind Fault and Anticline dips moderately steep (approx. 50 - 70^{o}) to the northwest with the hangingwall identified on the northeast side of the fault and footwall southeast. The top of the fault was also imaged at a depth of 300 m beneath the surface. This is 200 m shallower than what Beavan *et al.*, (2012) identified through InSAR surveys, and a lower angle. Assuming these interpretations are correct, this indicates it is possible to characterise these structures through near-surface seismic reflection investigations. Site investigations and RTK surveys provided detailed additional information about the Hororata Blind Fault with road cracking and deformed fencelines but were not able to pinpoint the location of the fault or characterise its structure without a surface trace. But Charing Cross seismic reflection survey indicated limitations in the reflection surveying in the Canterbury region particularly during period where there is a low water table. Thus, a combination of methods is best in characterisation near surface faults

Saunders Road survey profile of the Hororata Blind Fault also provides evidence that suggests the alluvial gravels beneath the Canterbury Plains do play a role in dissipating slip energy from the rupture of a fault. This is indicated in the top 300 m of the survey profile with the lithology boundary at 100 m being less disturbed and variable in depth that the deeper boundaries. Indicating the gravel is dampening in the amount of slip and it runs out of energy within the top 300 m. Thus if slip is being dissipated by gravels in the near surface, it is unlikely to be able to recognise slip on this structure geologically.

2.5.1 Future work

The site investigations and RTK results identified a number of areas worthy of further studies. These including Saunders Road, Rockwood Road, and Derrets Road in the Hororata area and Clintons Road, Ridgens Road, and Coaltrack Road around Charing Cross.

2.6 Conclusion

The seismic reflection survey along Saunders Road revealed that it is possible to characterise the structure of faults through near surface geophysical investigations. The Hororata Blind Fault was

found to be dipping northwest at an angle of 50-70^{o}. Furthermore the survey revealed that role gravels play in dissipating slip acting like a dampener. Limitations of the seismic survey method were also revealed within the Charing Cross profile, signifying the benefit of multiple investigation methods.

Part III: Can the New Zealand geodetic network be used for repeat cadastral surveys in determining surface deformation? What do they reveal about the patterns of surface deformation in the Canterbury earthquake sequence?

Outline:

3.1 Introduction

Large scale effects of fault rupture are typically documented by InSAR and regional GPS surveys of high order benchmarks. Getting 3-dimensions from InSAR relies on both ascending and descending tracks (Wright *et al.* 2004) or on combined GPS and InSAR (Beavan *et al.* 2010; Beavan *et al.* 2012). Resurveying of lower order cadastral marks has proven useful (Lee *et al.,* 2006; Lee *et al.,* 2010; Lee *et al.,* 2011; Duffy *et al.* accepted manuscript). In particular Lee *et al.* (2006; 2010; 2011) and Lee and Shih (2011) are iconic cadastral studies. Using the digital cadastral system, instead of the conventional way of surveying land and building boundaries, they collected data for co-seismic motion around a pop-up structure that occurred in the Shihkang area of Central Taiwan following the 1999 Chi-Chi earthquake.

A local study by Duffy *et al.* (accepted manuscript 2012) looked at dextral slip along the western end of the east-west striking Greendale fault during the 2010 M_W 7.1 Darfield earthquake transferred onto a northwest-trending segment, across an apparent trans-tensional zone, here named the Waterford releasing bend. To do this detailed surface mapping, differential analysis of pre- and post-earthquake LiDAR, and cadastral surveying was used (Duffy *et al.,* 2012). Of particular relevance was that the cadastral surveys involved re-occupation or re-survey of property boundary marks to produce high-resolution (cm-scale) estimates of co-seismic ground-surface displacements across the Waterford releasing bend.

After blind thrust features in Charing Cross and Hororata were identified by InSAR data, it was decided a small scale geodetic survey should be undertaken using the cadastral network to:

1. Re-occupy previously surveyed benchmarks in order to quantify the combined Darfield Earthquake (co-seismic) and post-seismic deformation field. In particular, to quantify surface deformation around the blind fault features at Charing Cross and Hororata in higher resolution than Beavan *et al.* (2010; 2012).
2. Create a dense high accuracy geodetic network to be used in future studies of this area to investigate the effects of future earthquakes on crustal deformation in the study area.
3. Use co-seismic displacements with relative shortening data to estimate recurrence intervals of major earthquakes on the Hororata and Charing Cross Faults.
4. Describe the Kinematics of the Hororata blind thrust and western West segment.

In a broader sense the repeat cadastral investigation was undertaken with the aim of testing the geodetic network in New Zealand to see if a similar study to that of Lee *et al.* (2006), Lee *et al.* (2010), Lee *et al.* (2011), and Lee and Shih (2011) could be completed. Completing this study would

provide additional insight into the patterns of surface deformation during the Canterbury Earthquake sequence. From the point of view of earthquake mechanics, this information could be used to further understand the afterslip mechanism for the Darfield earthquake, following on from Part I of this thesis. In addition, this survey may provide its significance in a broader context, for example, its relationship to the mechanisms of rupture nucleation and/or its influence on the relative proportions of co-seismic and post-seismic slip for the given earthquake (Marone *et al.*, 1991). Finally, by surveying these points with high accuracy in this study, I provide a framework that can be re-occupied to examine the effects of future earthquakes should they occur.

3.2 Study Area

3.2.1 The Darfield earthquake, Charing Cross and Hororata blind thrusts

Following the Darfield earthquake several studies were completed look at the earthquake sequence and determining the number of segments were responsible for the M_w 7.1 moment magnitude released during the earthquake (Beavan *et al.*, 2010, 2012; Duffy *et al.*, accepted manuscript; Jongens *et al.*, 2012; Elliot *et al.*, 2012). From these studies, the Darfield earthquake was found to be comprised of several segments – Charing Cross Blind Thrust Fault, Hororata Blind Thrust Fault, and western, central, and eastern segments of the Greendale Fault. For this study we were particular interested in deformation in the areas surrounding the HBT and CCBT as no surface fault scarp was found for either of these ruptures.

3.2.1.1 Hororata Blind Thrust and neighbouring Western Segment of the Greendale Fault

The Hororata Blind Fault is located approx. 3 km southwest of Hororata Township (see Figure 65). From seismic and InSAR data fault was modelled to be a north-westward dipping reverse fault that was equivalent to a M_w 6.3 ± 0.2 of the Darfield rupture sequence (Elliot *et al.*, 2012; Jongens *et al.*, 2012; Beavan *et al.*, 2012). These findings were consistent with the mechanism and location of an M_w 4.9 aftershock three days later (Elliot *et al.*, 2012). In addition, this aftershock provided evidence to continued suggestions that that the principle slip on this structure occurred during the mainshock sequence, and resulted in approx. ~400 mm uplift (Elliot *et al.*, 2012; Beavan *et al.*, 2012).

A recent study by Jongens *et al.* (2012) reviewed seismic survey lines completed in a 1998 oil exploration over the Canterbury Plains. Through interpretation the Hororata anticline and fault were imaged through survey line IP 98-004 (see Figure 64 previous section). Growth of the Hororata anticline appears to reflect movement along northwest-dipping thrusts may represent footwall splays from the neighbouring Hororata Fault (Jongens *et al.*, 2012). The location of the anticline and

underlying thrusts coincide with the deformation anomaly detected by differential InSAR post-Darfield Earthquake (Figure 65) near the western segment of the Greendale Fault (Jongens *et al.*, 2012).

The western-most segment of the Greendale Fault trace is located in-between Hororata Township and the Hororata Blind Fault. At approx. 15 km long, it strikes west-northwest (303^{o}) and dips northeast (75^{o}) with the trace petering out northwards (Elliot *et al.*, 2012; Beavan *et al.*, 2012). During the mainshock it predominantly resulted in strike slip motion, but it does consist of a small normal component which resulted in approx. 750 mm of uplift on the southern side of the fault (Elliot *et al.*, 2012; Beavan *et al.*, 2012). In stark contrast the northern and eastern segments of the Greendale Fault steeply dip to the south and resulted in right-lateral strike-slip displacements (Beavan *et al.*, 2010).

3.2.1.2 Charing Cross Blind Thrust and unnamed fault

The Charing Cross Blind Fault is located between Greendale and Charing Cross in Central Canterbury region (see Figure 65) (Beavan *et al.*, 2010; Holden *et al.*, 2011). Seismic modelling and InSAR inferred slip distributions indicate this fault ruptured on the 4th of September equivalent a M_w 6.44 ± 0.05 (Beavan *et al.*, 2010, 2012; Holden *et al.*, 2011; Elliot *et al.*, 2012). This fault is also believed to be responsible for initiating failure of the other segments and producing the M_w 7.1 of the Darfield Earthquake. The fault is characterised by a northeast strike (035^{o}) and a dip southeast (70^{o}) (Elliot *et al.*, 2012; Beavan *et al.*, 2012.

Through InSAR information, a recent study by Beavan *et al.* (2012) located an unnamed fault slightly north of the Charing Cross Blind Fault (see Figure 65). This fault was found to strike north-northwest to south-southeast of the epicentre (330^{o}) and dip 54^{o} to the north-east (Beavan *et al.*, 2012). The study identified this fault segment as the left lateral with up to approx. 1m of buried sinistral motion occurring. Because the rupture of these outlined structures resulted in no identifiable surface scarp and seismic surveying over this site return inconclusive results due to low frequency data, it was hope a cadastral study of lower order survey marks surrounding these faults would help to quantify and characterise co- and post-seismic deformation across the landscape more accurately.

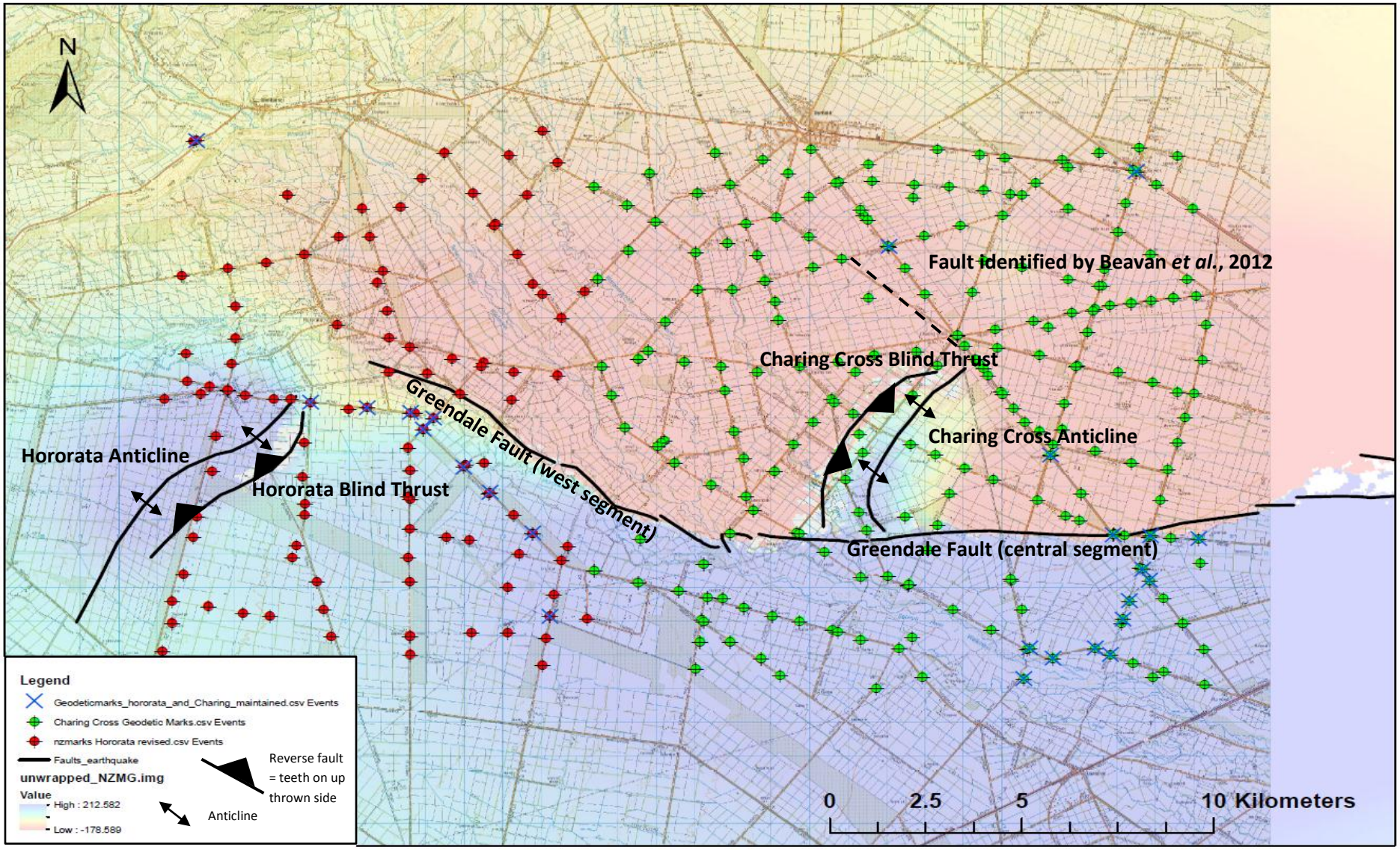

Figure 65: The available 0 -12th order geodetic survey marks in the Hororata (Red) and Charing Cross (Green) regions. It also shows those marks identified as being maintained (resurveyed) post September 4th 2010 Darfield earthquake (Survey marks locations courtesy of Linz online data service and InSAR image courtesy of J. Beavan and fault trace map courtesy of B. Duffy).

3.3 Methodology

After deciding to survey around Charing Cross/Greendale and Hororata areas, the next step was to locate all the possible survey marks for these areas. Geodetic survey marks were obtained from Land Information New Zealand (LINZ), in an online database (http://apps.linz.govt.nz/gdb/?mode=gmap).

Using the database, I selected survey marks and downloaded the following information for each site:

- Geodetic code,
- Name and Alternative name,
- Land district,
- Mark description and Mark type code,
- Beacon code,
- Maintenance date,
- Co-ordinates New Zealand Map Grid (NZMG) or New Zealand Transverse Mercator Projection (NZTM),
- Ellipsoidal Height,
- Horizontal Coordinate Order,
- Calculation date,
- Reference,
- Topo50 reference,
- Orthometric height and/or Orthometric height order,
- Orthometric height calculation date,
- Orthometric height reference, and
- Orthometric height datum.

For this study, the New Zealand Geodetic Datum 2000 (NZGD2000) was used and the above attributes of significant importance were; geodetic code, name, land district, mark description, mark type code, maintenance date, NZTM and NZMG co-ordinates, and orthometric height (see Appendix D Table D1).

The geodetic survey marks occupied prior to 4th September 2010 gave an indication of their reference position before the Darfield earthquake occurred. Thus, reoccupying them following the rupture will provide an indication of co- and post-seismic surface deformation. Additionally, survey marks that had been re-occupied after the Darfield earthquake by Beavan *et al.* (2010) provided the

opportunity to use these marker points as high quality reference markers, so that the quality of my surveys could be tested. This increased the accuracy reliability of the data collected during my surveys.

The equipment used for this surveying includes the following (see Figure 66):

- Trimble R8 base station and rover,
- Trimble repeater and aerial,
- 2 x tripods,
- 1 x staff,
- 1x stabilising poles,
- 4 x batteries + large 12V repeater battery,
- Hand held GPS, and
- 1x spade .

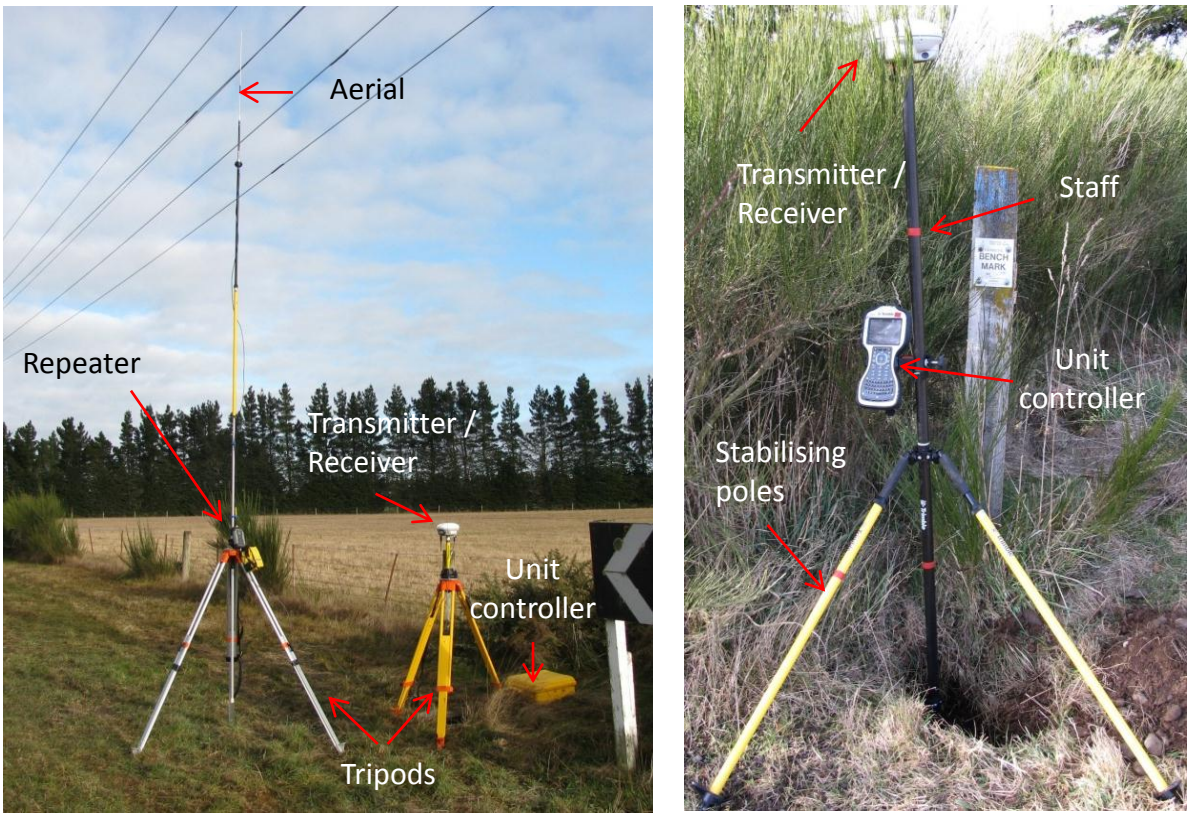

Figure 66: The Trimble R8 equipment used in the cadastral surveys.

3.3.1 Collection procedure

To collect robust and accurate data the survey required at least one maintained site (re-occupied post-September 2010) in each of the Charing Cross and Hororata survey areas. This enables all of the reoccupied survey marks to have a maintained reference point to be tied back to during processing. This aids in the production of accurate update locations.

Within the Charing Cross survey area, ACFA_vv45 a 9th order survey mark was used (see the yellow circle in Figure 67). It is located approx. 3.2 km north of Charing Cross on the corner of Telegraph and Essendon Roads. This was the most suitable position maintained survey mark, as it was away from tall hedges and trees. This enabled wide coverage to achieve closer to 5 km range of radio connection between the base station and rover when reoccupying other survey marks. Using this initial position the base station was then "leapfrogged" to four other locations to extend coverage and encompass the entire site area. These additional base locations included: cc126, cc 345 and cc 122 (see the yellow dots in Figure 67). Using these locations a total of 38 sites were tied back to ACFA_vv45.

Around the Hororata blind structure (HBS) the most suitable maintained location was EJ7W/cc178 no. 2 (see the yellow circle in Figure 68). A 10th order survey mark positioned in open space on the road side at the intersection between Derrets and Dunsandel Roads, within a central position of the site area. From this position only one other base position was required, vv79, to locate and reoccupy a further 22 survey marks (see the yellow dot in Figure 67). After completion of the surveys processing the raw collected data was required.

3.3.2 Post-processing

Using a Trimble software package provided with the Trimble R8 equipment, processing involved in-putting the collected raw data into the software to set the correct reference datum. In this case NZGD 2000 and New Zealand Transverse Mercator were selected. The data was then output as a shape file (.shp), to enable use in other software programs like ArcGIS and AutoCAD. Using these programs it was possible to produce maps showing the current position of each reoccupied point with respect to their original location. This is illustrated by Figure 67, which shows a map of all the data input into ArcGIS, including the; existing sites, maintained sites, unmaintained site, base locations, and the reoccupied locations of survey markers located in these surveys.

3.3.3 Data referencing

The data was georeferenced in AutoCAD by fixing the locations of the survey based on marks that had been occupied by both Beavan *et al.* (2010; 2012) and this study. For example, surveying undertaken from survey mark cc 126 as a base station involved the re-occupation of survey mark DOVF which was also occupied by Beavan *et al.* (2010; 2012). By highlighting all of these survey marks, then moving DOVF to match the location of DOVF from Beavan *et al.*'s (2012) survey, all of the reoccupied positions were shifted and tied back to a more accurate higher order survey mark.

The displacements of resurveyed marks were then measured relative to pre-earthquake locations published on the LINZ database. As expected based on the LINZ order descriptions (Table 7), only a few of the resurveyed marks (6^{th} order and higher) provided reliable displacements (Table 6). The majority of lower order survey marks (9^{th}-12^{th} order) were not accurate, with an accuracy of ± 1 to 10 m. Nevertheless, the resurvey of these marks provides improved constraints on their location that will facilitate future work.

Table 6: Difference in displacements and orientation following correction, note survey marks that corresponded to the same marks used by JB now have displacements of 0 as they were used to correct the sites below.

Survey Marks before correction				After Correction	
Order Number	**Mark Name**	**Displacement (m)**	**Orientation**	**Displacement (m)**	**Orientation**
4	BPMB	5.4860	SW	0.3333	E-SE
3	AA71	5.7238	SW	0.5600	E-SE
3	B2Q1	5.4712	SW	0.6940	E-SE
5	VV 46	5.3104	SE	0.5377	SW
5	AFCR_vv 81	5.9275	SW	0.0842	NW
9	AFC7_vv75	5.8371	SW	0.2245	E-SE
9	EJ7W_vv60	6.5431	SW	0.0625	NW

Table 7: shows the co-ordinate orders for the survey marks located after having issues with the accuracy of data (Table from Linz: http://www.linz.govt.nz/geodetic/datums-projections-heights/heights/coordinate-orders)

Order	Purpose	Tier (95% CI, m)	Class (95% CI)	
			Constant (m)	Proportional (m/m)
0	National reference frame	H 0.05 V 0.05	H 0.003 V 0.003	H 0.000 000 03 V 0.000 000 03
1	National deformation monitoring	H 0.05 V 0.10	H 0.003 V 0.003	H 0.000 000 1 V 0.000 000 3
2	Regional deformation monitoring	H 0.10 V 0.25	H 0.003 V 0.010	H 0.000 001 V 0.000 003
3	-	H 0.10 V 0.35	H 0.01 V 0.01	H 0.000 003 V 0.000 01
4	Local deformation monitoring	H 0.15 V 0.35	H 0.01 V 0.01	H 0.000 01 V 0.000 03
5	Cadastral horizontal control Basic geospatial network	H 0.15 V 0.35	H 0.01 V 0.02	H 0.000 05 V 0.000 1
6	Cadastral permanent reference marks	0.15	0.03	0.000 15
7	Class A boundary marks	0.2	0.06	0.000 15
8	Class B boundary marks	0.5	0.3	0.000 6
9	Class C boundary marks	5	1	0.003
10	-	20	3	0.01
11	-	50	10	0.03
12	-	-	-	-

Table 8: Indicates the accuracy of the pre and post-earthquake cadastral survey data.

Survey	Horizontal (m)		Vertical (m)	
	IGS05	Relative	Lyttelton 1937 Via NZGeoid05	Relative
Pre-quake cadastral	±0.05	±0.02	NA	±0.02
Post-quake cadastral	*	0<0.16	NA	±0.15

* sum of post-quake GPS and error ellipse dimensions.

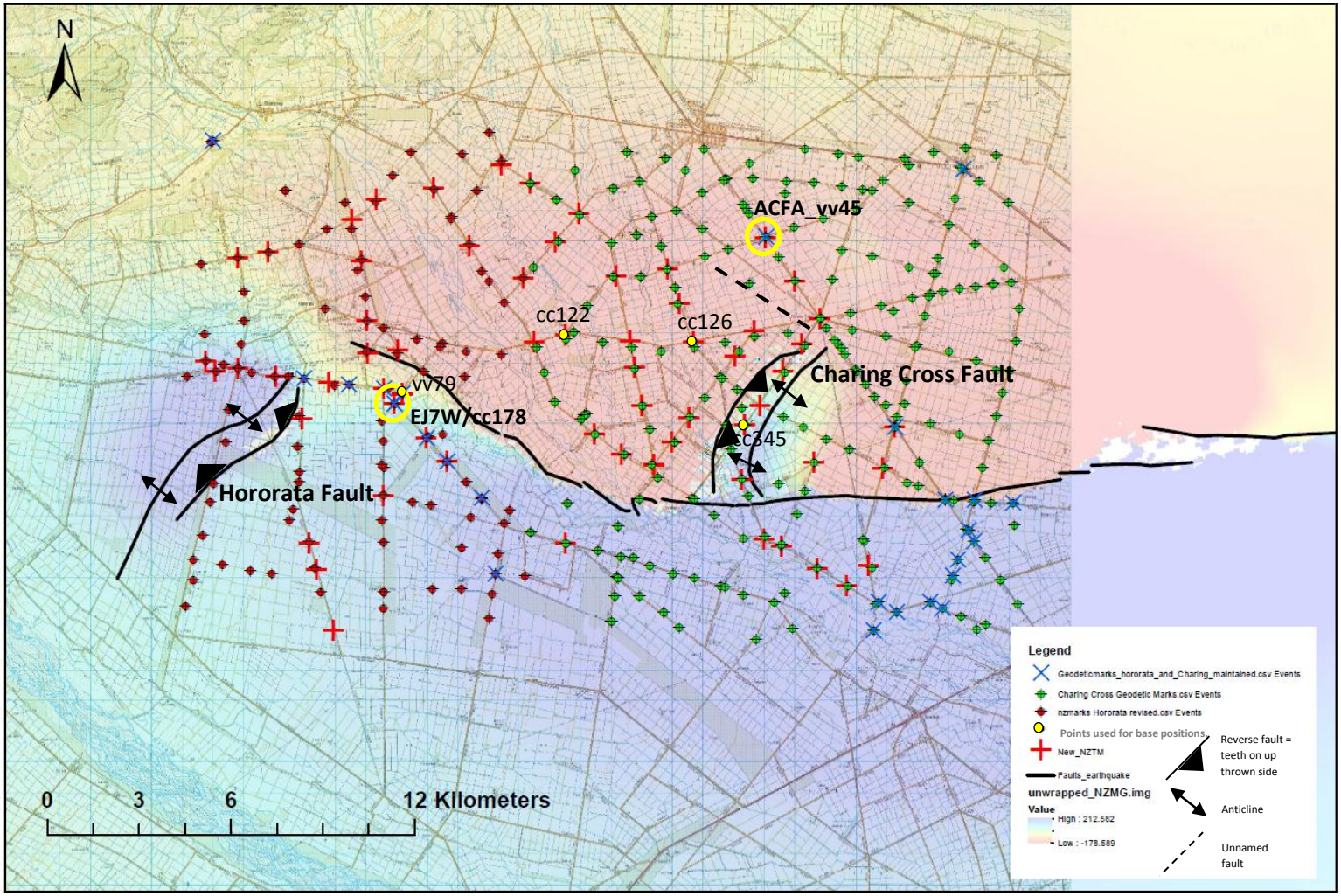

Figure 68: shows a map of all the existing marks as well as the reoccupied locations of some of these points. The green points visible are all the survey marks in the Charing Cross/Greendale area, with the red points corresponding to available survey marks in Hororata. The blue crosses highlight the maintained survey marks where the base station could be positioned in order to accurately tieback reoccupied locations. The yellow circles illustrate the maintained sites used as the original base positions for surveying around the Charing and Hororata areas. The red plus symbols indicate the reoccupied sites recorded during the surveys for this thesis.

Table 9: Crossover points corrected shown using Beavan et al (2010; 2012) studies.

				Pre-September Earthquake			Post-September Earthquake		
GeodeticCode	**Name**	**MaintDate**	**Order**	**NZTMEasting**	**NZTMNorthing**	**OrthHeight**	**EastingNZTM**	**NorthingNZTM**	**Elevation (m)**
BPMB	MOWBMCC263	7/12/2004	4	1512819.82	5180451.75	224.118	1512820.15	5180451.74	236.40
BPMC	MOWBMCC290	16/11/1999	4	1522353.91	5182883.29	199.361	1522353.91	5182883.29	211.70
BPMF	MOWBMCC93	15/02/2011	4	1517584.57	5176175.95	169.336	1517584.57	5176175.95	181.37
BPMG	MOWBMCC86	12/08/2008	4	1515142.54	5171169.53	191.458	1515142.54	5171169.53	203.27
BPMJ	MOWBMCC311	15/09/2008	4	1526013.39	5175618.48	143.661	1526013.39	5175618.48	155.52
D0VF	VV 47 NO 2	13/02/2008	5	1531827.69	5178478.02	150.7946	1531827.69	5178478.02	162.73

Table 10: Corrected values for the post-September earthquake. Also shown are the pre earthquake positions, maintenance date, order number, and horizontal displacements.

				Pre-September Earthquake			Post-September Earthquake			
Geodetic Code	**Name**	**MaintDate**	**Order**	**Easting NZTM**	**Northing NZTM**	**OrthHeight**	**Easting NZTM**	**Northing NZTM**	**Elevation (m)**	**Displacements (m)**
AA71	8233	4/04/2008	3	1512825.29	5176859.85	<Null>	1512825.83	5176859.71	215.94	0.560 ± 0.01
B2Q1	8231	21/03/2003	3	1517021.75	5178393.19	179.53	1517022.44	5178393.09	191.23	0.694 ± 0.01
ACFB	VV 46	31/07/1986	4	1530988.84	5179699.28	160.10	1530988.59	5179698.80	171.77	0.538 ± 0.01
AFC7	VV75	<Null>	4	1511770.64	5177095.22	211.68	1511770.85	5177095.15	224.29	0.225 ± 0.01
BPMB	CC263	7/12/2004	4	1512819.82	5180451.75	224.118	1512817.423	5180447.274	235.36	0.333 ± 0.01
ACFF	VV 50	<Null>	6	1534258.3	5174939.59	<Null>	1534256.41	5174921.06	127.35	0.065 ± 0.01
AFCR	VV81	23/02/2006	6	1517562.55	5172718.15	173.35	1517562.47	5172718.17	185.17	0.084 ± 0.03

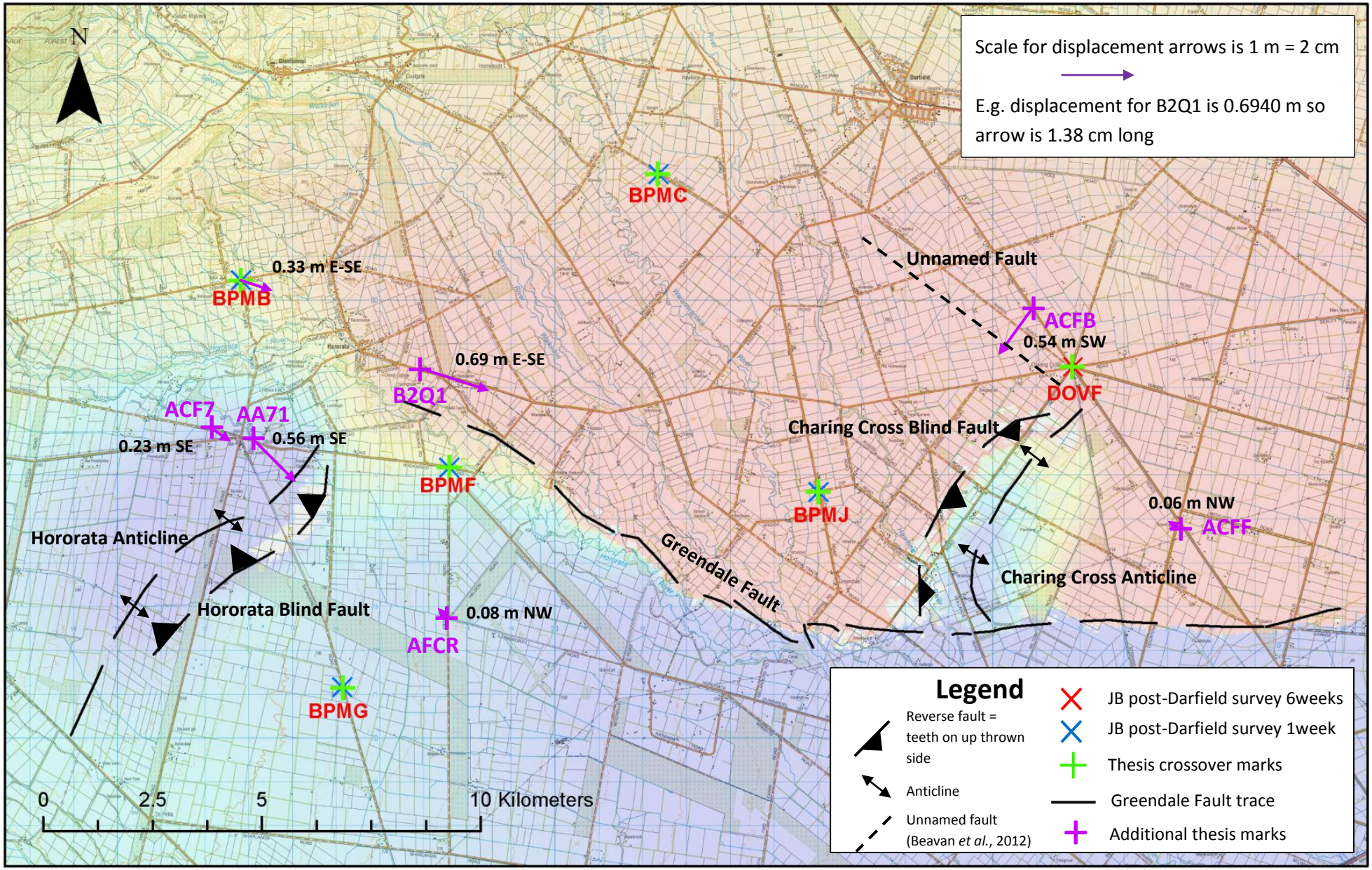

Figure 69: Relative horizontal deformation over the Hororata and Charing Cross areas as identified through cadastral surveys. The base layer shows an InSAR image which highlights the off main fault trace structures believed to be blind features that did not rupture the surface as well as the locations of geodetic survey pins. The survey marks and displacements illustrated in the image are points that were located during surveying that John Beavan also surveyed in the first week and 6 weeks following the Darfield earthquake

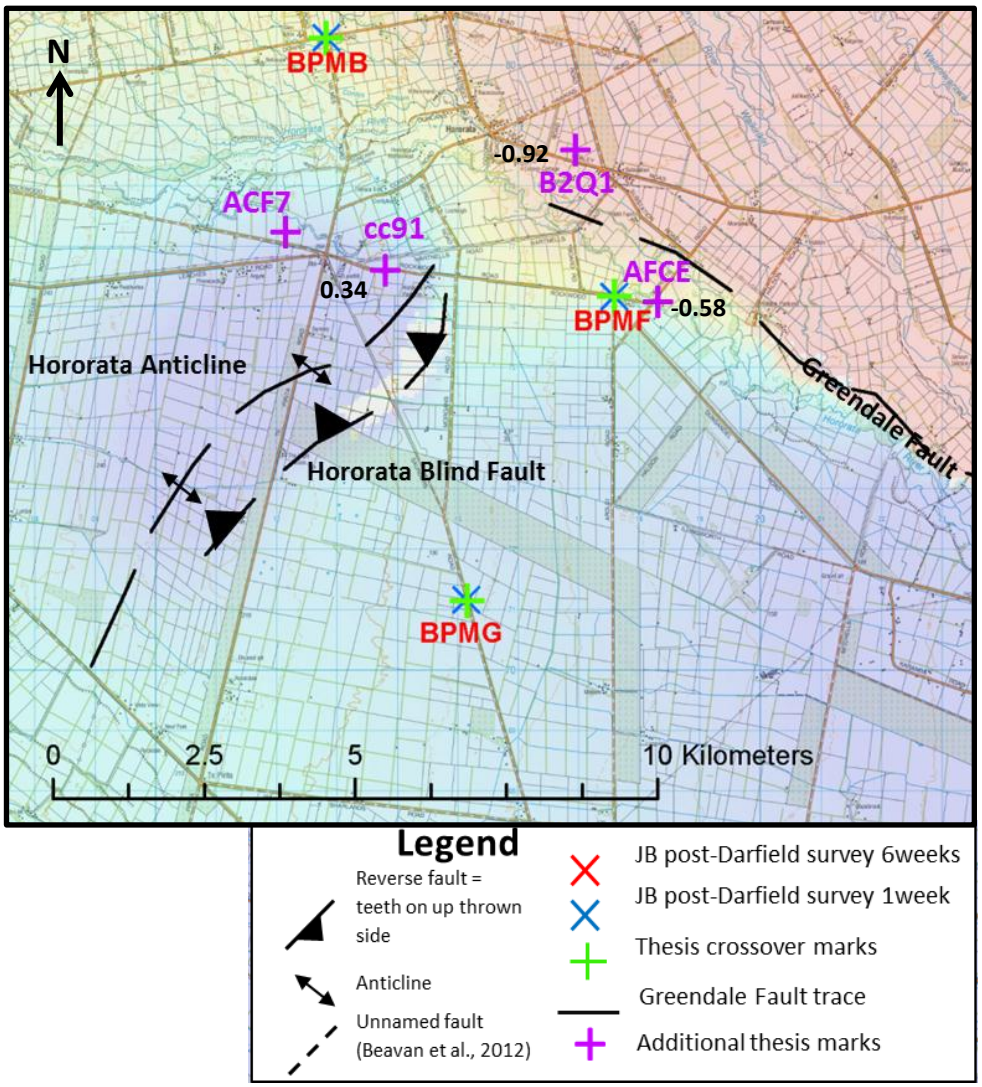

Figure 70: Vertical displacements across the Hororata Fault relative to survey mark ACF7. The base layer shows an InSAR image which highlights the off main fault trace structures believed to be blind features that did not rupture the surface as well as the locations of geodetic survey pins. The red survey marks illustrated within the image are points that were located during surveying that John Beavan also surveyed in the first week and 6 weeks following the Darfield earthquake.

Table 11: Relative elevation change matrix for cadastral marks surrounding the Hororata Fault.

	AFC7 vv75	AFCE vv79	B2Q1	cc91
AFC7 vv75	0	-0.5776	-0.9129	0.3361
AFCE vv79	0.5776	0	-0.3353	0.9137
B2Q1	0.9129	0.3353	0	1.249
cc91	-0.3361	-0.9137	-1.249	0

Note: Negative values indicate that the survey mark listed in the row has subsided relative to the mark listed in the column.

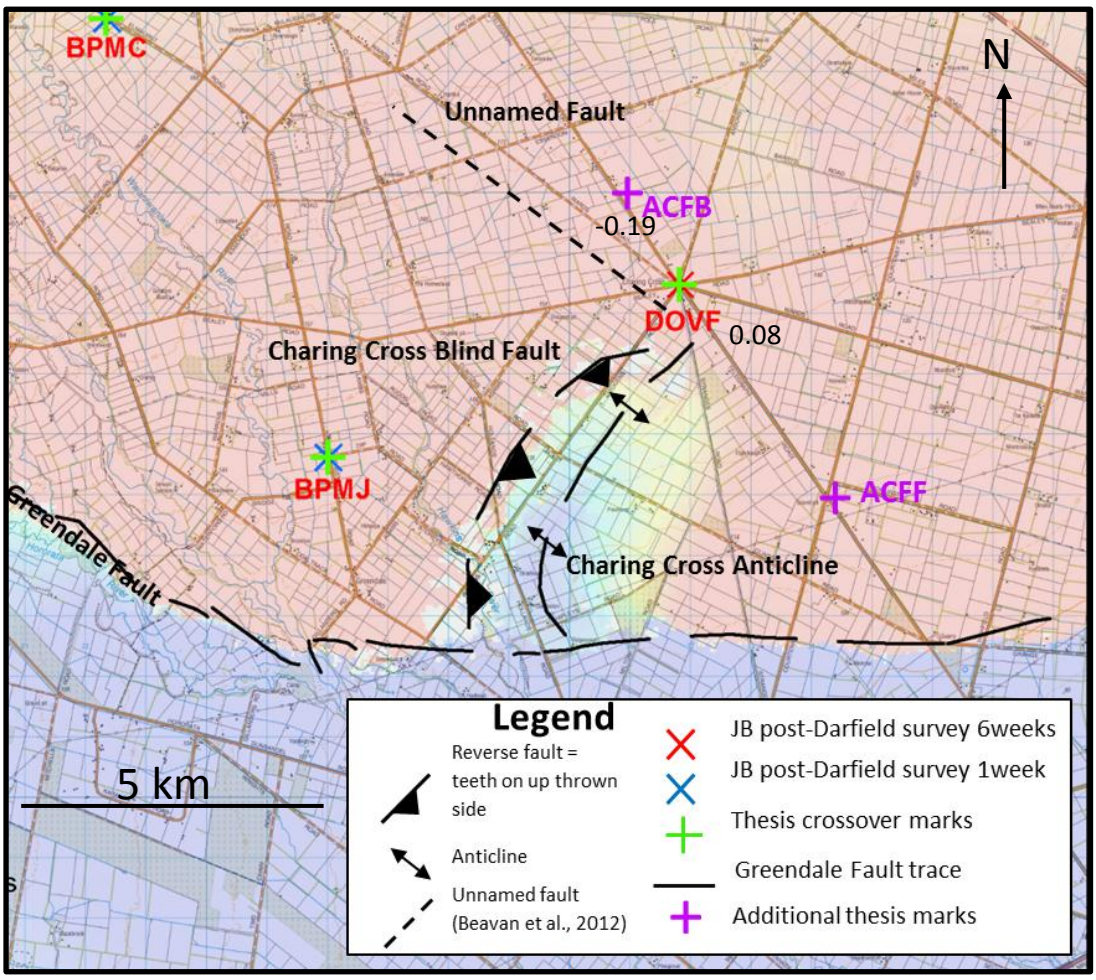

Figure 72: Survey marks that provide relative vertical deformation over the Hororata and Charing Cross areas as identified through cadastral surveys. The base layer shows an InSAR image which highlights the off main fault trace structures believed to be blind features that did not rupture the surface as well as the locations of geodetic survey pins. The red survey marks illustrated within the image are points that were located during surveying that John Beavan also surveyed in the first week and 6 weeks following the Darfield earthquake.

Table 12: Relative elevation change matrix for cadastral marks surrounding the Charing Cross Fault.

	BPMJ	DOVF	ACFB
BPMJ	0	0.0764	-0.189
D0VF	-0.0764	0	-0.2654
ACFB	0.189	0.2654	0

Note: Negative values indicate that the survey mark listed in the row has subsided relative to the mark listed in the column.

3.4 Results

Cadastral surveying undertaken in the period between May to July 2012 resulted in the re-occupation of 68 survey marks, mostly 12th order (60 marks). The post-earthquake positions of these marks are given in Table D1 in Appendix D. Of these, useful displacements were only provided by 6 marks 9th order or less (see Table 10).

3.4.1 Surface deformation around Charing Cross and Hororata

The corrected horizontal displacements, their orientation and their position relative to the Hororata, Charing Cross Blind Faults can be seen in Figure 69.

3.4.1.1 Kinematics of the Hororata Blind Fault and western segment of the Greendale Fault

Survey marks show a distinct pattern of displacement relative to the Hororata Blind Thrust Fault, Hororata Anticline and western segment of the Greendale Fault (see Figure 6 and 7). On each side of the fault, the marks showed moderate amounts of vertical movement relative to one another (average of ~0.72 m), but the marks on one side of the fault shifted substantially and consistently relative to those on the other side (Table 10). On the north-east side of the Hororata Blind Fault, marks were downthrown by an average of 1.08 ± 0.17 m (maximum 1.25 m) relative to cc91, the survey mark on the west side of the fault closest to the fault trace (Figure 70, Table 11). B2Q1 was also downthrown 0.34 ± 0.01 m relative to AFCE; indicating a further drop on the north-east side of the western segment of the Greendale Fault (Figure 70: Table 11). This motion is consistent with a normal component identified of the mainly dextral western segment of the Greendale Fault.

The southeast side of the Hororata Fault moved horizontally 0.08 ± 0.03 m toward 314^{o} (northwest); this vector moved perpendicular to the fault indicating the downthrown side (footwall) of the fault (Figure 69:Table 10). The northeast side of the western segment of the Greendale Fault moved 0.69 ± 0.01 m toward 112° (east-southeast) respectively (Figure 69:Table 10); this vector moved sub-parallel to the Greendale Fault indicating net slip of 0.63 m toward 117^{o}. These vectors are approximately perpendicular to the Hororata Fault and sub-parallel to the western segment. The northwest side of the Hororata Fault and anticline, horizontal displacement averaged 0.4 ± 0.15 m toward 135^{o} (southeast) (maximum of 0.56 ± 0.01 m toward 135^{o}), with displacement increasing eastwards toward the surface projection of the fault (see Figure 69: Table 10). This vector is approximately perpendicular to the fault trace and indicate patterns of displacement consistent with the up-thrown (hanging wall) of a thrust fault.

Nearby survey mark BPMB indicates relative displacements of 0.33 m toward 112° (east-southeast); this vector is consistent with sub-parallel vector at B2Q1 and reflecting right lateral net slip of 0.12 ± 0.01 m along the western segment of the Greendale Fault.

3.4.1.2 Kinematics of the Charing Cross Blind Fault

Survey marks around the Charing Cross are limited to ACFF and ACFB (see Figure 69). This is because DOVF and BPMJ were used to correct the data. The southeast side of the Charing Cross Blind Fault, ACFF moved horizontally 0.06 ± 0.01 m toward 315° (northwest); this vector moved perpendicular to the fault (see Figure 69 : Table 10). On the northwest side of the fault, ACFB moved horizontally 0.54 ± 0.01 m towards the 225° (southeast); this vector moved perpendicular to the fault.

Vertical displacements within the Charing Cross Fault site include survey marks BPMJ, DOVF and ACFB on north-western side (see Figure 72). DOVF was up-thrown by 0.0764 ± 0.01 m, whereas ACFB was downthrown -0.189 ± 0.01 m relative to BPMJ (see Figure 72: Table 12). Unfortunately no relative displacements were obtained for the south-eastern side of the fault as the LINZ data service did not have any available points.

Interpretation

Overall it can be seen hanging wall movement was towards the east and increased eastwards. This is reflected in net slip of that is greatest close to the fault. The increase toward the fault reflects increased displacement in the near surface. This is possible due to elastic rebound. In addition, near surface collapse due to slip distribution at depth may partly explain the observed motion in the Harper hills (BPMB), which is confined to the south of the west segment.

3.5 Discussion

3.5.1 Comparison of vertical and horizontal displacements to previous published data

Studies by Beavan *et al.* (2010; 2012) were completed using high order survey marks (3rd - 4th) around the Canterbury Region to measure displacements around the Greendale Fault following the Darfield Earthquake. Measurements of the horizontal and vertical location of survey marks were taken 1 and 6 weeks following the mainshock provided the opportunity to validate the results for the relative horizontal and vertical displacements measured through my cadastral survey. Relative to study area for this thesis survey marks resurveyed by Beavan *et al.* (2010; 2012) was limited to six (see Figure 69). Survey marks BPMB, BPMC, BPMF and BPMG are positioned relative to the Hororata Blind Fault and western segment of the Greendale Fault. Survey marks DOVF and BPMJ are located relative to the Charing Cross Fault and central segment of the Greendale Fault.

3.5.1.1 Hororata Blind Fault and western segment of the Greendale Fault

Relative to the Hororata Fault and western segment of the Greendale Fault, survey mark BPMB is positioned north-northwest and west respectively. Beavan *et al.* (2010; 2012) re-occupied the position of this mark 1 week and 6 weeks following the mainshock, which reflected an average horizontal movement of 0.54 ± 0.01 m toward 114^{o} (east-southeast) (see Table 13). A comparison of horizontal displacement for this point with my survey indicates a decrease in horizontal displacement of approx. 20 cm toward east-southeast (see Figure 74). Furthermore, my study reveals the average slip for hanging wall of the Hororata Fault and western segment of the Greendale Fault survey was 0.37 ± 0.2 m toward 129^{o} (from ACF7, AA71 and BPMB); with the displacement vector oriented perpendicular toward the strike of the Hororata Fault (see Figure 74). This difference in horizontal displacement of approx. 10 cm is likely to reflect post-seismic recovery in the few months following mainshock. This is supported by Beavan et al. (2010) revealing post-seismic recovery of ≤ 10 cm up to 8 weeks following the mainshock.

Across the southeast side of the Hororata Fault, survey marks occupied by Beavan *et al.* (2010; 2012) reflected average horizontal movement of 0.34 ± 0.07 m toward 205^{o} (south-southwest). Mark BPMF moved horizontally 0.28 m towards 134^{o} (southeast); sub-parallel to the western segment of the Greendale fault and perpendicular to the Hororata Fault. Mark BPMG indicated 0.41 m toward 245^{o} (southwest); perpendicular to the western segment of the Greendale fault and sub-parallel to Hororata Fault (Figure 77: Table 12). These were interesting findings by Beavan *et al.* (2010; 2012) as results from this study differed significantly in orientation. Survey mark ACFR indicated 0.08 m toward 315^{o} (northwest) or perpendicular toward the fault trace. From my results it was found that this mark lies on the footwall of the Hororata Fault making it likely that this reflects relative movement from the Hororata Fault. Whereas, Beavan *et al.* (2010; 2012) mark BPMF coincides with motion and orientation reflected by BPMB and the western segment of the Greendale Fault; (see Figure 74) and mark BPMG reflects broad scale dextral slip relative to the Greendale Fault.

Relative to original elevations of each of the survey marks re-surveyed by Beavan et al. (2010; 2012) BPMB was up-thrown by 0.0848 m northwest of the Hororata Fault and across the south-east side of the fault BPMF and BPMG were up-thrown by 0.1211 m by 0.0709 m, respectively. In contrast this study indicated ACFR was down thrust relative to the northwest side of the Hororata Bind Fault.

On the northern side of the western segment of the Greendale Fault, survey mark BPMC moved on average 1.03 ± 0.01 m towards 132^{o} (southeast) and was downthrown 0.16 m relative to its original position (see Table 12). Comparing this motion to B2Q1 (H 0.69 ± 0.01 m and 0.33 ± 0.01 m) also on

the northern side of the fault trace the horizontal movement of BPMC is 30 cm larger is oriented more southeast (see Figure 74). Looking at the vertical motion B2Q1 and BPMC both reflect downwards vertical displacement likely attributed to the normal component of the western segment (see Figure 73 and 74).

3.5.1.2 Charing Cross Blind Fault and unnamed fault

Survey marks BPMJ and DOVF reoccupied by Beavan *et al.* (2010; 2012) on the northwest side of the Charing Cross Blind Fault reflect combined average movement of 1.69 ± 0.01 m towards 113° (east-southeast); this vector moved perpendicular toward the fault trace from the footwall side of the reverser fault. BPMJ moved 1.87 m towards 123° whereas, DOVF moved 1.34 m towards 103° (see Figure 74: Table 13). Vertically DOVF was upthrown relative to BPMJ by 0.72 m. The movements of these points differ to that of ACFB which moved horizontal 0.54 m towards the 225° (southeast) and was downthrown relative to BPMJ 0.189 m (see Figure 74: Table 13 and 14). This difference is horizontal motion is likely to be ACFB reflecting motion from both the Chairing Cross Fault and unnamed fault northwest of Charing Cross. Comparisons could not be made across the southeast side of the Charing Cross Blind Fault as the study by Beavan *et al.* (2010; 2012) did not resurvey any marks in this area (see Figure 74).

Our study presents a complementary dataset to that of Beavan et al. that enables additional study to be conducted on the Horrarata, Charing Cross and unnamed fault.

Table 13: Post-Darfield earthquake displacements recorded by Beavan *et al.*, (2010; 2012) within my study site.

Post Darfield Displacements - Recorded from original position of survey marks				
	Horizontal Displacements		Vertical Displacements	
Survey Mark	1 week (m)	6 weeks (m)	Pre - 1 week (m)	Pre - 6 weeks (m)
BPMB	0.5435	0.5445	0.0848	0.0759
BPMC	1.0431	1.0278	-0.1566	-0.1410
BPMF	0.2680	0.2836	0.1211	0.0678
BPMG	0.4196	0.4241	0.0709	0.0695
BPMJ	1.8650	1.8758	-0.6057	-0.5757
DOVF	Not recorded	1.3471	Not recorded	0.1189

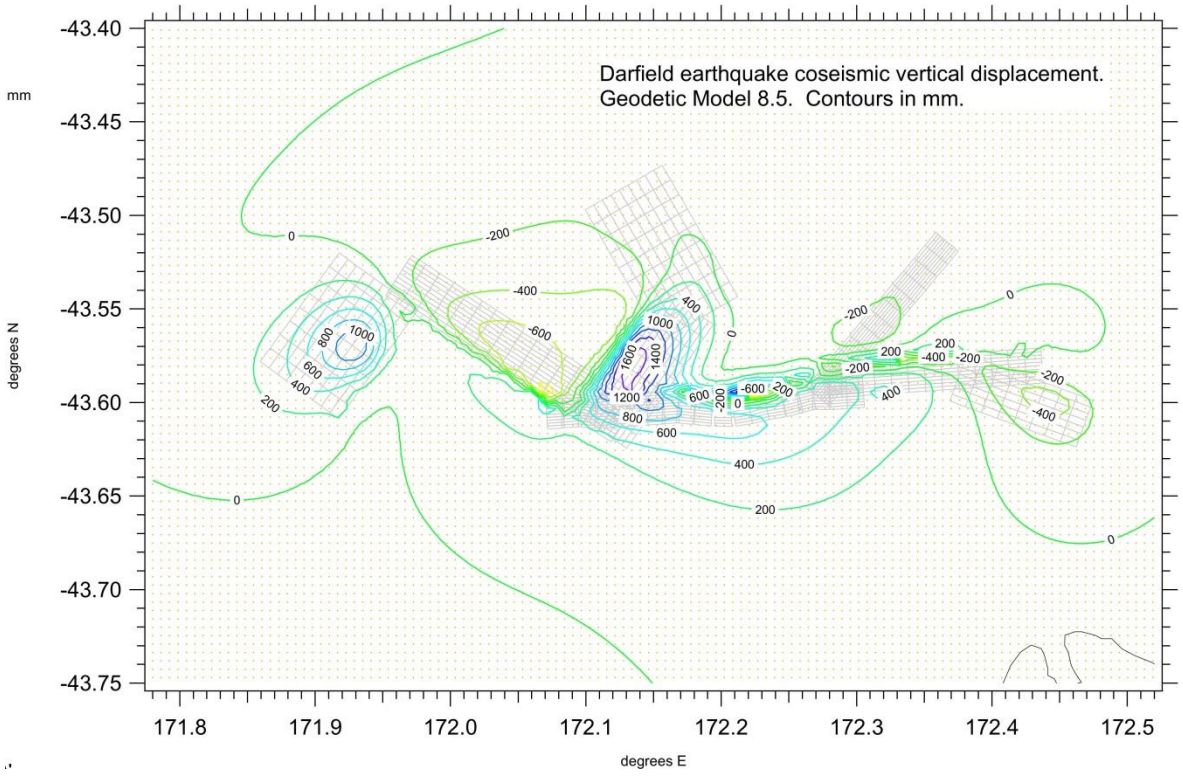

Figure 73: Vertical co-seismic displacements generated during the Darfield earthquake - modelled through geodetic surveys (Source: Beavan *et al.*, 2010).

Table 14: Relative vertical displacements located by *Beavan et al*. (2010: 2012)

	BPMB	BPMC	BPMF	BPMG	BPMJ	DOVF
BPMB	0	-0.2414	0.0363	-0.0139	-0.6905	0.0341
BPMC	0.2414	0	0.2777	0.2275	-0.4491	0.1566
BPMF	-0.0363	-0.2777	0	-0.0502	-0.7268	-0.0022
BPMG	0.0139	-0.2275	0.0502	0	-0.6766	-0.0848
BPMJ	0.6905	0.4491	0.7268	0.6766	0	0.7246
						0

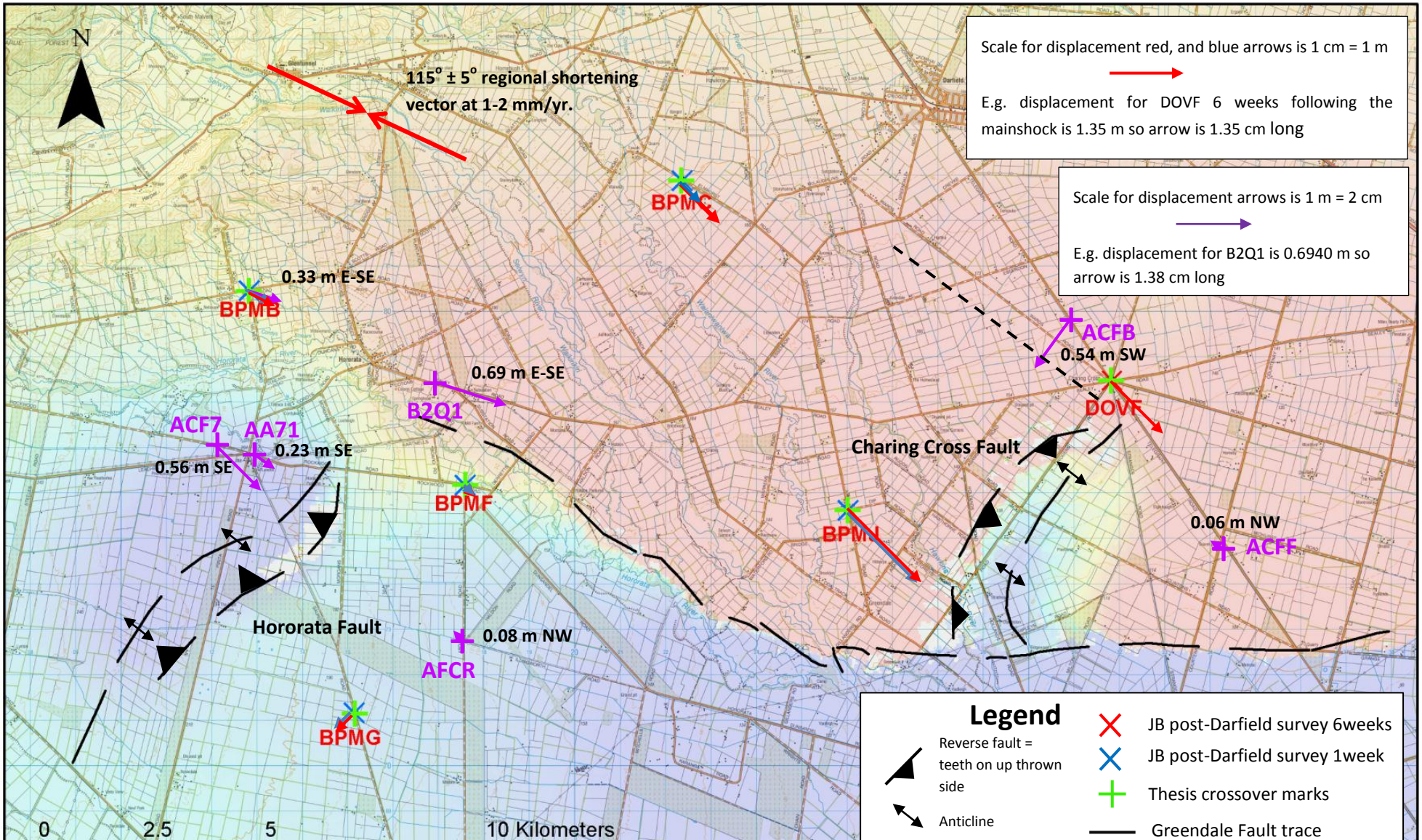
N
115° ± 5° regional shortening vector at 1-2 mm/yr.
Scale for displacement red, and blue arrows is 1 cm = 1 m
E.g. displacement for DOVF 6 weeks following the mainshock is 1.35 m so arrow is 1.35 cm long
Scale for displacement arrows is 1 m = 2 cm
E.g. displacement for B2Q1 is 0.6940 m so arrow is 1.38 cm long
BPMC
0.33 m E-SE
BPMB
ACFB
0.54 m SW
0.69 m E-SE
B2Q1
DOVF
ACF7
AA71
0.23 m SE
0.56 m SE
Charing Cross Fault
BPMF
BPMA
0.06 m NW
ACFF
Hororata Fault
0.08 m NW
AFCR
BPMG
0
2.5
5
10 Kilometers
Legend
Reverse fault = teeth on up thrown side
Anticline
JB post-Darfield survey 6weeks
JB post-Darfield survey 1week
Thesis crossover marks
Greendale Fault trace

3.5.2 Implications of displacement measurements for recurrence intervals on the Hororata and Charing Cross Faults

A comprehensive study by Wallace *et al.* (2007) on balancing the plate motion budget in the South Island, New Zealand provides an in depth look into the deformation kinematics across the transpressional collision tectonic boundary. More recently a study by Sibson *et al.* (2011) provides a more detailed look at stress control of on the strike slip faults involved in the 2010 and 2011 Canterbury earthquake sequence. Both these studies provide useful insight into the contraction pressures within the Hororata and Charing Cross areas of study. In particular, definition of constraints on regional shortening and direction and the rate at which it is occurring.

The studies reveal a uniform stress field across the Canterbury region, corresponding to a permanent compressive/contraction strain rate of 1-2 mm/yr. in a W-NW to E-SE orientation (115^{o} ± 8^{o} from Sibson *et al.*, 2011; 110 ± 8^{o} from Wallace *et al.*, 2007) across an approx. 125 km wide block (Sibson *et al.*, 2011; Wallace *et al.*, 2007). This corresponds to approx. 0.008 – 0.016 $\frac{mm}{yr.}/km$ of regional shortening. By combining these values with co-seismic and post-seismic displacements across a fault relative to the direction of regional shortening (i.e. 115^{o}) it is possible to estimate recurrence intervals of major earthquakes on the Hororata and Charing Cross Faults.

Steps to calculate the strain release which is approximately equal to the recurrence interval:

- Selecting survey marks from either side of a fault and resolve these displacements into co-seismic shortening in the regional shortening direction. For this study an orientation of 115^{o} will be used (Sibson *et al.*, 2011) (see Figure 74).
- Calculate the distance between the two marks in the direction of regional shortening.
- Combine the normalised co- and post-seismic.
    - Strain release; $\mathrm{SR} = {}^{D}/_{(d\ x\ Sr)}$

  Where D, is the combined displacements in direction of regional shortening; d, is the distance between survey marks in regional shortening; and Sr is the rate of regional shortening.

3.5.2.1 Hororata Fault Recurrence intervals

- From AA71 to BPMG (see Figure 74)
    - Survey mark AA71 indicates 56 cm of displacement, which is equivalent to 53 cm in the 115^{o} shortening direction using the Canterbury region value from Sibson *et al.,* 2011.

- On the eastern side survey mark BPMG shows 42 cm (Beavan *et al.*, 2010; 2012) displacement to the S-SE which is equivalent to 14 cm in the 115° shortening direction (Wallace *et al.*, 2007).
    - Therefore there is a total of approx. 67 cm or 670 mm co + post-seismic deformation in the regional shortening direction
- Rate of regional shortening :
    - 1-2 mm/yr. over 125 km (Wallace *et al.*, 2007; Sibson *et al.*, 2011)
      = 0.008 to 0.016 mm/yr. / km
    - Distance between AA71 and BPMG approx. 4.5 km in shortening direction therefore: 0.008 to 0.016 mm/yr. / km x 4.5 km
      = 0.03 to 0.072 mm/yr.
- Thus, the strain rate is equal to 500mm / rate of regional shortening over the Hororata Fault
    - $S.R. = \frac{670\ mm}{0.03\ to\ 0.072\ \frac{mm}{yr}} = 18{,}623\ to\ 9{,}311\ years$

An average recurrence interval for the Hororata Fault with a regional shortening rate of 1-2mm/yr. over 125 km is 7,403 ± 2,000 years to 14,785 ± 3,500 years (see Table 15).

3.5.2.2 Charing Cross Fault Recurrence intervals and Western Segment

Unfortunately, we were limited to the number of survey marks available around the Charing Cross Blind Fault. The sites used for determination of the Charing Cross recurrence interval include, BPMJ, ACFF, and DOVF to ACFF (see Figure 74). These sites produced an average recurrence interval with a regional shortening rate of 1-2mm/yr. over 125 km of 15,530 ± 5,000 years to 31,056 ± 8,000 years for the Charing Cross Fault (see Table 15).

Using marks, B2Q1 to BPMF and B2Q1 to AA71 across the western segment of the Greendale Fault the average recurrence intervals with a regional shortening rate of 1-2mm/yr. over 125 km was 15,530 ± 15,000 years to 31,056 ± 30,000 years (see Figure 74: Table 15).

3.5.2.3 Discussion

Cadastral surveying effectively captures co-seismic displacements for the Hororata fault. This is because the survey points are in close proximity (i.e. within 2-4.5 km) of the projected faults trace, which is moderately dipping (i.e. 45° Beavan et al., 2012) producing a broad deformation field. Because of this, our estimated minimum recurrence intervals for 1-2 mm/yr. strain of 7,403 ± 2,000 years to 14,785 ± 3,500 years are likely to be robust.

However, combinations of steep fault dip localising surface deformation, limited survey point density, and complicated surface deformation history in the Darfield Earthquake due to interacting reverse and strike-slip faults means the interpretation of Charing Cross and Greendale fault western segment data more challenging. As a result of this, the estimated recurrence intervals for these segments are more variable.

Table 15: Hororata Fault estimated recurrence intervals calculated from the strain release over the fault. Red values correspond to the Hororata fault; Blue corresponds to the Charing Cross Fault; and Green to the Western segment of the Greendale Fault.

Values in Direction of Regional Shortening (115°)			Strain Release / Recurrence Interval	
Across Fault Survey Marks used	Total Displacement (mm)	Distance between points (km)	From 2 mm/yr.	From 1 mm/yr.
AA71 to BPMG	669.84	4.50	9,311 yrs.	18,623 yrs.
ACF7 to BPMF	800.0	5.82	8,586 yrs.	17,173 yrs.
AA71 to BPMF	484.2	5.10	6,028 yrs.	12,056 yrs.
ACF7 to AFCR	605.0	6.70	5,686 yrs.	11,289 yrs.
BPMJ to ACFF	1908.2	8.87	13,455 yrs.	26,910 yrs.
DOVF to ACFF	1433.6	5.09	17,606 yrs.	35,213 yrs.
B2Q1 to BPMF	958.8	1.67	35,883 yrs.	71,766 yrs.
B2Q1 to AA71	906.8	2.72	20,851 yrs.	41,703 yrs.

3.5.3 LINZ data service

With earthquakes a common occurrence in New Zealand due to the tectonic setting, it was hoped research into cadastral surveying using the LINZ data service would pave the way for a new direction of focus for deformation monitoring following earthquakes or monitoring the build-up in strain around fault lines. However, throughout the completion of this study a number of inadequacies were revealed with the current LINZ geodetic database, with the most consistent problem being with positional accuracy of survey marks.

It was found that a large percentage of the marks are useless because of the poor positional accuracy. In particular, I refer to the lower order marks. Currently low order marks (9^{th} to 12^{th}) have a horizontal accuracy of 1 to >10 m making them unhelpful for accurate centimetre scale deformation monitoring. Through correspondence with LINZ I was informed these lower order

marks are used for their vertical location or accuracy rather than the horizontal, however, this is not the case either. Table D1 in Appendix D shows survey marks re-occupied as part of this study and also included is the LINZ downloaded pre-earthquake positions. Of the approx. 68 reoccupied marks only 14 of them had pre-earthquake elevations. The majority of these were 10 to 12th order, but even 5th and 3rd order marks were without elevation data. This was a major limiting factor not only with the database but also with the opportunity to quantitatively represent motion across the Charing Cross Fault, the western segment of the Greendale Fault and unnamed fault near Charing Cross.

In order to provide a more accurate and reliable network it is believed that the LINZ network requires a shift or upgrade from the current vector based system into a coordinate based system. In doing so, the survey marks will no longer be connected to one another via a large vector system, instead each survey mark will have an individual co-ordinate. This has been shown to be extremely successful in Taiwan through Lee and Shih, (2011) and Lee *et al.* studies. Local Christchurch Surveyors, who were approached to recover more accurate locations for the lower order marks have experienced similar issues with the LINZ network. They have begun updating survey marks themselves from a vector based system into co-ordinate based system.

Though expensive, if the whole country's system was upgraded, an additional benefit would be that it would provide scientists with a great opportunity for future insight into the earthquake mechanics and kinematic.

3.5.4 Future work

By introducing this section into this thesis, an opportunity for further investigation(s) was created. In particular, with future work on along the Greendale Fault, use of the network elsewhere and upgrade of the LINZ network/survey marks.

The cadastral trial study completed as part of this thesis was limited to the immediate areas surrounding the Hororata and Charing Cross blind structures. It was used to provide additional support to findings from other sections of this thesis. Therefore, there is plenty of room for a whole Masters or PhD project in cadastral surveying alone looking at Darfield earthquake or the Canterbury earthquake sequence 2010 and 2011 as a whole. This could involve reoccupation of not only at survey marks but also boundary pegs over the whole area of the fault similar to Lee and Shih (2011) and Lee *et al.* studies following the 1999 Chi-Chi earthquake overseas. Furthermore, should another

earthquake occur near Greendale Fault, a detailed network of accurate survey marks is available and the network would be able to be used to its true potential.

The network as it stands can be used for future monitoring of deformation of faults or earthquake events on a larger scale. This is provided higher order marks (1-6) and maintained sites lie nearby to the desired site or investigation area. However, an upgrade of the network from a vector based system in to an individual co-ordinate based system would provide scientists unique and vast research opportunities into the mechanics of earthquake and deformation processes.

Conclusions

Cadastral surveys effectively capture co-seismic displacements for the Hororata Fault. However, combinations of steep fault dip localising surface deformation, limited survey point density, and complicated surface deformation history meant interpretations of the Charging Cross Fault and the Western segment of the Greendale Fault were not as robust.

In addition the study reflects inadequacies with the current LINZ geodetic database limiting the potential for future research opportunities. Recommendations were provide use the network as it currently as well as providing an option for upgrading to create a better service for future deformation monitoring studies in New Zealand.

Conclusions from the Thesis

Using fault displacement GPS surveying, detailed surface investigations and deformation feature mapping, seismic reflection surveying and survey mark (cadastral) re-occupation this study revealed interesting finding for the patterns of crustal deformation associated with the Darfield earthquake.

Fault displacement surveys reveal that no resolvable post-seismic creep occurred along the Greendale Fault relative to the survey sites. Near-field post-seismic deformation identified appears to be driven by on-going creep on adjacent thrust faults (e.g. Charing Cross).

Near surface investigations identified and characterised the Hororata Blind Fault to be dipping northwest at an angle of 50-70^{o}. These investigations also reveal that gravels do play a role in dissipating slip, inhibiting the opportunity to view subsurface fault structures geologically at the surface.

Re-occupation of survey marks in the cadastral surveys effectively captures co-seismic displacements for deformation on the Hororata Fault enabling generation of robust interpretation and recurrence intervals. However, combinations of steep fault dip localising surface deformation, limited survey point density, and complicated surface deformation history meant interpretations of the Charging Cross Fault and the Western segment of the Greendale Fault were not as robust. The cadastral surveys indicated inadequacies with the current LINZ geodetic database limiting the potential for future research opportunities, therefore recommendations for upgrading the LINZ network an using the network in its current state were discussed.

Bibliography

Aki, K. (1979). Characterization of barriers on an earthquake fault. *Journal of Geophysical Research, Vol. 4*, pp. 6140-6148.

Allen, J., Ashford, S., Bowman, E., Bradley, B., Cox, B., Cubrinovski, M., et al. (2010). Geotechnical Reconnaissance of the 2010 Darfield (Canterbury) Earthquake. *Bulletin of the New Zealand Society for Earthquake Engineering, Vol. 43*(No. 4), pp. 243-320.

Barbot, S. F. (2009). Postseismic deformation due to theMw6.0 2004 Parkfield earthquake: stress-driven creep on a fault with spatially variable rate-and-state friction parameters. *Journal of Geophysical Research: Solid Earth, Vol.114*(no.B07405), pp.1-26.

Barbot, S., Hamiel, Y., & Fialko, Y. (2008). Space geodetic investigation of the coseismic and postseismic deformation due to the 2003 Mw 7.2 Altai earthquake: implications for the local lithospheric rheology. *Journal of Geophysical Research: Solid Earth, Vol. 113*(no.B03403), pp.1-10.

Barka, A., Akyuz, H., Altunel, E., Sunal, G., Cakir, Z., Dikbas, A., et al. (2002). The Surface Rupture and Slip Distribution of the 17 August 1999 Izmit Earthquake (M 7.4), North Anatolian Fault. *Bulletin of the Seimological Society of America*, 43-60.

Barrell, D. (2010). *GNS Science Immediate Darfield (Cantebury Earthquake) of 04 Sept 2010 Further Reconnaissance of Surface Deformation - 24 & 25 October 2010.* Dunedin, New Zealand: GNS Science.

Barrell, D., & Jongens, R. (2010). *GNS Science Immediate Report Canterbury Earthquake of 04 September 2010 - Wider reconnaissance of surface deformation 24 Sept and 26 Sept 2010.* Dunedin, New Zealand: GNS Science.

Barrell, D., Litchfield, N., Townsend, D., Quigley, M., Van Dissen, R., Cosgrove, R., et al. (2011). Strike-Slip ground-surface rupture (Greendale Fault) associated with the 4 September 2010 Darfield earthquake, Canterbury, New Zealand. *Quarterly Journal of Engineering Geology & Hydrogeology, Vol. 44* (no. 3), pp. 283-291.

Beavan, J., Motagh, M., Fielding, E., Donnelly, N., & Collet, D. (2012). Fault Slip models of the 2010-2011 Canterbury, New Zealand, earthquakes from geodetic data, and observations of post-seismic ground deformation. *New Zealand Journal of Geology and Geophysics*, pp.1-30.

Beavan, J., Samsonov, S., Motagh, M., Wallace, L., Ellis, S., & Palmer, N. (2010). The Darfield (Canterbury) Earthquake: Geodetic Observations and Preliminary Source Model. *Bulletin of teh New Zealand Society for Earthquake Engineering, Vol.43*(no.4), pp.228-235.

Berryman, K., & Beanland, S. (1988). The rate of tectonic movement in New Zealand from Geological evidence. *Transactions of the Institute of Professional Engineers of New Zealand, Vol. 15*, pp. 25-35.

Berryman, K., Beanland, S., Cooper, A., Cutton, H., Norris, R., & Wood, P. (1992). The Alpine Fault, New Zealand: Variation in Quaternary structure style and geomorphic expression. *Annales Tectonicae Suppliment to Volume, Vol. 6*, pp.126-163.

Bjornsson, G., Flovenz, O. G., Saemundsson, K., & Einarsson, E. H. (2001). *In Proc. 26th Workshop on Geothermal Reservoir Engineering.* Stanford: Stanford University.

Bock, Y., Wdowinski, S., Fang, P., Zhang, J., WIlliams, S., Johnson, H., et al. (1997). Southern California Permanent GPS Geodetic Array: Continuous measurements of regional crustal deformation between the 1992 Landers and 1994 Northridge earthquakes. *Journal of Geophysical Research* , 18,013-18,033.

Bouchon, M., Toksöz, N., Karabulut, H., Bouin, M., Dietrich, M., Aktar, M., et al. (n.d.). Seismic imaging of the 1999 Izmit (Turkey) rupture inferred from the near-fault recordings. *Geophysical Research Letters, Vol. 27*(No. 18), pp.3013-3016.

Brown, L., & Weeber, J. (1992). *Geology of the Christchurch Urban Area.* Lower Hutt, New Zealand: Institute of Geological & Nuclear Sciences Ltd.

Burbank, D., & Anderson, R. (2009). *Tectonic Geomorphology.* Hoboken: Wiley-Blackwell .

Burg, J.-P. (2011). *Strike-slip and Oblique-slip Tectonics* . Retrieved 2012 August, from University of Zurich - Structural Geology: www.files.ethz.ch/structuralgeology/JPB/files/English/5wrench.pdf

Burgmann, R., Ergintav, S., Segall, P., Hearn, E., McClusky, S., Reilinger, R., et al. (2002). Time-space variable afterslip on and deep below the Izmit earthquake rupture. *Bulletin of the Seismological Society of America, Vol.92*, pp.126-137.

Burgmann, R., Segall, P., Lisowski, M., & Svarc, J. (1997). Postseismic strain following the 1989 Loma Prieta earthquake from GPS and leveling measurements. *Journal of Geophysical Research, Vol.102*, 4933-4955.

Byerlee, J. (1978). Friction of rock. *Pure Applied Geophysics, Vol. 116* , pp.615–-626.

Caltrans . (2006, September). *Survey Manual - Total Station Survey System (TSSS) Survey Specifications.* Retrieved July 15, 2012, from California Department of Transportation: http://www.dot.ca.gov/hq/row/landsurveys/SurveysManual/07_Surveys.pdf

Cetin, E., Meghraoui, M., Cakir, Z., Akoglu, A., Mimouni, O., & Chebbah, M. (2012). Seven years of postseismic deformation following the 2003 Mw = 6.8 Zemmouri earthquake (Algeria) from InSAR time series. *Geophysical Research Letters, Vol.39*, L10307 pp.1-6.

Cheng, L. L. (2009). Coseismic and postseismic slip distribution of the 2003 Mw = 6.5 Chengkung earthquake in eastern Taiwan: Elastic modeling from inversion of GPS data . *Tectonophysics*, 335-343.

Cousins, J., & McVerry, G. (2010). Overview of strong-motion data from the Darfield Earthquake. *Bulletin of the New Zealand Society for Earthquake Engineering, Vol. 43*(No. 4), pp. 222-227.

Cowan, H. (1991). The North Canterbury earthquake of 1 September 1888. *Journal of the Royal Society of New Zealand, 21*, 1 - 12.

Cowan, H., Nicol, A., & Tonkin, P. (1996). A comparison of historical and paleoseismicity in a newly formed fault zone and a mature fualt zone, North Canterbury, New Zealand. *Journal of Geophysical Research, Vol. 101*, pp. 6021-6036.

Davis, G. H., & Reynolds, S. J. (1996). *Structural Geology of Rocks and Regions - 2nd Edition.* Hoboken: John Wiley & Sons, Inc.

DeMets, C., Gordon, R., D.F., A., & Stein, S. (1990). Current plate motions. *Geophysical Journal International, Vol. 101*, pp. 425-478.

Dorn, C., Carpentier, S., Kaiser, A., Green, A., Horstmeyer, H., Campbell, F., et al. (2010). First seismic imaging results of tectonically complex structures at shallow depths beneath the northwest Canterbury Plains, New Zealand. *Journal of Applied Geophysics, Vol.70*, pp. 317-331.

Downes, G., Science, G., Tectonophysics, Yetton, M., & Ltd., G. C. (2012). Pre-2010 historical seismicity near Christchurch, New Zealand: The 1869 Mw 4.7-4.9 Christchurch and 1870 Mw 5.6-5.8 Lake Ellesmere earthquakes. *New Zealand Journal of Geology and Geophysics, Vol.55*(no.3), pp.1-16.

Duffy, B. Q. (12). Fault kinematics and surface deformation across a releasing bend during the 2010 MW 7.1 Darfield, New Zealand, earthquake revealed by differential LiDAR and cadastral surveying. *Duffy, B, Quigley, M, Barrell, D, Dissen, RV, Stahl, T, Leprince, S, McInnes, C & Bilderback, E accepted manuscript, 'Fault kinematics and surface deformation acrossAccepted Manuscript*.

Elder, D., McCahon, I., & Yetton, M. (1991). *The earthquake hazard in Christchurch: a detailed evaluation.* Christchurch, New Zealand: A Research Report to the EQC. Soils and Foundations Ltd.

Ellsworth, W., & Beroza, G. (1995). Seismic evidence for a seismic nucleation phase. *Science, Vol. 268*, pp. 851-855.

Erdik, M., & Durukal, E. (2000). Strong ground motion from the Kocaeli and Duzce earthquakes. *Nato Advanced Research Seminar: Integration of Earth Sciences Research on the 1999 Turkish and Greek Earthquakes and Needs for Future Cooperative Research Seminar Abstract Book*, (p. 108). Istanbul.

Ergintav, S., Burgmann, R., McClusky, S., Cakmak, R., Reilinger, R., Lenk, O., et al. (2002). Postseismic Deformation near the Izmit Earthquake (17 August 1999, M 7.5) Rupture Zone. *Bulletin of the Seismological Society of America, Vol.92*(no.1), pp.194-207.

Failko, Y., & Barbot, S. (2010). A unified continuum representation of post-seismic relaxation mechanisms: semi-analytic models of afterslip, poroelastic rebound and viscoelastic flow. *Geophysical Journal International, Vol.182*, pp.1124-1140.

Fialko, Y. (2004). Evidence of fluid-filled upper crust from observations of postseismic deformation due to the 1992 Mw7.3 Landers earthquake. *Journal of Geophysical Research, Vol.109* (no.B08401), pp.1 - 17.

Fialko, Y. (2004). Probing the mechanical properties of seismically active crust with space geodesy: Study of the co-seismic deformation due to the 1992 Mw 7.3 Landers (southern California) earthquake. *Journal of Geophysical Research, Vol. 109*(B03307), pp. 1-23.

Fialko, Y., Sandwell, D., Simons, M., & Rosen, P. (2005). Three-dimensional deformation caused by the Bam, Iran, earthquake and the origin of shallow slip deficit. *Nature*, 295-299.

Field, B., & Browne, G. (1989). Cretaceous and Cenozoic sedimentary basins and geological evoluiton of the Canterbury region, South Island, New Zealand. *New Zealand Geological Survey Basin Studies 2. Lower Hutt, New Zealand Geological Survey*, pp.94.

Forsyth, P., Barrell, D., & Jongens, R. (2008). *Geology of the Christchurch Area.* Lower Hutt, Wellington, New Zealand: GNS Science - Institute of Geological & Nuclear Sciences.

Freed, A. (2007). Afterslip (and only afterslip) following the 2004 Parkfield, California, earthquake. *Geophysical Research Letters, Vol.34*.

Freed, A., & Burgmann, R. (2004). Evidence of power-law flow in the Mojave desert mantle. *Nature, Vol.430*, pp.548-551.

Freed, A., Burgmann, R., Calais, E., Freymueller, J., & Hreinsdottir, S. (2006). Implications of deformation following the 2002 Denali, Alaska, earthquake for postseismic relaxation processes and lithospheric rheology. *Journal of Geophysical Research, Vol. 111*(no. B01401), pp.1-23.

Freymueller, J., King, N., & Segall, P. (1994). The Co-seismic Slip Distribution of the Landers Earthquake. *Bulletin of the Seismological Society of America, Vol. 84*(No. 3), pp. 646-659.

Geonet. (2012). *Historic Earthquakes M 7.1 Darfield (Canterbury), September 4 2010*. Retrieved May 12, 2012, from Geonet: http://www.geonet.org.nz/earthquake/historic-earthquakes/top-nz/quake-13.html

Gledhill, K., Ristau, J., Reyners, M., Fry, B., & Holden, C. (2011). The Darfield (Canterbury, New Zealand) Mw 7.1 Earthquake of September 2010: Preliminary Seismological Report. *Sesimological Research Letters*, 378-386.

Grapes, R., Little, T., & Downes, G. (1998). Rupturing of the Awatere Fault during the 1848 October 16 Marlborough earthquake, New Zealand: historical and present day evidence. *New Zealand Journal of Geology and Geohpysics, Vol. 41*, pp. 387-399.

Grijalva, K., Burgmann, R., & Banerjee, P. (2007). *Using Geodetic Data to Understand Post-seismic Processes following the Sumatra-Andaman Earthquake.* Retrieved August 23, 2012, from Berkeley Seismological Laboratory Annual Reports: http://seismo.berkeley.edu/annual_report/ar09_10/node6.html

Hamiel, Y., & Fialko, Y. (2007). Structure and mechanical properties of faults in the North Anatolain Fault system from InSAR observations of coseismic deformation due to the 1999 Izmit (Turkey) earthquake. *Journal of Geophysical Research*, 1-12.

Harris, R., Archuleta, R., & Day, S. (1991). Fault steps and the dynamic rupture process: 2-d numerical simulations of a spontaneusly propogating shear fracture. *Geophysical Research Letters, Vol. 18*, p. 893-896.

Harris, R., Dolan, J., Hartleb, R., & Day, S. (2002). The 1999 Izmit, Turkey, Earthquake: A 3D Dynamic Stress Transfer Model of Intraearthquake Triggering. *Bulletin of the Seismological Society of America*, 245-255.

Hauksson, E., James, L., & Hutton, K. (2002). The 1999 Mw 7.1 Hector Mine, California, earthquake sequence: complex conjugate strike-slip faulting from space geodetic observations. *Bulletin of the Seismological Society of America , 92*(4), 1154-1170.

Hauksson, E., Jones, L., Hutton, K., & Eberhart-Phill, D. (1993). The 1992 Landers Earthquake Sequence' Seismological Observations. *Journal of Geophysical Research, Vol. 98*(no. BII), pp. 19,835-19,858.

Hearn, E., Burgmann, R., & Reilinger, R. (2002). Dynamic of Izmit earthquake postseismic deformation and loading of the Duzce hypocentre. *Bulletin of the Seismological Society of America, Vol.92*, pp.172-193.

Holden, C., Beavan, J., Fry, B., Reyeners, M., Ristau, J., Van Dissen, R., et al. (2011). Preliminary source model of the Mw 7.1 Darfield earthquake from geological, goedetic and seismic data . *Proceedings of the Ninth Pacific Conference on Earthquake Engineering Building an Earthquake Resilient Society* (pp. 1-8). Auckland: New Zealand Society of Earthquake Engineering.

Hosseini, K., Mahdavifar, M., Bakhshayesh, M., & Rakhshandeh, M. (2004). *Engineering Geology and Geotechnical Aspects of Bam Earthquake (Preliminary Report).* Tehran, Iran: International Institute of Earthquake Engineering and Seismology.

Howard, M., Nicol, A., Campbell, J., & Pettinga, J. (2005). Holocene paleoearthquakes on the strike-slip Porters Pass Fault, Canterbury, New Zealand. *New Zealand Journal of Geology and Geophysics, Vol. 48*, pp. 59-74.

Hsu, Y., Bechor, N., Segall, P., Yu, S., Kuo, L., & Ma, K. (2002). Rapid afterslip following the 1999 Chi-Chi, Taiwan Earthquake. *Geophysical Research Letters, Vol.29*(no.16), pp. 1754.

Hsu, Y., Simons, M., Avouac, J., Galetzka, J., & Sieh, K. (2006). Friction afterslip following the 2005 Nias-Simeulue earthquake, Sumatra. *Science, Vol.312* , pp.1921–1926.

Hudnut, K., & et al. (1994). Coseismic Displacements of the 1992 Landers Earthquake sequence. *Bulletin of the Seismological Society of America, Vol. 84*, pp. 806-816.

Hudnut, K., & Larsen, S. (1993). Slip distribution in the Landers Califiornia, earthquake sequence determined from geodetic data. *EOS, 74*(43), 183.

Hudnut, K., BLock, Y., Cline, M., Fang, P., Feng, Y., Freymueller, J., et al. (1993). Co-seismic displacments of the 1992 Landers earthquake sequence. *Bulletin of the Seismological Society of America, Vol. 84*(No. 3), pp. 625-645.

Husseini, M., Jovanovich, D., Randall, M., & Freund, L. (1975). The fracture energy of earhtquakes. *Geophysical Journal of the Royal Astronomical Society, Vol. 43*, pp. 367-385.

Johanson, I., Fielding, E., Rolandone, F., & Bürgmann, R. (2006, September). Coseismic and Postseismic Slip of the 2004 Parfield Earthquake from Space-Geodetic Data. *Bulletin of the Seismological Society of America, 96*(4B), S269-S282.

Johnson, K., Burgmann, R., & Larson, K. (2006). Frictional Properties on the San Andreas Fault near Parkfield, California, Inferred from Models of Afterslip following the 2004 Earthquake. *Bulletin of the Seismological Society of America, Vol. 96*(No. 4B), S321-S338.

Jonsson, S., Segall, P., Pedersen, R., & Bjornsson, G. (2003). Post-earthquake ground movements correlated to pore-pressure transients. *Nature, Vol.424*, pp.179-183.

Karakaisis, G. (2003). Accelerating seismic crustal deformation before the Izmit (NW Turkey) large mainshock of 1999 August 17 and the evolution of its aftershock sequence. *International Journal of Geophysics*, 103-110.

Kerr, J., Nathan, S., Van Dissen, R., Webb, P., Brunsdon, D., & King, A. (2003, July). *A guideline to assist resource management planners in New Zealand.* Retrieved August 2012, from Ministry for the Environment New Zealand: http://www.mfe.govt.nz/publications/rma/planning-development-active-faults-dec04/planning-development-faults-graphics-dec04.pdf

Keuken, H., & Groenewoud, P. (1992). *Sevices: Seismic Surveys*. Retrieved July 30, 2012, from Resolution Resources Internation (RRI): http://www.rri-seismic.com/Frame%20Pages/Tech%20Pages/Seismic/seismic.htm

Kisslinger, C., & Jones, L. (1991). Properties of aftershocks in southern California. *Journal of Geophysical Research, Vol.96*, pp.11,947-11,958.

Lee, Y.-H., & Shih, Y.-X. (2011). Coseismic displacement, bilateral rupture, and strucural characteristics at the southern end of the 1999 Chi-Chi earthquake rupture, central Taiwan. *Journal of Geophysical Research, 116*(B07402), 1-18.

Lee, Y.-H., Chen, Y.-C., Chen, C.-L., Rau, R.-J., Chen, H.-C., Lo, W., et al. (2011, June). Revealing Coseismic Displacement and Dosplacemnt Partitioning at the Northern End of the 1999 Chi-Chi Earthquake, Central Taiwan, Using Digital Cadastral Data. *Bulletin of the Seismological Society of America, 101*(3), 1199-1212.

Lettis, W., Bachhuber, J., Witter, R., Brankman, C., Randolph, C., Barka, A., et al. (2002). Influence of Releasing Step-Overs on Surface Fault Rupture and Fault Segmentation: Examples form the 17 August 1999 Izmit Earthquake on the North Anatolian Fault, Turkey. *Bulletin of the Seismological Society of America*, 19-42.

Li, Y., Vidale, J., Aki, K., Xu, F., & Burdette, T. (1998). Evidence of shallow fault zone strengthening after the 1992 Mw 7.5 Landers, California, earthquake. *Science, Vol. 279*, pp. 217-219.

Li, Y., Vidale, J., Day, S., Oglesby, D., & Cochran, E. (2003). Post-seismic fault healing on the rupture zone of the 1999 Mw 7.1 Hector Mine, California, earthquake. *Bulletin of the Seismological Society of America, Vol. 93*, pp. 854-869.

Lin, A., Ren, Z., Jia, D., & Wu, X. (2009). Co-seismic thrusting rupture and slip distribution produced by the 2008 Mw 7.9 Wenchuan earthquake, China. *Tectonophysics, 471*, 203-215.

Lyons, S., & Sandwell, D. (2003). Fault creep along the southern San Andreas from interferometric synthetic aperture radar, permanent scatterers, and stacking. *Journal of Gepphysical Research, Vol. 108*, doi:10:1029/2002JB001831.

MacDonald, J., Burton, C., Winstanley, I., & Lapidus, D. (2003). *Collins internet-linked dictionary of Geology.* London: HarperCollins.

Main, I. (2000). A damage mechanics model for power-law creep and earthquake aftershock and foreshock sequences. *Geophysics Journal International, Vol.142*, pp.151-161.

Manning, C., & Ingebritsen, S. (1999). Permeability of the continental crust:Implications of geothermal data and metamorphic systems. *Reviews of Geophysics, Vol. 37*, pp.127–-150.

Marone, C. (1998). Laboratory-derived friction laws and their application to seismic faulting. *Annual Reviews - Earth and Planetary Sciences, Vol. 26*, pp. 643–-696.

Marone, C., Scholz, C., & Bilham, R. (1991). On the mechanics of earthquake afterslip. *Journal of Gephysical Research, Vol.96*, pp.8441-8452.

Masterlark, T., & Wang, H. (2002). Transient stress-coupling between the. *Bulletin of the Seismological Society of America, Vol.92*(no.4), pp.1470-1486.

McCaffrey, R., & Gupta, K. (2011). *Encyclopedia of Solid Earth Geophysics.* Netherlands: Springer.

Melbourne, T., Webb, F., Stock, J., & Reigber, C. (2002). Rapid postseismic transients in subduction zones from continuous GPS. *Journal of Geophysical Research, Vol.107*(no.B10), pp.2241.

Miyahsita, K., Vijaykumar, K., Kato, T., Aoki, Y., & Reddy, C. (2001). *Postseisimc crustal deformation deduced from GPS observations, in a comprehensive survey of the 26 January 2001 Earhtquake (Mw 7.7) in the State of Gujarat, India. Edited by T. Sato et al.,.* Retrieved August 11, 2012, from Hirosaki University, Faculty of Science and Technology: http://www.st.hirosaki-u.ac.jp/~tamao/Gujarat/print/Gujarat_4.pdf

Norris, R., & Cooper, A. (2001). Late Quaternary slip rates and slip partitioning on the Alpine Fault, New Zealand. *Structural Geology, 23 (2-3)*, 507-520.

Norris, R., Koons, P., & Cooper, A. (1990). The obliquely-convergent plate bourndary in the South Island of New Zealand: implications for ancient collision zones. *Structural Geology, 12 (5-6)*, 715-725.

Nur, A., & Booker, J. R. (1972). Aftershocks caused by pore fluid flow? *Science, Vol.175*, pp.885–887.

Omori, F. (1894). On the aftershocks of earthquakes. *Journal of the College of Science, Imperial University of Tokyo, Vol. 7* , pp. 111–200.

Owen, S., Anderson, G., Agnew, D., Johnson, H., Hurst, K., Reilinger, R., et al. (2002). Early postseismic deformation from the 16th October 1999 Mw Hector Mine, California,

earthquake as measured by survey-mode GPS. *Bulletin of the Seismological Society of America, Vol.92*, pp.1423-1432.

Papathanassiou, G., Pavlides, S., & Ganas, A. (2005). The 2003 Lefkada earthquake: Field observations and preliminary microzonation map based on liquefaction potential index for the town of Lefkada. *Engineering Geology*, 12-31.

PCE. (2001, March). *Building on the edge the use and development of land on or close to fault lines.* Retrieved August 2012, from Paliamentary Commissioner for the Environment New Zealand: http://www.pce.parliament.nz/assets/Uploads/Reports/pdf/Building_edge.pdf

Peltzer, G., Rosen, P., & Rogez, F. (1998). Poroelastic rebound along the Landers 1992 earthquake surface rupture. *Journal of Geophysical Research, Vol. 103*(No. B12), pp. 30,131-30,145.

Perfettini, H., & Avouac, J. (2004). Postseismic relaxation driven by fault creep: A possible mechanism to reconcile geodetic measurements and the decay rate of aftershocks, application to the Chi-Chi earthquake, Taiwan. *Journal of Geophysical Research, Vol.109*, pp.B02304.

Perfettini, H., & Avouac, J. (2007). Modeling afterslip and aftershocks following the 1992 Landers earthquake. *Journal of Geophysical Research, Vol.112*(no.B07409), pp.1-19.

Pettinga, J. R., Yetton, M., Van Dissen, R., & Downes, G. (2001, December). Earthquake Source Identification and Characterisation for the Canterbury Region, South Island, New Zealand. *Bulletin of the New Zealand Society for Earthquake Engineering, 34*(4), 282-317.

Pollitz, F. F., Wicks, C., & Thatcher, W. (2001). Mantle flow beneath a continental strike-slip fault: Post-seismic deformation after the 1999 Hector Mine earthquake. *Science, Vol.293*, pp.1814-1818.

Pollitz, F., Burgmann, R., & Segall, P. (1998). Joint estimation of afterslip rate and postseismic relaxation following the 1989 Loma Prieta earthquake. *Journal of Geophysical Research, Vol. 103*, pp. 26,975-26,992.

Pollitz, F., Nyst, M., Nishimura, T., & Thatcher, W. (2006). Inference pf post-seismic deformation mechanisms of the 1923 Kanto earthquake. *Journal of Geophysical Research, 111*(B05408).

Pollitz, F., Peltzer, G., & Burgmann, R. (2000). Mobility of continental mantle: evidence from postseismic geodetic observations following the 1992 Landers earthquake. *Journal of Geophysical Research: Solid Earth, Vol.105*(no.B4), pp.8035-8054.

Quigley, M., Van Dissen, R., Villamor, P., Duffy, B., Barrell, D., Furlong, K., et al. (2012). Surface rupture during the 2010 Mw 7.1 Darfield (Canterbury) earthquake: Implications for the fault rupture dynamics and seismic-hazard analysis. *Geology, Vol. 40*(No. 1), pp. 55-58.

Quigley, M., Van Dissen, R., Villamor, P., Litchfield, N., Barrell, D., Furlong, K., et al. (2010). Surface Rupture of the Greendale Fault during the Mw 7.1 Darfield (Canterbury) Earthquake, New Zealand: Initial Findings. *Bulletin of the New Zealand Society for Earthquake Engineering, 43*(3), 236-242.

Quigley, M., Villamor, P., Furlong, K., Beavan, J., Van Dissen, R., Litchfield, N., et al. (2010). Previously Unknown Fault Shakes New Zealand's South Island. *EOS, Vol. 91*(No. 49), pp. 469-488.

Ran, Y., Shi, X., Wang, H., Chen, L., Chen, J., Liu, R., et al. (2010). The maximum coseismic vertical surface displacement and surface deformation pattern accompanying the Ms 8.0 Wenchuan earthquake. *Chinese Science Bulletin, Vol. 55*(No. 4), pp. 841 - 850.

Reid, H. (1910). *The Mechanics of the Earthquake, The California Earthquake of April 18, 1906, Report of the State Investigation Commission, Vol. 2.* Washington, DC: Carnegie Institution of Washington.

Reilinger, R., Ergintav, S., Burgmann, R., McClusky, S., Lenk, O., Barka, A., et al. (2000, September 1). Coseismic and Postseismic Fault Slip for the 17 August 1999, M = 7.5, Izmit, Turkey Earthquake. *Science, 289*, 1529-1523.

Reyners, M. (2011). Lessons from the Destructive Mw 6.3 Christchurch, New Zealand, Earthquake. *Seismological Research Letters, Vol. 82*(no. 3), 371-372.

Reyners, M., & Cowan, H. (1993). The transition from subduction to continental collision: crustal structure in the North Canterbury region, New Zealand. *Geophysical Journal International, Vol. 115*(No. 3), pp. 1124-1136.

Reyners, M., Eberhart-Phillips, D., & Bannister, S. (2011). Tracking repeated subduction of the Hikurangi Plateau beneath New Zealand. *Earth and Planetary Science Letter*.

Rick, J. (1996). *Total Stations in Archaeology.* Retrieved August 2012, from Society for American Archaeology 14 (4): http://www.saa.org/portals/0/saa/publications/saabulletin/14-4/saa16.html

Roeloffs, E. (1996). Poroelastic techniques in the study of earthquake-related hydrologic phenomena. *Adances in Geophysics*, 27, 135–195.

Rymer, M. J., Langenheim, V. E., & Hauksson, E. (2002). The Hector Mine, California, Earthquake of 16 October 1999: Introduction to the Special Issue. *Bulletin of the Seismological Society of America*, 1147-1153.

Rymer, M., Tinsley III, J., Treiman, J., Arrowsmith, J., Clahan, K., Rosinski, A., et al. (2006, September). Surface Fault Slip Associated wiht the 2004 Parkfield, California, Earthquake. *Bulletin of the Seismological Society of America, Vol. 96*(No.4B), S11-S27.

Savage, J. C. (1980). *Dislocation in seismology, in Dislocation in Solids, Vol. 3.* North-Holland, Amsterdam: F.R.N. Nabarro (Editor).

Savage, J. C. (1990). Equivalent strike-slip earthquake cycles in half-space and lithosphere-asthenosphere Earth models. *Journal of Geophpysical Research, Vol.95*, pp.4873-4879.

Savage, J. C., & Prescott, W. (1978). Asthenospheric readjustment and the earthquake cycle. *Journal of Geophysical Research, Vol.83*, pp.3369–3376.

Savage, J., & Svarc, J. (1997). Postseismic deformation associated with the 1992 Mw = 7.3 Landers earthquake, southern California. *Journal of Geophysical Research*, 7565-7577.

Schaff, D., Beroza, G., & Shaw, B. (1998). Postseismic response of repeating aftershocks. *Geophysical Research Letters*, 4549-4552.

Scholz, C. H. (1988). The critical slip distance for seismic faulting. *Nature, Vol.336*, pp.761–763.

Segall, P. (2010). *Earthquake and Volcano Deformation.* Princeton: Princeton University Press.

Segall, P., & Pollard, D. D. (1980). Mechanics of discontinuous faults. *Geophysics*, 4337-4350.

Segall, P., Burgmann, R., & Matthews, M. (2000). Time dependant triggered afterslip following the 1989 Loma Prieta earthquake. *Journal of Geophysical Research, Vol.105*, pp.5615-5634.

Shakal, A., Haddadi, H., Grizer, V., Lin, K., & Huang, M. (2006). Some Key Features of the Strong-Motion Data from the Mw 6.0 Parkfield, California, Earhtquake of 28 September 2004. *Bulletin of the Seismological Society of America, Vol. 96*(No. 4B), S90-S118.

Shao, Z., Wang, R., Wu, Y., & Zhang, L. (2011). Rapid afterslip and short-term viscoelastic relaxation following the 2008 Mw 7.9 Wenchuan Earthquake. *Earthquake Science, Vol. 24*(No.2), pp. 163-175.

Shaw, B., & Wesnousky, S. (2008). Slip-Length Scaling in Large Earthquakes: the Role of Deep-Penetrating Slip below the Seismogenic layer. *Bulletin of the Seismological Society of America*, 1633-1641.

Shcherbakov, R., Turcotte, D., & Rundle, J. (2004). A generalized Omori's law for earthquake aftershock decay. *Geophysical Research Letters, Vol. 31*(L11613), pp.1-5 .

Shen, Z., Jackson, D., Feng, Y., Cline, M., Kim, M., Fang, P., et al. (1994). Post-seismic deformation following the Landers earthquake, California, 28th June 1992. *Bulletin of the Seismological Society of America, Vol. 84*, pp. 780-791.

Sibson, R. (1985). Stopping of earthquake ruptures at dilational fault jogs. *Nature, Vol. 316*, p. 248-251.

Sibson, R. (1986). Rupture interactions with fault jogs, in Earthquake Source Mechanics. *Geophysical Monographs, Maurice Ewing Series 6, American Geophysical Union*, p. 157-167.

Sieh, K., Jones, L., Haukksson, E., Hudnut, K., Eberhart-Phillips, D., Heaton, T., et al. (1993). Near-field investigations of the Landers earthquake sequence. *Science, 260*, 171-176.

Simons, M., Fialko, Y., & Rivera, L. (2002, May). Co-seismic Deformation from the 1999 Mw 7.1 Hector Mine, California, Earthquake as Inferred from InSAR and GPS Observations. *Bulletin of the Seismological Society of America, 92*(4), 1390-1402.

Smith, S., & Wyss, M. (1968). Displacement on the San Andreas Fault subsequent to the 1966 Parkfield Earthquake. *Bulletin of the Seismological Society of America, Vol.58*, pp.1955-1973.

Stein, S., & Wysession, M. (2003). *An Introduction to Seismology, Earthquakes, and Earth Structure.* Victoria, Australia: Blackwell Publishing Ltd.

Stein, S., & Wysession, M. (2009). *An Introduction to Seismology, Earthquakes, and Earth Structure.* Victoria: Wiley-Blackwell Publishing Ltd.

Stirling, M., Pettinga, J., Berryman, K., & Yetton, M. (2001). Probablistic seismic hazard assessment of the Canterbury Region, New Zealand. *Bulletin of the New Zealand Society for Earthquake Engineering, 34*(4), 318-334.

Sutherland, R. (1999). Cenozoic bending of New Zealand basement terranes and Alpine Fault displacement: A brief review. *New Zealand Journal of Geology and Geophysics, Vol. 42*(No. 2), pp. 295-301.

Sutherland, R., & Norris, R. (1995). Late Quaternary displacement rate, paleoseismicity, and geomorphic evolution of the Alpine Fault: evidence from Hokuri Creek, South Westland, New Zealand. *New Zealand Journal of Geology and Geophysics, Vol. 38*, pp. 419-430.

Sutherland, R., Berryman, K., & Norris, R. (2006). Quaternary slip rate and geomorphology of the Alpine Fault: implications for kinematics and seismic hazard in the southwest New Zealand. *Bulletin for the Geological Society of New Zealand*, 118(3-4):464-474.

Sutherland, R., Eberhart-Phillips, D., Harris, R., Stern, T., Beavan, R., Ellis, S., et al. (2007). Do great earthquakes occur on the Alpine Fault in Central South Island, New Zealand? *Geophysical Monograph Series, Washington, DC (American Geophysical Union)*, 235-251.

Talebian, M., Fielding, E., Funning, G., Ghorashi, M., Jackson, J., Nazari, H., et al. (2004). The 2003 Bam (Iran) earthquake: Rupture of a blind strike-slip fault. *Geophysical Research Letters, Vol. 31*(L11611), pp. 1-4.

Terres, R., & Sylvester, A. (1981). Kinematic analysis of rotated fractures and blocks in simple shear. *Bulletin of the Seismological Society of America, Vol.71*, pp. 1593-1605.

Thatcher, W. (1983). Nonlinear strain buildup and the earthquake cycle on the San Andreas fault. *Journal of Geophysical Research, Vol.88*, pp.5893–5902.

Toke, N., Arrowsmith, J., Young, J., & Crosby, C. (2006). Paleoseismic and Postseismic Observations of Surface Slip along the Parkfield Segment of the San Andreas Fault. *Bulletin of the Seismological Society of America, Vol.96*(No. 4B), S221-238.

Totalstation.org. (2012). *Some explanation about Total Station and Theodolite.* Retrieved August 13, 2012, from Totalstation.org: http://totalstation.org/theodolite.php

Townend, J., Sutherland, R., & Toy, V. (2009). *Deep Fault Drilling Project- Alpine Fault, New Zealand Scientific Drilling.* Scientific drilling.

Tse, S., & Rice, J. (1986). Crustal earthquake instability in relation to the depth variation of frictional slip properties. *Journal of Geophysical Research, Vol. 91*, pp.9452–9472.

Tuttle, M. P. (2001). The use of liquefaction features in paleoseismology: Lessons learned in the New Madrid seismic zone, central United States. *Journal of Seismology*(5), 361-380.

USGS. (2012, June 27). *Earthquake Facts and Statistics*. Retrieved June 19, 2012, from United States Geological Survey - USGS: http://earthquake.usgs.gov/earthquakes/eqarchives/year/eqstats.php

Utsu, T., Ogata, Y., & Matsu'ura, R. (1995). The centenary of the Omori formula for a decay law of aftershock activity. *Journal of the Physics of the Earth, Vol.43*, pp.1-33.

Van Dissen, R., Barrell, D., Litchfield, N., Villamor, P., Quiley, M., King, A., et al. (2011). Surface rupture displacement on the Greendale Fault during the Mw 7.1 Darfield (Canterbury) earthquake, New Zealand, and its impact on man-made structures. *Proceedings of the Ninth Pacific Conference on Earthquake Engineering Building an Earthquake Resilient Society* (pp. 1-8). Auckland, New Zealand: NZSEE.

Wallace, L., Beavan, J., McCaffrey, R., Berryman, K., & P., D. (2007). Balancing the plate motion budget in the South Island, New Zealand using GPS, geological, and seismological data. *Geophysics Journal International, Vol. 168*, pp.332-352.

Wallace, R. (1970). Earthquake recurrence intervals of the San Andreas fault. *Bulletin of the Seismological Society of America, Vol. 81*, p. 2875-2890.

Wang, R., Xia, Y., Grosser, H., Wetzel, H., Kaufmann, H., & Zschau, J. (2004). The 2003 Bam (SE Iran) earthquake: precise source parameters from satellite radar interferometry. *Geophysics Journal International, Vol. 159*, pp. 917-922.

Wellman, H. (1953). Data for the study of Recent and Late Pleistocene faulting in the South Island of New Zealand. *New Zealand Journal of Science and Technology, 34 (4)*, 270-288.

Wesnousky, S. G. (2006). Predicting the endpoints of eathquake ruptures. *Nature*, 358-360.

Wiemer, S. (2006, January 10). *Earthquake statistics and Earthquake Prediction Research.* Retrieved July 2012, from Earthquake Statistics Group: http://www.earthquake.ethz.ch/education/NDK/NDK

Wood, R., Andrews, P., & Herzer, R. (1989). Cretaceous and Cenozoic geology of the Chatham Rise region, South Island, New Zealand. *New Zealand Geologcial Survey Basin Studies 3. Lower Hutt, New Zealand Geological Survey*, pp.76.

Yetton, M. (2000). *The Probablilty and Consequence of the next Alpine Fault Earthquake, South Island, New Zealand. UNpublished PhD Thesis, Lodged in the University of Canterbury, Library, Christchurch, NZ. 312 pages.*

Table of Figures

Appendices

The following are included in the appendix:

- Appendix A – Literature Review
- Appendix B – Fault Creep Surveys
- Appendix C – Site Investigations, RTK and Seismic Reflection Surveys
    - Site Investigations
        - Photos from site investigations around the Canterbury Region
    - RTK Surveying
        - Survey data sheets
    - Seismic Reflection Surveys
        - Survey log sheets
- Appendix D – Cadastral/ Geodetic Surveys

Table A1: shows approx. 30 historical strike slip earthquakes and observations from 1868 – 1999 involving step-overs (Source: Lettis *et al.*, 2002)

ID	Fault Name; Country; Pull-Apart Basin	Name of EQ; Magnitude; Event Date (mm/dd/yy)	Rupture Length (km)	Segments Ruptured	Displacement (m)		Rupture Through (Y/N)	Separation and Overlap (Pull-Apart Basin Dimensions)			Reference	Comments
					At Basin	Maximum*		Length (km)	Width (km)	Area (km_2)		
1a	Hayward fault California, USA Tule Pond	Hayward M_s 6.8 10/21/1868	48	27		1.9 0.9 avg.	Y	0.35	0.1	0.035	Yu and Segall (1996), Wells *et al.* (1994), Lienkaemper (1992)	Only available map was a poor scale to measure step-over dimensions
1b	Hayward fault California, USA Lake Elizabeth						Y	0.40	0.15	0.06		
2a	Owens Valley fault, California, near Manzanar airport	Owens Valley M_s 8.0 3/26/1872	108	3	3.40	11 6.2 avg.	Y	4.5	2	9	Wells and Coppersmith (1994), Beanland and Clark (1994)	Both ends of rupture do not appear to be step-over boundaries; rupture from south to north
2b	Owens Valley fault, California Calvert Lake region						Y	−1.3	0.6	~0.8		
3a	Hope River fault New Zealand Hope–Boyle Basin	North Canterbury *M* 7–7.3 9/1/1888	30	1	2.40	1.5–2.6 max.	N	~5	~4	~20	Cowan (1990, 1991), Cowan *et al.* (1991)	Hope–Boyle basin is a releasing bend; right lateral; measured fencelines to determine offsets; rupture from the west to the east
3b	Hope River fault New Zealand Hanmer Basin				1.50		N	~2	(4–6.5) ~5	~10		
4	San Andreas fault California, USA Golden Gate	1906 San Francisco EQ *M* 7.8 4/10/1906	435–470		−3	6 hor. 1 ver.	Y	−10	3.5	~35	Lawson *et al.* (1908); Wesnousky (1989)	Right lateral; length of overlap is approximate (at Golden Gate)
5	Haiyun fault China Salt Lake	Haiyuan (Kansu) *M* 8.7 12/16/1920	200	2	6.0	10 8 avg.	Y	6.5	2–4	34.0	Weiqi *et al.* (1987)	Displacement at basin noted from W to E along fault (no rupture direction noted); left lateral; poor scale map, difficult to measure steps/basin dimensions
6a	Fu-yun fault China	Ketetuohai-Ertai M_s 7.9 8/10/1931	180		5.5–7.5	14.6 8 avg.	Y	10	4	40	Wells and Coppersmith (1994), Baljinnyam *et al.* (1993), Knuepfer (1989)	
6b	Fu-yun fault China						Y	3	2	6		
6c	Fu-yun fault China						Y	−2	3	6		

ID	Fault Name; Country; Pull-Apart Basin	Name of EQ; Magnitude; Event Date (mm/dd/yy)	Rupture Length (km)	Segments Ruptured	Displacement (m)		Rupture Through (Y/N)	Separation and Overlap (Pull-Apart Basin Dimensions)			Reference	Comments
					At Basin	Maximum*		Length (km)	Width (km)	Area (km_2)		
7a	North Anatolian fault, Turkey Erzincan	Erzincan M_s 7.9 12/26/1939	360.0	2	2.5 0	6–8 max. 2.5 avg.	N	20	5	100	Barka (1997), Barka *et al.* (1988)	Primary right lateral; 1 step restraining-not measured; Susehri is a double bend, not measured; rupture from east to west
7b	North Anatolian fault, Turkey Niksar				3.7 0		N	12	10	120		
8a	Imperial fault California	Imperial Valley *M* 7.1 5/18/1940	60	2	1–1.5	5.2	N	9	8–12	90	Wells and Coppersmith (1994)	Northern termination at step-over to San Andreas fault; southern termination at step-over to Cervo Prieto fault
8b	Imperial fault California				1–1.5		N	—	12			
9	North Anatolian fault Turkey	Erba M_s 7.1 12/20/1942	47–60	1	1.8 0	1.8	N	~5	1.5	7.5	Hempton and Dunne (1984), Aydin and Nur (1982), Barka (1996), Wells *et al.* (1994)	Primary right lateral; basin is a lazy z shape, in an oblique orientation to master faults; east end termination not at segment boundary; epicenter near Erbaa
10a	North Anatolian fault, Turkey Ladik	Kastamanu (Ladik Tosya) *M* 7.3 8/16/1943					Y	5	2	10	Barka (1996), Barka *et al.* (1988)	Rupture from east to west
10b	North Anatolian fault, Turkey Kamil				1.60		Y	4	1.5	6		
10c	North Anatolian fault, Turkey Kargil		360	4		6 2.5 avg.	Y	3	1.5	4.5		
10d	North Anatolian fault, Turkey Kirkpinar						Y	2	0.5	1		
10e	North Anatolian fault, Turkey Bayramoren						Y	1.5	1.5	2.25		
11a	North Anatolian fault, Ismetpasa Turkey	Bolu–Gerode M_s 7.5 2/1/1944					Y	2.5	1.5	3.75	Barka (1996), Wells and Coppersmith (1994)	Rupture from east to west; epicenter north of Kursunlu.
11b	North Anatolian fault, Yenicaga Turkey		150	3		4.5 2 avg.	Y	3	2	6		
11c	North Anatolian fault, Turkey				1.0 0.5		N	15	5	75		
12	San Miguel fault	San Miguel *M* 6.8 2/9/1958	20.0	1		0.9 0.5 avg.	N	2.8	1.4	4	Brune and Simons (1979)	Right lateral

ID	Fault Name; Country; Pull-Apart Basin	Name of EQ; Magnitude; Event Date (mm/dd/yy)	Rupture Length (km)	Segments Ruptured	Displacement (m)		Rupture Through (Y/N)	Separation and Overlap (Pull-Apart Basin Dimensions)			Reference	Comments
					At Basin	Maximum*		Length (km)	Width (km)	Area (km_2)		
13	North Anatolian fault (southern strand) Turkey	Abant M_s 7.0 5/26/1957	40.0	1		1.65 0.55 avg.	N	1	1.5	1.5	Barka *et al.* (1988), Wells and Coppersmith (1994), Kneupfer (1989)	West end of rupture at restraining bend, not measured
14	San Andreas fault California, USA	Parkfield *M* 5.5 6/28/1986	35	2		0.10	Y	−1.25	1	1.3	Knuepfer (1989), Scholz (1990)	Ruptured from north to south; Scholz noted the rupture did not extend beyond step-over
15a	Tuleet Uul fault Mongolia Huljiyn Basin	Mogod M_w 7.4 1/5 & 20 1967	36		1.35	3.50	N	15	4	60	Baljinnyam *et al.* (1993)	Right lateral, with thrust faulting to the south and normal faulting to the north
15b	Tuleet Uul fault Mongolia				1.50		Y	1.5	0.75	1.12		
16	North Anatolian fault, Turkey Mudumu Valley	Mudumu M_s 7.1 7/22/1967	80–106	1		1.9	N	8	5.3	42.4	Pinar and Honkura (1996), Barka (1996)	1–3-km wide shear zone; east end did not terminate at segment boundary
17a	Dasht-e-Bayaz Iran	Dasht-e-Bayaz *M* 7.2 8/31/1968	80		3 2.5	5.2 2.3 avg.	Y	1.7	1.5	2.5	Tchalenko and Ambraseys (1970), Wells and Coppersmith (1994)	Left lateral
17b					0.20		Y	0.75	1	0.75		
18a	Qujang fault China	Tonghai *M* 7.5 1970	48	5±		2.7	Y	5	0.4	0.60	Zhou *et al.* (1983)	
18b	Qujang fault China						Y	1–2	0.3	0.36		
19	East Anatolian fault Turkey	Bingol M_s 6.7 5/22/1971	39	1		0.6 0.25 avg.	N	3	12.5	37.5	Barka *et al.* (1988), Knuepfer (1989), Wells and Coppersmith (1994)	Rupture propagated west from triple junction
20	Lake Managua Nicaragua	Managua *M* 6.2 12/23/1972	15	4	0.33	0.35	N	−9	~0.75	6.75	Brown *et al.* (1972), Wells and Coppersmith (1994)	Left lateral
21a	Calidran fault Turkey	Calidran M_s 7.3 11/24/76					Y	0.6	0.75	0.45	Barka *et al.* (1988), Knuepfer (1989), Wells and Coppersmith (1994)	Bilateral faulting

ID	Fault Name; Country; Pull-Apart Basin	Name of EQ; Magnitude; Event Date (mm/dd/yy)	Rupture Length (km)	Segments Ruptured	Displacement (m)		Rupture Through (Y/N)	Separation and Overlap (Pull-Apart Basin Dimensions)			Reference	Comments
					At Basin	Maximum*		Length (km)	Width (km)	Area (km_2)		
21b	Calidran fault Turkey		55	4		3.5 2.05 avg.	Y	3	1.5	4.5		
21c	Calidran fault Turkey						Y	0.75	0.4	0.34		
21d	Calidran fault Turkey						N	5	10	50		
22	Imperial fault California, USA	Imperial Valley *M* 7.1 10/15/1979	30.5	2		0.8 0.15 avg.	N	−9	10–14	108	Johnson and Hill (1982), Wells and Coppersmith (1994)	North termination at step-over to San Andreas fault
23a	Gowk fault southern Iran	Golba *M* 6.7 6/11/1981	16	2	0.04	0.11	N	10	3	30	Knuepfer (1989), Wells and Coppersmith (1994)	Right-lateral fault with large component of thrust (dominantly compressional)
23b	Gowk fault southern Iran						Y	3	1.5	4.5		
24a	Gowk fault northern Iran	Sirch *M* 7.1 7/28/1981	65	3		0.5	Y	2.5	1	2.5	Knuepfer (1989), Wells and Coppersmith (1994)	Primary component of thrust faulting (dominantly compressional); rupture did not terminate at segment boundary
24b	Gowk fault northern Iran						Y	3.5	2	7		
24c	Gowk fault northern Iran						Y	0.5	1	0.5		
25a	Superstition Hills California, USA Old Lake Coahuila	Superstition Hills M_s 6.6 11/24/1987	30	3	0.35 0.23		Y	3	0.2	0.6	Rymer (1989), Hwang *et al.* (1990)	(a) North Strand–Imler (b) Imler–Wienert Ruptures to the southeast
25b	Superstition Hills California, USA				0.25 0.2	0.96	Y	3	1	3		
26	North Anatolian fault, Turkey Erzincan	Erzincan *M* 6.8 3/13/1992	16–20	1	0.10–1.0	1.0 (at depth)	N	20	5	100	Hempton and Dunne (1984), Bernard *et al.* (1997)	Primary right lateral; rhomboidal shape basin; rupture terminated at basin
27a	Landers, Homestead California, USA	Landers M_w 7.3 6/28/1992	85	5	2–3		Y	10	1–3	10–30	Sowers *et al.* (1994), McGill and Rubin (1999)	Ruptured to the northwest (a) Johnson–Homestead (via the Kickapoo fault) (b) Homestead–Camprock; not a segment boundary at endpoints
27b	Homestead, Emerson California, USA				2–3	1.5–5.3	Y	~9	2–3	18–27		
28	Suma, Suqayama, Gosukebashi Japan basin offshore	Hyogu-ken Nanbu (Kobe) *M* 7.2 1/17/1995	30–50		0.26	1.8	Y	5	2	10	Holzer (1996), Sekiguchi *et al.* (2000)	Right lateral fault; bilateral rupture

ID	Fault Name; Country; Pull-Apart Basin	Name of EQ; Magnitude; Event Date (mm/dd/yy)	Rupture Length (km)	Segments Ruptured	Displacement (m)		Rupture Through (Y/N)	Separation and Overlap (Pull-Apart Basin Dimensions)			Reference	Comments
					At Basin	Maximum*		Length (km)	Width (km)	Area (km_2)		
29a	Abiz fault eastern Iran Zirchuh Plain	Zirkuh (Qa'enat) M_w 7.2 5/10/1997			1.4 1.9		Y	6	1.6	9.6	Berberian *et al.* (1999)	Sistan right-lateral suture zone; north end is in proximity of the east west fault zone; ruptured from north to south; multiple segments, with some left steps noted
29b	Abiz fault eastern Iran		125	zone	0.5 0.25	2 avg.	Y	3	1.5	4.5		
29c	Abiz fault eastern Iran				0.25 0		N	7	6	42		
30a	North Anatolian fault, Turkey Karamursel	Izmit (Kocaeli) M_w 7.4 8/17/1999	126	4	3–5 avg. (offshore)	5.5	N	16–19 (17.5 avg.)	4–5 (4.5 avg.)	80–95 (87.5 avg.)	Toksöz *et al.* (1999), Lettis *et al.* (2000)	Refer to this article for details regarding fault rupture, segmentation and step-over geometries
30b	North Anatolian fault, Turkey Gölcük				3–5 avg.	5.5	Y	7.5	1–2 (1.5 avg.)	7.5–15 (11.25 avg.)		
30c	North Anatolian fault, Turkey Lake Sapanca				2–3 avg.	3.3	Y	9	1–2 (1.5 avg.)	9–18 (13.5 avg.)		
30d	North Anatolian fault, Turkey Eften Lake				1–1.5	1.5	N	10	2–4 (3 avg.)	20–40 (30 avg.)		

Table A2: shows surface attributes and observations from historical earthquake ruptures from 1857 – 2002 (Source: Wesnousky, 2008).

Date (mm/dd/yyyy)	Location	Number	Type*	Length (km)‡	$S^{\dagger}$(Average Net Slip) (m)	S^{max} Max Slip (m)	Depth (km)	Rigidity μ (10^{11} dyne cm^2)	M_0^G(10^{26} dyne cm)	P_0^G(10^{15} cm^3)	M_w^G	Reference§	Notes‖
01/09/1857	San Andreas, CA	1	SSR	360	4.7	9.1 (12)	15	3	76	25.4	7.9	1	a
05/03/1887	Sonora, MX	2	N/60	70	2.2	4.1	15	3	8.0	2.7	7.2	2, 3, 48	b
10/28/1891	Neo-Dani, Japan	3	SSL	80	3.1	7.9	15	3	11.3	3.8	7.3	4	c
08/31/1896	Rikuu, Japan	4	R/45	37	2.5 (3.5)	6.2 (8.8)	15	3.0	8.2	2.7	7.2	5	d
10/02/1915	Pleasant Valley, NV	5	N/45	61	1.8 (2.6)	5.8 (8.2)	15	3.1	10.3	3.4	7.3	6	e
11/02/1930	Kita-Izu, Japan	6	SSL	35	1.1	3.5	12	3.3	1.6	0.48	6.7	7	f
12/25/1939	Erzincan, Turkey	7	SSR	300	4.2	7.4	13	3.2	52.5	16.4	7.7	8	g
05/19/1940	Imperial, CA	8	SSR	60	1.6	3.3	13	2.5	3.0	1.2	6.9	9	h
12/20/1942	Erbaa-Niksar, Turkey	9	SSR	28	1.66	1.9	13	3.2	1.8	0.6	6.8	8	I
11/26/1943	Tosya, Turkey	10	SSR	275	2.5	4.4	13	3.2	28.7	9.0	7.6	8	j
09/10/1943	Tottori, Japan	11	SSL	10.5	0.6	1.5	15	3.3	0.3	0.09	6.3	10	k
02/01/1944	Gerede-Bolu, Turkey	12	SSR	155	2.1	3.5	13	3.2	13.3	4.2	7.35	8	l
01/31/1945	Mikawa, Japan	13	R/30	4.0	1.3	2.1	8	3.0	0.24	.08	6.2	11	m
12/16/1954	Fairview Peak, NV	15	NSSR/60	62	1.1	5.2	15	3.0	3.5	1.2	7.0	13	n
12/16/1954	Dixie Valley, NV	16	N/60	47	0.8 (0.9)	3.1 (3.5)	12	3.0	1.76	0.6	6.8	13	t
08/18/1959	Hebgen Lake, MT	14	N/50	25	2.5	5.4	15	3.0	3.7	1.25	7.0	12	s
07/22/1967	Mudurnu, Turkey	17	SSR	60	0.9	2.0	12	2.4	1.6	0.65	6.7	8	u
04/08/1968	Borrego Mtn, CA	18	SSR	31	0.13	0.4	12	3.3	0.16	0.05	6.1	14	v
02/09/1971	San Fernando, CA	19	R/45	15	0.95	2.5	15	3.4	1.0	0.30	6.7	59	ap
06/02/1979	Cadoux, Australia	20	R/35	10	0.6	1.2	6	3.2	0.20	0.06	6.1	49	x
10/15/1979	Imperial Valley, CA	21	SSR	36	0.28–0.41	0.6–0.78	13	2.5	0.33–0.48	0.13–0.19	6.3–6.4	15, 16	w
10/10/1980	El Asnam, Algeria	22	R/50	27.3	1.2	6.5	12	3.0	1.55	0.5	6.7	60	aq
07/29/1981	Sirch, Iran	23	SS/69	64	0.13	0.50	15	3.3	0.43	0.13	6.4	50	aj
10/28/1983	Borah Peak, ID	24	N/45	34	.94 (1.3)	2.8 (4.0)	14	3.2	2.9	0.89	6.9	17	y
03/03/1986	Marryat, Australia	25	R/35	13	0.24 (sec) (0.42)	0.70 (sec) (1.2)	3	3.2	0.09 (sec)	0.03 (sec)	5.9 (sec)	46	z
					0.26*u* (0.46)	0.8*u* (1.4)			0.10*u*	0.03*u*	5.9*u*		
03/02/1987	Edgecumbe, NZ	27	N/60	15.5	0.6 (0.7)	2.6 (3.0)	10	2.6	0.33	0.13	6.3	19	ao
11/23/1987	Super. Hills, CA	26	SSR	25	0.3–0.6	0.5–1.1	12	2.5	0.22–0.47	.09–.19	6.2–6.4	18	aa
01/22/1988	Tennant Crk, Australia	28	R/45	30	0.7 (1.0)	1.8 (2.5)	8	3.3	1.1	0.34	6.6	43	ab
07/16/1990	Luzon, Philippines	29	SSL	112	3.5	6.2	20	3.5	27.4	7.84	7.6	20, 21	am
06/28/1992	Landers, CA	30	SSR	77	2.3	6.7	15	3.0	8.1	2.7	7.2	22	ac
03/14/1998	Fandoqa, Iran	31	SSN/54	25	1.1	3.1	10	3.3	1.2	0.36	6.6	50	ag
08/17/1999	Izmit, Turkey	34	SSR	107 (145)	1.1	5.1	13	3.2	4.9	1.5	7.1	47	ae
09/21/1999	Chi-Chi, Taiwan	32	R/70	72	3.5 (4.0)	12.7 (16.4)	20	3.0	18.4	6.1	7.4	23	ad
10/16/1999	Hector Mine, CA	33	SSR	44	1.56	5.2	12	3.0	2.5	0.82	6.9	57	an
11/12/1999	Duzce, Turkey	35	SSR	40	2.1	5.0	13	3.2	3.5	1.1	7.0	24	af
11/14/2001	Kunlun, China	36	SSL	421	3.3	8.7	15	3.0	62.5	20.8	7.8	53	am
11/14/2001 (spot)	Kunlun, China	36a	SSL	428	2.4	8.3	15	3.0	46.8	15.6.	7.8	61	al
11/03/2002	Denali, AK	37	SSR	302	3.6	8.9	15	3.2	51.6	16.1	7.7	52	ak

TELEGRAPH ROAD

Point	Date	Bearing (D,M,S)			Distance (m)	X	Y	Correction of angle
RN 2	9 Sep 10	186	03	50	20.879	0.000	-20.879	6.0639
RN 3	9 Sep 10	186	01	45	40.702	0.000	-40.702	6.0292
RN 4	9 Sep 10	186	03	45	62.121	0.000	-62.121	3.0625
RN 5	9 Sep 10	186	02	00	82.975	0.000	-82.975	6.0333
RN 6	9 Sep 10	186	03	55	104.175	0.000	-104.175	6.0653
RN 7	9 Sep 10	186	07	00	124.369	0.000	-124.369	6.1167
RN 8	9 Sep 10	186	09	10	143.885	0.000	-143.885	6.1528
RN 9	9 Sep 10	187	01	20	191.937	0.000	-191.937	7.0222
RN 10	9 Sep 10	186	54	50	212.261	0.000	-212.261	6.9139
RN 11	9 Sep 10	186	53	25	232.610	0.000	-232.610	6.8903
RN 12	9 Sep 10	186	49	10	252.650	0.000	-252.650	6.8194
RN 13	9 Sep 10	186	45	55	271.220	0.000	-271.220	6.7653
RN 14	9 Sep 10	186	42	20	290.507	0.000	-290.507	6.7056
RN 15	9 Sep 10	186	39	40	309.085	0.000	-309.085	6.6611
RN 2	13 Sep 10	186	03	25	20.882	0.003	-20.882	
RN 3	13 Sep 10	186	01	30	40.707	0.003	-40.707	
RN 4	13 Sep 10	186	03	25	62.116	0.006	-62.116	
RN 5	13 Sep 10	186	01	45	82.975	0.006	-82.975	
RN 6	13 Sep 10	186	03	40	104.189	0.008	-104.189	
RN 7	13 Sep 10	186	06	45	124.377	0.009	-124.377	
RN 8	13 Sep 10	186	08	50	143.894	0.014	-143.894	
RN 9	13 Sep 10	187	01	05	191.932	0.014	-191.932	
RN 10	13 Sep 10	186	54	40	212.260	0.010	-212.260	
RN 11	13 Sep 10	186	53	20	232.616	0.006	-232.616	
RN 12	13 Sep 10	186	49	00	252.640	0.012	-252.640	
RN 13	13 Sep 10	186	45	45	271.218	0.013	-271.218	
RN 14	13 Sep 10	186	42	15	290.498	0.007	-290.498	
RN 15	13 Sep 10	186	39	20	309.081	0.030	-309.081	
RN 2	18 Sep 10	186	01	50	20.880	0.012	-20.880	
RN 3	18 Sep 10	186	01	10	40.722	0.007	-40.722	
RN 4	18 Sep 10	186	03	10	62.133	0.011	-62.133	
RN 5	18 Sep 10	186	01	45	82.966	0.006	-82.966	
RN 6	18 Sep 10	186	03	35	104.178	0.010	-104.178	
RN 7	18 Sep 10	186	06	20	124.373	0.024	-124.373	
RN 8	18 Sep 10	186	08	30	143.897	0.028	-143.897	
RN 9	18 Sep 10	187	00	55	191.951	0.023	-191.951	
RN 10	18 Sep 10	186	54	25	212.272	0.026	-212.272	
RN 11	18 Sep 10	186	53	00	232.624	0.028	-232.624	
RN 12	18 Sep 10	186	48	55	252.646	0.018	-252.646	

RN 13	18 Sep 10	186	45	35	271.216	0.026	-271.216
RN 14	18 Sep 10	186	42	10	290.480	0.014	-290.480
RN 15	18 Sep 10	186	39	05	309.069	0.052	-309.069
RN 2	13 Oct 10	186	03	00	20.875	0.005	-20.875
RN 3	13 Oct 10	186	02	00	40.698	-0.003	-40.698
RN 4	13 Oct 10	186	03	15	62.110	0.009	-62.110
RN 5	13 Oct 10	186	02	05	82.960	-0.002	-82.960
RN 6	13 Oct 10	186	04	05	104.165	-0.005	-104.165
RN 7	13 Oct 10	186	07	05	124.366	-0.003	-124.366
RN 8	13 Oct 10	could	not	find			
RN 9	13 Oct 10	187	01	30	191.929	-0.009	-191.929
RN 10	13 Oct 10	186	55	15	212.255	-0.026	-212.255
RN 11	13 Oct 10	186	53	45	232.602	-0.023	-232.602
RN 12	13 Oct 10	186	49	30	252.626	-0.024	-252.626
RN 13	13 Oct 10	186	46	20	271.207	-0.033	-271.207
RN 14	13 Oct 10	186	43	00	290.480	-0.056	-290.480
RN 15	13 Oct 10	186	40	05	309.074	-0.037	-309.074
RN 2	1 Jul 11	186	01	06	20.860	0.017	-20.860
RN 3	1 Jul 11	186	00	30	40.706	0.015	-40.706
RN 4	1 Jul 11	186	02	42	62.107	0.019	-62.107
RN 5	1 Jul 11	186	01	20	82.952	0.016	-82.952
RN 6	1 Jul 11	could	not	find			
RN 7	1 Jul 11	could	not	find			
RN 8	1 Jul 11	could	not	find			
RN 9	1 Jul 11	could	not	find			
RN 10	1 Jul 11	could	not	find			
RN 11	1 Jul 11	186	52	38	232.591	0.053	-232.591
RN 12	1 Jul 11	186	48	24	252.605	0.056	-252.605
RN 13	1 Jul 11	186	45	07	271.191	0.063	-271.191
RN 14	1 Jul 11	186	41	42	290.453	0.054	-290.453
RN 15	1 Jul 11	186	38	39	309.054	0.091	-309.054

HIGHFIELD ROAD

Point	*Date*	*Bearing (D,M,S)*			*Distance (m)*	*X*	*Y*	Correction of Angle
RN 2	9 Sep 10	184	29	00	19.446	0.000	-19.446	4.4833
RN 3	9 Sep 10	184	45	05	52.062	0.000	-52.062	4.7514
RN 4	9 Sep 10	184	35	05	71.777	0.000	-71.777	4.5847
RN 5	9 Sep 10	184	40	55	91.496	0.000	-91.496	4.6819
RN 6	9 Sep 10	185	47	30	182.927	0.000	-182.927	5.7917
RN 7	9 Sep 10	185	43	05	194.424	0.000	-194.424	5.7181
RN 8	9 Sep 10	185	39	25	214.055	0.000	-214.055	5.6569
RN 9	9 Sep 10	185	35	40	234.610	0.000	-234.610	5.5944
RN 10	9 Sep 10	185	32	10	254.632	0.000	-254.632	5.5361
RN 11	9 Sep 10	185	29	05	274.255	0.000	-274.255	5.4847
RN 12	9 Sep 10	185	28	00	294.572	0.000	-294.572	5.4667
RN 13	9 Sep 10	185	26	15	314.571	0.000	-314.571	5.4375
RN 2	13 Sep 10	184	26	45	19.448	0.013	-19.448	
RN 3	13 Sep 10	184	44	45	52.057	0.005	-52.057	
RN 4	13 Sep 10	184	34	30	71.755	0.012	-71.755	
RN 5	13 Sep 10	184	40	25	91.490	0.013	-91.490	
RN 6	13 Sep 10	185	46	50	182.923	0.035	-182.923	
RN 7	13 Sep 10	185	42	30	194.412	0.033	-194.412	
RN 8	13 Sep 10	185	38	50	214.052	0.036	-214.052	
RN 9	13 Sep 10	185	35	05	234.606	0.040	-234.606	
RN 10	13 Sep 10	185	32	20	254.633	-0.012	-254.633	
RN 11	13 Sep 10	185	28	30	274.240	0.047	-274.240	
RN 12	13 Sep 10	185	27	20	294.556	0.057	-294.556	
RN 13	13 Sep 10	185	25	35	314.555	0.061	-314.555	
RN 2	18 Sep 10	184	28	45	19.440	0.001	-19.440	
RN 3	18 Sep 10	184	45	20	52.073	-0.004	-52.073	
RN 4	18 Sep 10	184	34	40	71.774	0.009	-71.774	
RN 5	18 Sep 10	184	40	40	91.503	0.007	-91.503	
RN 6	18 Sep 10	185	47	10	182.913	0.018	-182.913	
RN 7	18 Sep 10	185	42	50	194.417	0.014	-194.417	
RN 8	18 Sep 10	185	39	25	214.052	0.000	-214.052	
RN 9	18 Sep 10	185	35	35	234.597	0.006	-234.597	
RN 10	18 Sep 10	185	33	00	254.629	-0.062	-254.629	
RN 11	18 Sep 10	185	28	50	274.234	0.020	-274.234	
RN 12	18 Sep 10	185	27	55	294.555	0.007	-294.555	
RN 13	18 Sep 10	185	26	10	314.560	0.008	-314.560	
RN 2	13 Oct 10	184	26	30	19.444	0.014	-19.444	

RN 3	13 Oct 10	184	44	45	52.052	0.005	-52.052
RN 4	13 Oct 10	184	34	30	71.762	0.012	-71.762
RN 5	13 Oct 10	could	not	find			
RN 6	13 Oct 10	185	47	05	182.909	0.022	-182.909
RN 7	13 Oct 10	185	42	50	194.410	0.014	-194.410
RN 8	13 Oct 10	185	38	55	214.047	0.031	-214.047
RN 9	13 Oct 10	185	35	15	234.594	0.028	-234.594
RN 10	13 Oct 10	185	32	35	254.625	-0.031	-254.625
RN 11	13 Oct 10	185	28	30	274.244	0.047	-274.244
RN 12	13 Oct 10	185	27	35	294.547	0.036	-294.547
RN 13	13 Oct 10	185	26	00	314.570	0.023	-314.570

KIVERS ROAD

Point	*Date*	*Bearing (D,M,S)*			*Distance (m)*	*X*	*Y*	Correction of Angle
RN 2	10 Sep 10	186	29	00	19.304	0.000	-19.304	6.4833
RN 3	10 Sep 10	186	27	15	55.282	0.000	-55.282	6.4542
RN 4	10 Sep 10	186	31	10	74.376	0.000	-74.376	6.5194
RN 5	10 Sep 10	186	32	15	91.691	0.000	-91.691	6.5375
RN 6	10 Sep 10	187	24	30	167.887	0.000	-167.887	7.4083
RN 7	10 Sep 10	187	19	05	187.282	0.000	-187.282	7.3181
RN 8	10 Sep 10	187	15	35	205.646	0.000	-205.646	7.2597
RN 9	10 Sep 10	187	11	05	224.812	0.000	-224.812	7.1847
RN 10	10 Sep 10	187	09	15	243.948	0.000	-243.948	7.1542
RN 11	10 Sep 10	187	05	55	263.219	0.000	-263.219	7.0986
RN 2	13 Sep 10	186	28	40	19.316	0.002	-19.316	
RN 3	13 Sep 10	186	27	15	55.274	0.000	-55.274	
RN 4	13 Sep 10	186	31	05	74.377	0.002	-74.377	
RN 5	13 Sep 10	186	32	15	91.700	0.000	-91.700	
RN 6	13 Sep 10	187	24	15	167.893	0.012	-167.893	
RN 7	13 Sep 10	187	18	50	187.299	0.014	-187.299	
RN 8	13 Sep 10	could	not	find				
RN 9	13 Sep 10	187	10	45	224.819	0.022	-224.819	
RN 10	13 Sep 10	187	08	50	243.962	0.030	-243.962	
RN 11	13 Sep 10	187	05	15	263.224	0.051	-263.224	
RN 2	18 Sep 10	186	28	55	19.316	0.000	-19.316	
RN 3	18 Sep 10	186	27	45	55.275	-0.008	-55.275	
RN 4	18 Sep 10	186	31	00	74.370	0.004	-74.370	
RN 5	18 Sep 10	186	32	15	91.690	0.000	-91.690	
RN 6	18 Sep 10	187	24	25	167.884	0.004	-167.884	
RN 7	18 Sep 10	187	19	00	187.274	0.005	-187.274	
RN 8	18 Sep 10	187	15	20	205.634	0.015	-205.634	

RN 9	18 Sep 10	187	11	00	224.790	0.005	-224.790
RN 10	18 Sep 10	187	09	05	243.941	0.012	-243.941
RN 11	18 Sep 10	187	05	40	263.204	0.019	-263.204
RN 2	13 Oct 10	186	28	45	19.319	0.001	-19.319
RN 3	13 Oct 10	186	27	35	55.294	-0.005	-55.294
RN 4	13 Oct 10	186	30	05	74.371	0.023	-74.371
RN 5	13 Oct 10	186	31	45	91.707	0.013	-91.707
RN 6	13 Oct 10	187	24	30	167.902	0.000	-167.902
RN 7	13 Oct 10	187	19	15	187.279	-0.009	-187.279
RN 8	13 Oct 10	187	15	15	205.659	0.020	-205.659
RN 9	13 Oct 10	187	11	15	224.819	-0.011	-224.819
RN 10	13 Oct 10	187	09	05	243.963	0.012	-243.963
RN 11	13 Oct 10	187	05	40	263.228	0.019	-263.228
RN 2	1 Jul 11	186	28	17	19.316	0.004	-19.316
RN 3	1 Jul 11	186	27	51	55.293	-0.010	-55.293
RN 4	1 Jul 11	186	30	42	74.366	0.010	-74.366
RN 5	1 Jul 11						
RN 6	1 Jul 11						
RN 7	1 Jul 11	187	19	09	187.300	-0.004	-187.300
RN 8	1 Jul 11	187	15	26	205.653	0.009	-205.653
RN 9	1 Jul 11	187	10	58	224.824	0.008	-224.824
RN 10	1 Jul 11	187	08	58	243.955	0.020	-243.955
RN 11	1 Jul 11	187	05	27	263.220	0.036	-263.220

KERRS ROAD

Point	*Date*	*Bearing (D,M,S)*			*Distance (m)*	*X*	*Y*	**Correction of Angle**
RN 2	10 Sep 10	258	30	00	20.441	0.000	-20.441	78.5000
RN 3	10 Sep 10	258	17	25	43.514	0.000	-43.514	78.2903
RN 4	10 Sep 10	258	16	15	73.280	0.000	-73.280	78.2708
RN 5	10 Sep 10	258	19	25	104.012	0.000	-104.012	78.3236
RN 6	10 Sep 10	258	26	40	135.664	0.000	-135.664	78.4444
RN 7	10 Sep 10	258	32	25	166.855	0.000	-166.855	78.5403
RN 8	10 Sep 10	258	37	05	199.149	0.000	-199.149	78.6181
RN 2	13 Sep 10	258	29	40	20.423	0.002	-20.423	
RN 3	13 Sep 10	258	17	15	43.519	0.002	-43.519	
RN 4	13 Sep 10	258	16	30	73.286	-0.005	-73.286	
RN 5	13 Sep 10	258	19	40	104.019	-0.008	-104.019	
RN 6	13 Sep 10	258	27	00	135.674	-0.013	-135.674	
RN 7	13 Sep 10	258	32	50	166.871	-0.020	-166.871	

RN 8	13 Sep 10	258	37	20	199.153	-0.014	-199.153
RN 2	19 Sep 10	258	29	20	20.427	0.004	-20.427
RN 3	19 Sep 10	258	16	50	43.516	0.007	-43.516
RN 4	19 Sep 10	258	16	05	73.277	0.004	-73.277
RN 5	19 Sep 10	258	19	05	104.013	0.010	-104.013
RN 6	19 Sep 10	258	26	50	135.664	-0.007	-135.664
RN 7	19 Sep 10	258	32	35	166.856	-0.008	-166.856
RN 8	19 Sep 10	258	36	53	199.154	0.012	-199.154
RN 2	13 Oct 10	258	29	50	20.420	0.001	-20.420
RN 3	13 Oct 10	258	17	10	43.518	0.003	-43.518
RN 4	13 Oct 10	258	15	55	73.282	0.007	-73.282
RN 5	13 Oct 10	258	19	25	104.015	0.000	-104.015
RN 6	13 Oct 10	258	26	55	135.673	-0.010	-135.673
RN 7	13 Oct 10	258	32	45	166.870	-0.016	-166.870
RN 8	13 Oct 10	258	37	15	199.156	-0.010	-199.156
RN 2	1 Jul 11	258	29	37	20.441	0.002	-20.441
RN 3	1 Jul 11	258	17	21	43.512	0.001	-43.512
RN 4	1 Jul 11	258	16	00	73.291	0.005	-73.291
RN 5	1 Jul 11						
RN 6	1 Jul 11						
RN 7	1 Jul 11						
RN 8	1 Jul 11	258	37	23	199.158	-0.017	-199.158

RAILWAY ROAD

Point	***Date***	***Bearing (D,M,S)***			***Distance (m)***	***X***	***Y***	**Correction of Angle**
RN A	10 Sep 10	61	29	05	126.879	0.000	-126.879	-118.5153
RN B	10 Sep 10	70	26	10	127.619	0.000	-127.619	-109.5639
RN C	10 Sep 10	77	39	45	130.533	0.000	-130.533	-102.3375
RN D	10 Sep 10	85	54	00	136.696	0.000	-136.696	-94.1000
RN E	10 Sep 10	93	30	25	144.119	0.000	-144.119	-86.4931
RN F	10 Sep 10	100	17	35	154.081	0.000	-154.081	-79.7069
RN A	13 Sep 10	61	30	05	126.871	-0.037	-126.871	
RN B	13 Sep 10	70	27	30	127.611	-0.049	-127.611	
RN C	13 Sep 10	77	41	05	130.526	-0.051	-130.526	
RN D	13 Sep 10	85	55	20	136.691	-0.053	-136.691	
RN E	13 Sep 10	93	31	55	144.109	-0.063	-144.109	

RN F	13 Sep 10	Did	not	find			

RN A	19 Sep 10	61	29	55	126.873	-0.031	-126.873
RN B	19 Sep 10	70	26	50	127.617	-0.025	-127.617
RN C	19 Sep 10	77	40	25	130.527	-0.025	-130.527
RN D	19 Sep 10	85	54	54	136.694	-0.036	-136.694
RN E	19 Sep 10	93	31	30	144.113	-0.045	-144.113
RN F	19 Sep 10	100	18	35	154.080	-0.045	-154.080

RN A	13 Oct 10	61	30	20	126.867	-0.046	-126.867
RN B	13 Oct 10	70	27	50	127.611	-0.062	-127.611
RN C	13 Oct 10	77	41	25	130.525	-0.063	-130.525
RN D	13 Oct 10	85	55	30	136.691	-0.060	-136.691
RN E	13 Oct 10	93	31	50	144.113	-0.059	-144.113
RN F	13 Oct 10	100	19	30	154.077	-0.086	-154.077

RN A	1 Jul 11	61	30	24	126.875	-0.049	-126.875
RN B	1 Jul 11	70	27	38	127.617	-0.054	-127.617
RN C	1 Jul 11	77	41	10	130.544	-0.054	-130.544
RN D	1 Jul 11	85	55	17	136.713	-0.051	-136.713
RN E	1 Jul 11	93	32	24	144.159	-0.083	-144.159
RN F	1 Jul 11	100	19	40	154.128	-0.093	-154.128

Table 16: Earthquakes within the vicinity of Greendale Fault > Mag 4 from the survey period 9th to 13th September 2010 (Source: data courtesy of Geonet - http://magma.geonet.org.nz/resources/quakesearch/).

Earthquakes (> Mw 4) During Survey Period 9th to 13th September									
NUMBER	**ORI_DAY**	**TIME**	**MAG**	**DEPTH**	**LAT**	**LONG**	**NZMGE**	**NZMGN**	**CUSP_ID**
1	9-Sep-10	0:38	4.104	11.1123	-43.3248	171.8959	2420473	5764335	3369269
2	9-Sep-10	6:27	4.071	7.2129	-43.5889	172.5845	2476468	5735495	3369391
3	9-Sep-10	12:25	4.275	8.5696	-43.579	172.4004	2461588	5736507	3369525
4	9-Sep-10	19:10	4.444	9.0165	-43.5755	172.3992	2461487	5736901	3369682
5	10-Sep-10	10:04	4.244	10.9045	-43.6114	172.4207	2463251	5732920	3370029
6	10-Sep-10	20:36	4.188	7.0916	-43.6196	172.4583	2466294	5732032	3370255
7	10-Sep-10	21:01	4.057	6.9564	-43.4698	172.1114	2438120	5748437	3370260
8	11-Sep-10	18:03	4.614	9.7135	-43.6408	172.3925	2460999	5729634	3370677
9	11-Sep-10	23:39	4.111	10.3699	-43.5361	171.8751	2419101	5740837	3370794
10	12-Sep-10	5:27	4.483	8.2252	-43.5759	172.3886	2460638	5736850	3370916
11	12-Sep-10	19:54	4.085	6.649	-43.6074	172.4952	2469270	5733401	3371231
12	12-Sep-10	21:05	4.148	7.0821	-43.5433	172.191	2444643	5740329	3371253
13	13-Sep-10	1:05	4.148	15.7226	-43.5339	172.5354	2472463	5741582	3371335
14	13-Sep-10	9:15	4.007	7.9247	-43.5683	172.1476	2441163	5737523	3371514

Table 17: Earthquakes within the vicinity of Greendale Fault > Mag 4 from the survey period 13th to 18th September 2010 (Source: data courtesy of Geonet - http://magma.geonet.org.nz/resources/quakesearch/).

Earthquakes (> Mw 4) During Survey Period 13th to 18th September

NUMBER	ORI_DAY	TIME	MAG	DEPTH	LAT	LONG	NZMGE	NZMGN	CUSP_ID
1	13-Sep-10	21:12	4.29	9.9226	-43.5978	172.3349	2456319	5734377	3371762
2	13-Sep-10	23:40	4.271	9.3211	-43.596	172.3368	2456466	5734575	3371814
3	14-Sep-10	12:36	4.363	7.335	-43.5734	172.3964	2461265	5737122	3372087
4	15-Sep-10	8:30	4.058	9.2431	-43.5642	172.0539	2433582	5737894	3372516
5	15-Sep-10	10:42	4.313	9.6734	-43.5797	172.5217	2471389	5736493	3372561
6	15-Sep-10	15:13	4.486	9.0591	-43.6275	172.497	2469422	5731168	3372661
7	15-Sep-10	16:35	4.228	9.1425	-43.6258	172.4981	2469509	5731359	3372691
8	16-Sep-10	5:53	4.193	9.3978	-43.6003	172.3484	2457412	5734106	3372984
9	16-Sep-10	10:36	4.11	10.1353	-43.5381	172.4511	2465655	5741085	3373082
10	16-Sep-10	10:58	4.306	8.2178	-43.6237	172.4839	2468363	5731581	3373091
11	16-Sep-10	12:08	4.462	7.8975	-43.5296	171.93	2423528	5741616	3373119
12	17-Sep-10	13:37	4.445	6.6793	-43.4593	172.1606	2442087	5749637	3373723
13	17-Sep-10	22:03	4.564	9.6229	-43.5873	172.3937	2461058	5735585	3373925

Table 18: Earthquakes within the vicinity of Greendale Fault > Mag 4 from the survey period 18th September to 13th October 2010 (Source: data courtesy of Geonet - http://magma.geonet.org.nz/resources/quakesearch/).

Significant Earthquakes During Survey Period 18th September to 13th October

NUMBER	ORI_DAY	TIME	MAG	DEPTH	LAT	LONG	NZMGE	NZMGN	CUSP_ID
1	19-Sep-10	12:30	4.546	8.4387	-43.5595	172.3902	2460750	5738664	3374803
2	19-Sep-10	23:50	4.098	5	-43.0116	172.0883	2435698	5799312	3375067
3	22-Sep-10	18:22	4.547	8.9834	-43.5649	172.4276	2463776	5738094	3376639
4	23-Sep-10	15:40	4.448	11.0779	-43.5822	172.405	2461963	5736150	3377148
5	24-Sep-10	7:50	4.329	9.0689	-43.5797	172.3872	2460527	5736425	3377550
6	24-Sep-10	21:22	4.288	9.4829	-43.5982	172.3984	2461445	5734375	3377880
7	25-Sep-10	4:46	4.013	9.4019	-43.5707	172.0488	2433182	5737162	3378064
8	25-Sep-10	7:58	4	7.427	-43.5349	172.6526	2481938	5741523	3378131
9	29-Sep-10	20:39	4.355	9.7299	-43.6071	172.3668	2458902	5733365	3380440
10	30-Sep-10	16:53	4.101	14.2835	-43.824	171.6528	2401651	5708593	3380862
11	4-Oct-10	9:21	5.15	10.3314	-43.5627	172.4031	2461799	5738324	3382676
12	4-Oct-10	17:29	4.289	5	-43.6168	172.1586	2442105	5732143	3382841
13	5-Oct-10	10:10	4.076	11.711	-43.6395	172.4142	2462754	5729790	3383183
14	7-Oct-10	10:10	4.218	10.9549	-43.6052	172.3241	2455455	5733549	3384170
15	7-Oct-10	17:17	4.388	10.4969	-43.7141	172.3641	2458770	5721481	3384315
16	7-Oct-10	17:29	4.18	15.5298	-43.7137	172.3749	2459639	5721528	3384322
17	13-Oct-10	0:28	4.093	9.1257	-43.5924	172.4074	2462164	5735025	3388240
18	13-Oct-10	3:42	5.123	10.3521	-43.5899	172.4131	2462623	5735304	3388384

Appendix C – Site Investigations, RTK and Seismic Reflection Surveys

Site Investigations

Lincoln – Ladbrooks Area

Springs Road,

A number of surface deformation features were identified in a section along Springs Road south of Hamptons Road outside the Neville R. Stud Farm. Cracking and liquefaction (sand blows) was present cutting through the tarseal in an NE-SW orientation. Also identified was a power-pole along the roadside that had sunk by approx. 15-20 cm. Further inspection revealed it was a lot more extensive than just localised to the road. Discussion with the staff at Neville R. Stud farm led to the following discoveries:

- A number of linear en-echelon stepping sand blows emanated in the back paddocks as well as some ground cracks. They then jumped through onto the neighbours (Bromac Lodge) front paddock. Gates for the paddocks have become stuck. The whole carpark at Neville R. Stud Farm was underwater from surface flooding (see Figure 59).
- Inspection of the paddocks at back of the farm showed there a general trend in orientation of the cracks and sand blows (NW-SE) and there was a slight offset in the fence at the back of the property.

To determine whether the en-echelon liquefaction features extended in either of the NW or SE orientations, it was decided to investigate neighbouring roads where the feature was likely to intersect if it continued to propagate through the landscape. It was identified that along Shands Road near the intersection with Hamptens Road, was where the feature was likely to pass through if it did continue from the Neville R. Stud farm and Springs Road. However, no evidence could be found anywhere along Shands Road that suggested any deformation features had occurred. This was later confirmed when reviewing satellite imagery of the site on Google Earth.

Tracking the pattern in the SE direction instead meant, the next road likely to be intersected was Birchs Road approx. 200m south of the intersection with Leadleys Road. Once again there was no sign of any liquefaction or cracking. Further inspection up the road, at the intersection with Leadleys Road a few features were identified, including:

- A series of cracks were located cutting through the tarseal east-west along Birchs Road and at the intersection of Birchs and Leadleys Roads.
- There was a slight indication of sand blows on the horse track next to the intersection with Google earth confirming the presence of liquefaction feature with the same NW-SE orientation (see Figure 60).

Projecting this feature further east led down Leadleys Road to an intersection with the next north-south oriented road, Ellesmere Road. Again, at this location there was no evidence suggestion liquefaction or cracking, but up the road approx. 500m and heading south along the road approx. 1 km there was sand blows and cracking at each of these locations. Furthermore sand blows were also visible along McDrurys Road.

Figure C1: Earthquake attributed features, sand blows, offset fence posts and cracking the road identified near Neville R Stud farm immediately following the September 4th earthquake (Image sourced courtesy of Google earth).

Figure 75: En-echelon liquefaction features on the corner of Birchs and Leadleys Road, inside the horse training circuit immediately following the September 4th earthquake (Image sourced courtesy of Google earth

Tai Tapu – Halswell Area

Tai Tapu Road,

- A series of cracks cut E-W through the tarseal of Tai Tapu Road between Hayes and Leadleys Road; in particular a cluster is opposite 182 and beside 173 Tai Tapu Road.
- En-echelon liquefaction features returned to this location, in the paddock beside 173 Tai Tapu Road. They had the same NW-SE alignment as the features located previously.
- Slight dextral offset can be seen as the cracks displace the centreline. Also observed was a slight bend in the road first identified by Barrell and Jongens (2010).

Old Tai Tapu Road,

At this location there were a number of surface deformation features identified in an initial inspection by Barrell and Jongens (2010). Unfortunately at the time of this site inspection (Late October early November 2010) some repair had begun, concealing features. Therefore the following list is a mixture of those features still visible during this these investigations:

- Liquefaction damage to the road and deformation of fence lines out front of properties 319 (Delana Farm) and 321 (Larnark Downs) Old Tai Tapu Road identified by Barrell and Jongens, (2010) had been ripped up and gravelled over. However, damage to the fence

lines and tracking of the liquefaction through the road was observed in the grassed verges at either end of the road.

- In particular, the driveway and fence line leading into the Delana Farm portrayed less than 0.5 m of left lateral offset in Barrell and Jongens, 2010 was still prominent. Barrell and Jongens, (2010) also noted that there were discrete offset en-echelon open fractures striking at approx. 350^{o} to 010^{o} which step southwest along strike to the south passing through and causing extensive damage to 321 Old Tai Tapu Road, these were identified to continue through into the neighbour paddocks at 339 Old Tai Tapu Road (Duncans Property).
- Also identified at the Duncans property was a series of cracks related to the en-echelon features cutting north-south through the driveway and by the letterbox.
- Cracks east-west in orientation, continued sporadically along the road from outside the properties above down to Osterholts Bridge. Some of the cracks were identified to have approx. 2 cm of sinistral offset through the centreline.
- At the bridge there was a combination of east-west and north-south trending cracks.
- These continued through the neighbour ' Duncans' property, 339 Old Tai Tapu Road,
- Also noted, was a severely deformed and partially collapsed cow shed in a paddock across the road from Larnack Downs as well as lateral spreading that went into the river channel at and just south of the Osterholts Road intersection, first identified in a report by Barrell and Jongens, (2010).
- Extensive areas of liquefaction were also noted by Barrell and Jongens (2010) with sand blows and linear fissures close to Halswell River. These were seen to continue into the Duncans Property forming a large cluster of sand blows and ground fissuring in the front paddocks.

Also identified within this area were extensive linear fracturing and liquefaction along Trices Road, Longstaffs Road, Sabys Road, and the top end of Ellesmere Road.

Figure 76: Earthquake features along Tai Tapu Road, Old Tai Tapu Road and Osterholts Road immediately following the September 4th earthquake (Image source courtesy of Google earth).

South of Christchurch

Site investigation and RTK surveys south of Christchurch highlighted interesting deformation features, including a number of linear en-echelon stepping sand blows emanated in the back paddocks as well as some ground cracks, and cracks in the road from Springs Road through to Old Tai Tapu. Tracking and inspecting these features identified a general trend in orientation of the cracks and sand blows (NW-SE) with slight offsets identified in places. Also observed towards the southern end of Tai Tapu Road was a broad linear ridge, trending 190°, several 10's of metres wide, and up to 2 m high first identified by Barrell and Jongens (2010). Ground fissures along Old Tai Tapu Road are position on the crest of this feature but "step-off" progressively westward towards the south. Continuing south near Holmes Road, the ridge interacts with the Port Hills volcanics. Both Barrell and Jongens (2010) and I agree, the way these features line up is not deemed a coincidence mainly because you can track these features from Springs Road through to Old Tai Tapu Road. Two possibilities are that these features may correspond to either tectonic origin or closer to old Tai Tapu Road reflect old stream or river channels.

Unfortunately due to time controls this section was not able to be further investigated. Using detailed aerial photos captured following each of the earthquakes this work could be undertaken again in the future. It would be very interesting to see whether these features were indicating tectonic origin or not. Through seismic investigation it would be interesting to see what influence the volcanics from the Port Hill had on the area also. Areas of interest include**:**

- Springs Road,
- Birchs Road,
- Tai Tapu Road, and
- Old Tai Tapu Road.

A joint detailed study of this region was undertaken by the University of Canterbury and University of Calgary, using a vibro-truck very deep detailed seismic reflection surveys were completed. This data could also prove to be very helpful in finding out what caused these deformation features south of Christchurch.

Map of everything on the Eastern Side – Lincoln, Halswell/Tai Tapu areas

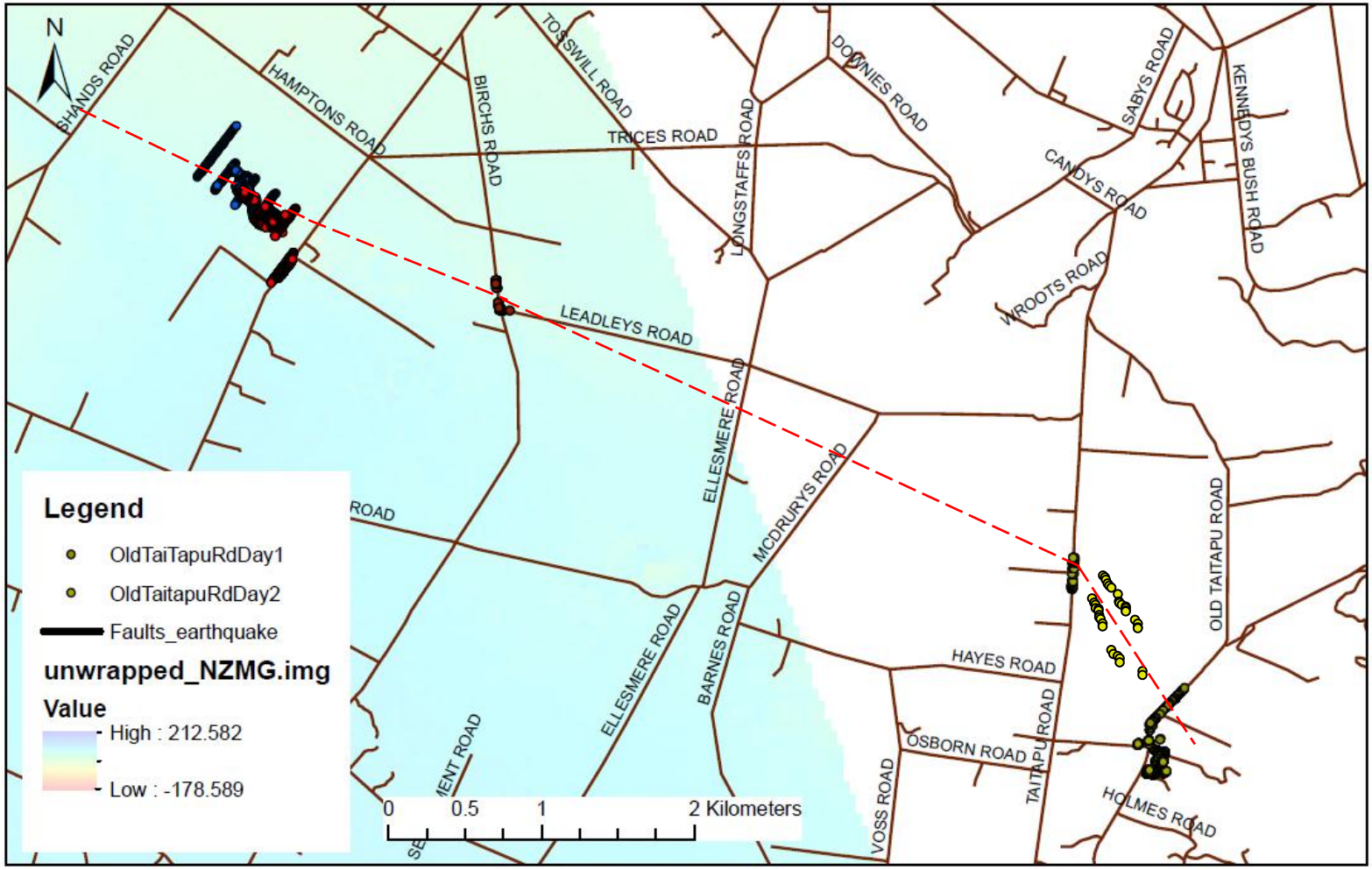

Figure C4: RTK sites along the eastern end of the Greendale Fault Trace. The alignment of these features may indicate a projection of the fault trace. Further work is required to confirm this.

Eastern Side

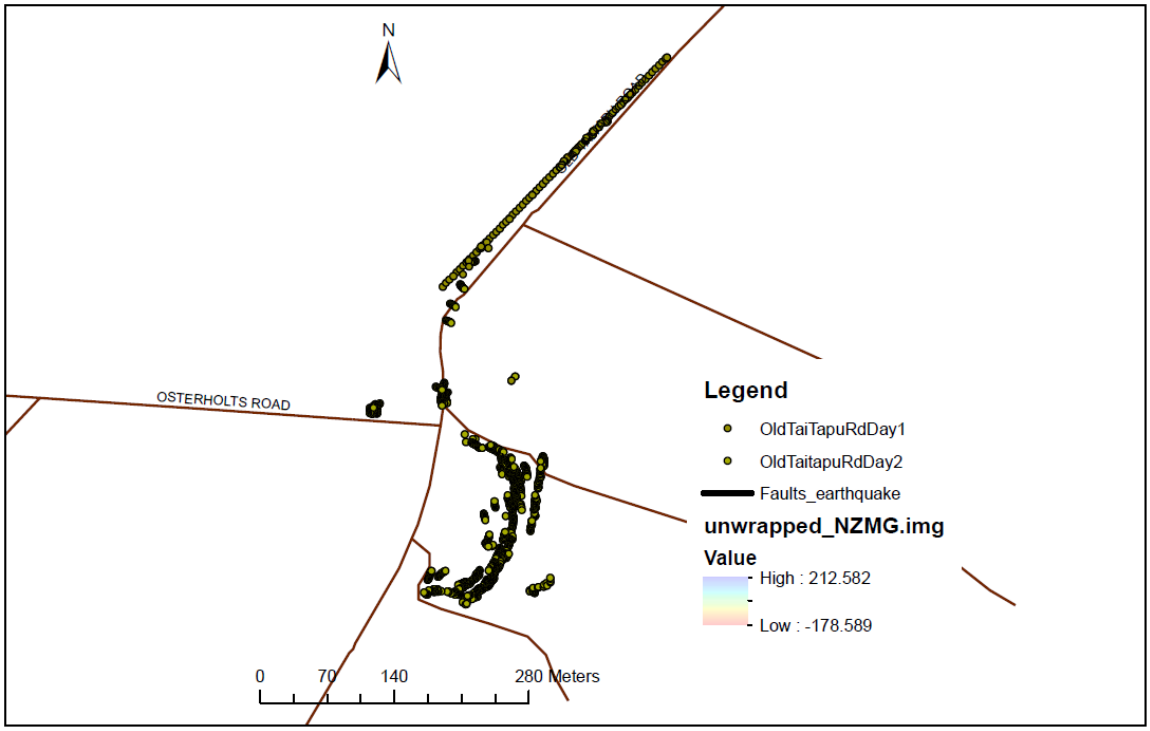

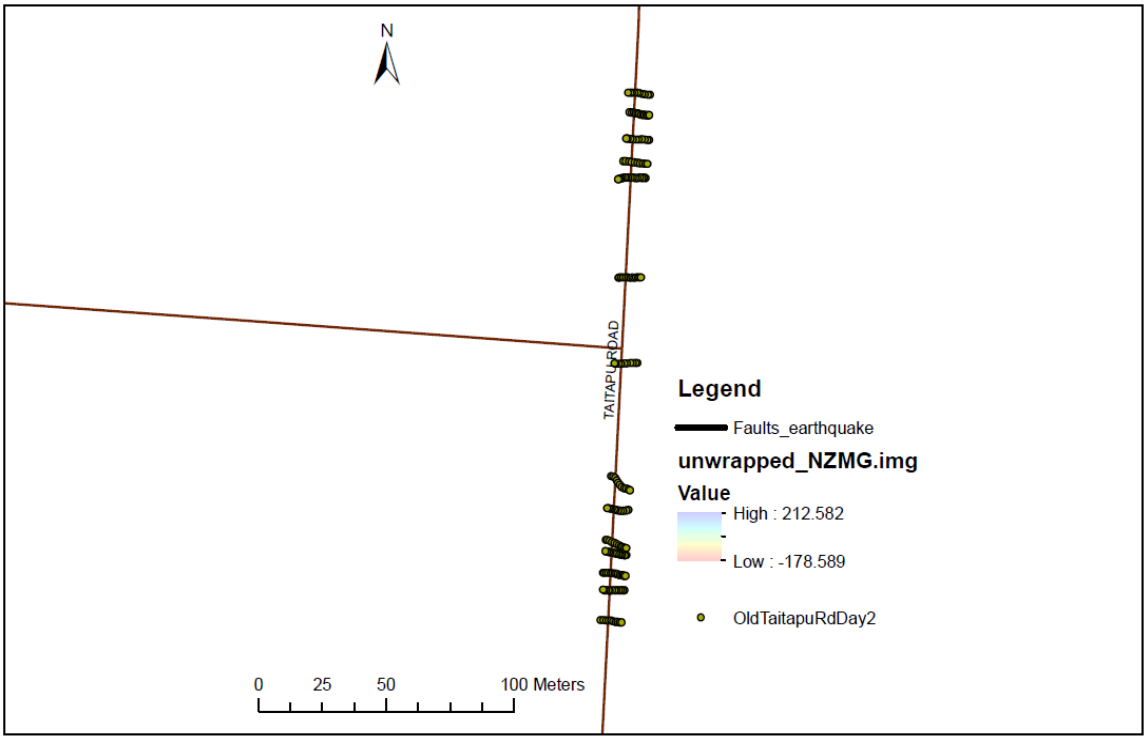

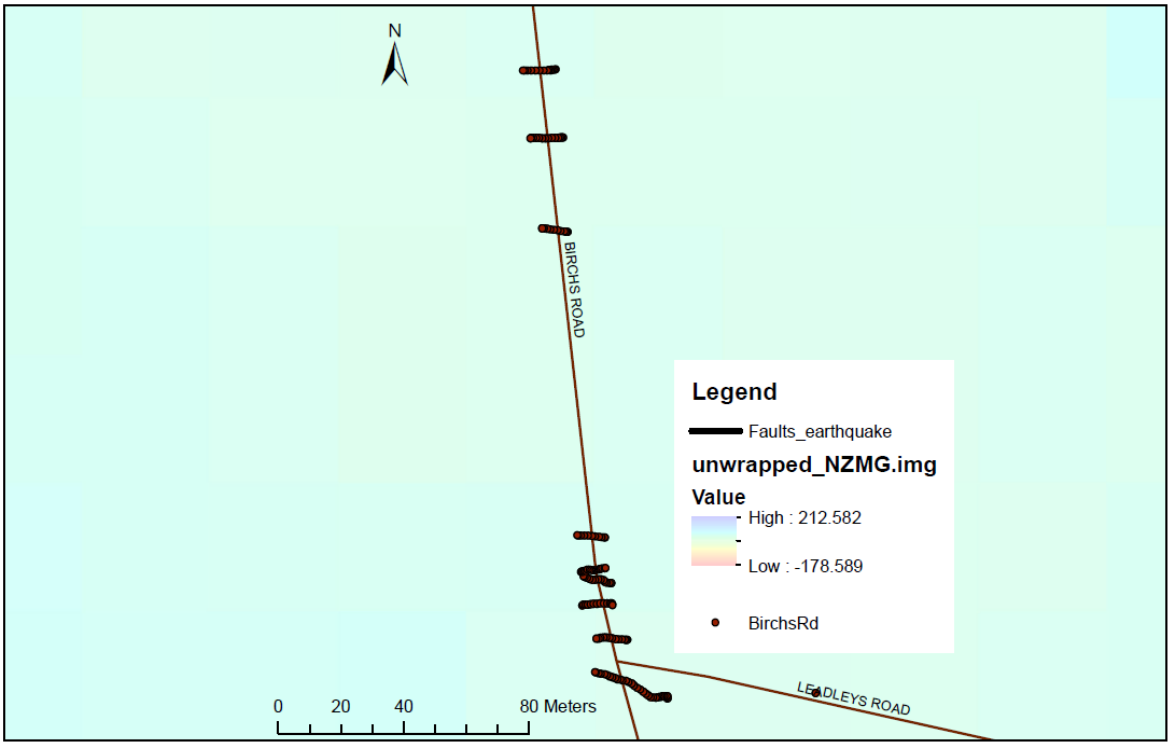
N
BIRCHS ROAD
LEADLEYS ROAD
Legend
Faults_earthquake
unwrapped_NZMG.img
Value
High : 212.582
Low : -178.589
BirchsRd
0 20 40 80 Meters

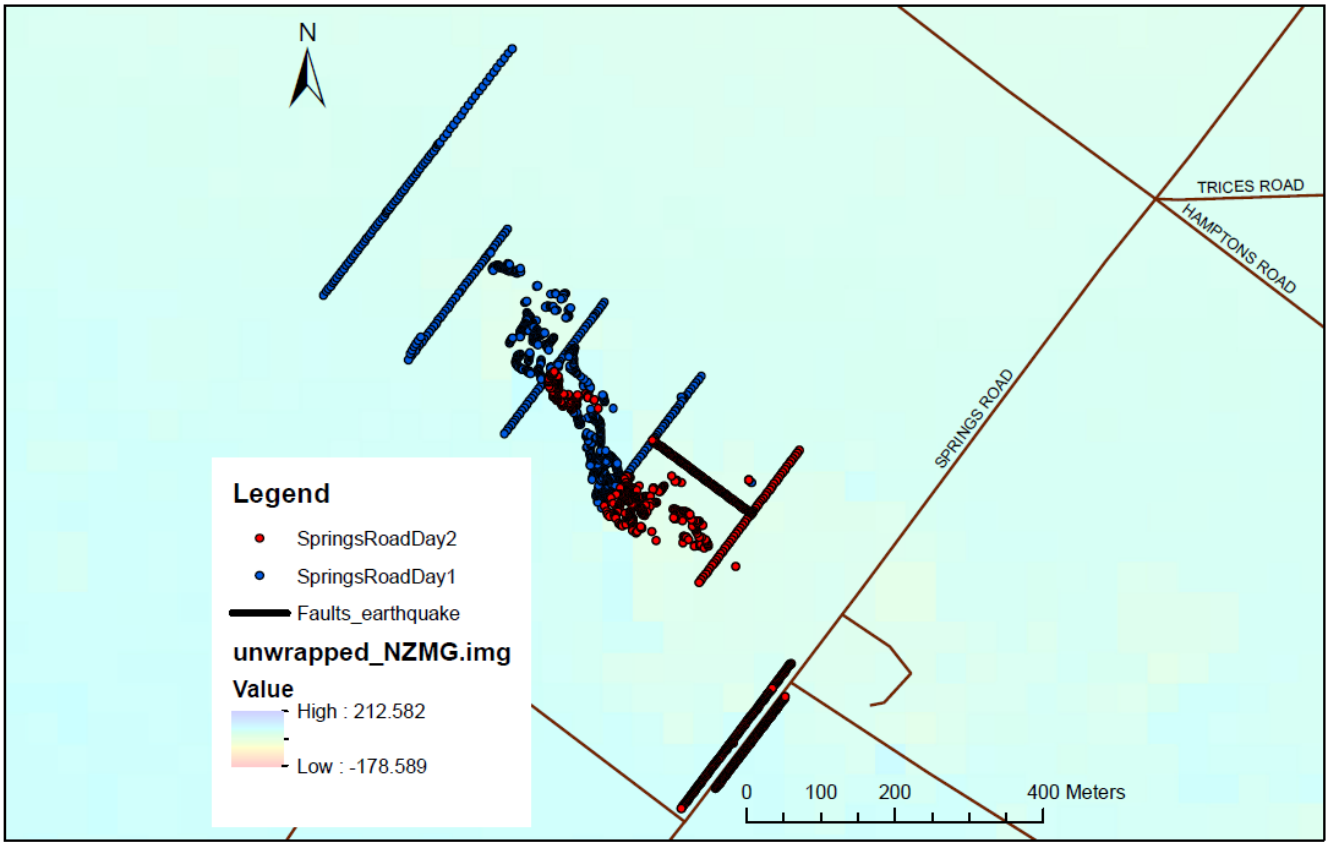
N
TRICES ROAD
HAMPTONS ROAD
SPRINGS ROAD
Legend
SpringsRoadDay2
SpringsRoadDay1
Faults_earthquake
unwrapped_NZMG.img
Value
High : 212.582
Low : -178.589
0 100 200 400 Meters

Western Side

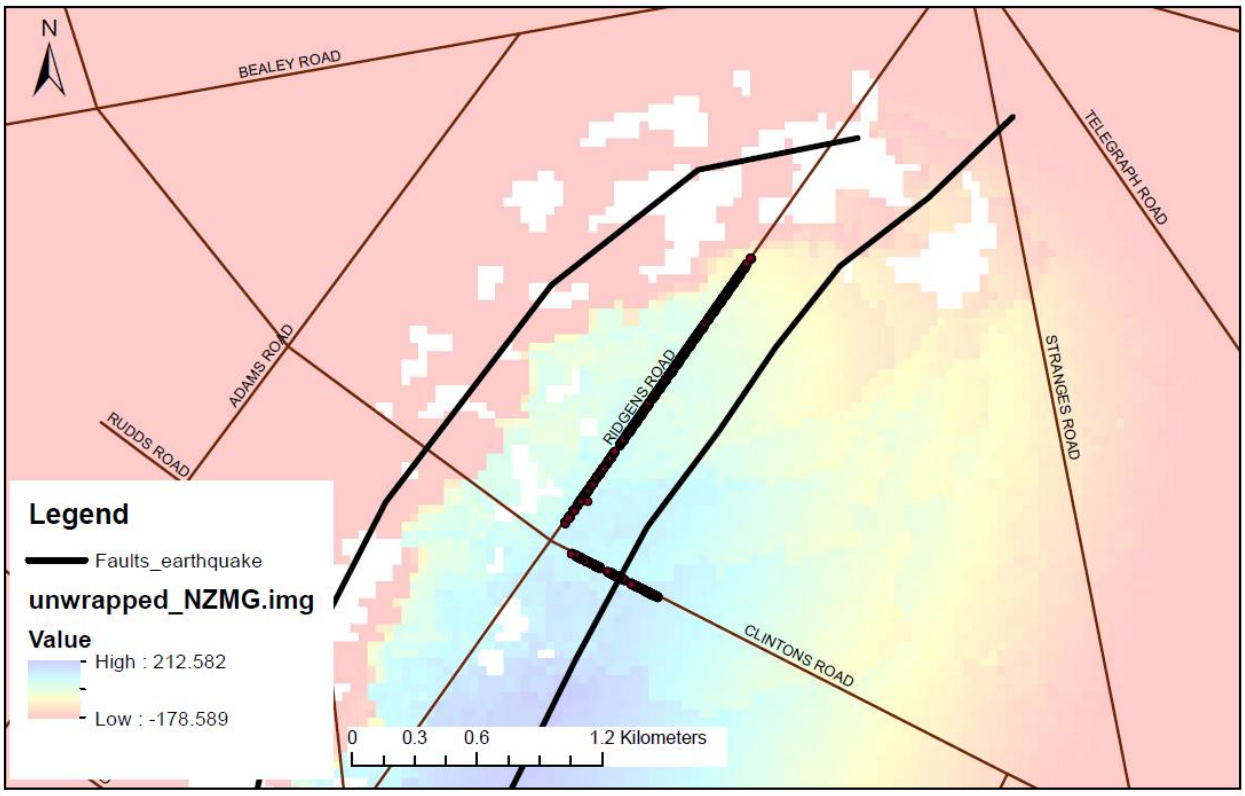

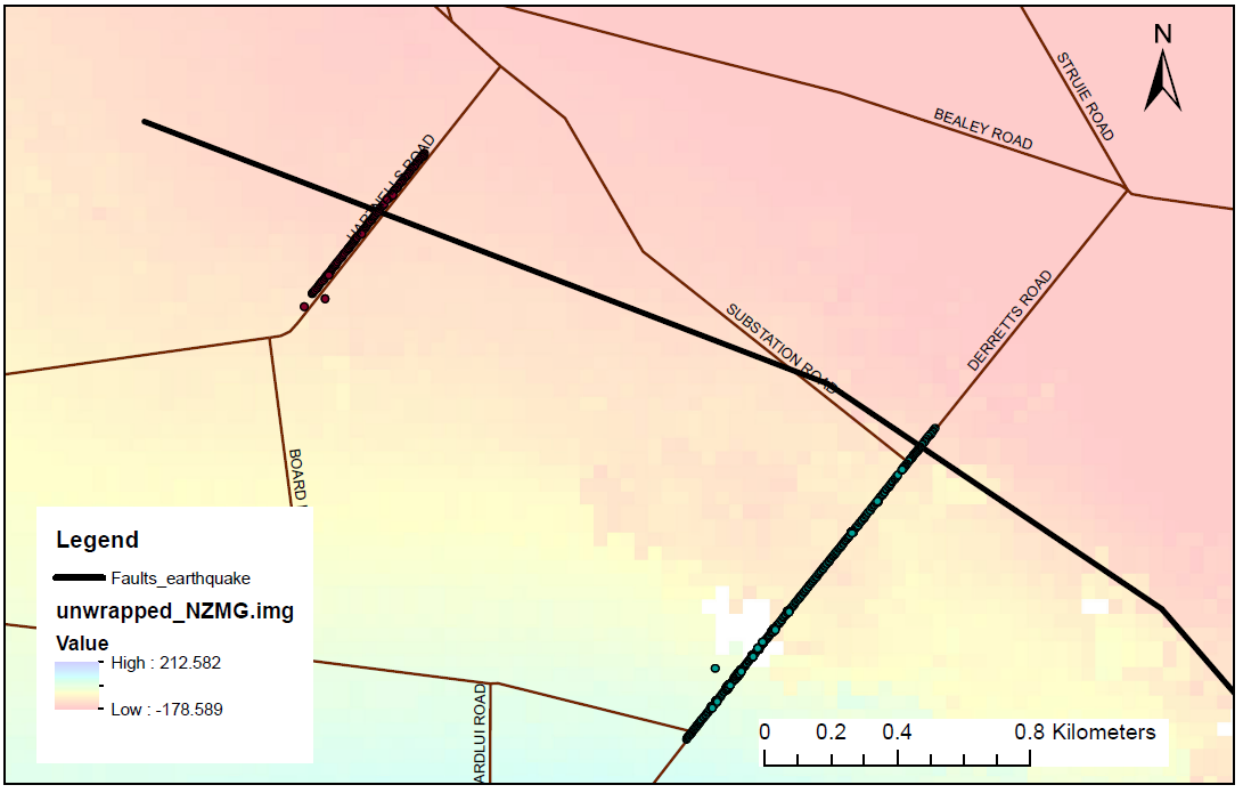

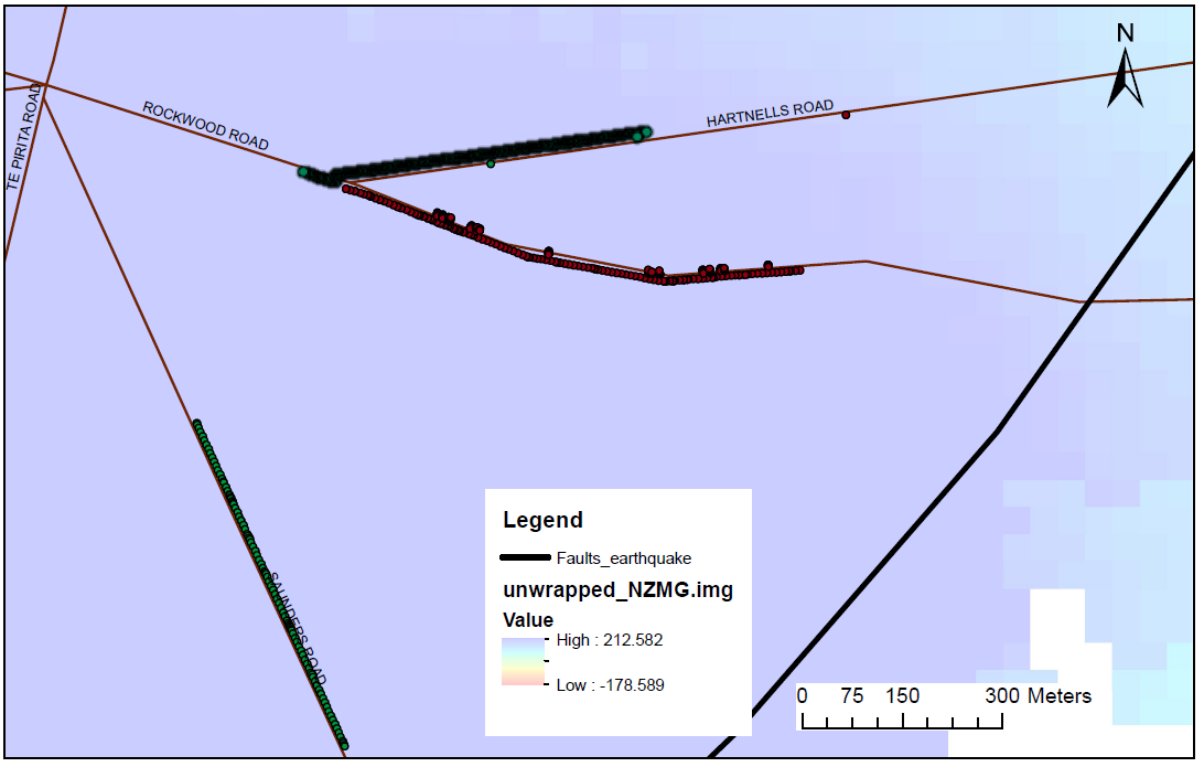

Seismic Surveys

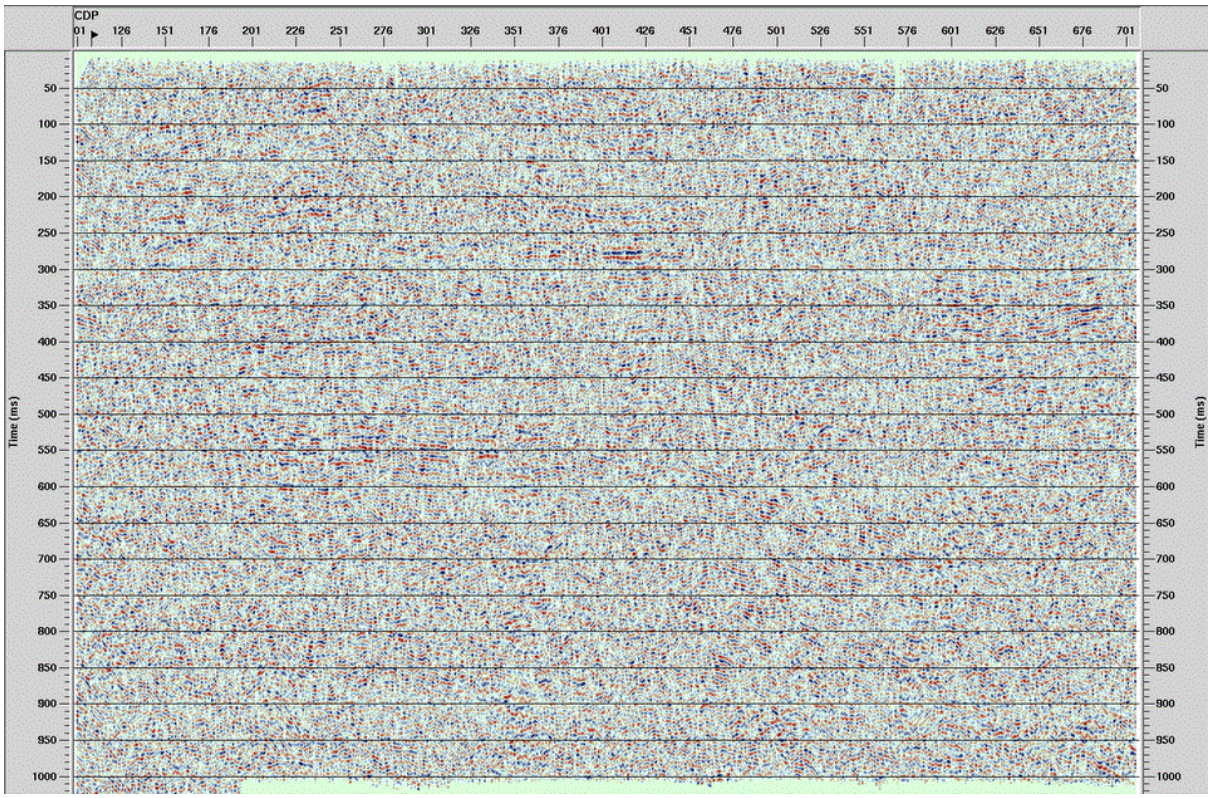

FigureC: Saunders Road raw profile.

Appendix D – Cadastral / Geodetic Surveys

Table D19: All reoccupied cadastral survey marks with pre (brown) and post (blue) September locations. Red marks indicate crossover points with Beavan *et al.*, 2010 study 9Pre earthquake locations download from lindz.govt.nz geodetic data base.

				Pre-September Earthquake			Post-September Earthquake		
GeodeticCode	Name	MaintDate	CrdOrder	NZTMEasting	NZTMNorthing	OrthHeight	EastingNZTM	NorthingNZTM	Elevation (m)
AA71	8233	4/04/2008	3	1512825.29	5176859.85	<Null>	1512833.017	5176837.87	212.346749
B2Q1	8231	21/03/2003	3	1517021.75	5178393.19	179.53	1517019.717	5178388.628	190.19133
BPMB	MOWBMCC263	7/12/2004	4	1512819.82	5180451.75	224.118	1512817.423	5180447.274	235.360897
BPMC	MOWBMCC290	16/11/1999	4	1522353.91	5182883.29	199.361	1522350.169	5182881.307	205.657935
BPMF	MOWBMCC93	15/02/2011	4	1517584.57	5176175.95	169.336	1517581.841	5176171.484	180.329957
BPMG	MOWBMCC86	12/08/2008	4	1515142.54	5171169.53	191.458	1515149.721	5171147.681	199.675031
BPMJ	MOWBMCC311	15/09/2008	4	1526013.39	5175618.48	143.661	1526013.427	5175617.292	153.784003
ACFB	VV 46	31/07/1986	4	1530988.84	5179699.28	160.0958	1530985.389	5179697.175	166.124792
AFC7	VV75	<Null>	4	1511770.64	5177095.22	211.6771	1511778.037	5177073.306	220.692078
D0VF	VV 47 NO 2	13/02/2008	5	1531827.69	5178478.02	150.7946	1531824.481	5178476.389	157.083164
DBQN	BM CC 349 DP 79436	12/10/2000	5	1531623.08	5173779.2	<Null>	1531621.43	5173776.892	128.710361
AFCR	VV81	23/02/2006	6	1517562.55	5172718.15	173.3509	1517569.652	5172696.326	181.567241
AFCA	VV76	<Null>	6	1513268.6	5176707.6	199.757	1530037.673	5181108.111	177.194672
AFCE	VV79	20/11/2010	6	1518180.53	5176021.07	165.4447	1518191.068	5176004.076	173.802888
EJ7J	CC177NO2	10/12/2011	10	1518971.77	5174568.93	<Null>	1518970.405	5174563.644	171.727162
EJ7V	CC 336 NO 2	10/12/2011	10	1534256.45	5174921.01	<Null>	1534253.492	5174918.65	127.352747
EJ7W	CC178NO2	10/12/2011	10	1517917.09	5175686.58	<Null>	1517917.236	5175685.365	175.979682
EJ81	CC176NO2	10/12/2011	10	1519649.26	5173810.97	<Null>	1519647.899	5173805.681	168.032959
DYWP	CC39	22/05/2007	12	1512118.47	5176735.86	<Null>	1512081.921	5176740.709	218.099953
DYY0	CC85	22/05/2007	12	1515318.2	5170337.74	<Null>	1515393.985	5170277.959	196.689528
DYY5	CC90	22/05/2007	12	1514817.92	5175286.43	<Null>	1514909.64	5175181.632	198.04351
DYY6	CC91	22/05/2007	12	1514018.01	5176586.05	193.791	1514053.372	5176589.995	203.139396

DYY7	CC92	22/05/2007	12	1515967.55	5176286.27	181.952	1515785.621	5176368.456	190.430525
DYYD	CC98	22/05/2007	12	1517017.2	5177386.07	<Null>	1517047.309	5177340.039	181.188404
DYYE	CC99	22/05/2007	12	1518016.95	5177336.16	<Null>	1518041.165	5177456.815	179.092272
DYYH	CC116	22/05/2007	12	1516517.07	5181385.01	<Null>	1516548.941	5181701.384	219.522972
DYYJ	CC117	22/05/2007	12	1516717.1	5180035.37	<Null>	1516859.864	5180343.061	205.914937
DYYN	CC121	22/05/2007	12	1522565.74	5177536.44	<Null>	1522492.299	5177691.485	169.42047
DYYP	CC122	22/05/2007	12	1523515.46	5177786.44	<Null>	1523504.427	5177936.097	169.235463
DYYR	CC124	22/05/2007	12	1525664.88	5177536.65	<Null>	1525618.403	5177726.445	163.581885
DYYU	CC 126	22/05/2007	12	1527714.3	5177536.81	<Null>	1527685.428	5177717.258	160.104107
DYYU	CC 126	22/05/2007	12	1527714.3	5177536.81	<Null>	1529359.152	5174990.32	139.856049
DYYW	CC 128	22/05/2007	12	1529663.72	5177886.84	<Null>	1529663.67	5178065.468	158.604866
E010	CC171	22/05/2007	12	1523515.97	5171138.28	<Null>	1523506.312	5171140.446	144.616362
E02W	CC 237	22/05/2007	12	1532713.44	5169739.49	<Null>	1532690.123	5169731.425	100.232023
E02X	CC 238	22/05/2007	12	1531713.69	5170339.22	<Null>	1531727.206	5170320.954	106.175403
E02Y	CC 239	22/05/2007	12	1530563.97	5171088.9	<Null>	1530558.718	5171036.271	112.008397
E030	CC 240	22/05/2007	12	1530014.11	5171338.77	<Null>	1529989.706	5171285.035	115.272358
E036	CC 246	22/05/2007	12	1525415.2	5174037.62	<Null>	1525333.516	5174037.359	141.088526
E037	CC247	22/05/2007	12	1524465.42	5174687.36	<Null>	1524449.321	5174694.351	146.295035
E03D	CC253	22/05/2007	12	1520366.1	5180885.38	<Null>	1520378.06	5180844.399	195.829269
E03F	CC255	22/05/2007	12	1519216.29	5182684.84	<Null>	1519199.69	5182732.968	214.206708
E03K	CC259	22/05/2007	12	1517316.81	5182284.82	<Null>	1517339.112	5182353.503	226.903448
E03N	CC262	22/05/2007	12	1513817.79	5180635.02	<Null>	1513802.972	5180630.816	221.868952
E04D	CC288	22/05/2007	12	1521415.67	5183584.74	<Null>	1521414.758	5183472.293	207.590374
E04K	CC294	22/05/2007	12	1523965.08	5181835.36	<Null>	1523957.402	5181894.926	195.593088
E04L	CC295	22/05/2007	12	1523265.32	5180985.55	<Null>	1523181.381	5180983.484	188.865852
E04M	CC296	22/05/2007	12	1522115.7	5179785.79	<Null>	1522134.747	5179785.92	183.600084
E04W	CC308	22/05/2007	12	1525064.89	5179835.98	<Null>	1525149.226	5179861.983	180.824188
E04Y	CC310	22/05/2007	12	1525764.9	5176836.86	<Null>	1525755.38	5176880.622	157.850226
E052	CC 313	22/05/2007	12	1526314.98	5173687.79	<Null>	1526396.209	5173699.847	136.150415

E057	CC 318	22/05/2007	12	1526814.4	5180086.02	<Null>	1526842.706	5180089.999	178.244752
E058	CC 319	22/05/2007	12	1527164.37	5178936.37	<Null>	1527223.089	5178969.737	168.949301
E05E	CC 330	22/05/2007	12	1527064.71	5174437.63	<Null>	1526982.495	5174447.411	139.89531
E05F	CC 331	22/05/2007	12	1527564.51	5175237.45	<Null>	1527542.198	5175238.273	144.795293
E05J	CC 334	22/05/2007	12	1529163.9	5177386.94	<Null>	1529042.102	5177262.341	154.131657
E05R	CC 341	22/05/2007	12	1533912.76	5173588.43	<Null>	1533867.498	5173581.975	120.376417
E05W	CC 345	22/05/2007	12	1529364.01	5174987.66	<Null>	1529354.453	5174989.2	139.360892
E05X	CC 346	22/05/2007	12	1529264.17	5173238.16	<Null>	1529257.365	5173203.322	128.511492
E064	CC 352	22/05/2007	12	1530663.51	5176687.26	<Null>	1530609.094	5176739.907	150.099414
E065	CC 353	22/05/2007	12	1531313.26	5177587.04	<Null>	1531228.198	5177621.728	152.366542
E06C	CC 360	22/05/2007	12	1533513.15	5170339.38	<Null>	1533404.023	5170413.921	103.180949
cc83							1515945.39	5168306.636	188.285965
unknown							1529847.131	5175637.059	143.171124

Table D2: Reoccupied cadstral marks and survey base stations

Base Station	Mark Collected	EastingNZTM	NorthingNZTM	elevation	CrdOrder
Charing Cross Sites:					
Acfa_vv 45		1530037.673	5181108.111	177.194672	9
	cc126	1527685.428	5177717.258	160.104107	12
cc126					
	cc128	1529663.67	5178065.468	158.604866	12
	DOVF	1531824.481	5178476.389	157.083164	5
	ACFB vv46	1530985.389	5179697.175	166.124792	5
	cc318	1526842.706	5180089.999	178.244752	12
	cc319	1527223.089	5178969.737	168.949301	12
	cc308	1525149.226	5179861.983	180.824188	12
	cc124	1525618.403	5177726.445	163.581885	12
	cc310	1525755.38	5176880.622	157.850226	12
	bpmj_cc311	1526013.427	5175617.292	153.784003	3
	cc313	1526396.209	5173699.847	136.150415	12
	cc330	1526982.495	5174447.411	139.89531	12
	cc331	1527542.198	5175238.273	144.795293	12
	cc334	1529042.102	5177262.341	154.131657	12
	unknown	1529847.131	5175637.059	143.171124	
	cc349	1531621.43	5173776.892	128.710361	12
	cc341	1533867.498	5173581.975	120.376417	12
	cc345	1529354.453	5174989.2	139.360892	12
	cc352	1530609.094	5176739.907	150.099414	12
	cc353	1531228.198	5177621.728	152.366542	12
cc345					
	cc346	1529257.365	5173203.322	128.511492	12
	cc240	1529989.706	5171285.035	115.272358	12
	cc360	1533404.023	5170413.921	103.180949	12
	cc237	1532690.123	5169731.425	100.232023	12
	cc238	1531727.206	5170320.954	106.175403	12
	cc239	1530558.718	5171036.271	112.008397	12
	cc246	1525333.516	5174037.359	141.088526	12
	cc247	1524449.321	5174694.351	146.295035	12
	cc122	1523504.427	5177936.097	169.235463	12
	EJ7V	1534253.492	5174918.65	127.352747	10
cc122					
	cc295	1523181.381	5180983.484	188.865852	12
	cc296	1522134.747	5179785.92	183.600084	12
	cc253	1520378.06	5180844.399	195.829269	12
	cc255	1519199.69	5182732.968	214.206708	12
	BPMC	1522350.169	5182881.307	205.657935	3
	cc288	1521414.758	5183472.293	207.590374	12
	cc294	1523957.402	5181894.926	195.593088	12

	cc121	1522492.299	5177691.485	169.42047	12
Hororata Sites:					
EJj7W/cc178		1517917.236	5175685.365	175.979682	10
	AFCE vv79	1518191.068	5176004.076	173.802888	9
	cc98	1517047.309	5177340.039	181.188404	12
	cc99	1518041.165	5177456.815	179.092272	12
	cc117	1516859.864	5180343.061	205.914937	12
	cc116	1516548.941	5181701.384	219.522972	12
	AA71	1512833.017	5176837.87	212.346749	3
	AFC7 vv75	1511778.037	5177073.306	220.692078	9
	cc39	1512081.921	5176740.709	218.099953	12
	cc90	1514909.64	5175181.632	198.04351	12
	bpmg/mowbmcc3	1515149.721	5171147.681	199.675031	3
	cc85	1515393.985	5170277.959	196.689528	12
	cc83	1515945.39	5168306.636	188.285965	12
	AFCR vv81	1517569.652	5172696.326	181.567241	5
	cc91	1514053.372	5176589.995	203.139396	12
	cc92	1515785.621	5176368.456	190.430525	12
AFCE vv79					
	cc171	1523506.312	5171140.446	144.616362	12
	ej81/cc176	1519647.899	5173805.681	168.032959	10
	ej7j/cc177	1518970.405	5174563.644	171.727162	10
	BPMF	1517581.841	5176171.484	180.329957	3
	cc259	1517339.112	5182353.503	226.903448	12
	cc262	1513802.972	5180630.816	221.868952	12
	BPMB	1512817.423	5180447.274	235.360897	3
	B2Q1	1517019.717	5178388.628	190.19133	3